AN INVESTIGATION OF THE THERMAL BEHAVIOUR OF SOME IONIC COMPOUNDS BY CRYSTALLOGRAPHIC AND PHYSICAL METHODS

A Thesis submitted for the

Degree of Doctor of Philosophy

by

JAJNESWAR HATIBARUA

Department of Chemical Engineering
and Chemical Technology
Imperial College of Science and Technology
London S.W.7.

September 1968

ABSTRACT

Detailed investigations of thermal behaviour of potassium acetate and some preliminary studies on rubidium and caesium acetates have been described. Properties have been studied by X-ray diffraction and other physical methods. Three crystallographically distinct but closely related polymorphs of potassium acetate have been found:

Form I : From 155°C upwards ..... orthorhombic

Form II : From 155°C to ~ 75°C ... monoclinic

Form III : From ~ 75°C to room temperature ... monoclinic with a multiple cell.

The two solid-solid phase transitions have been studied. X-ray diffraction photographs of single crystal and co-operative pretransition-increase in dielectric and thermal properties have shown that the transition I → II is of "displacive" (martensitic) type whose structural basis has been established.

The transition II → III which did not show up in dielectric and thermal analysis measurements has been structurally characterised by the appearance of additional layer lines, resembling superlattice reflexions in an ordered structure. Intensity of these reflexions has been used to study the hysteresis of this transition.

Thermal expansion of the lattice parameters has been studied. Very high values of the thermal expansion along the a-axis and

contraction along b and c axes have been measured. In the dielectric study, the relative permittivity and loss-factor rapidly increased at higher temperature, starting from about the T_c = 155°C of II ⟶ I transition. This has been attributed to thermal activation of the cations from lattice site to the void in the lattice.

The basic structures of form I and II have been established as formed by ionic double layers parallel to $\{100\}$ of potassium ions co-ordinated by six oxygen atoms from five different acetate ions, - four from four different acetate ions of the same half of the layers as the potassium ion and two from the same acetate ion of the other half of the layer. Only probable models of form III have been discussed.

For comparison, some crystallographic and dielectric work have also been done with rubidium and caesium acetates.

ACKNOWLEDGEMENTS

The author wishes to express his gratitude to Dr G.S. Parry for constructive supervision and invaluable help at each and every stage of this research.

It is also a pleasure to thank Professor A.R. Ubbelohde F.R.S. for his continued interest and helpful suggestions during this work.

Thanks are due to Dr D.A. Young for his suggestions on different matters, to Dr D.E. Nixon for correcting part of the manuscript, to Dr E.A.D. White of the Crystal Growth Laboratory for growing some crystals, to Dr I.S. Kerr of the Chemistry Department for allowing the use of the microdensitometer and to Dr J.A. Barrie of the Polymer Characterisation Laboratory for allowing the use of the Differential Thermal Analyser.

The co-operation of the following members of the College technical staff is gratefully acknowledged: Mr A. Jones and his staff for the construction of the glass apparatus and Mr J. Oakley and his staff for construction of the glove box.

The author is grateful to the State Government of Assam, India, for the award of an Overseas Scholarship.

CONTENTS

Chapter 1

GENERAL INTRODUCTION

1.1. Introduction

1.1.1. Introduction to crystal forces. The forces of inter-atomic interaction which play the dominating role in the formation of crystal structures may be divided into four types: (a) metallic, (b) covalent, (c) ionic (d) Van der Waals'.

(a) In the present work metallic forces are of no interest, so the characteristic features of only the other three types will be discussed.

(b) In covalent bonding, two or more atoms attain a stable inert gas configuration by a sharing of pairs of electrons. For example, the existence of the hydrogen molecule is due to this type of bonding. A hydrogen atom has only one electron. When the two atoms come together to form a molecule, their two electrons belong to both atoms and each can be assumed to attain helium atom configuration. Thus, in the case of co-valent bonding, the number of neighbours is limited by the number of available electrons that can be shared. Another important feature of this type of bonding is that in most cases, the bonds from the atoms are directed. Thus, the covalent bonds of a carbon atom are directed towards the corner of a regular tetrahedron. The properties mentioned above, restrict the number of types of crystal structure formed with such bonds. The covalency fixes the number of neighbours that an atom may have and because

co-valency is small, the number of structures bound entirely by covalent forces is small. In the majority of molecular crystals, these forces generally operate within a single molecule and the different molecules are held together by other forces. The well known example of a crystal formed purely by co-valent forces is the diamond structure, in which each carbon atom is surrounded by four others and these neighbours are arranged at the corners of a regular tetrahedron.

(c) The forces interacting between ions are electrostatic in nature, varying inversely as the square of the distances between them. This assumes that the electron distribution function of an ion is spherically symmetrical, so that interactions between ions are undirected and unsaturated. The unsaturated nature of ionic forces is shown by the fact that each ion tends to draw as many oppositely charged ions as is geometrically possible, that is, the co-ordination number is as large as possible. The possible maximum value of the co-ordination number is determined by the ratios of the ionic radii. An increase in the ratio = (radius cation/radius anion) is accompanied by an increase in co-ordination number. Although the number of co-ordinating ions does not generally exceed the maximum allowed by the contact radii, the number can be less. In the following table (Table 1) radius ratios and the observed co-ordination numbers of some alkali metals with oxygen are used to illustrate the variation of co-ordination number with radius ratio.

Table 1

Co-ordination number for some cations with oxygen ion[1]

ion	radius ratio	co-ordination number
Li^+	.34	4
Na^+	.54	6, 8
K^+	.75	6, 7, 8, 9, 10, 12
Cs^+	.96	12

Because of the high energy of the ionic bond, these crystals have fairly high melting points. A few ionic crystals with their melting points are given in Table 2.

Table 2

Some crystals with their melting points

Material	melting point °C
Ionic:- monoatomic anion	
NaCl	804
LiBr	547
AgBr	434
	304
Polyatomic anion	
CH_3COONa	329
CH_3COOK	304
CH_3COORb	246
CH_3COOCs	194

(d) Van der Waals forces arise from the instantaneous polarization of the neighbouring atoms by the fluctuating fields of an atom. The interaction energy in this case varies inversely as the sixth power of the distance between atoms. These forces are undirected, so there are no restrictions as to the number of neighbours in a crystal formed due to these forces. Hence they form close packed structures as in ionic crystals. For instance, helium gas at low temperature and high pressure ($\sim$ 25 atm.) forms hexagonal-close-packed crystals and other inert gases are cubic close packed in the solid state.

From an analysis of the distribution of crystals according to their space group symmetry, it was found that crystals in which ionic or metallic forces predominate crystallise in more symmetrical space groups within the cubic and hexagonal systems. Organic molecular crystals, on the other hand, crystallise in less symmetrical space groups within the monoclinic and orthorhombic systems[2]. In the organic structures the molecules can be represented by ellipsoids whose close packing leads to less symmetrical space groups[3].

Although these are the basic types of chemical binding forces, in reality a large number of intermediate types of bonds are possible. However, in indicating the type of a particular crystal, only the predominant forces are mentioned. Thus, potassium cyanide and sodium nitrate are referred to as ionic crystals, because the forces forming these crystals are mainly

ionic although the forces forming the complex $(CN)^-$ or $(NO_3)^-$ are covalent. There are many such groups in which the atoms in the group are bound more tightly than with the rest of the structure. These groups may, at sufficiently high temperatures, execute hindered or free rotation. Such motions are likely to take place readily in groups of pseudo-spherical or pseudo-cylindrical forms and in the latter case, motion is restricted to rotation about an axis of pseudo-symmetry. For example, the $(NO_3)^-$ group can rotate about the triad axis and as a consequence such a rotation can often take place without any increase in the symmetry of the structure. Thus, in $NaNO_3$, the transition to the rotating form takes place gradually over an extended temperature range without alteration in the structure, but with a small change in the angle of the rhombohedral unit cell[4]. On the other hand, a more or less spherical group such as NH_4^+ can rotate about any axis.

The packing of the organic crystal structures has already been mentioned. Each organic substance has its own distinctive molecular structure, and often the molecules in such a crystal might have a distorted and complex shape. For example, they may form sheets, or chains, or helices, or other shapes. Nevertheless, the crystal structures may be essentially ionic. Thus, the metal salts of organic acids and certain other compounds such as ammonium halides or salts, form ionic structures, the component ions of which are held together by electrostatic forces. If the complex ion is small, these organic ionic crystals may form the

same type of simple structures as inorganic ionic compounds. Thus, in the sodium oxalate structure[5], each sodium atom is octahedrally co-ordinated by six oxygen atoms of adjacent $(COO)_2^{2-}$ ions. In this crystal, and in many others, no distinction can be made between the two oxygen atoms of the same planar ion, which suggests that complete resonance takes place between the two equivalent configurations:

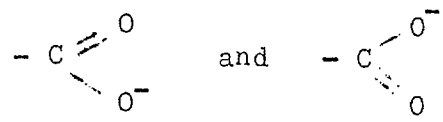

For this reason, the C-O distance in these crystal structures is intermediate between those of single and double bonds[6].

The relevance of the above description will be apparent when the chemical representation of the acetate structures studied in the present work is considered. The carboxylic ion shown above is the co-ordinating group around the alkali metal ion. The covalent bonding between the carbon of this ion and a methyl group CH_3 forms the acetate ion.

1.1.2. Introduction to the present work. Earlier it was mentioned that the metal salts of organic acids form ionic structures. During studies of the melting mechanism and melt properties of the alkali metal salts of various univalent organic acids, Hazlewood et al.[7] have investigated some alkali metal acetates. Few of these salts yield stable melts, and of these, the most stable were the acetates.

Potassium acetate differs from other acetates in several respects. For instance, unlike sodium acetate, it has the rare property of a contraction in the specific volume on melting, it is extremely deliquescent and does not form crystalline hydrates.

The dilatometric studies of potassium acetate by Hazlewood et al. established at least three irregularities in the variation of the molar volume with temperature. The irregularities could be interpreted as three changes in volume expansion coefficient of the solid salt and were assumed to be due to three solid state phase transformations. When discussing the possible structural changes involved, it was suggested that these must involve an increase in the statistical symmetry of the molecular anion prior to melting. Now, the contributions to the entropy of melting of these crystals may be written as:

$$S_f = S_{positional} + S_{orientational}$$

Positional randomisation of the acetate ion will lead to an increase in entropy; this is a common mechanism in these salts. The molecular symmetry of the acetate ion is a function of the methyl group and libration of the group about the C-C bond raises the symmetry of this ion to mm2. An anion with such symmetry is capable of various modes of motion. The methyl group may rotate about the C-C bond, it may librate, the whole acetate ion may rotate about the C-C bond, or from head-to-tail. Of these, Hazlewood et al. considered that rotation of the methyl group

about C-C might be involved at least in one transformation because the energy involved in such rotation is small. Another transformation may occur due to head-to-tail rotation of the acetate ion. In such a case, because the acetate ion must carry a strong dipole, marked change in dielectric properties would be observed. If such a rotation of the ionic dipoles were possible, they could be aligned along an external field which might be the structural basis of a ferro ~~para~~ → para electric transformation in the solid. The present investigation is concerned mainly with the nature of the structural changes, with temperature, of potassium acetate crystals. Two techniques are used for the purpose:-

(i) X-ray diffraction: This was used to obtain information on the average structures.

(ii) Dielectric measurements: For information on molecular relaxation.

Moreover, a qualitative observation on the heat capacity of potassium acetate was made on the basis of a thermogram obtained from its differential thermal analysis.

The acetates of rubidium and cesium have also been studied although in less detail. The results provide an interesting comparison with those of potassium acetate and show the influence of the increase in size of the cations on the properties of those compounds.

1.2. Polymorphism : Thermodynamic Aspects

Let us suppose that there are two distinct phases 1 and 2 of a crystal with free energies that vary with temperature as shown in the figure (Fig.1). At the transition temperature T_c the two phases can remain in equilibrium, for the change in free energy on passing from phase 1 to 2 at constant temperature and pressure is zero, i.e.

$$dG_{1\to 2} = d(U - TS + pV)_{1\to 2} = 0$$

This means that the Gibb's free energy for the assembly is constant during the change, for, if the mass of one phase decreases by dm_1, the mass of the other phase increases by the same amount. Thus, the condition of equilibrium can be written as,

$$dm\ (\frac{\partial G}{\partial m_1})_{p,T} - dm(\frac{\partial G}{\partial m_2})_{p,T} = 0$$

i.e., the Gibb's functions per unit mass or chemical potentials g_1, g_2 for phases 1 and 2 are equal. There is no explicit relation connecting G, p and T and indirect methods must be used. Assuming that $g_1 = g_2$ at the point (p_o, T_o), the effect of a small change in p, T can be found by the expansion,

$$g_1(p,T) = g_1(p_o,T_o) + dp(\frac{\partial g_1}{\partial p})_T + dT(\frac{\partial g_1}{\partial T})_p +$$

$$+ \frac{(dp)^2}{2}(\frac{\partial^2 g_1}{\partial p^2})_T + \frac{(dT)^2}{2}(\frac{\partial^2 g_1}{\partial T^2})_p +$$

$$+ dp\ dT\ (\frac{\partial^2 g_1}{\partial p \partial T}) + \ldots$$

with a similar expression for $g_2(p,T)$.

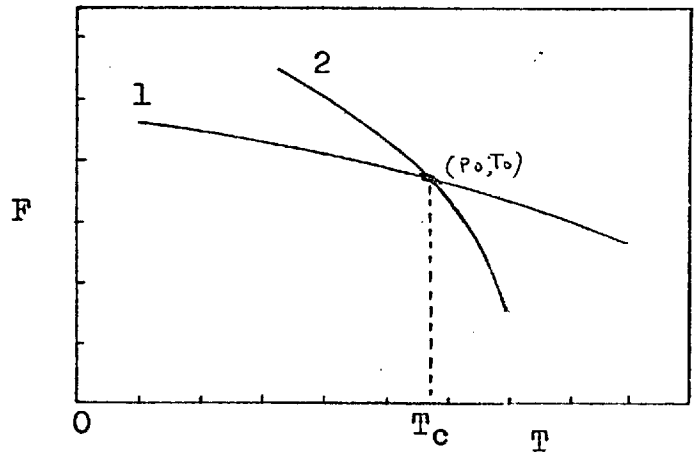

Fig.1. The nature of variation of free-energies with temperature, of two polymorphic phases 1 and 2.

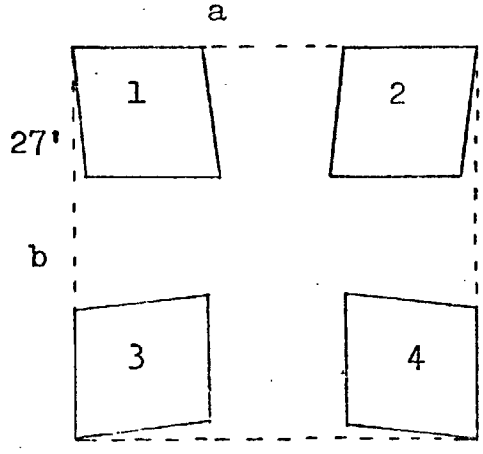

Fig.2. Diagrammatic representation of hybrid crystal (The dotted rectangle represents the original tetragonal KH_2PO_4 crystal. Four equivalent monoclinic options have developed within the original, below T_c - after Ubbelohde et al., see text)

Since, $g_1(p_o,T_o) = g_2(p_o,T_o)$, it is possible to express the ratio $\frac{dp}{dT}$ in terms of changes in chemical potentials with p and T.

Three different situations can arise:

(a) There may be finite changes in

$$\left(\frac{\partial g}{\partial p}\right)_T \quad \text{and/or} \quad \left(\frac{\partial g}{\partial T}\right)_p .$$

(b) The first order differentials for the two phases

$$\frac{\partial g_1}{\partial T} \quad \text{and} \quad \frac{\partial g_2}{\partial T} , \quad \frac{\partial g_1}{\partial p} \quad \text{and} \quad \frac{\partial g_2}{\partial p}$$

may have the same values and be continuous at the transition.

(c) The above expansion of g may not be permissible in any phase.

Case (a): Since $\left(\frac{\partial g}{\partial p}\right)_T = v$ = specific volume and $(\partial g/\partial T)_p = s$ = entropy per unit mass, discontinuity in v means a finite change in density and that in s a finite latent heat. Thus

$$\frac{dp}{dT} = -(\partial g_{1/\partial T} - \partial g_{2/\partial T}) \;/\; (\partial g_{1/\partial p} - \partial g_{2/\partial p}) = \frac{s_1 - s_2}{v_1 - v_2}$$

This gives the Clausius Clapeyron's equation:

$$dp/_{dT} = L/T(v_1 - v_2) = \frac{s_1 - s_2}{v_1 - v_2}$$

The transformation involves a discontinuous change of volume, and latent heat is involved. This is the thermodynamic first order transformation.

Case (b): When there is no latent heat and no change of volume $dp/_{dT} = 0/_0$ is indeterminate and to find $dp/_{dT}$, the second derivatives must be used - i.e.

$$g_1 - g_2 = 0 = \frac{(dp)^2}{2}((\partial^2 g_1/\partial p^2)_T - (\partial^2 g_2/\partial p^2)_T) + \frac{(dT)^2}{2}((\partial^2 g_1/\partial T^2)_p - (\partial^2 g_2/\partial T^2)_p) + dpdT((\partial^2 g_1/\partial p\partial T) - (\partial^2 g_2/\partial p\partial T)) + \ldots$$

In this equation

(a) $(\partial^2 g/\partial p^2)_T = (\partial v/\partial p)_T$ is the isothermal compressibility.

(b) $(\partial g/\partial T^2)_p = -(\partial s/\partial T)_p = -cp/T$ is the specific heat at constant pressure.

(c) $\partial^2 g/\partial p\partial T = (\partial v/\partial T)_p$ is coefficient of thermal expansion.

A discontinuity in any one of these derivatives can be recognised by a discontinuity in the appropriate physical property.

Some authors such as Ehrenfest[8], Von Laue and Justi[9] and others[10] have attempted to apply the thermodynamic classification of the different order transitions to transformations taking place exclusively within the solid state. Although relations involving the changes in the physical properties such as specific heat and thermal expansion, which are represented by second order terms of the Taylor expansion of g given above, have been deduced, it is extremely difficult in practice to decide whether a genuine discontinuity in the property really exists.

In addition to these difficulties, there is a possibility that the Taylor expansion itself may not be valid near the transition. It is possible that some of the derivatives of g in one or both phases become infinite, indicating an infinite specific heat or thermal expansion coefficient at a particular temperature or pressure. The existence of such infinite values

would invalidate the Taylor expansion. This in itself suggests that Ehrenfest's classifications of solid-solid phase transformations are not complete.

The complexity of the problem arises from the fact that in a solid-solid transformation, the phases are not distinct. Hence, it is not correct to assume that the free energy of a phase has the same significance at the transition point. These make the behaviour of solids undergoing structural transition variable; in some cases the thermal, electrical magnetic and structural properties change continuously, in others, discontinuously. Ehrenfest's treatment does not account for the solid-solid transformations where there is anomalous change in properties before and after the transitions and where the changes in those properties are continuous. Hysteresis of the properties still further invalidates the classical treatments, because it indicates that work is done during the transformation.

Hence, in order to avoid prejudging the situation, the transitions in which the properties vary in a continuous manner along a path of similar form to the Greek letter Lambda, Λ, are often referred to as Lambda point transitions.

There are numerous examples of such transitions. For instance such transitions occur in,

(i) alloys, when an ordered atomic structure becomes disordered (see section on order-disorder), e.g. the alloy CuZn[11] has an order-disorder transition at about $470^{\circ}C$.

(ii) inorganic salts when molecular or ionic-disorder takes place, e.g. in KCN crystal[12] the Lambda point transition takes place at $-106^{\circ}C$.

(iii) ferroelectric crystals, when dipoles in the crystal which are aligned in the direction of an external field become disordered at a critical temperature, e.g. $BaTiO_3$[13] ($T_c = 120^{\circ}C$).

(iv) ferromagnetic crystals, when the permanent magnets are suddenly demagnetised, e.g. iron ($T_c \sim 1000^{\circ}C$).

(v) superconductors, when the resistivity of a material vanishes completely (as it becomes superconducting), e.g. mercury[14] ($T_c \sim 4.2^{\circ}K$).

An interpretation of the λ-point phenomenon that links the thermodynamics and structural arrangements has been presented by Ubbelohde[15]. He has pointed out that the premonitory range and the tail of the specific heat curve cannot be accounted for by classical thermodynamics. In these transformations, instead of forming completely independent phases, the new phase must nucleate within the matrix of the original structure. This means that the equilibrium surfaces for the two phases are not independent, but their curvatures rapidly change as they approach the point of intersection, thereby reducing the angle of intersection of the two surfaces. This range of anomalous behaviour is referred to as a premonitory range.

When the new crystal structure is a derivative of the original, Ubbelohde[16] has proposed that the transformation be called "continuous". A structurally discontinuous transformation only arises when the new structure is completely independent of the original. In the continuous case, the finite change in volume and heat content, which should occur at a single temperature according to the classical first order transition then, is replaced by anomalous maxima in the specific heat and thermal expansion curves, for the transition is now spread over a range of temperature.

Structurally, even in such a case, there is usually a small discontinuity in the lattice parameters. But this misfit is very small and can be accommodated within the original lattice forming a "hybrid" crystal. The units or the domains of the new structures are oriented in a definite relationship to the original structure (Fig.2). The regions of different structures (domain) in such a hybrid cannot be regarded as twins.

There have been other cases where the axes of the transformed structure have been related to the original direction. For example, in the study of the thermal transformations of KNO_3[17] and or nitrites and nitrates[18], persistence of crystal axes have been observed.

Thus, although it is rather difficult to label a transformation thermodynamically as first or second order because of the experimental uncertainties involved, it can be definitely decided

on structural grounds whether a transformation is continuous. Those transformations are continuous in which specific orientation relations exist between the lattices of the two structures. Thus, the two lattices are "tied together" and can only appear in this set orientation. In a discontinuous transformation, no such orientation relationships exist. From this viewpoint, one of the transformations of thallous nitrate[19], - from orthorhombic to rhombohedral - has been stated to be structurally and hence thermodynamically discontinuous.

Another phenomenon which cannot be explained on the basis of the classical thermodynamics is the occurrence of "hysteresis" in a continuous transition.

Hysteresis is due to the difficulties of nucleation of the new phase inside the matrix of the old. The composite crystal contains both the phases in the "hybrid" crystal (Ubbelohde[20]). This is Buerger's[21] composite crystal of "obversed" and "reversed" positions. Hybrid formation and hysteresis have been studied in KNO_2[22a,b], thallous nitrate[19], potassium cyanide[23] etc. In KCN[23], the hysteresis which was 2.3°C wide with a pure sample narrowed to only 0.8°C when 1.2% of sodium impurity was introduced.

Ubbelohde[24] has discussed the difficulties and conditions of nucleation of one phase inside the other. Three cases may arise: (1) The specific volume of the new phase (proportional to the unit cell volume) differs appreciably from that of the

parent phase so that the transformed crystal must break up into a polycrystalline powder in which the crystallographic axes occur at random. (2) When the volume of the new phase differs appreciably, but can be nucleated on the surface or at dislocations. In such cases, although the crystallites have independent axes, these may have some preferred orientation. (3) When the volume difference is small enough, domains of one form may nucleate and grow inside the parent phase, with the persistence of axes even after several cycles through the transformation temperature.

Generally speaking, the specific volume of the two phases are not exactly the same and hence growth of domains of the other phase introduces strain. It is necessary therefore to modify the free energy expressions of the two phases which must now include terms for the surface energy η and strain energy ξ [24]:

$$G_1 = f_1 (p, T, \eta_1, \xi_1)$$

$$G_2 = f_2 (p, T, \eta_2, \xi_2)$$

The terms η and ξ must have a range of values because nucleation is a random process. ξ may vary within the original single crystal, it will vary from crystal to crystal, and it will depend on the thermal history of the sample. Hence G is characteristic of a small volume element only. This means that the free energy surfaces of the two phases of the single crystal do not intersect sharply, thus producing smeared transitions. It has been shown that because either or both of these arbitrary parameters in the

free energy equations are not equal for the two phases, nucleation of one phase inside the other is opposed. This causes hysteresis in transformations of this type.

The relative importance of the role of the energy of the domain boundaries and the compression and tension energies appear to vary from crystal to crystal. When the interfaces of the unit cells of the structures of the two forms match closely, the interface energy is negligible compared with the bulk energy. In such cases, the difference in specific volumes ΔV_c indicates the spread of the hysteresis. Ubbelohde[25] compared ΔV_c and ΔT_c (spread of the hysteresis loop) for some ammonium salts. He cautioned, however, that such comparison might not be a general feature.

The onset temperature of a Lambda point transition of the same substance may vary from crystal to crystal. But the temperatures lie inside the hysteresis loop. It is rather difficult to detect the exact onset temperature of such a transition because it is detectable only after an appreciable amount of the co-operative process has proceeded. This is particularly true for X-ray diffraction methods. Onset temperatures of potassium cyanide[23], rochelle salt[27], acetylene dicarboxylic acid dihydrate[28] etc, have been studied and show this variation from crystal to crystal.

1.3. Polymorphism : Structural Aspects

In the previous section, some thermodynamic aspects of solid-solid phase transitions have been described. Thermodynamic treatments are fundamental to the understanding why specific phases are stable and why transitions to other phases occur. On the one hand it is an exact science with strict mathematical apparatus, on the other it is flexible to cope with problems of a widely varied nature. But it is so general that it provides little insight into the mechanisms of phase transitions. This is a serious limitation when considering how transitions take place. In the solid state an examination of the crystal structure before and after the transformation provides additional ways of classifying such phase transformations.

In the following section it is proposed to discuss structural aspects of solid state phase transformations.

For a transformation to proceed certain energy barriers must be overcome, so that the transformation requires an activation energy. From the thermodynamic point of view, these energy barriers may involve surface energy, strain energy etc. It is necessary to investigate the structural nature of these energy barriers.

A solid is formed, when atoms condense, under the influence of forces in such a way that the arrangement exhibits long range order. For convenience, these interactions between atoms may be described in terms of bonds. Now a bond may be defined as

a binding or attachment between two atoms or groups of atoms due to forces acting between them in such a way as to lead to the formation of an aggregate. During a solid solid phase transformation, changes in the bonding between atoms in the structure take place which correspond to the change in the internal energy. On heating, if there is heat absorption during a transformation, the net bonding is weakened because the change is towards higher energy bonding.

This weakening may be effected by:

(i) reduction in bond energy or

(ii) complete change in bonding type.

Structurally, the reduction in bond energy means a reduction of the interaction between the neighbouring atoms. This weakening may be limited to more distant neighbours or involve even the nearest neighbours. Now, one convenient way of looking at a crystal structure is to consider how the neighbouring atoms are arranged around an atom, i.e. from the standpoint of co-ordination. Thus, solid state transformations may be classified on the basis of co-ordination changes as was done by Buerger[29]:

1. Transformation of secondary co-ordination: Here the primary co-ordination involving atoms in contact remains unchanged, so the structural differences between the two phases are small. It occurs widely in inorganic crystals. The change in the co-ordination of non-nearest neighbours accounts for the energy change of transformation. If it is assumed that the most important contribution to the total energy comes from nearest neighbour

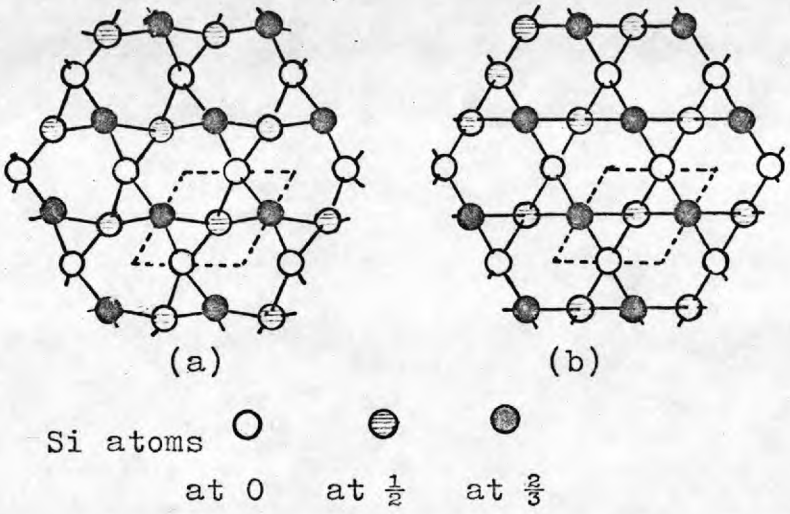

Fig.3. (a) α - quartz structure (rhombohedral)
(b) β - quartz structure (hexagonal). Only Si atoms are shown. The oxygen atoms are tetrahedrally arranged about those of Si in such a way that all corners of the (SiO_4) tetrahedra are shared (Reproduced from "Crystal Chemistry" -by R.C.Evans, Cam.U.P. 1966.)

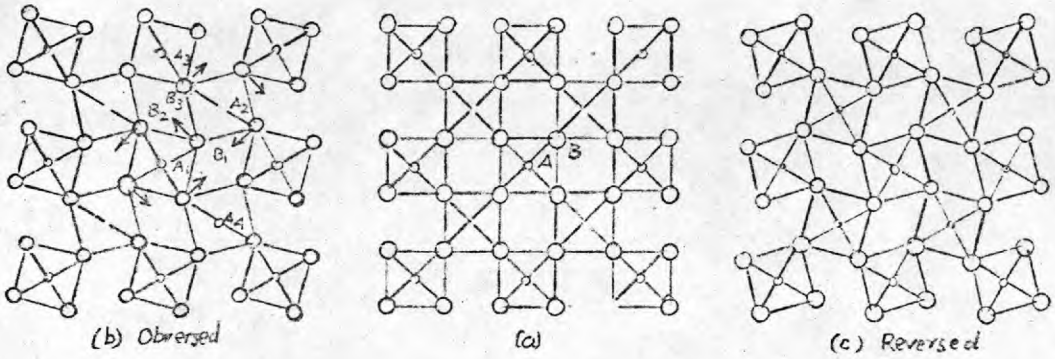

Fig.4. " Low-high" displacive transformation
(Reproduced from Ref. 28)

interactions, this type of transformation can be said to involve a change in the residual co-ordination energy. Now, an assembly of atoms may be arranged in several ways that satisfy a given primary co-ordination geometry. The energy differences between these different ways is the energy contribution of secondary co-ordination.

It is possible to go from one kind of secondary co-ordination to another by two different mechanisms. One is the 'displacive' and the other 'reconstructive' type of transformation.

(a) Displacive transformation: In this type of transformation, the nearest neighbour contacts of the atoms are maintained, and the structure is distorted by the relative displacement of the non-nearest neighbours. An example of such a change is quartz (Fig.3) which can exist in two forms, α and β. The β-form is stable from 573°C to 870°C and the α-form is stable below 573°C. The ideal (β) and distorted (α) forms are shown in the figure. Such transformations are rapid because the movement of the atoms is limited.

(b) Reconstructive transformation: This involves the disruption of the old structure, i.e. the temporary breaking of primary bonds which are subsequently re-formed. The new network will be different and yet the primary co-ordination will be the same after this transformation. As an example, the transformation of Zincblende structure to that of Wurtzite can be cited. Because the energy barrier is high, the transformation rate is slow in this case.

Another type of transformation involving secondary co-ordination is the order-disorder transformation, or transformation of disorder. It is discussed in a separate section because of its importance in the present work. This type of transformation has the characteristics of both the displacive and reconstructive transformations discussed above.

The transformation involving first co-ordination will not be discussed, because they are not relevant to the present investigation.

As transformation of the displacive type is relevant to the study of the transformations in the present work, a discussion of its mechanism now will make it easier to explain things later.

Suppose there are two forms of the same planer lattice containing atoms of opposite type A and B (Fig.4). The high temperature form may be called an open form and the low temperature one, a collapsed form. In both forms the atoms A and B have four and two nearest neighbours of the opposite kind of atoms respectively. On examining the next nearest neighbours of opposite type, it is observed that they are nearer in the collapsed form than in the open form. When A and B atoms are different, they will have different electronegativities. As a result, non-nearest A's and B's will attract each other with a small force. The nearer they are the less is their residual energy. The collapsed form has lower residual energy and is therefore more stable.

A rise of temperature in the collapsed form may effect the structure in the following way:

For simplicity, we assume that the atoms of the type A are fixed and those of the type B can vibrate. If, as a result of acquisition of thermal energy, B_1 moves in the direction shown in the figure (Fig.4) it comes nearer to B_2 and B_3 which it repels. Because they are free to move, B_1's motion will be communicated to B_2 and B_3 and they in their turn will force their neighbours to move and so on, thus producing a "co-operative distortion" of the whole neighbourhood. Hence, the result of thermal agitation is the co-operative rotation of the squares in this imaginary lattice.

If the thermal agitation is increased, at a certain temperature, the vibrations would be so large, that B atoms will be able to overcome the attractions of non nearest neighbours and swing past to the reversed configuration shown in the figure. This is the displacive transformation. After the transition, the crystal would be composed of mosaics of small regions of "obversed" and "reversed" configurations in equal amounts. The regions will of course be continually changing. Now this new form is the open form as shown in the figure (Fig.4b) because, as B vibrates between the obverse and reverse configurations, the time average of the positions of the B atoms would be the same as the position of B in the static open form. In other words, B atoms oscillate about positions which are statistically the same as the positions

of the open form. This form can be regarded as the disordered equivalent of the collapsed form. So it is the form of higher entropy.

The above description indicates that the high temperature form has the higher symmetry. The positions of the atoms in the high temperature structure is only the statistical average of the obversed and reversed configurations and that is a position higher symmetry.

Because the high temperature form is a combination of both "obverse" and "reverse" orientations, twinning takes place after the transformation to the low temperature form[30]. This is a macroscopic expression of a microscopic behaviour.

Assuming Buerger's theory on derivative structure[31], the low temperature structure should be a subgroup of the symmetry of the high temperature basic structure, the derivative being formed by the suppression of symmetry elements of the basic structure.

The above description presents the basic structural mechanism of a displacive transformation. A phenomenological description of the same is presented here to complete the picture. The displacive transformations are designated as shear transformations or martensitic transformations[32] when they occur in metals and alloys. The name martensitic transformation is derived from the austenite-martensite transformation which occurs in steel. Austenite is an iron carbide stable over about 700°C. When

quenched it still contains only austenite, but controlled heating allows partial transformation to the stable form, martensite.

Martensitic transformations are shear-like. They entail a co-operative movement of the atoms, so that the region undergoes a change in shape. It has been postulated that the lattice deformation arising from small atomic movements in a martensitic transformation is homogeneous only over a very small region and that in between the parent crystal and the homogeneously deformed boundary a region of heterogeneous deformation must occur.

A transformed region in the body of the parent crystal has an interface which connects the transformed region with the untransformed surroundings. Hence it cannot be rotated and disturbed when averaged over macroscopic distances. It must also provide a link between the two phases, so that as the interface moves forward, the atoms are systematically displaced from one lattice to the other in the correct orientation.

The overall homogeneous displacement and heterogeneous strain are accomplished at the interface as it proceeds through the parent phase. Frank[33] proposed that the interface has dislocation arrays which travel along with the interface and produce the heterogeneous strain. This means that the two lattices cannot be perfectly coherent.

It has been shown[33] that the mobility of the interface does not seem to depend on the thermal activation. The interface

motion is wave-like and does not involve atom by atom transfer across the interface, nor is a diffusion process involved. Actual relative movements of the atoms are very much less than one lattice spacing. It has been concluded that the activation energy for the growth mechanism of martensite is effectively zero.

Supercooling and hysteresis:[34] Another characteristic feature of the martensitic transformation is its hysteresis. This has been discussed with reference to continuous transformations. It is one of the features which identifies martensitic transformations in metallurgy and displacive transformations in inorganic salts. Hysteresis occurs because, in addition to the overall free energy, the non-chemical factors such as interfacial energy η and strain energy ξ must also be considered before the transformation may start[35]. In other words,

$$\Delta G_{I \to II} + (\eta_{I \to II} + \xi_{I \to II}) > 0 \text{ cal./mol.}$$

or

$$\Delta G_{I \to II} > (\eta_{II \to I} + \xi_{II \to I}) \text{ cal./mole.}$$

Hence η, ξ may be considered as the restraining force opposing the driving force, when these forces become positive below the critical point T_c. Thus, for the formation of the second phase during cooling, the temperature must be decreased sufficiently to make ΔG_{I-II} not only greater than zero, but greater than some finite quantity $(\eta_{II \to I} + \xi_{II \to I})$.

1.3.1. Positional order-disorder in alloys. It has been mentioned in the section on the structural aspects of polymorphic transitions that order-disorder transformations involve secondary co-ordination. It is proposed to discuss here in what way the secondary co-ordination is involved due to movement of the atoms in a structure which undergoes an order disorder transition.

Insight into the origin of order-disorder phenomenon can best be explained with the help of an example. Let a metal B be dissolved in another metal A. The structure of the alloy AB is essentially that of A, except that some of the lattice sites are now occupied by atoms of B. Such an alloy AB is called a 'substitutional solid solution'. The atoms of B may not be randomly arranged in the lattice of A, but may have particular order in their arrangements, depending on the interactions between them. If they do interact, one type of atom, A, may require its neighbour to be of the other type, B, and the structure is ordered.

In an ordered structure, the lattice can be regarded as being composed of two interpenetrating sub-lattices, one of which contains most of the A atoms and the other most of the B atoms. Such an arrangement may give rise to a superlattice. A hypothetical perfectly ordered two dimensional lattice is shown in Fig.5. It is evident from the figure that the ordered structure defines two types of lattice sites: a and b; A atoms arranging themselves

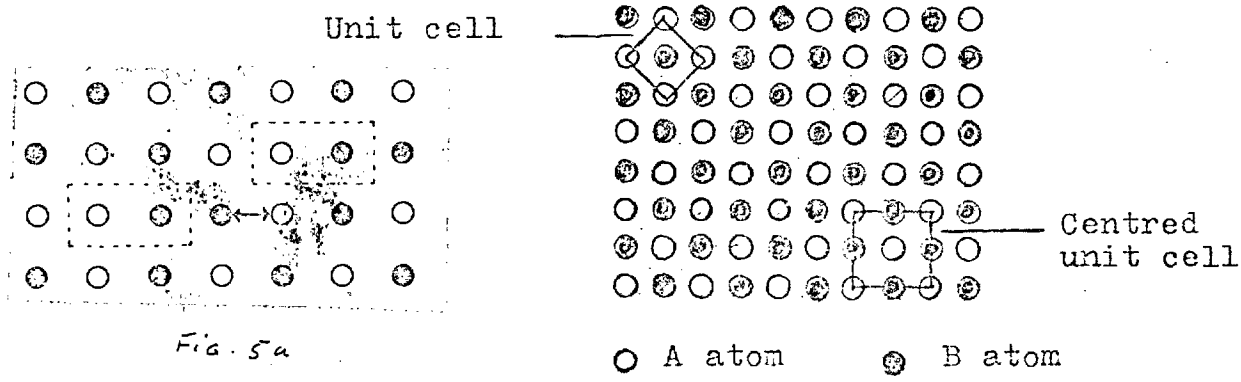

Fig. 5a

Fig.5. Completely ordered structure of alloy AB

Fig.5a. Increase in disorder with increasing temperature.

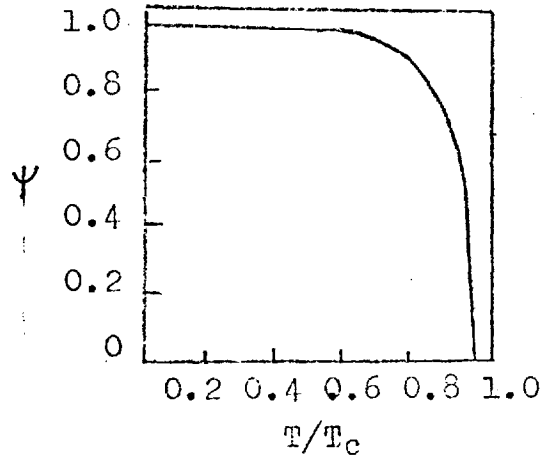

Fig.6. Long range order Ψ vs. temperature of an alloy AB. (Bragg & Williams, see text)

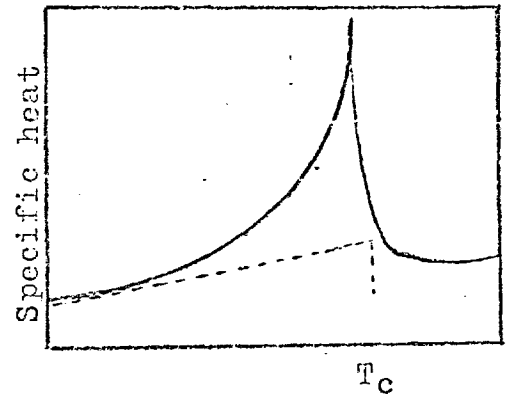

Fig.7. Schematic representation of excess specific-heat near order-disorder transition.

in the a site and B on the b site. With the idea of a particular site for a particular atom, a parameter ψ, measuring the amount of order can be defined, starting from a perfectly ordered lattice, when all A atoms are in a site and B atoms in b site. Two kinds of order can be considered. The long range order parameter measures how many, on the average, A (or B) atoms are occupying a (or b) sites. The short range order parameter defines how well, on the average, A (or B) atoms are surrounded by nearest neighbour B(or A) atoms.

The effects of increase of temperature on a perfectly ordered structure, defined as above, can now be considered.

As the temperature of the alloy is increased there will be an increase in the amplitudes of thermal vibrations of the atoms. As the temperature is increased higher and higher, pairs of atoms or small group of atoms will acquire enough energy to break away from their equilibrium positions and exchange sites. The atoms A (or B) occupying b (or a) sites may be called 'wrong' atoms. This would mean that like atoms are forced to be nearest neighbours contrary to their tendency. But this tendency still operates. At a particular temperature, below a critical temperature, there will be an equilibrium state, characterised by a definite number of wrong atoms. The number of wrong atoms will increase with temperature, not only because of thermal vibrations but from the co-operative effect arising as follows. In Fig.5(a) thermal vibration produces a wrong pair (indicated as in the figure).

Each of the wrong atoms has three like atoms as its nearest neighbours. This can be taken as a state of higher energy, which is lowered by the interchange as shown by arrowheads. The interchange requires less energy than that which led to the initial disorder. Thus, with increasing temperature, it will be easier to create more disorder as disorder increases. This decrease of order with increasing temperature leading to order-disorder transition is discussed below.

Let the same alloy AB be considered with the two sites a and b as before. If there are R atoms in the correct positions and W atoms in the wrong positions, the order parameter is defined by,

$$\psi = (R - W)/N = (R - N + R)/N = (2R - N)/N \quad \ldots \quad (a)$$

Here $W + R = N$ = total number of atoms, with $N/2$ atoms of both A and B. When all atoms are in correct sites, $R = N$, so that $\psi = \pm 1$, for complete order. When $R = N/2$, $\psi = 0$, which is taken as complete disorder, so the range of ψ is from 0 to 1. At the absolute zero of temperature there would be complete order, so that the energy which must be supplied to create disorder is always positive.

In the alloy AB, where the number of right and wrong atoms are R and W respectively, let an atom A in a go to b and an atom B in b go to a, at a temperature T° absolute. Thus, one atom of A and one atom of B are put in wrong sites. If ΔR is change in R and ΔW in W due to the above exchange,

$$\Delta W = 2 = -\Delta R.$$

The energy required to introduce the above exchange in positions in a perfectly ordered crystal lattice has been calculated by Bragg and Williams[36] in the following manner.

Let the energy required to produce the pair of wrong atoms in the state R,W be V(R,W). At thermal equilibrium, the change in free energy ΔF associated with ΔW must vanish.

The configurational entropy associated with the state (R,W) is

$$S_{con.} = k\ (N \log N - R \log R - W \log W)$$

where k is Boltzmann constant.

The change $\Delta S_{con.}$ associated with ΔW is $\Delta S_{con.} = 2k \log R/W$.

In equilibrium, therefore,

$$R/W = \exp\ (V(R,W)/2kT) \quad \ldots \qquad (b)$$

Assuming only the interaction between only the nearest neighbour pairs of atoms, the total potential energy (internal) in interchanging A and B atoms, is shown as,

$$V_{(R,W)} = V_o \psi \quad \ldots \qquad (c)$$

where $V_o = 2V_{AB} - V_{AA} - V_{BB}$. Here V_{AA} and V_{BB} are the energies of interaction of an AA and BB pair of nearest neighbours and V_{AB} is that of an AB pair.

When $\psi = 1$, $V = V_o$ is the energy required to produce a pair of wrong atoms in a completely ordered lattice. Again, from this equation it is seen that as order parameter ψ decreases, V the energy required to produce disorder decreases.

From (a) using (b) and (c)

$$\psi = \tan h \left(\frac{V_o \psi}{4kT} \right)$$

putting $\frac{V_o \psi}{4kT} = x$ or $\psi = \frac{4kT}{V_o} x$ ... (d)

and $\psi = \tan x$ ... (e)

The equation can be solved graphically. The solutions show that ~~below~~ above a certain value of temperature T, called T_c, order disappears completely.

Theoretical values of ψ, when plotted against T gives curves of the nature as shown in the figure (Fig.6).

It is seen from the graph that in the vicinity of the transition temperature T_c, there is a rapid drop of order. Thus, as order decreases the easier it is to increase disorder. This curve is characteristic of the order-disorder phenomenon. This suggests that any order parameter, such as intensity of reflexions of X-rays produced by a superlattice of an ordered structure should behave similarly (diffraction theory of formation of superlattice reflexions will be given in Chapter 4).

1.3.2. Rotational disorder. In addition to positional disordering described above, there may be rotational disordering, i.e. molecules or groups of atoms in some crystals can disorder by rotation. If rotation sets in as the temperature rises, a number of transitions revealed by specific heat measurements can be explained on the

basis of Pauling's[37] treatment. On the other hand, Fowler's[38] treatment of molecular rotation using partition functions is unable to account for the smaller range of temperature in the specific heat rise. Thus, although a large number of crystals have transformations of the order-disorder type, no theory can predict the observed ~~behaviour~~ behaviours correctly. The effect of the molecular rotation on the structure of the crystal can be considered generally without the help of the above theories. As the molecular rotation tends to lower the internal field, it raises the symmetry of the structure. If the molecule is fairly symmetrical, the rotation gives rise to a close packed cubic or hexagonal structure. Some examples of transformations of this type will be discussed in the section on dielectric measurements. To visualise the onset of rotation in a crystal the following simplified picture is given.

Above the absolute zero of temperature, the molecules or groups of atoms of all solids possess energy of translational and rotational vibration about equilibrium positions. The amplitude of the rotational vibrations depends on the way in which the potential energy of the molecule or the group varies with orientation and the temperature. Now, the average energy of a classical oscillator is kT. If the potential energy of the equilibrium position of the molecule is less than that of any other possible orientations by an amount which is much larger than kT, it will execute oscillations of small amplitude. If, on the other hand, the energy difference between the equilibrium position and other

possible orientation is small in comparison to kT, the kinetic energy of the molecule will be sufficient to overcome the potential barrier, so that the molecule would move to this orientation, and so on. This is not a free rotation as is found in gases or liquids, but hindered rotation. The onset of such rotation in a crystal contributes to the specific heat of the crystal.

Configurational Specific Heat. The major part of the specific heat of a crystal consists of contributions from the internal energy associated with thermal vibrations of the lattice, given by the well known formula of Einstein[39]. This was modified by Debye[40], Blackman[41] and others[42] to take account of the internal energy associated with the vibrational spectrum of the lattice, instead of Einstein's single frequency vibrations. When disordering takes place in a crystal, in addition to usual vibrational specific heat, there also appears an extra specific heat contributed by the internal energy associated with increasing disorder as the temperature is increased. This excess specific heat is known as configurational specific heat.

If the entire change in energy takes place at a single temperature, there will be latent heat instead of an extra specific heat. But in order-disorder transition, the total change in energy dE on heating is gradually absorbed over a range of temperature. Above the critical temperature the long range order vanishes. So the specific heat value drops, for,

on further heating, the only change will be in the short range order (Fig.7).

This excess specific heat can be calculated as follows:

The energy required to increase R by dR is $dE = -V_o \psi^{dR/2}$ from (c).

From (a) $Nd\psi = dR - dW = dR + dR = 2dR$

or $dR = Nd\psi/2$

So, $dE = -V_o \psi (Nd\psi)/4 = -V_o N/4 . \psi d\psi$

Thus, the specific heat increase for disorder of an atom is

$\Delta C_v = 1/N\ (dE/dT) = -\phi_o \psi/4 .\ d\psi/dT.$

The plot of this function is shown in Fig.7, with the dotted curve.

This theoretical curve drops to zero at T_c whereas in practice the curve tails off, as can be seen from the CuZn curve of specific heat given in the same figure. However, the curves agree insofar as they both show the excess specific heat in the form of a peak and a sudden drop. Apart from this, there are disagreements in detail. The range of temperature predicted for the transition is much too large; actual order-disorder transformations take place in a narrower range of temperature.

Chapter 2

POTASSIUM ACETATE

2.1. A Review of Previous work

The unusual thermal behaviour of potassium acetate was first observed by Hazlewood et al.[7] and has already been described in the introduction. In this section a few further observations will be discussed.

The values of molar volumes at different temperatures of polycrystalline acetates were obtained in the work referred to above using dilatometric method of measurement; the graphs and linear equations of molar volume and temperature are reproduced from Hazlewood et al.'s paper. (Fig. 8a,b and Table 2.1). The anomalous expansions at the temperatures 80°, 160° and 230°C and contraction on melting at 304°, which are obvious from these graphs, were attributed to polymorphic transitions occurring at those temperatures.

Table 2.1

Molar volumes of polycrystalline potassium acetate (Hazlewood et al.[7])

Temp. range °C	Molar vol., $cm^3 mole^{-1}$
25 - 75	62.04 + 0.0281 (T - 25)
76 - 84	increase of 0.5 $cm^3 mole^{-1}$
85 - 155	64.26 + 0.0446 (T - 83)
156 - 216	67.53 + 0.0196 (T - 156)
217 - 287	68.20 + 0.0452 (T - 217).

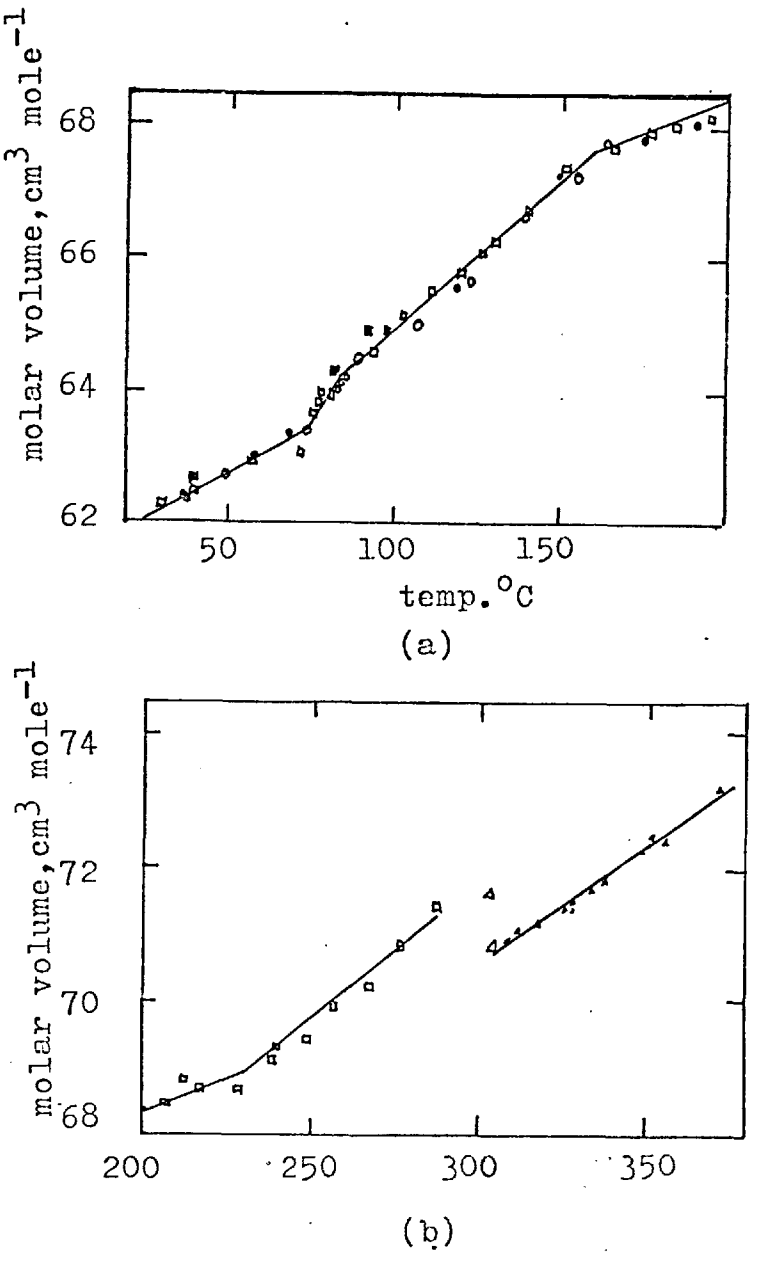

Fig.8. Molar volume of potassium acetate
(a) 20 -200°C; (b) 200 - 370°C solid and melt.
(after Hazlewood et al.[7])

These equations give a density for potassium acetate at 25°C of D = 1.60 and at 155°C of D = 1.52 g $cm.^{-3}$.

The observation that the salt contracts on melting may be significant from a structural point of view. It might mean, for example, below the melting point the crystal structure is loosely packed, a point which could be checked by a study of the crystal structure at specified temperature. This was one of the aims of the present investigation.

The suggestion that the acetate ion and the methyl group might be involved in the polymorphic transitions has already been discussed before. Only crystal structure determination can show their role in the transformations. It should be mentioned here that practically nothing was known about the structural features of potassium acetate before this study began, since no previous work on this structure has been reported apart from a card for the material in the ASTM X-ray Diffraction Data file which lists the first five prominent d spacings as:

13.6Å, 10.7 Å, 9.2 Å, 3.6 Å, 3.47 Å.

The only other property previously studied is the solubility reported by Seidell[43]. The values found by different workers appear to be consistent. The solubility of potassium acetate in 100 g of water is 217 g at 0°C and 396 g at 90°C. The solubility in methyl alcohol at 15°C is 24.2 g of the acetate per 100 g of the solvent. In ethyl alcohol, the solubility is 33 g per 100 g. Liquid sulphur dioxide dissolves 0.006 at 0°C and liquid ammonia

dissolves 1.026 g at -33.9°C. The problems of recrystallisation for crystallographic work are closely connected with the range of solvents and temperatures which are available. This is discussed in detail in the section that follows.

2.2. Preliminary Experiments and Conclusions

2.2.1. Introduction: Laboratory reagent grade polycrystalline potassium acetate as supplied by M & B was used for making single crystals. The nominal purity of the material was 99% (the main impurities were the chloride and sulphate).

Another laboratory reagent grade potassium acetate of lower nominal purity (98%) supplied by B.D.H. was also tried, but the crystals formed were less satisfactory. During the process of growing crystals from the melt, crystals formed from this material appeared to be slightly charred. This behaviour is consistent with Hazlewood's[7] finding that in ionic acetates, the thermal stability of the melts is sensitive to impurities capable of promoting electron transfer. In fact, the presence of traces of metal ions (Pb .001%, Fe .001%) was indicated in the composition by the manufacturers. Hence the use of this material was subsequently abandoned.

2.2.2. Recrystallisation : Preliminary. To study the properties of potassium acetate by X-ray diffraction methods single crystals were needed. Because practically nothing was known about how

such crystals should be grown, various methods have been tried and techniques developed to overcome the difficulties encountered. Once this was done, use of similar methods in the preparation of crystals of rubidium and cesium acetates presented no difficulties.

Potassium acetate is highly soluble in water (see review of previous works) and very deliquescent. Even so, a saturated aqueous solution covered by a thin film of silicone oil gave crystals in the form of extremely thin flakes when seeded. These crystals were, however, useless for X-ray diffraction studies. Other solvents were considered for growing crystals from solution. Potassium acetate dissolves in dry methyl alcohol, but the resulting crystals are the alcoholates and not acetates[43]. Dried ethyl and propyl alcohols, methyl, ethyl and acetic esters, benzene, acetone, and carbon tetrachloride were unsuccessfully tried. Liquid ammonia and liquid sulphur dioxide should dissolve potassium acetate[43] but at very low temperatures and the solubility in them was very low. Hence they were not tried.

The method of sublimation on to a water cooled surface was then tried. No significant amount of material evaporated on to the cold surface even at temperatures where the original potassium acetate began to decompose.

As many of the conventional methods of growing crystals had failed, attempts were made to grow crystals from melt even though there was a danger[7] of slight decomposition of the melt. Potassium acetate powder was put into thin walled pyrex capillaries

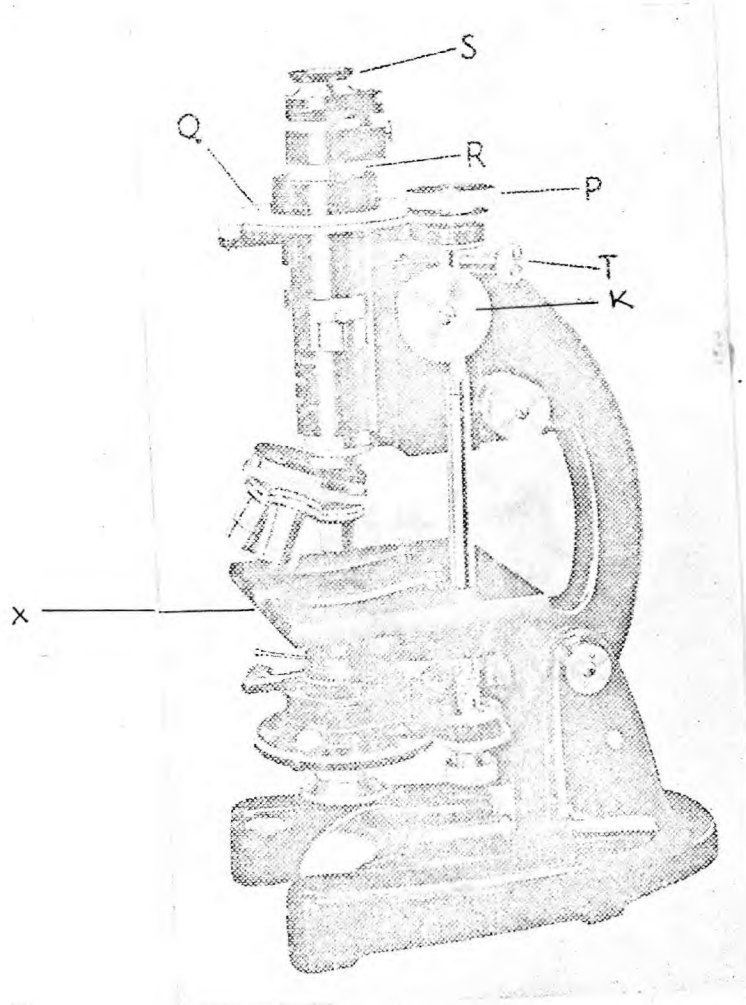

Fig.9. The Swift " Model PD (Dick)" polarising microscope. For recrystallisation, the hot stage was attached to the microscope stage X. (reproduced from Hartshorne and Stuart's "Crystals and the polarising Microscope"

which had been sealed; the powder was subsequently melted in a dry atmosphere by placing it on the hot stage of a polarising microscope which was totally enclosed by a plastic bag through which dry nitrogen was passed. As an additional precaution against the entry of moisture, the microscope stood on a dish containing silica gel.

The microscope used was a Swift "Model PD (DICK)" in which the stage is fixed. The polariser, analyser and the eyepiece rotate together, but the mechanical linkages allow focussing in the normal way, ((Fig.9) coarse focussing knob, K; polariser/analyser rotation, knob f.) The main advantage of this type of microscope is that ancillary equipment (in this case an electrical hot-stage) can be mounted on the microscope stage without any inconvenience.

The hot stage consisted of an ebonite frame with a long opening along its length. A microscope slide over which was wound a nichrome wire, was clamped horizontally to the frame. The heating current to the hot-stage was controlled by a Variac Autotransformer.

Despite these precautions, the experiments were unsuccessful when the melt was cooled slowly. X-ray diffraction photographs of the sample showed the formation of highly strained multiple crystals and in one case, what appeared to be a glass.

After attempts to grow crystals inside the cylindrical capillaries had proved unsuccessful, recrystallisation on a flat

microscope slide was tried. A little of the powder was placed on a glass slide over the hot stage, so that it was visible under the microscope. A cover slip was placed over the powder and a second cover slip was placed beside the powder, so that when the powder melted, a wedge was formed between the upper cover slip and the microscope slide; capillary forces drew the melt inside the wedge. On cooling, single crystal regions could be identified by rotating the crossed polariser and analyser of the microscope. Where necessary, the sample was remelted and the process repeated until satisfactory single crystal regions were formed. After cooling to room temperature, the crystalline block was removed from the slide by means of a razor blade, transferred to a petri dish and covered by oil which had previously been carefully dried. The block was then manipulated under the oil and suitable single crystals extracted which were subsequently cut to the required size and orientation.

Later, the facilities of the Crystal Growth Laboratory were used to recrystallise a sample of potassium acetate from the melt using a variation of the Bridgman method. The dried material was sealed in a glass tube about half an inch in diameter and passed slowly (2 mm/hour) through the furnace so that the crystals formed were cooled slowly. Afterwards, one end of the glass tube was cut and slices of crystals were chopped off on to the oil in a beaker, all operations being done in dry atmosphere. Single crystal regions were obtained as before.

Mounting for X-ray work. Once the crystal had been cut to size and shape, it had to be mounted in a capillary for X-ray study. At first the crystal was removed to a cleaner part of the dish by a needle and transferred to a glass slide mounted under the microscope, using a dry brush. One end of a glass capillary was then brought up to the crystal which entered the capillary together with a small quantity of oil. This method was found to be unsuitable because of contamination with water on transfer. It was found more satisfactory to draw the crystal into the capillary directly from the dish. When the crystal was well inside the capillary, excess oil was withdrawn from it, and the ends were sealed with a micro coal gas flame, or for reasons to be explained later, by electrical heating. In the later case, a very small loop of thin resistence wire whose diameter was slightly larger than that of capillary diameter was passed over the capillary containing the crystal. An electric current was passed through the loop until the wire was white hot, and at the same time the capillary was slowly pulled out forming the seal. This method avoided the production of water which appears as a by-product in gas sealing.

The sealed pyrex capillary containing the crystal was mounted in a brass mount which could be fitted on to the tip of the arcs as shown in the figure (Fig.10). A little paste of alumina cement and water glass diluted with water was placed on the brass head and the end of the capillary was mounted in the paste so that it

remained vertical. When the ceramic paste was dry the head was baked in an oven at about 250°C for about 12 hours, and subsequently fitted to the goniometer arcs.

From the experience gained during these preliminary experiments the following conclusions were drawn:

(1) Material as supplied must be properly dried before being melted in recrystallisation experiments. Water vapour coming out of the material during melting often condensed in the cooler part of the slide and subsequently attacked the freshly prepared crystals. Thus it became necessary to construct a vacuum drying system.

(2) Any trace of moisture in the accessories - microspetulum, razor blade, oil, petri dish, slides, cover slips, or even the naked hands released moisture which subsequently attacked and even destroyed the crystals. This led to the construction of a glove box in which all operations involved in preparing and mounting the crystals could be performed from the outside.

(3) Dried silicone oil used as a confining fluid by previous workers[7] was not as effective in protecting the crystal from attack by moisture as the light hydrocarbon oil (3 in 1 oil).

(4) During the trial sealing of the sample by micro-coal-gas flame, water vapour often appeared inside the capillaries and destroyed the crystal after a period of time which varied from minutes to days. This might be due to vapour from the flame or to improper sealing through charring of oil around the seal.

The method of electrical sealing was found to lead to less failures, but needed careful manipulation to avoid the risk of breaking the capillaries.

(5) The linear absorption coefficient of potassium acetate for CuK_α radiation is high (μ = 102) and even a crystal 0.07 mm thick absorbed about 50% of the characteristic radiation. Nevertheless, although thick crystals transmit very little, they were found to give strong surface reflexions, even with a relatively short exposure, which made such crystals useful in following the process of transformations during subsequent X-ray studies. Very small crystals were soft, however, and could not be handled without damage, so that medium sized crystals ($\sim$ .07 mm) have had to be used for measurement of the diffraction intensities.

(6) The internal diameter of the microthermostat used to control the temperature of the crystal set an upper limit to the inclination of the capillary to the central axis of the micro-thermostat, of about 8°. This meant that the crystals must be cut and mounted very accurately, so that one of the crystallographic axes was almost exactly parallel to the capillary axis. Otherwise, the crystal could not be oriented, so that the layer lines were horizontal. Although the crystal was not positively located in the capillary, it remained in position because of a thin oil film between the crystal and the capillary wall.

(7) The quality of the crystals grown could be influenced to some extent by controlling the heating current of the hot-stage of the

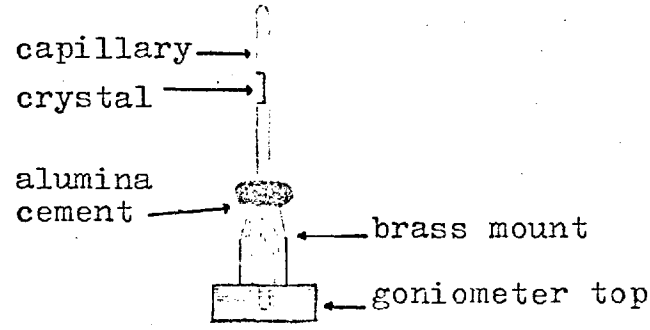

Fig.10. Mounting of the crystel for high temperature oscillation photography.

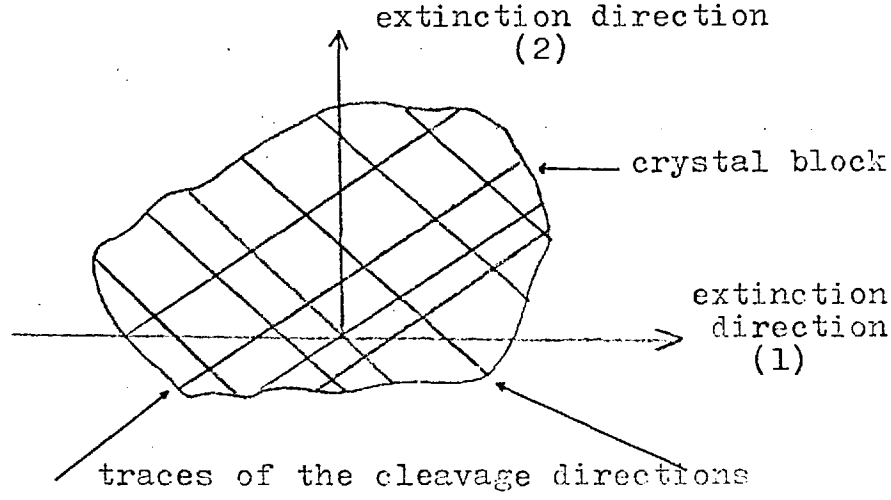

Fig.11. Relative orientation of the traces of the cleavage direction on the surface of the potassium acetate crystal block and the extinction directions.

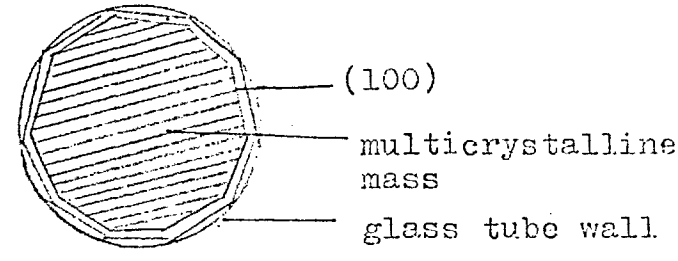

Fig.12. Shape of the cross section of potassium acetate crystal grown in a glass tube from melt.

Fig. 13. Vacuum Drying System.

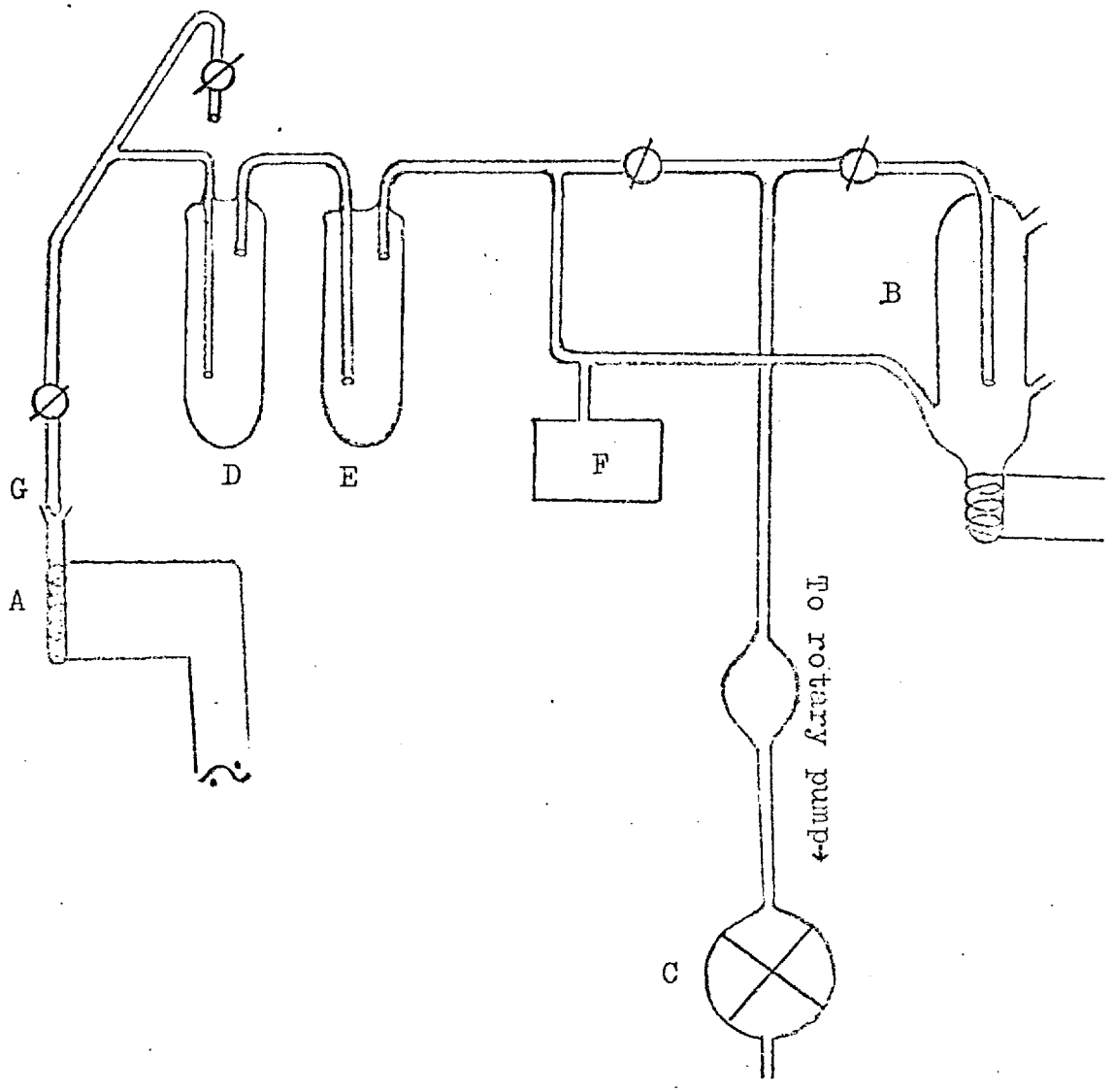

microscope. Very fast cooling gave samples in which crystals were in multiple orientations. Thick crystals ($\sim$ .5 mm) did not extinguish completely under the crossed polariser and analyser indicating that crystals in different orientations overlap each other.

(8) During recrystallisation from the melt, it was noticed that when a large single crystal plate was formed, it was invariably traversed by a network of cleavage fissures as it cooled. The temperatures at which these cracks appeared varied widely and did not correlate with any transformation temperature. Such cracks might be due to unequal thermal contraction of the glass slide and the crystal. The traces of the cleavage directions were found to be oriented at fixed angles relative to the extinction directions as shown in the figure (Fig.11).

X-ray photographs taken later showed that extinction directions (1) and (2) coincided with the two axes having the repeat distances 23 Å and 4 Å respectively. Examination of the birefringence by a quartz wedge identified direction (1) with the greater refractive index. Subsequently, the directions (1) and (2) were identified as the b and c axes respectively.

(9) The crystals formed from the melt by the Bridgman method had a characteristic appearance. The predominant crystal face (100) was always approximately parallel to the circumference of glass tube. Thus, the cross-section of the polycrystalline mass appeared as shown in the figure (Fig.12). This behaviour was

found to be consistent with the structure of potassium acetate and will be discussed later. The poor quality of crystals grown within a capillary was probably due to the tendency of (100) to lie parallel to a glass surface.

2.3. High vacuum drying system and handling of materials.

The first measure taken in the light of the conclusions given above to improve the experimental techniques of sample preparation was to construct the vacuum drying system shown in Fig.13. As stated earlier, the potassium acetate supplied must be thoroughly dried before use.

The vacuum drying system consisted of an oil diffusion pump B, backed by a rotary pump C, with two vapour traps D and E, to remove the oil and moisture from the system. Pressure was measured by a Pirani gauge inserted into the system at F. The sample powder was placed in a pyrex tube A, connected to the vacuum system as shown in the figure.

In order to facilitate release of any trace of water from the crystallites, the powder was alternately heated electrically through the transformations to about 180°C and then cooled down to about 50°C. This was repeated several times a day for at least 72 hours before using the material for recrystallisation or for measuring any physical property. The pressure was kept at about 10^{-5}mm of Hg.

Next, a glove box was made to provide a dry atmosphere during sample preparation from the dried powder.

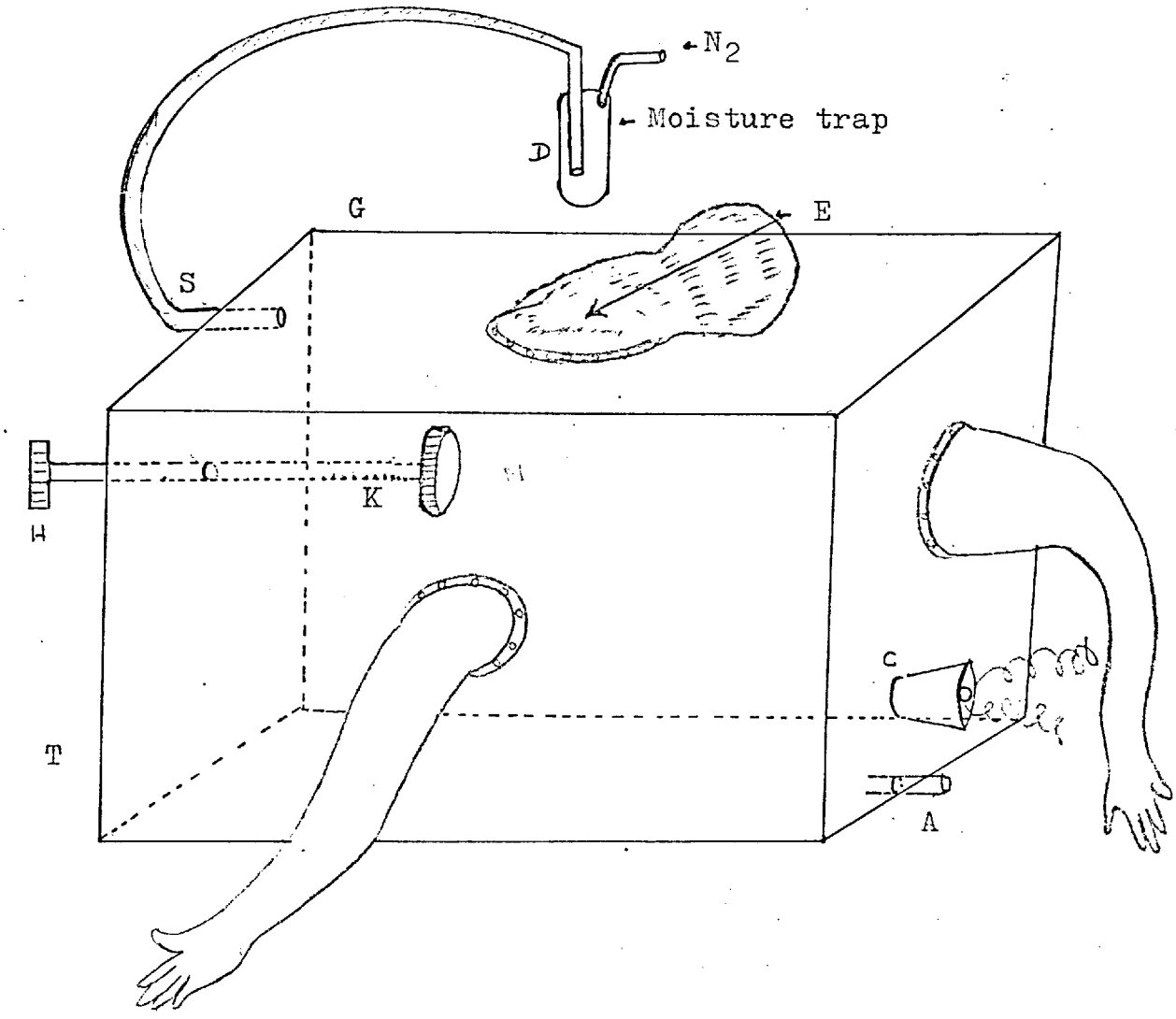

Fig. 14. The glove-box for handling the materials

The Glove Box (Fig.14). This was made from perspex panels, of which the front one (T) could be removed. Everything needed for a particular experiment (including the microscope where necessary) was arranged inside the box before the start of the experiment. The front panel was then slid into position and the edges sealed with Sellotape. Throughout an experiment, nitrogen dried by the liquid nitrogen trap D entered the box at S and left at A. A dish containing phosphorous pentoxide was also kept within the box to accelerate the initial removal of water vapour.

The polarising microscope could be focussed remotely from outside the box by rotating the milled head H which was directly linked to the coarse focussing control K of the microscope M.

Electrical connections for the hot-stage were passed through a rubber bung inserted into the hole C. A circular opening (E) in the upper panel was closed by a clean transparent polythene bag. This allowed the analyser to be inserted or removed and the analyser/polariser system to be rotated by the milled head P of the microscope (Fig.9).

2.4. The Thermostat and the Temperature Control Unit

The design of the microthermostat used in the present work was the same as that used in the earlier study of the thermal transformations of potassium nitrite[44]. The initial experiments actually utilised the furnace constructed by Dr A. Schuyff, but when this developed an electrical defect, the furnace had to be rewired (Fig.15).

The microthermostat consisted of a beryllium tube (A), about 2.5 4.0 cm long, 1 cm diameter and 1 mm wall thickness in which two circular apertures were drilled (B) to allow the incident beam to pass through without obstruction. A thin mica sheet C was wrapped round the beryllium tube for electrical insulation. On top of this a layer of Fiberfrax D was laid, to prevent the movement of the platinum wire (E) wound round it as a temperature sensing element. This 1 ohm platinum resistance thermometer was made of two 2 ohm sections of thermopure (40 s.w.g.) wire connected in parallel and wound non-inductively. One section was wound above the main beam apertures B and the other below. The common leads (F) for external connections were constructed of heavier gauge platinum wire of negligible resistance and all electrical connections were hard soldered.

A layer of paste made from alumina cement mixed with water-glass diluted with water was placed over the platinum thermometer to insulate it electrically and to prevent movement of the wires. On this cement layer, a 15 ohm nichrome heater (N) was wound non-inductively in three layers separated by alumina cement and distributed between upper and lower part of the thermostat. Then the thermostat was built up with alumina cement paste to a convenient external profile (S).

The platinum resistance wire terminals (F) projected out of the furnace in a direction normal to the holes for the X-ray beam and the furnace wire terminals (M) came out near the top of the

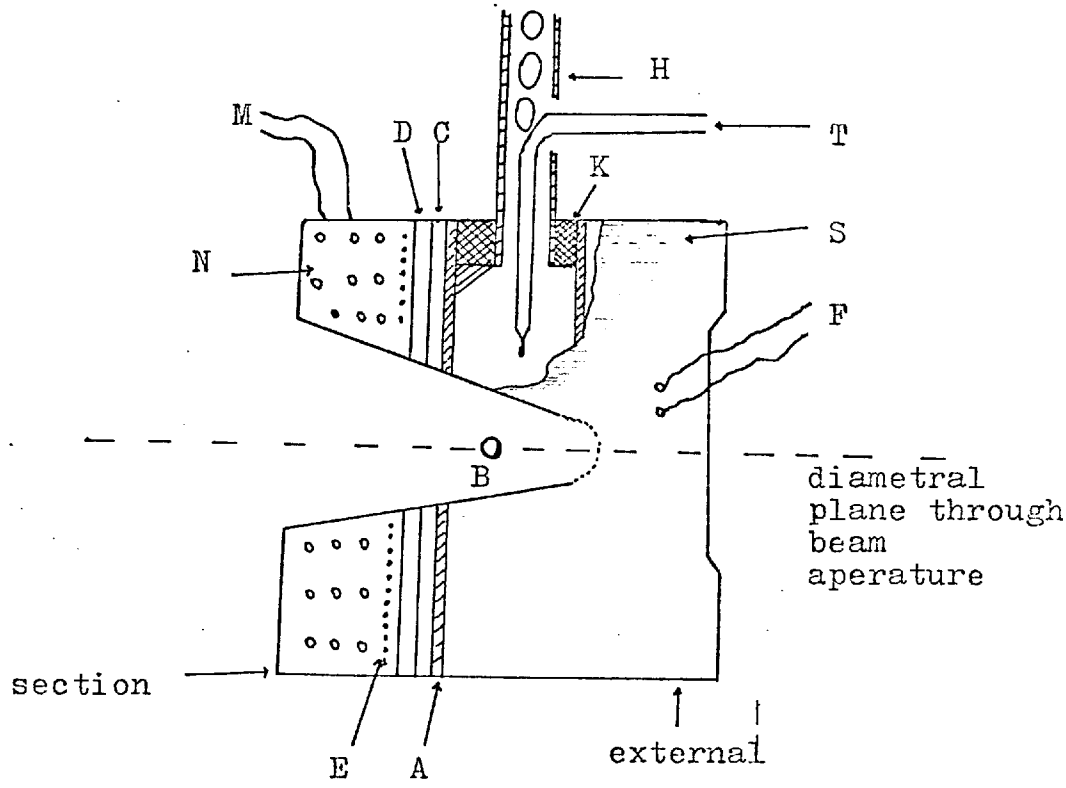

Fig.15. The Microthermostat.

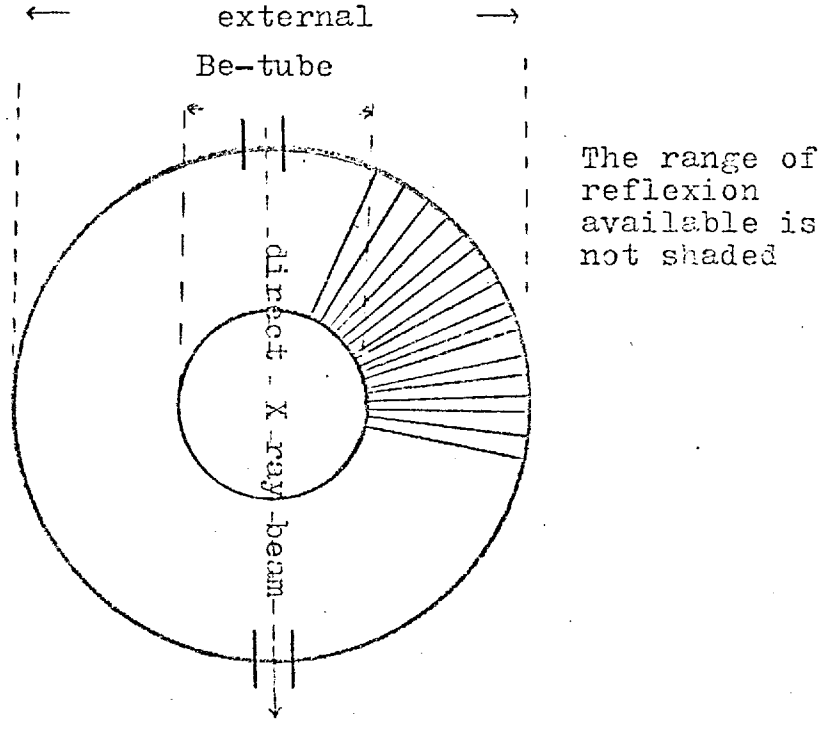

Fig16. Horizontal cross-section of Fig.15.

furnace. Thus, the beryllium tube was left uncovered over an angular arc from about $+180^{\circ}$ to -90° with respect to the line of the beam aperture (Fig.16) in the diametral plane and about $\pm 20^{\circ}$ in elevation. On one side the diffracted beam could pass unobstructed through the beryllium tube for all Bragg angles, whereas on the other side the high angle quadrant was obstructed by ceramic which protected the platinum resistance thermometer leads and the heater connections between the upper and lower parts of the furnace.

The completed furnace was fired for about 18 hours by raising the temperature of the furnace very slowly till it was red hot.

The top end of the beryllium tube was closed by a copper plug (K) which could be screwed to one end of a perforated, hollow stainless steel tube (H). This, in turn, was suspended from a frame, attached to the X-ray goniometer, so that the furnace could be raised or lowered by an adjusting screw. The frame from which the furnace was suspended, was provided with a centering adjustment allowing the furnace to be laterally adjusted on the X-ray beam. It was necessary to avoid the direct beam hitting the beryllium tube, for this gives rise to beryllium powder lines on the diffraction photographs.

The furnace temperature was measured by a copper-constantan thermocouple (T), calibrated at three temperatures - room temperature ($22^{\circ}C$), the boiling point of water at normal pressure ($100^{\circ}C$) and the melting point of naphthalene ($218^{\circ}C$). The deviation

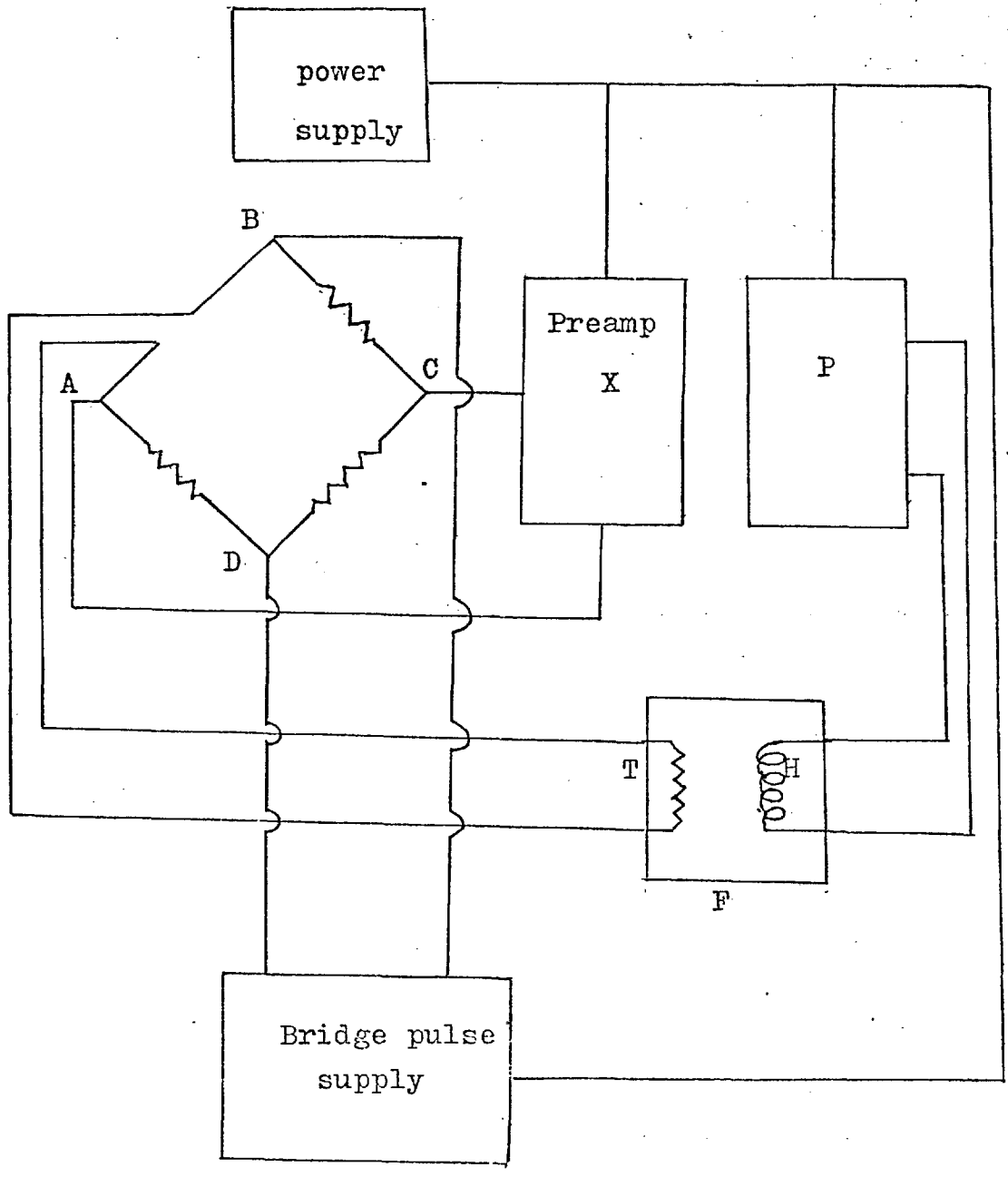

Fig.17. A block diagram of the temperature control unit.

from tabulated values was found to be negligibly small and the standard values have been used for interpolation.

The thermocouple was lowered through the stainless steel tube (H), so that the tip of the thermocouple was brought as near the crystal as practicable. The bottom of the thermostat was closed by aluminium foil to reduce the vertical gradient in the furnace to around 0.1°C/mm. The temperature was measured by a potentiometer (Pye, Cambridge) which was sensitive to ~~0.1~~ 1.0 μV. To keep the temperature of the thermostat constant, the temperature control unit described below was constructed by the electronics workshop.

The Temperature Control Unit The control unit is shown in Fig.17. ABCD is a resistance a.c. bridge, one arm of which is the sensing thermometer (T) of the microthermostat (F). Any variation of temperature in F throws the bridge out of balance, the resulting signal being amplified (X) and fed into the Proportional and Integral Controller P. This varies the heater current so as to reduce the out of balance signal. Thus, at a particular temperature an optimum steady value of current is maintained through the heater H.

The temperature control appeared to improve as the temperature was raised. From room temperature up to 80°C, the control was not better than ± 0.2°C. At 200°C, the temperature could be maintained at about ± 0.1°C. The range of controlled temperatures used was nominally from room temperature to about 350°C.

2.5. Recording of Diffraction Patterns

It was mentioned earlier that the photographic method was used in the present work to record the diffraction pattern from single crystals.

An accurate determination of a structure requires the reciprocal lattice to be scanned as completely as possible in order to have the maximum data available. In the case of a low symmetry crystal this means that at least a half or a quarter of the available reciprocal lattice must be covered to record the intensity of each independent reflexion. This requires data to be recorded about at least three crystallographic axes. In moving film techniques such as the Weissenberg camera each layer line along an axis is recorded in turn, each reflexion being completely resolved. Thus for purely structural work, it is usual to use such a photographic method. The rotation photographs, on the other hand, give data for all available layers simultaneously, but reflexions overlap and the problem of measuring the intensity becomes too complex.

Thus, for a room temperature structure determination, a moving film technique is undoubtedly the best and was used in the present work to obtain data for form III. For low temperature structural work there are commercial Weissenberg cameras, but no cameras are available for high temperature work.

However some attempts have been made to modify the standard Weissenberg camera for high temperature work on the lines suggested

by other workers. In one modification[45] the main shaft is replaced by a hollow one, through which the electrical leads pass to a microfurnace of a few turns of platinum wire. In another[46] a narrow jet of hot air is blown on to the crystal from a glass nozzle clamped on the open side of the film holder. Because the first modification required drastic changes, the second method was tried. But in the absence of a cooling device, the film deteriorated at high temperature. A more serious difficulty encountered with these modifications was the large fluctuations of temperature (of the order of $\pm$ 10°C), which may be negligible for some structures with small thermal expansion but which are quite unacceptable for structures with large expansions (such as potassium acetate - see section on cell dimensions at different temperatures).

In principle ordinary oscillation photographs can also be used for structural work, but considerable effort is required to identify every reflexion correctly, even for a relatively simple crystal structure, since small oscillation angles must be used. Moreover, two consecutive oscillation ranges must overlap to record the reflexions at the extremities of a range. For a complex structure with a very large real cell, the large number of possible reflexions complicate the problem of uniquely assigning hkl indices to a reflexion. Apart from these difficulties, however, there are several good features of rotation and oscillation cameras which were used with advantage in the present work. The

problem was to record the maximum amount of data in the minimum of time because of difficulties regarding the control of temperature and the thermal history of the sample (see section on thermal expansion and hysteresis). The rotation photographs record several layers in the same time as a Weissenberg records one layer. An oscillation photograph samples the reciprocal lattice in a general way in a much shorter exposure time.

Therefore, for all high temperature diffraction photographs, oscillation and rotation techniques were used. The 3 cm cylindrical camera could not be used for high temperature work because of the microthermostat and its support, so a hemicylindrical film holder of radius 5.73 cm was used, which did not interfere with the heating arrangement for the crystal. This film holder allowed reflexions up to a maximum Bragg angle of 45° to be recorded.

For intensity measurements at high temperatures, rotation photographs with the same film-holder were taken, once it had been established that there would be no ambiguities in indexing. The multiple film technique was used to cover the intensity range.

For oscillation photographs with large crystals about an hour's exposure was sufficient under normal conditions. For rotation photographs with smaller crystals, the exposure time was increased to two days.

Temperature fluctuations and overheating of the film proved to be the main difficulties. Overheating increased the background

while the temperature fluctuations caused by draughts were minimised by surrounding the camera and the furnace on all sides with cardboards.

To get the structural data for room temperature phases, 15^{o} oscillation photographs were taken at 12^{o} intervals with the 3 cm cylindrical camera. In addition, a few Weissenberg photographs were taken to confirm the deductions based on oscillation photographs.

2.6. Relative intensity and line profile measurement

Introduction: To compare the intensities predicted on the basis of the different models of the crystal structures of potassium acetate, the intensity of each available reflexion was measured in the present work. The quality of the intensity data required is determined in each case by the nature of the study pursued. Early workers determined simple crystal structures by the photographic method, merely by estimating the intensities qualitatively. Now it is usual for routine structural work using photographic methods to estimate intensity visually by comparing the diffraction intensities with a known graded intensity scale. Sometimes microphotometers are used for the measurement of integrated or peak intensity. It is customary to estimate the relative intensity only, unless the absolute intensity is required for special reasons.

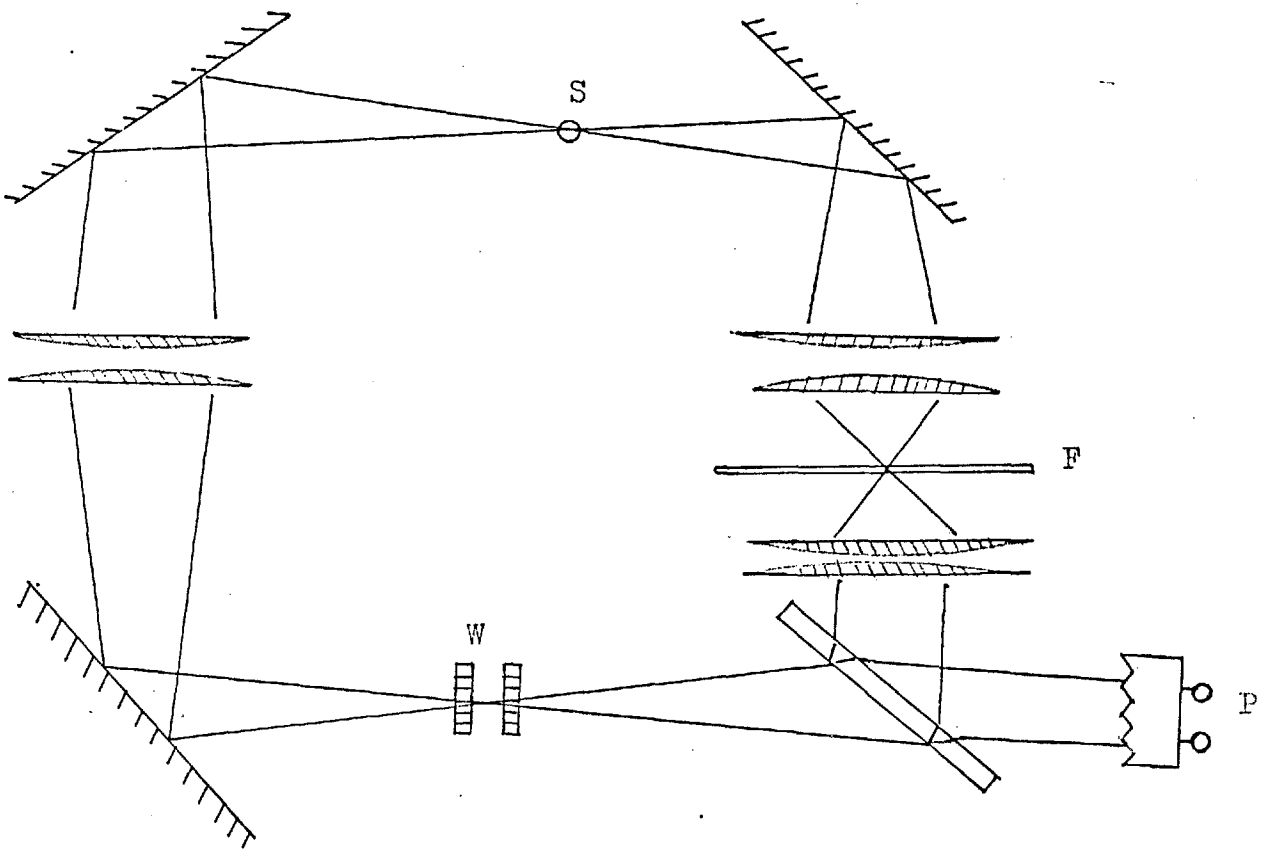

Fig.18. The woking principle of the microdensitometer used.

Apparatus: In the present measurements data on the shape and magnitude of the diffraction spots was obtained with a Joyce Loebl Automatic recording microdensitometer, Mark III (Fig.18). This is a double beam null point instrument in which an optical wedge of graded density is progressively inserted into one beam to balance the absorption by the sample of the other beam. The pen displacement is limited to the displacement of the density wedge at the null position.

Light from a source S is split into two beams which are switched alternately to a single photomultiplier P. If the two beams have different intensities, a difference signal is produced by the photomultiplier which after amplification causes a servo motor to move an optical attenuator so as to reduce the intensity difference to zero. In this way a continuously balancing system is obtained in which the position of the attenuator is made to record the optical density at any particular part of the specimen F.

The advantage of this instrument is that the variation in the source intensity is eliminated by using the same source to illuminate both the film and the wedge.

Theoretical: The degree of blackening or density of a film on exposure to any light is defined as

$$D = \log \frac{\text{incident light}}{\text{transmitted light}}$$

Exposure is defined as

$$E = I \times t$$

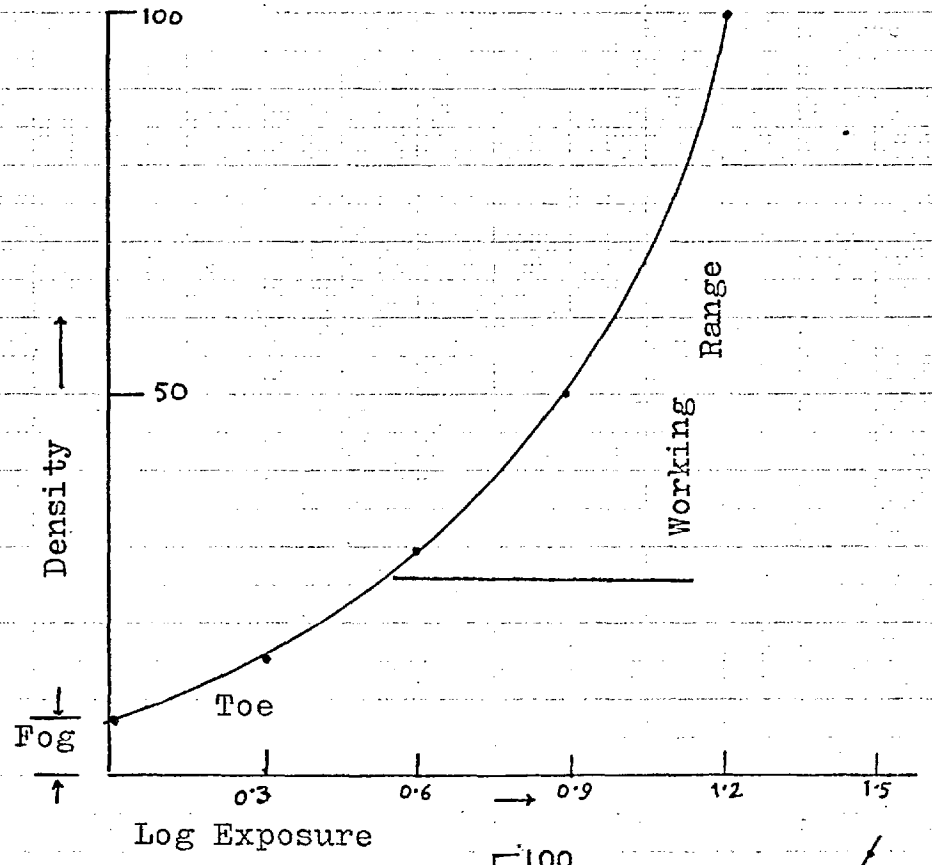

Fig.19. Characteristic curve of the film used.

Fig.20. (below) Density vs. Exposure curve, showing the linear range from 0 to about density= 40

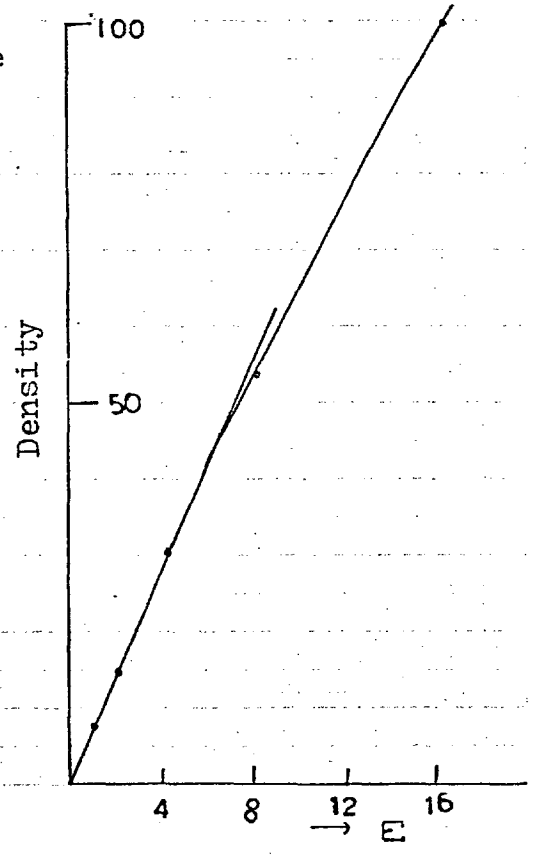

where I is the beam intensity and t is the time of exposure. When D was plotted against log E, the characteristic curve of the film was obtained (Fig.19).

In the present case a graded intensity scale was prepared by allowing a collimated X-ray beam, reduced in intensity by passing through a number of aluminium plates, to fall on a pack of films for 1 second. The film was then displaced and again exposed for 2 seconds. The process was repeated for the geometrical progression, 4, 8, 16 etc seconds. The exposure was made at normal tube voltage and the photographs were processed under controlled conditions. The intensity scale was then photometered. The density (heights of the peaks) were found to be a linear function of intensity (exposure) up to a maximum peak height of ~~35~~ 46 mm from zero background (Fig.20). Within this limit the peak heights were taken directly to represent relative intensity.

In the multiple film technique, as each film in a pack acts as a uniform absorber, the intensity transmitted to the film beneath is reduced by a certain constant factor (transmission factor). This factor for the films used, ~~were~~ was found by comparing the heights of the same reflexion on successive films. The average value of the transmission factor of x.42, obtained from a number of reflexions, was used to convert all intensities to the same scale.

2.7. Preliminary Crystallographic work : Identification of phases

While the techniques of preparing crystals were still being improved, preliminary crystallographic work was started.

Using crystals showing complete extinction under the crossed polars and mounted as described previously, X-ray oscillation photographs were recorded at room temperature on a 3 cm cylindrical camera. The radiation used was CuKα (λ = 1.54178Å). Photographs about an axis parallel to extinction direction (2) showed layer lines indicating a lattice repeat distance in this direction of about 4 Å. This was taken to be a unit cell axis and labelled c. Similarly, the oscillation photographs taken about extinction direction (1) also showed layer lines and was taken to be second unit cell axis b. Inspection of the photograph showed zero, first, third, fourth, fifth, seventh ... layer lines, for which k = 0, 1, 3, 4, 5, 7 ... The repeat distance along the b axis was about 23 Å. Further, strong reflexion intensities were found only on layer lines for which k = 4n. Layer lines for which k was odd contained only the weaker intensities and no reflexion at all was visible on layer lines for which k = 4n + 2.

This crystal was subsequently heated and 15° oscillation photographs recorded on a flat plate film holder (the furnace prevented the cylindrical film holder being used) at temperatures of about 60°, 100°, 130°, 200° and 280°C, and finally at room temperature. It was found that the layers with k odd, which as

noted above, contained only weak reflexion, became significantly weaker at 60°C and were absent in the photograph recorded at 100°C. Thus, the photographs taken at 100°C contained only those layer lines for which k = 4n, at room temperature, so that the b-axis was reduced to one quarter of its former value. The photographs at 200°C and above were much clearer, for there was a reduction in the number of reflexions within each layer, compared to photographs taken at lower temperatures. Room temperature photographs taken after the heating cycle showed that the weak layer lines had re-appeared apparently with the same intensity as before.

Attempts to take oscillation photographs about an axis perpendicular to the plane of the crystal plate in order to locate the third axis of the crystal cell were unsuccessful. Excessive exposure times were required because of the unsuitable crystal shape and the higher absorption coefficient. Nevertheless, some idea of the length of the a-axis was obtained by identifying the hoo reflexions in the zero-layer lines of photographs taken about the b and c axes. These formed a sequence of prominent reflexions with ξ values that were multiples of .16, so the interplaner spacing d_{100} was taken to be either $\lambda/0.16$ or some simple multiple of it, giving a minimum value for the a axis of about 9.7Å.

Some tentative conclusions, to be verified by more sophisticated experiments later, were drawn from the above observations.

(i) At room temperature, the unit cell dimensions were approximately

$a \sim 9.7$ Å, $b \sim 23$ Å, $c \sim 4$ Å.

(ii) Potassium acetate has at least three crystal structures. One form existed from room temperature to the temperature when the weak layer lines disappeared. This temperature was provisionally identified, with the phase transition at 80°C reported by Hazlewood et al.[7]. This new phase underwent a further transformation between 135° and 200°C characterised by a reduction in the number of reflexions. This change was provisionally identified with the second phase transition reported to occur at 160°C. No evidence of the third transition at 230°C was found as there was no difference in the appearance of diffraction photographs taken at 200°C and 280°C. Accordingly, the phases were designated from room temperature upwards: form III → form II → form I.

(iii) During the heating cycle, the b and c axes did not show any observable change of orientation. Crystals mounted about these axes remained "set" throughout both phase transitions.

2.8. Determination of Cell Dimensions at Specific Temperatures

Reference has already been made to the difficulties of recording diffraction patterns from crystals mounted about the a-axis and to the abortive attempts at modifying the Weissenberg camera for high temperature operation. Hence for most of this

work it was necessary to use oscillation photographs of crystals about the b and c axes, to establish the cell dimensions of the different forms of potassium acetates. Improved estimates of b and c for form III were easily obtained from measuring the layer line separation of photographs recorded with a cylindrical film holder by means of a travelling microscope, but nothing was known about the values of the interaxial angles initially. As there were a large number of reflexions on the zero layer line of the c-axis oscillation photographs of form III, a zero layer Weissenberg photograph was taken at room temperature. This established that the a^*b^* net was orthogonal with $a^* = .0825$ $b^* = .0654$, and the photograph was subsequently indexed with a standard Weissenberg chart. Thus, it was possible to assign unambiguous indices to all the reflexions of the c-axis oscillation photographs. Although in principle it would have been possible to obtain all values of the cell angles from Weissenberg photographs, an attempt (which proved to be successful) was made to solve the problem by oscillation photographs alone, in order to gain experience for the interpretation of photographs at higher temperatures, where the Weissenberg camera could not be used.

A close examination of the reflexions in the first layers of c-axis oscillation photographs taken at room temperature showed that in one crystal, the diffraction intensities did not exhibit the mm-symmetry commonly found when the crystal was oriented parallel to X-ray beam along the b* axis. The intensities of

pairs of reflexions in the first layer line on the upper half of the film were in reverse order on the lower half (Fig.21). Moreover, the stronger reflexions were relatively sharp whereas the weak reflexions were badly arced along curves of constant θ. Thus the diffraction photograph could not be that of an orthorhombic single crystal but proved beyond doubt that this crystal (and by inference all similar crystals) were twins with a monoclinic angle β, which could be roughly measured from the photograph. Such a diffraction pattern requires the crystal to have the following twin texture (Fig.22).

The two orientations of the twin (1) and (2) have a common c axis and a axes that diverge at an angle 2β. Likewise both a^*_1 and a^*_2 are perpendicular to c and therefore lie in the same straight line whereas c^*_1 and c^*_2 are inclined at an angle $(180-2\beta^*)$. In both components the b-axis must be parallel, for, otherwise, the angle would be detectable on the b-axis oscillation photographs, which was not experimentally observed. Thus b^*, which is perpendicular to a^* and c^* must be perpendicular to the plane of the paper in Fig.22. It is evident that (100) is the twinning plane.

Thus, with c as the oscillation axis, reflexions of the type hoo or hko in the zero layer are split into pairs of reflexions hol and $ho\bar{l}$ or hkl and $hk\bar{l}$ in the first layer line. Although in the present case the two components of the twin were of unequal volume so that the intensities of the pair of reflexions were

unequal, in general this is found not to be the case.

The appropriate value of the monoclinic angle β was found by measuring the separation of the pairs of reflections 701 and $70\bar{1}$, 611 and $61\bar{1}$, 501 and $50\bar{1}$, 301 and $30\bar{1}$ on two separate photographs.

Thus, the above arguments lead to the conclusion that the room temperature structure is monoclinic and twinned, the twinning plane being (100), $a^* = .085$, $b^* = 0.0654$, $c^* = .39$, $\beta = 92.3^\circ$.

Confirmation that this was a selfconsistent set of cell parameters was obtained by successfully indexing all reflexions on a set of b-axis photographs.

A more accurate method used to determine the change of β with temperature will be given later.

Having verified that it was possible to index the room temperature photographs an attempt was made to index the b-axis photographs at $207^\circ C$, because here the diffraction patterns showed fewer reflexions. Bearing in mind that the lattice is likely to gain symmetry elements as the temperature rises, it was thought possible that the lattice was now orthogonal. The orientation of a* was found to be unchanged and a central reciprocal lattice row identified as the new c*(I) was found perpendicular to a*(I) (parentheses refer to the three forms). An a*c* net was drawn on the basis of these two dimensions and it was soon evident that all reflexions could be accounted for by making:

$$a^*(I) = \tfrac{2}{3}a^*(III).$$

Using the fact that $b(I) \sim \frac{1}{4}$ (III) from layer line measurements, it was concluded that the form I structure belonged to the orthorhombic system, with the appropriate cell dimensions:

$$a^* = 0.160,\ b^* = 0.27,\ c^* = 0.390.$$

The problem of indexing photographs taken at 107°C (about the middle of the temperature range over which form II is stable) was next tackled.

The reflexions of the type hoo could be identified from their positions and overall similarity in intensity to those of form I and II. This helped to define the range of oscillations to sweep those regions of reciprocal space which contained reflexions of the types other than hoo. For a number of reflexions in the zero layer line, the photographs about b-axis were found to be more akin to those of form III. Hence an attempt was made to index the photographs on a twin reciprocal net of form III. Soon it was apparent that if the form was a monoclinic twin, the monoclinic angle must be larger than in form III. After trial and error adjustments of β^*, finally a non-orthogonal twin net was found on which all reflexions on the zero and first layer limes could be indexed. The corresponding cell dimensions were: $a^* = 0.165$, $b^* = 0.27$, $c^* = 0.39$, $\beta = 94.8°$.

It was subsequently verified that the cell dimension deduced for the forms III and II of potassium acetate could be

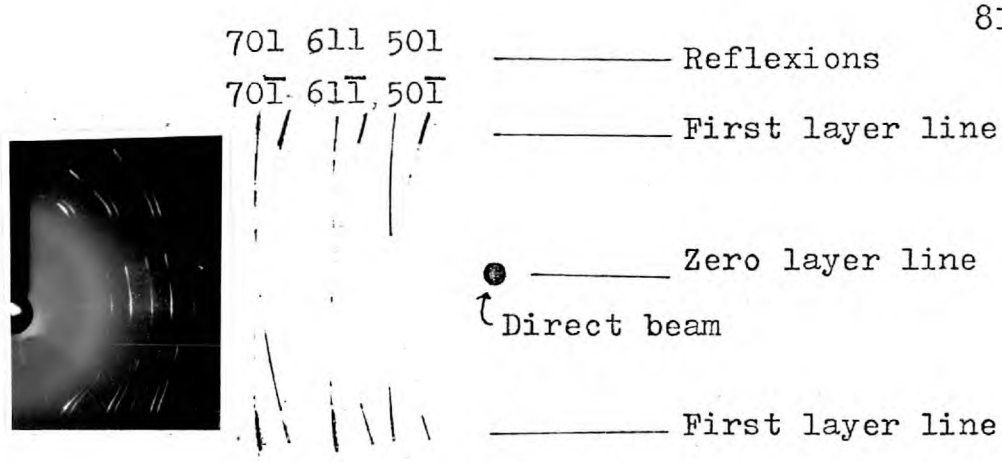

Fig.21. Schematic diagram of a room temperature c axis oscillation photograph of potassium acetate, which showed splitting of reflexions in the first layer line, due to twinning.

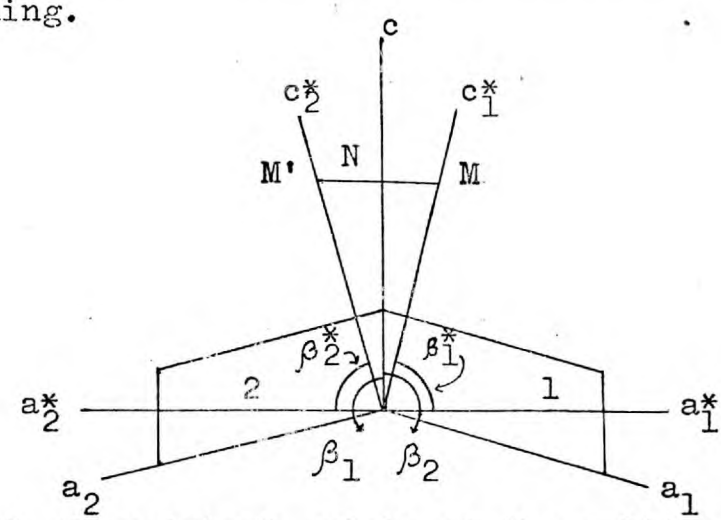

Fig.22. Geometrical origin of the split-reflexions of Fig.21.

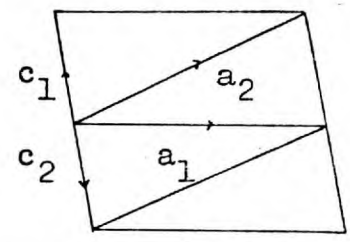

Fig.23. Transformation of axes; b.c. to f.c. lattice in Form II and Form III potassium acetate.

used to index photographs taken about the c-axis. This provided an independent check on the correctness of the cell dimensions quoted in Table 2.8 and justified the use of the indices of observed reflexions to determine the translational elements of symmetry present in the space groups.

The present axial systems involve an increase in the monoclinic angle β from 92.3° in form III to $\beta = 94.8^{\circ}$ in form II, followed by a reduction in form I where this angle must be 90° by orthorhombic symmetry. Subsequent inspection of photographs taken at different temperatures revealed that this discontinuity in the β angle was not a real effect but due to the choice of unit cell in forms II and III. To avoid this artificial change in the unit cell, the orientation of reciprocal axes chosen for indexing the monoclinic forms were transformed, to ensure that β decreases progressively through the transformations III $\rightarrow$ II $\rightarrow$ I. This was done by defining the new axes a_2 and c_2 whose transformation equations in terms of the original a_1 and c_1 are given by (Fig.23) (for both forms III and II)

$$\underline{c}_2 = -\underline{c}_1$$

$$\underline{a}_2 = \underline{a}_1 + \underline{c}_1$$

This leads to a similar transformation in the Miller indices

$$h_2 = h_1 + \ell_1$$

$$\ell_2 = -\ell_1$$

After assignment of new indices to all reflexions of the photographs taken for the three forms, the space groups from the systematic reflexion conditions, relative to these new axes were found to be as follows:

In form III, reflexions of the type,

hkl were present only for h+k = 2n

Thus, the allowed space groups are

Cm, C2/m or C2.

In addition, other reflexion conditions were found that were not required by any monoclinic space group. These conditions were

oko present only for k = 8n and hkl absent when k = 4n ± 2.

The only reflexion condition in form II is that

oko present only for k = 2n.

The space groups are, therefore,

$P2_1$ or $P2_1/m$.

The reflexion conditions for form I are okl present only for k ± l = 2n.

These are the conditions for the space groups

Pnmm, $Pn2_1m$ or $Pnm2_1$.

Table 2.8

Summary of crystallographic data of Potassium Acetate
(Transformed)

Form	temp.	a*	b*	c*	β*	aÅ	bÅ	cÅ	β°
III	22°C	.0825	.0654	.39	79.6°	18.38	23.65	4.00	100.4
II	107°C	.165	.27	.39	82.6°	9.38	5.72	3.99	97.4
I	207°C	.160	.27	.39	90°	9.71	5.90	3.96	90

	Reflexion condition	Space groups
(III)		
	hkl present only for h+k = 2n	Cm, C2/m or C2
	(oko present only for k = 8n	
	hkl absent when k = 4n+2)	
(II)		
	oko present only for k = 2n	$P2_1$ or $P2_1/m$
(I)		
	okl present only for k+l = 2n	Pnmm, $Pn2_1m$ or $Pnm2_1$

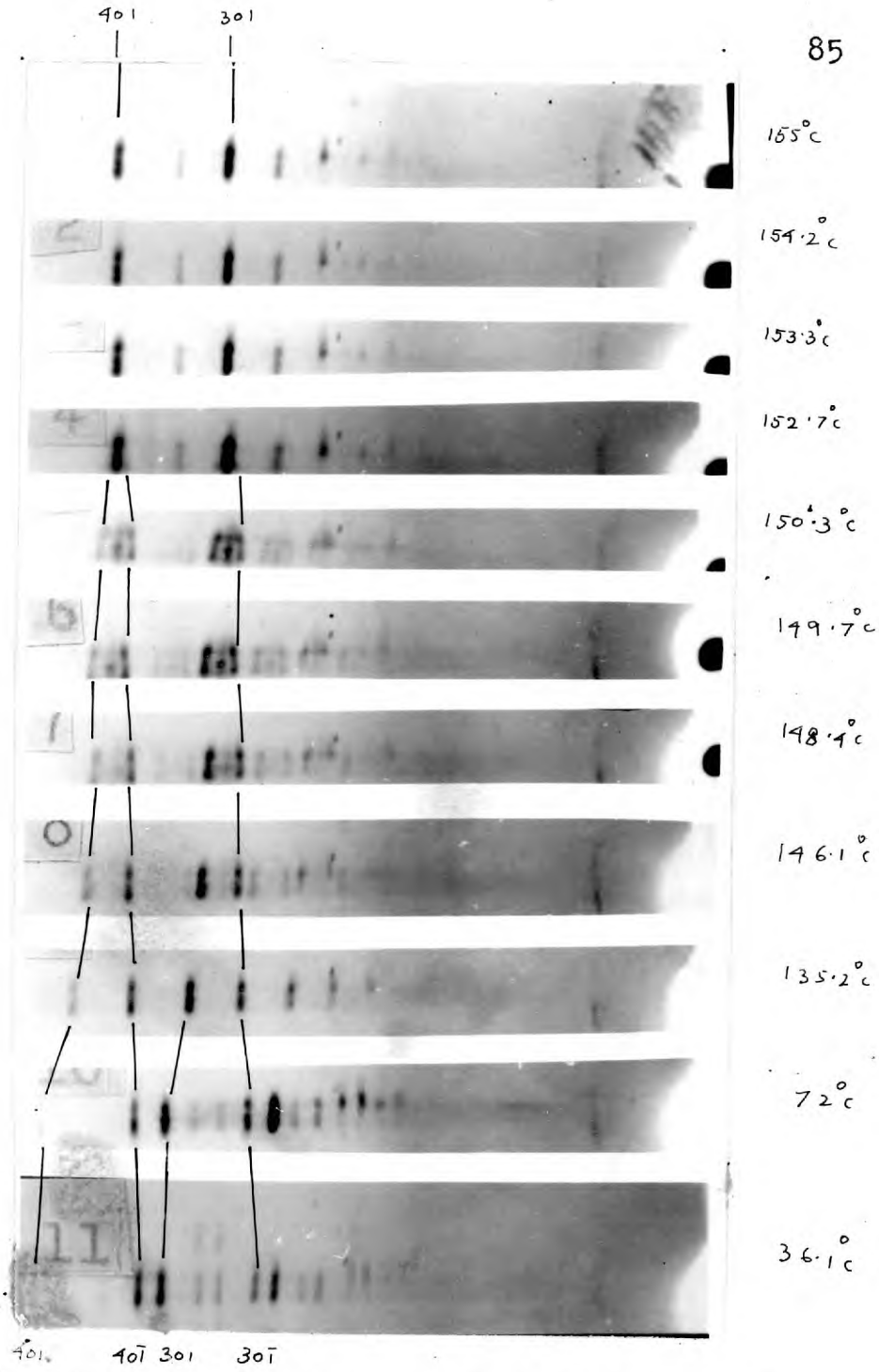

Fig.24. The movement of pairs of reflexions of the type h0l and h0$\bar{1}$ towards each other with increasing temperature (in between room temperature and T_c (II → I)).

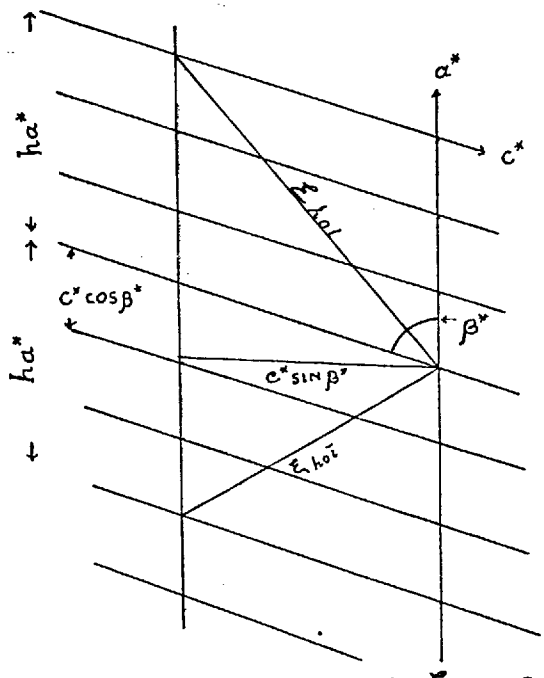

Fig.25. Relation of β^* and ξ --values of h0l and $\bar{h}$0l
(or h0$\bar{l}$ of twin orientation)

2.9. Determination of Cell Dimensions at a Series of Temperatures

In the foregoing section, the cell dimensions of the three forms were determined only at three specific temperatures. But the following observations led to the study of the cell dimensions at different temperatures.

While identifying the changes in the b-axis diffraction pattern due to the phase transformation, it was found that,

(i) reflexions of the type hoo moved noticeably towards low θ with increasing temperature, indicating large thermal expansion of d_{100}.

(ii) Pairs of zero layer reflexions identified as the type hol and $ho\bar{l}$, with one from each orientation of the twin, moved towards each other with increasing temperature and coalesced between 136°C and 200°C (Fig.24). This phenomenon was investigated further by taking a series of b-axis oscillation photographs with the hemicylindrical camera at different temperatures.

The positions of these two reflexions are related to the monoclinic angle in the following way:

From the geometry of the Fig.25,

$$\zeta^2_{hol} = c^{*2} + (ha^*)^2 + 2ha^*c^* \cos \beta^*$$

$$\zeta^2_{ho\bar{l}} = c^{*2} + (\bar{h}a^*)^2 - 2ha^*c^* \cos \beta^*$$

so that,

$$\zeta^2_{hol} - \zeta^2_{ho\bar{l}} = 4.\ h.\ a^*c^* \cos \beta^* \qquad (1)$$

For all zero layer reflexions $\zeta = 2 \sin \theta$

Hence $\cos \beta^* = (\sin^2\theta_{hol} - \sin^2\theta_{hol\bar{}})/ha^*c^*$ (2)

Thus, to find β at a particular temperature three photographs were taken, one to obtain θ_{hol} and $\theta_{hol\bar{}}$ and the other two to obtain $\underline{a}^*$ and $\underline{c}^*$.

The reflexions used for measurement and their approximate Bragg angles are shown in the Table 2.9.

Table 2.9

Approximate Bragg angles for lattice parameter determination

Reflexion Indices	Approx. Bragg angle θ^o
400 (800)	20
002	23
301 - 30$\bar{1}$ (601, 60$\bar{1}$)	20
040 (0, 16, 0)	32

The indices in parentheses are those for form III.

Near the transitions, photographs were taken at frequent temperature intervals and a few photographs were taken above II ⟶ I transition temperature, to see if there was any detectable change in the diffraction pattern.

Once it had been verified that it was possible to obtain meaningful measurements of β and therefore of $\underline{a}$ and $\underline{c}$, another crystal was mounted about the c-axis in order to record the oko reflexion from which the remaining cell dimension $\underline{b}$ could be obtained.

The variation with temperature of the cell parameters that were measured directly, namely, d_{100}, $d_{010} = b$, and d_{001} are shown in Fig. 26, 27, 28. Using the relations,

$$\underline{a}^* = \lambda/d_{100}, \quad \underline{c}^* = \frac{\lambda}{d_{001}}, \quad \beta = 180 - \beta^*$$

in equation (2), the variation of β with temperature was derived and is plotted in Fig.29. Values of $\underline{a}$ and $\underline{c}$ were calculated from the equations $\underline{a} = \frac{d_{100}}{\sin\beta}$ and $\underline{c} = \frac{d_{001}}{\sin\beta}$ and plotted (Fig.30,28).

The Bragg angles of the reflexions chosen were considerably lower than are desirable for accurate measurement, but this is partly counteracted by the large change in the parameters to be measured. Nevertheless, to obtain a self consistent set of results, certain precautions were necessary. The reproducibility of measurements in the travelling microscope was quite satisfactory, an average of 11 readings having a standard deviation of $\pm$ 0.002 cm. Given the camera radius of 5.73 cm, this corresponds to an error in the Bragg angle $\Delta\theta$ of 0.02° and a precision of spacing measurement $\frac{\Delta d}{d} = -\cot\theta . \Delta\theta$ of about 0.1%. This precision was not achieved in photographs repeated under identical conditions. No correction for film shrinkage was possible but random variations in the shrinkage were minimised by processing films under identical conditions and measuring the films without delay. Thus, film shrinkage will change the absolute value of the spacing, but the random error in the relative value is probably less significant. The most likely

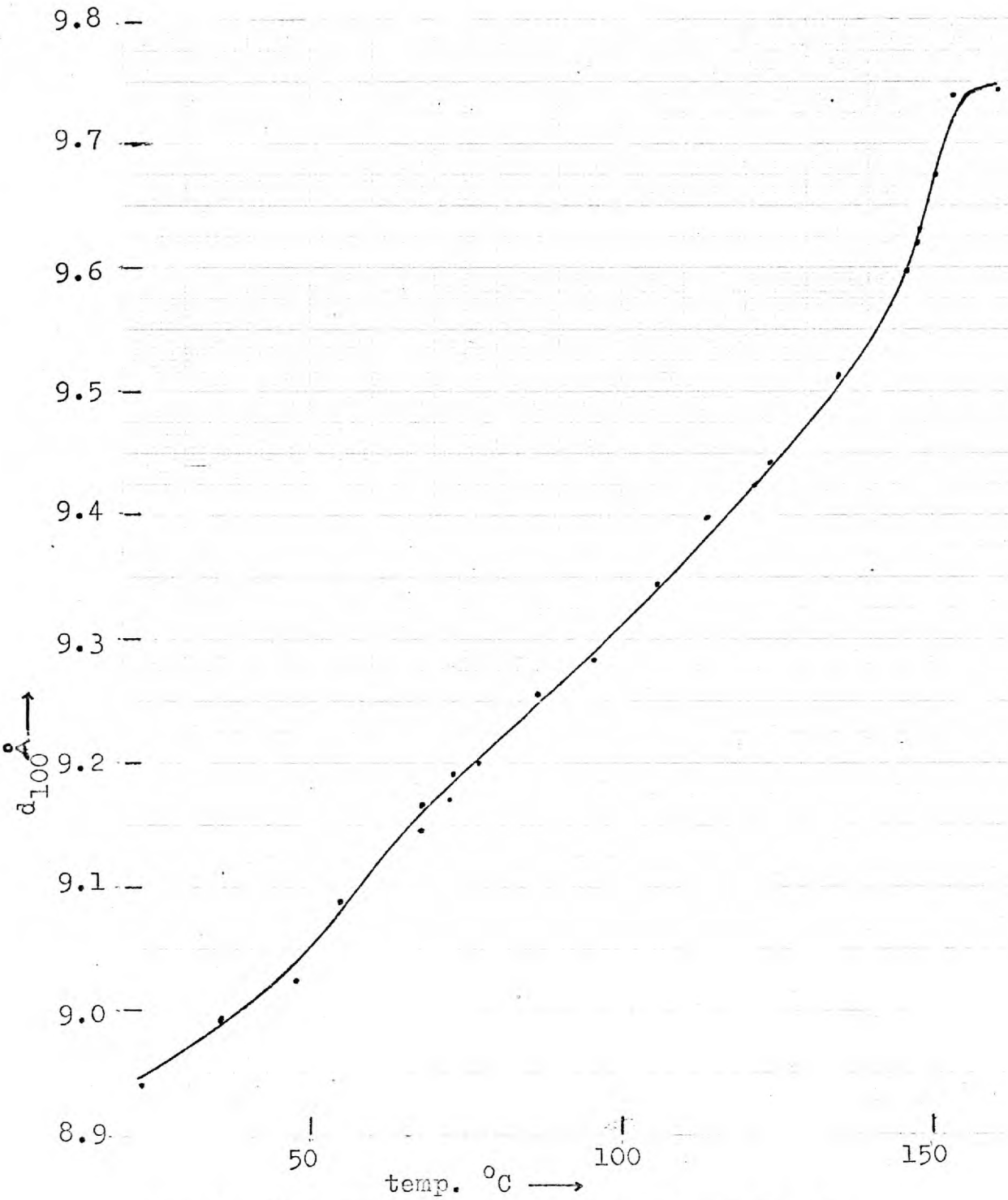

Fig.26. Variation of d_{100} with temperature in potassium acetate. (numerical data given in Appendix)

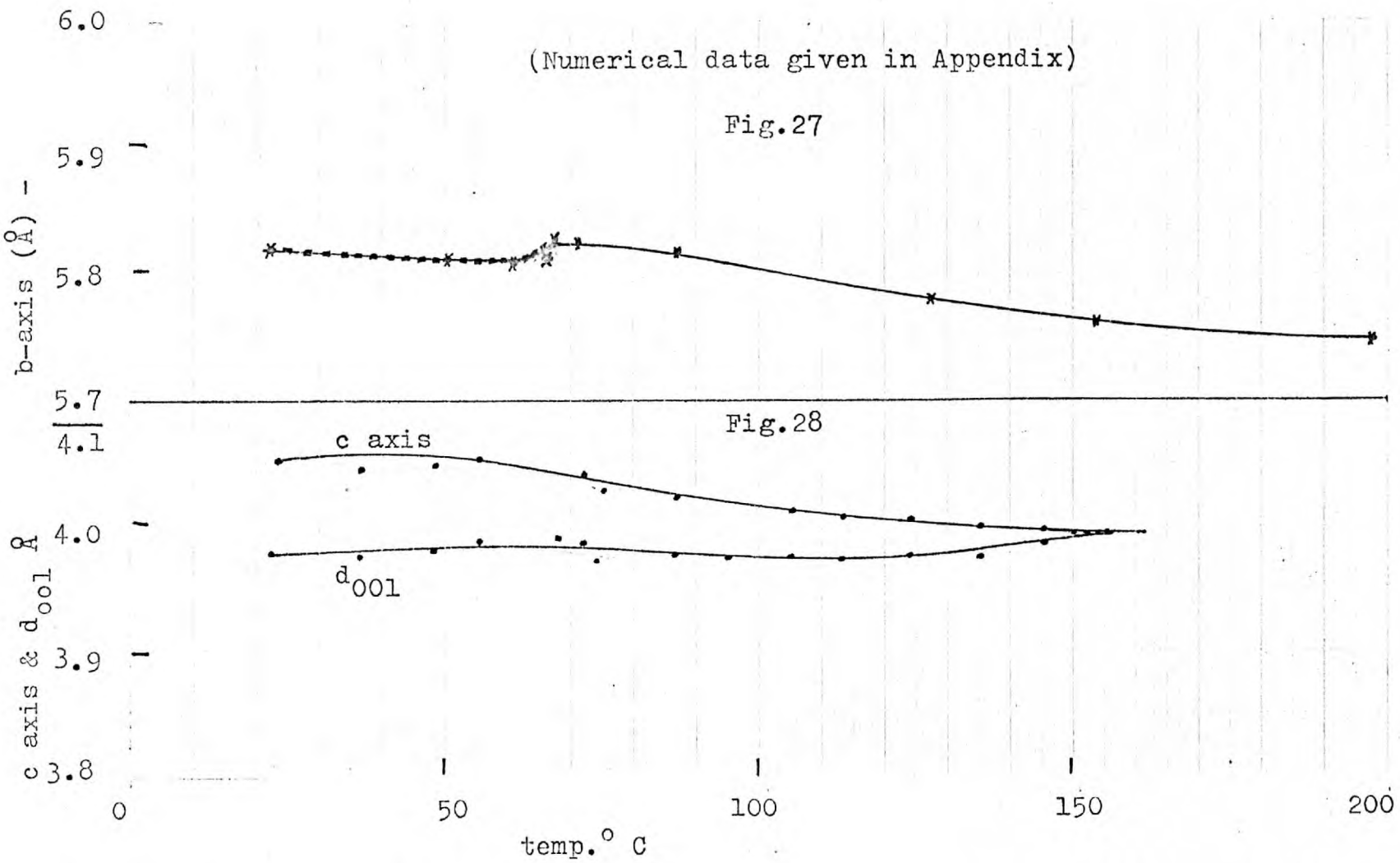

(Numerical data given in Appendix)

Fig.27

Fig.28

Fig.27. Variation of b axis with temperature; - - - b/4 (form III), ___ b (II & I)

Fig.28. Variation of c axis and d_{001} with temperature (sample: potassium acetate)

Fig.29. Variation of β with temperature. (numerical data given in Appendix) (sample: potassium acetate)

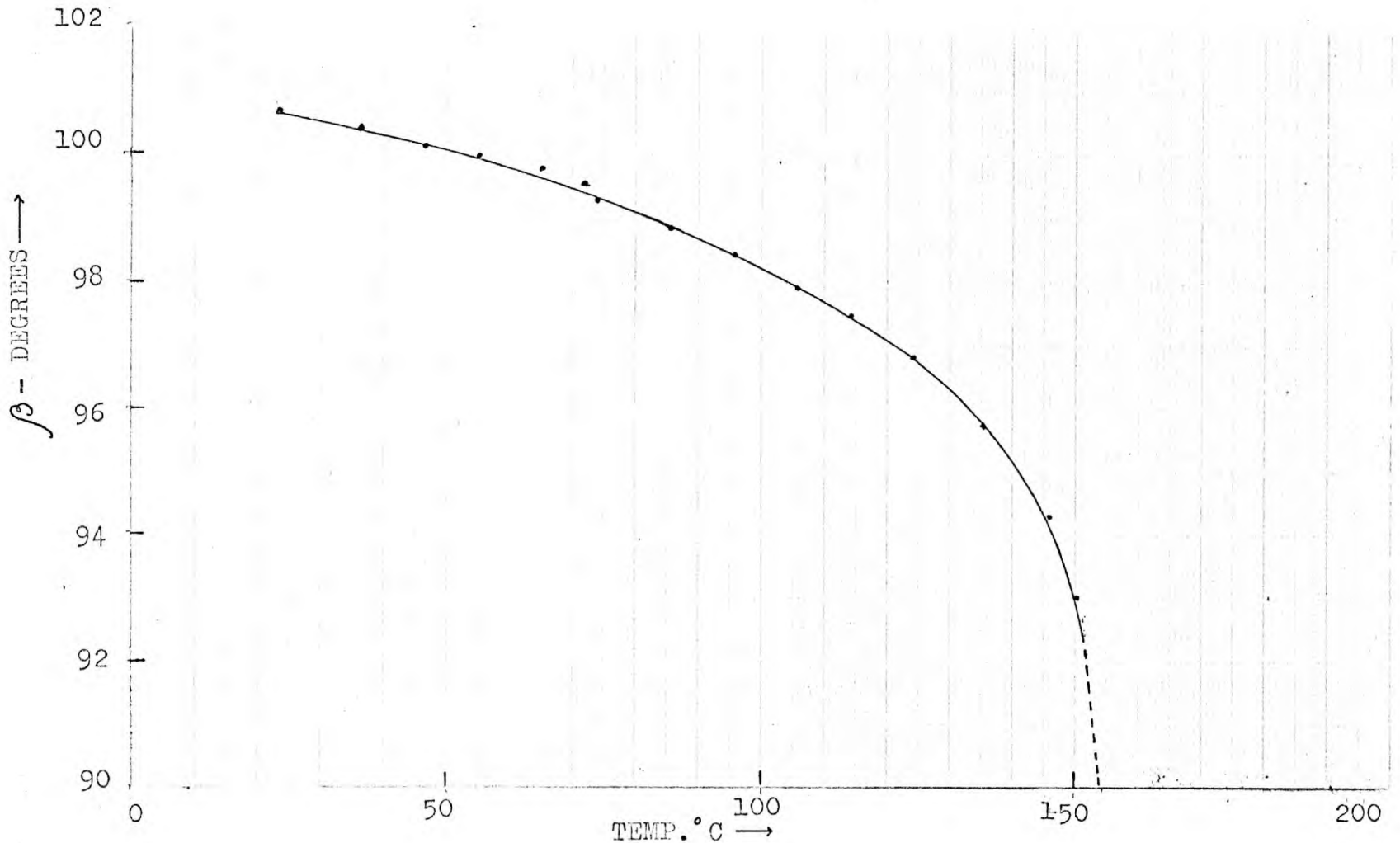

(Nunerical data given in Appendix)

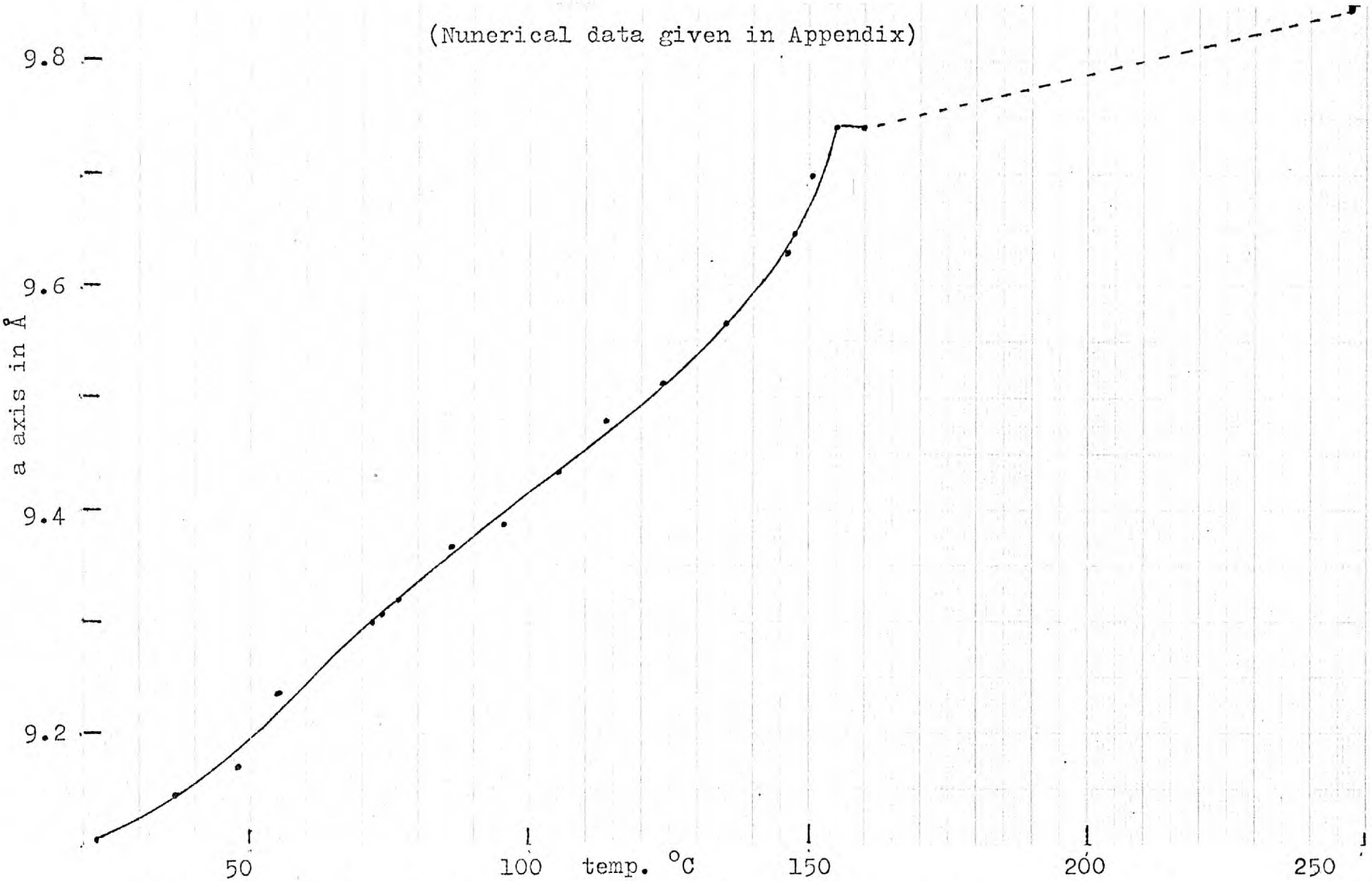

Fig.30. Variation of a axis with temperature (sample: potassium acetate)

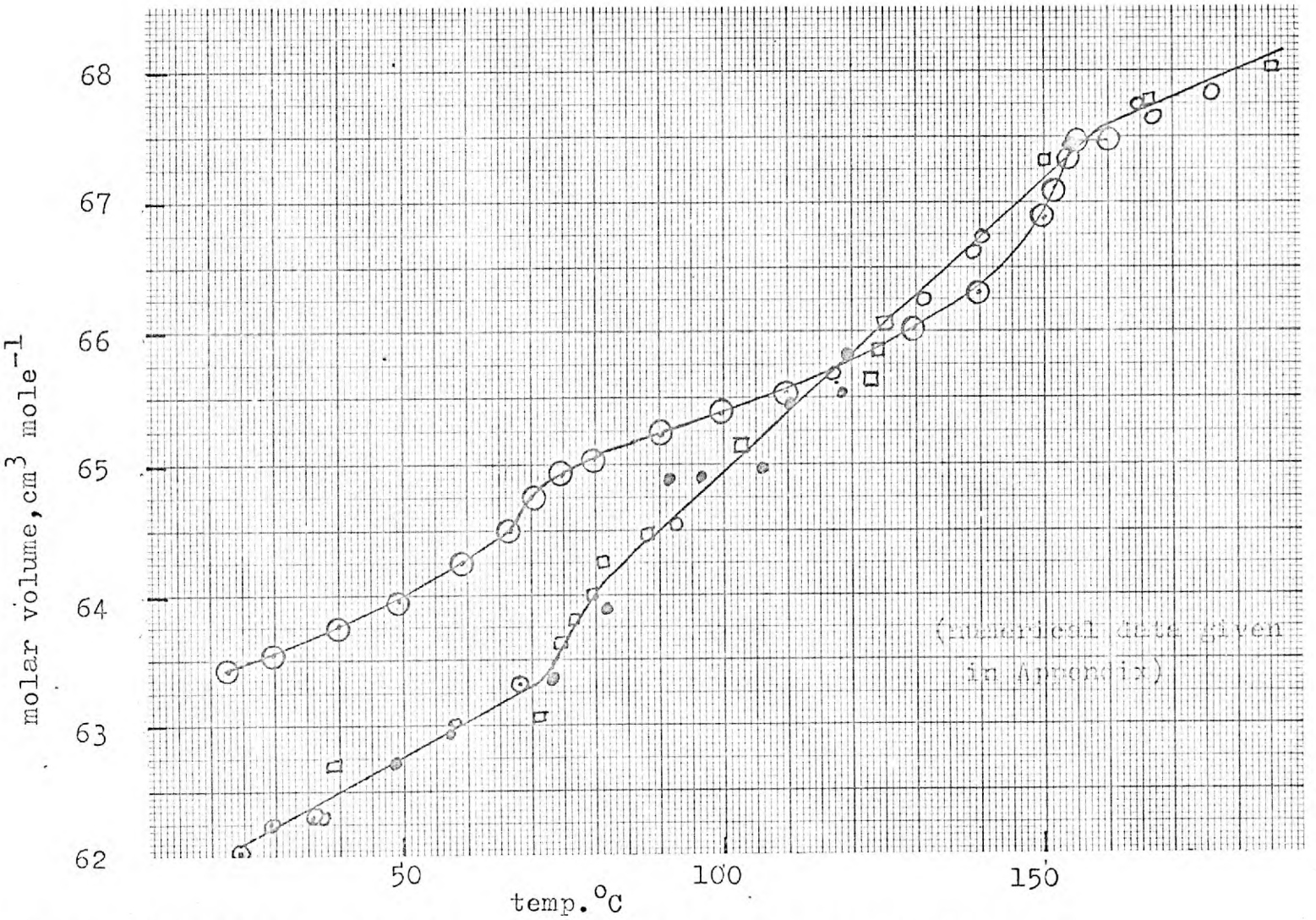

Fig.31. Comparision of molar volumes:-⊙-⊙- X-ray; ○—□—● dilatometer.
(sample: potassium acetate)

cause of the irreproducibility was thought to be slight differences in the positioning of the film within the film holder leading to an uncertainty in the value of the effective camera radius. On the basis of all available evidence, the relative accuracy of these results appears to be about 0.005 Å in a spacing of 4 Å. The absolute accuracy is unknown but is unlikely to be better than 1%.

From the graphs of cell dimensions (Fig. 26, 27, 28 and 29), values of d_{100}, d_{010}, d_{001} and β were intrapolated at regular intervals of temperature. Then the cell volumes $V = (d_{100} \cdot b \cdot c)$ were determined over the temperature range 23°C - 160°C. For comparison with the dilatometric data of Hazlewood et al. these unit cell volumes were converted to molar volumes by multiplying by N/2. The two curves are shown in Fig.31, where it can be seen that the only point of detailed agreement is the density of form I at 160°C.

It should be noted that dilatometric graph is an average one of the heating and cooling cycles of two samples whereas the present data were obtained only while the crystal was being cooled, so a comparison is not justified. Nevertheless studies of the structural hysteresis (next Section) suggest that an average X-ray curve of heating and cooling cycles might follow a different path, narrowing the differences between the two curves. Of greater significance probably is that the dilatometric measurements give the macroscopic expansion of polycrystalline samples having a mass

of about 3 g whereas the present measurement relates to the lattice parameters of a single crystal of mass ($\sim 8 \times 10^{-6}$ g). But it is not clear why the macroscopic volumes should be smaller than those found using X-rays. While Schottky defect formation on heating, will effect the thermal expansion[48], it would predict that the macroscopic volumes should be larger than the microscopic values. Further comment on the origin of this discrepancy is deferred to Chapter 6.

From these graphs it is evident that the a-axis expands rather rapidly from room temperature to 155°C, but the rate of increase is less when the crystal has undergone the transformation II $\longrightarrow$ I. The diffraction photograph taken at 247°C shows that a = 9.583 Å an increase of 0.109 Å from its value at 155°C giving an estimated thermal expansion between these temperatures of α_a(average) 155° - 247°C $\sim 150 \times 10^{-6}$ C deg^{-1}.

It is apparent that no such average figure can be given for the expansion of the a-axis over the entire temperature range from 23°C to 155°C. The overall thermal expansion can be represented only graphically (Fig.32).

Rather surprisingly, the two other axes contract on heating. The slight c-axis contraction $\alpha_c \simeq -40 \times 10^{-6}$ C deg.$^{-1}$ remained approximately constant up to 155°C, but the value at 247°C indicated that α_c becomes positive between 155° and 247°C.

The variation of b is more complex (Fig.33). From room temperature to about 68°C, the axis contracted with an average

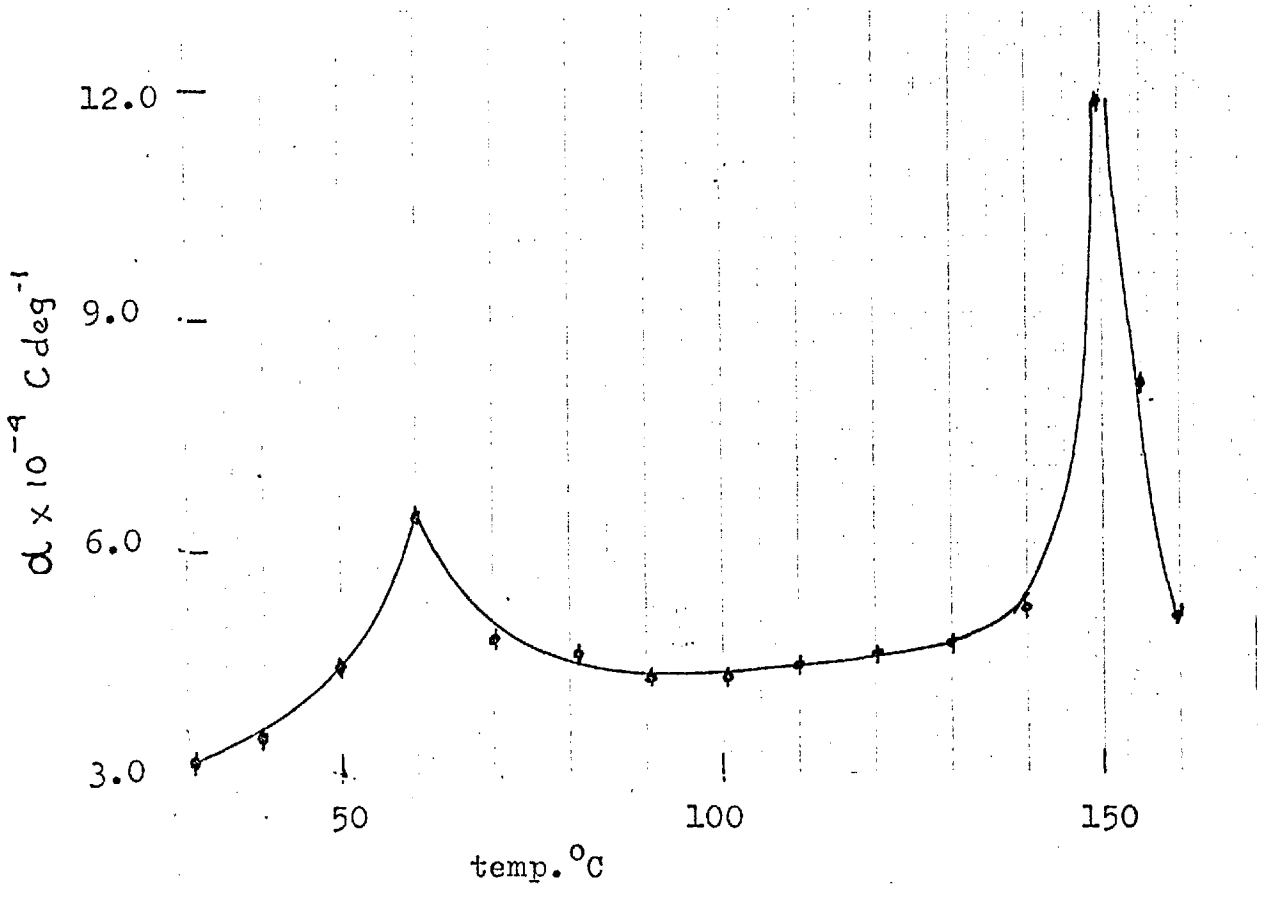

Fig.32. The coefficients of thermal expansion of potassium acetate along a-axis.

coefficient $\alpha_b \approx -10 \times 10^{-6}$ C deg.$^{-1}$. Then at the transformation III $\longrightarrow$ II, there is a rapid but continuous expansion followed by a contraction after about 75°C. This contraction continues up to 200°C and shows no discontinuity at transition II $\rightleftharpoons$ I. The average coefficient of expansion in this temperature range is $\alpha_b \sim -100 \times 10^{-6}$ C deg.$^{-1}$.

The monoclinic angle β determined by the method given above decreases continuously with increasing temperature up to 150.3°C. Above this temperature the β angle is increasing very rapidly; the observations are reported in the next section. Above this temperature, β was estimated by plotting the separation of the doublet from room temperature to 150.3°C against the values of β subsequently deduced and extrapolating the resulting straight line to 90° (Fig. 34).

2.10. Transition Temperatures, Hysteresis and Persistence of Axes

As has been stated only three polymorphs (involving two solid-solid transitions) have been detected by the present X-ray methods, compared to the four polymorphs proposed from the dilatometric study[7]. Once the characteristic features in the changes in the diffraction patterns for the two transitions were understood, it became possible to explore the crystallographic behaviour in the vicinity of the transition temperatures by taking diffraction photographs at small temperature intervals. Using a crystal of dimensions 0.5 x 0.1 x 0.1 mm, the transformations

form II $\rightarrow$ form I, from monoclinic (twinned) to orthorhombic (single crystal) diffraction pattern was followed during a thermal cycle form II $\underset{\text{cooling}}{\overset{\text{heating}}{\rightleftharpoons}}$ form I, by noting the separation of 401 and $40\bar{1}$ and 301 and $30\bar{1}$ doublets obtained from the two orientations of the twin in the zero layer of the b-axis photographs. On heating, the doublets coalesced, at 154.3°C to form the 401 and 301 reflexions of the orthorhombic form I. On cooling, the single reflexion split into two components at 153.1°C. Thus, there was hysteresis of about a degree wide in the transformation. The co-existence of the two forms at a single temperature could not be verified because of the temperature gradient (about 0.1°C/mm) between different parts of the crystal, the upper part being always hotter than the lower. There was no doubt, however, that the two forms could co-exist within one hybrid crystal, for, the separation of the hol and $ho\bar{l}$ was variable through the composite diffraction spot (Fig.24), some one or two degrees before the transition. The inclination of the two reflexions defining the β angle in form II suggests that in this temperature range the angle is continuously variable in one part of the crystal and is co-existing with another part of the crystal that has already completed its transformation to form I. For practical reasons the minimum observable separation of hol and $ho\bar{l}$ corresponded to a β of 93.1° but there was no indication of any discontinuity in β as it approached 90°.

The progress of the transition III $\longrightarrow$ II could be followed by observing the weak layer lines with k odd, obtained at room temperature b-axis photographs. These grow weaker in intensity with rise of temperature and finally disappear at the transition temperature. Using the same crystal, the reduction in the intensity of the reflexions $\{710\}_{III}$ and $\{510\}_{III}$, which were relatively strong in relation to other reflexions in the layer line, was observed. On heating, these could not be observed at 75°C and reappeared on cooling at about 68°C. With another smaller crystal ($\sim .08$ mm^2), the reflexions disappeared between 85°C and 95°C on heating, but did not appear even at 65°C on cooling. Thus, the transition III $\longrightarrow$ II probably has no well defined transition temperature, but depends on the particular crystal used. Size and perfection of the crystal is likely to be important, for, with the smaller and more perfect crystal, the hysteresis in the transition temperature was very much greater than that found with the bigger crystal. Defects may also play some part. The greater perfection of the small crystal was indicated by the absence of slight θ-arcing of the reflexions in some orientations. The thermal history of both crystals was effectively the same, both having passed through several thermal cycles.

The similarity in the appearance of these additional reflexions with the superlattice reflexions in ordered alloys (mentioned in Chapter 1 and discussed in detail in Chapter 4) suggests that two

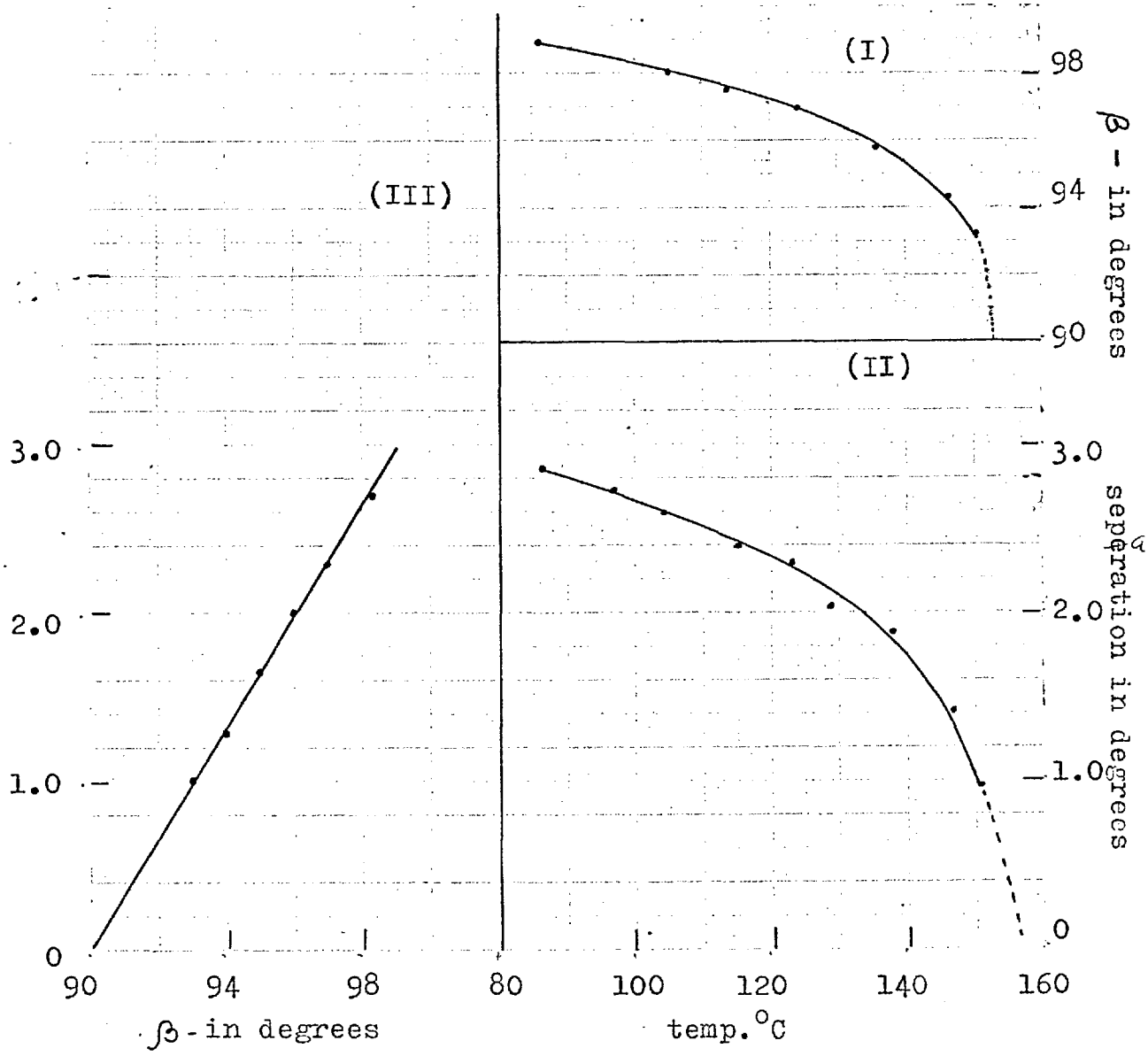

Fig.34. Curves to obtain extrapolated value of
(I) β - vs. temp.
(II) Separation (in degrees) vs. temp.
(III) Separation (... ...) vs. β

* seperation means the seperation of 301-30$\bar{1}$ reflexions.

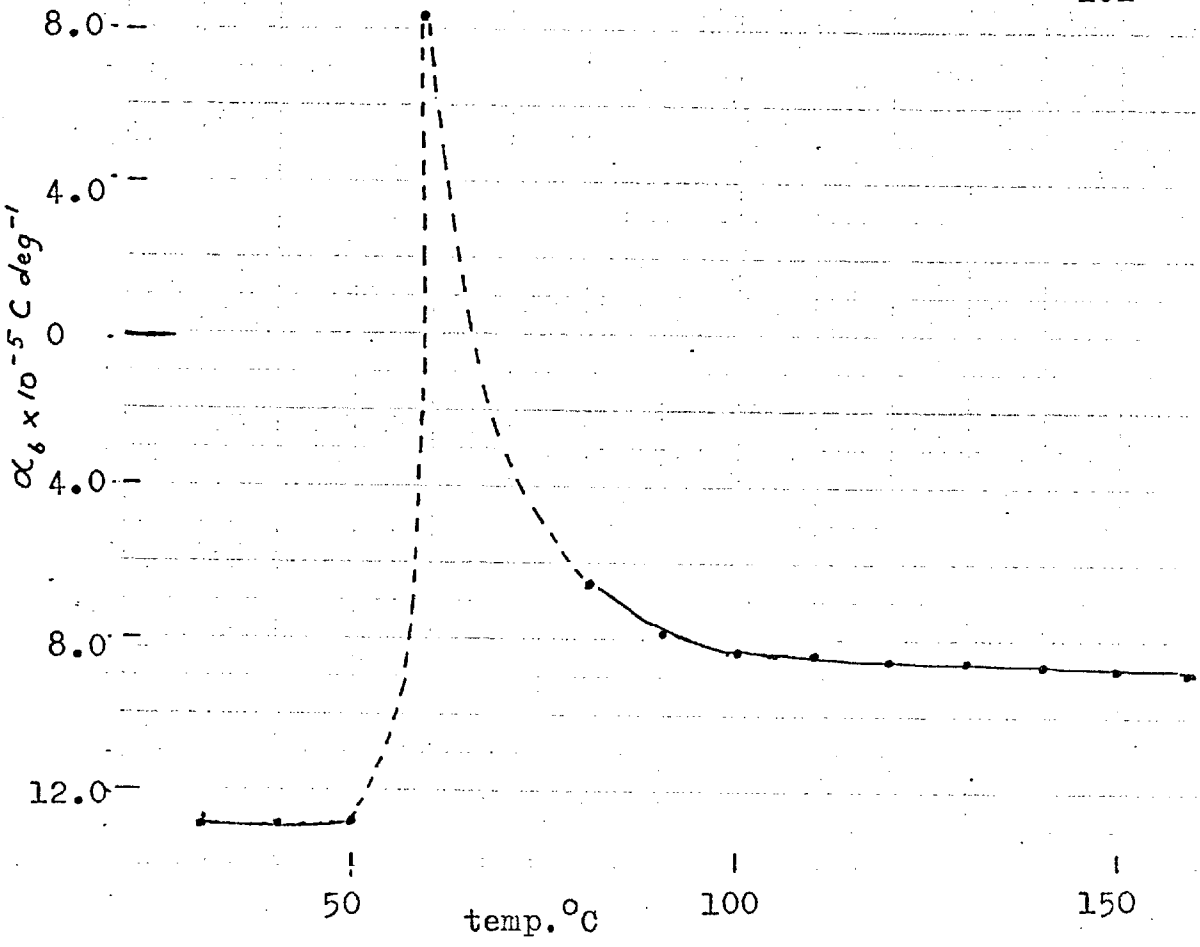

Fig.33. Co-efficient of thermal expansion of b axis of potassium acetate.

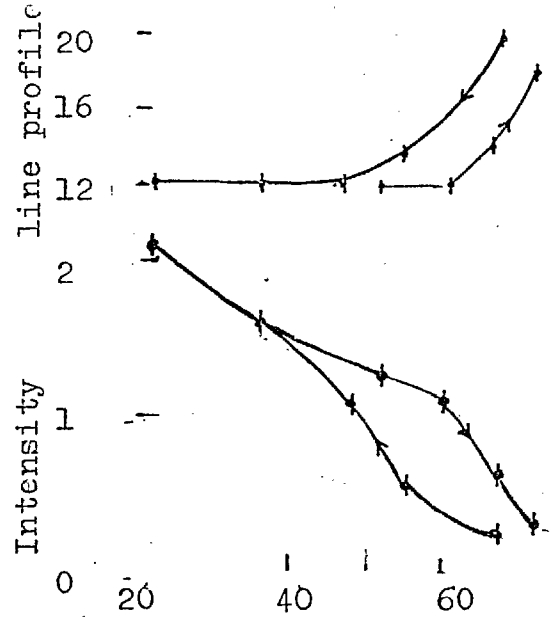

Fig.35. . Intensity and line profile vs. temperature of the 710 reflexion in the additional layer line of potassium acetate (form III).

features relating to the degree of order (if any) in the structure deserve further study. These are the integrated intensity and line profile of the additional reflexions. These two quantities may be taken to indicate the physical state of the sample. Photographic recording can only give relative intensity data. The intensity of the 710 reflexion was therefore placed on a comparative scale by comparing its intensity with that of the $CuK\beta$ reflexion from 400 which occurred at roughly the same Bragg angle and was of a convenient intensity. Although there was no justification for assuming that the intensity of 400 remained constant the intensity ratio must still be characteristic of the state of the sample.

Valu s of this ratio I(710)/I(400β) were plotted against temperature during both heating and cooling (Fig.35). The integrated intensity was taken as the product of the half widths and the heights of the photometer traces through the reflexions. The curve relating the half breadth of the line profile with temperature is also plotted in Fig.35. It is of interest to note that there is a significant change in intensity before there is any change in the breadth of the reflexion.

The following points can be made from these graphs:

(1) The progressive broadening means that the transformation temperature will be impossible to detect by X-ray diffraction alone.

(2) The intensity and profile do not change together as in the order disorder transformation in alloys.

(3) The intensity curve differs fundamentally from that found in order-disorder in alloys.

(4) The maximum width of the hysteresis loop was about 15°C.

Thus, in neither of the transformations were any discontinuities in the diffraction patterns observed. Intensity and positional changes of diffraction spots, all occur smoothly and continuously.

Chapter 3

A. DIELECTRIC PROPERTIES OF POTASSIUM ACETATE

3.1. Introduction

3.1.1. Polarisation in homogeneous materials. Measurements of the dielectric properties of a material give information about the structural behaviour of the dielectric. The electrons in a dielectric cannot generally leave the atoms or molecules to which they are bound. An external electric field applied to the material by means of condenser plates can, however, cause relative displacements of the electrons and atomic nuclei, thus polarising the atoms.

In addition to electronic polarisation, the external field tends to orient molecules having permanent dipole moments so that the dipole is aligned along the field direction. The field may also change the interatomic or interionic distances and bond angles. Thus, with molecules with permanent dipole moments,

total polarisation $P = P_{electronic} + P_{atomic} + P_{orientational}$.

Polarisation is related to the static (or low frequency) dielectric constant through the equation:

$$\frac{\epsilon - 1}{\epsilon + 2} \cdot \frac{M}{d} = P = \frac{4\pi N}{3} \alpha = \frac{4\pi N}{3} \left(\alpha_o + \frac{\mu^2}{3kT}\right)$$

where: ϵ is the static dielectric constant; M is the molecular weight; d is the density, N is Avogadro's number; α_o is the polarizability of electronic and atomic distortion; μ is the permanent dipole moment, k, the Boltzmann constant and T, the absolute temperature.

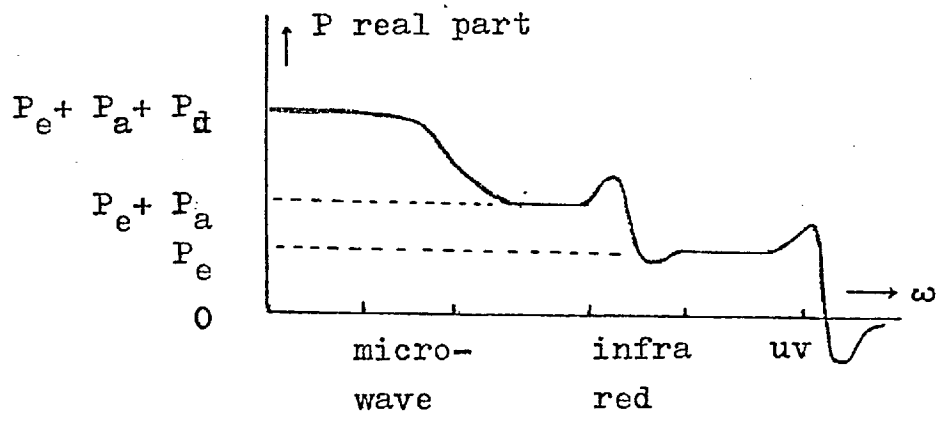

Fig.36. Schematic diagram showing the contributions of different polarisation to the total polarization (reproduced from Dekkar's "Solid State Physics")

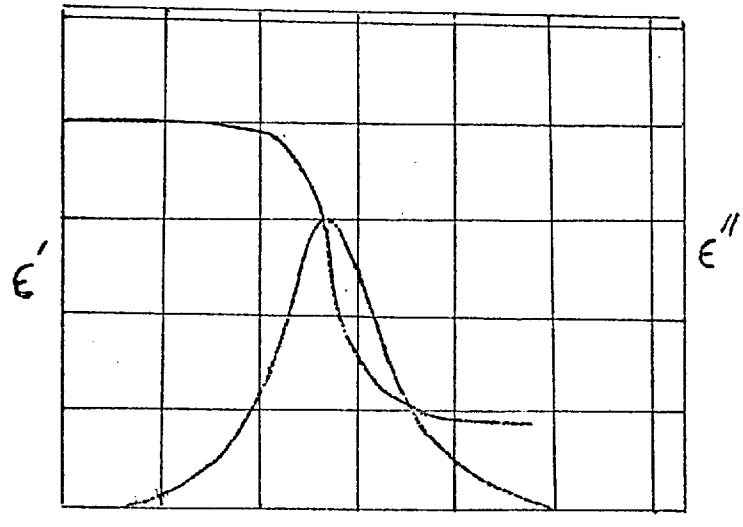

Fig.37. Schematic representation of Debye relaxation

From this equation, it is evident that the total polarization P decreases with increasing temperature because of the decrease in the orientation of molecules along the field.

When a low-frequency alternating electric field is applied, the polarization of electrons, atoms, ions or dipoles tend to follow the field and contribute to the total polarization. As the frequency becomes higher, the polarization cannot follow the field and there is an observable lag in attaining equilibrium. This lag in response to the stimulus (here, the field) is known as relaxation. Generally, up to about 10^{10} Hz, the electronic, atomic or orientation effects, all contribute to the total polarization. With increasing frequency the orientation contribution ceases. Between 10^{12}-10^{14} Hz the atomic contribution also ceases. Up to about 10^{15} Hz the only contribution is from the electronic polarization. Contributions for different sources are shown in Fig.36, where total polarisation is plotted against log frequency.

In a real dielectric placed in an alternating field, some energy is always absorbed and dissipated as heat. The displacement current of a condenser with an alternating field has therefore two components. One is the loss or ohmic current which is in phase with the field and given by $E\omega\epsilon''C_o$ and the other component is 90^o out of phase with the alternating potential charging current and is given by $E\omega\epsilon'C_o$. These two components form the complex dielectric constant $\epsilon^* = \epsilon' - i\,\epsilon''$ giving rise to two dielectric constants ϵ' and ϵ''. This complex dielectric constant is $(90 - \delta)^o$ out of phase with the field, where δ, the loss angle is given by $\tan^{-1} \epsilon''/\epsilon'$. The two dielectric constants

vary with frequency according to the Debye equations,

$$\epsilon' = \epsilon_\infty + \frac{\epsilon_o - \epsilon_\infty}{1 + \omega^2\tau^2}$$

$$\epsilon'' = \frac{(\epsilon_o - \epsilon_\infty)\,\omega\tau}{1 + \omega^2\tau^2}$$

Here ω is the angular frequency and ϵ_∞ and ϵ_o are the dielectric constants at high and low frequency respectively. τ is defined by the equation,

$$\alpha(t) = \alpha(o)\, e^{-t/\tau}$$

where $\alpha(t)$ represents the decay (or rise) of polarization after a sudden removal (or application) of a field with steady polarization $\alpha(o)$ (or with zero polarization). When time $t = \tau$ $\alpha(t)/\alpha(o) = \frac{1}{e}$ i.e. τ is the period of time during which the polarization changes to 1/e of its initial value. τ is known as the relaxation time. The variation of ϵ' and ϵ'' with frequency predicted by the Debye equations is shown schematically in Fig.37. The equation of ϵ'' shows that $\epsilon'' \rightarrow 0$ for large and small values of $\omega\tau$ and is maximum for $\omega\tau = 1$ or $\tau = 1/\omega_{max}$. In the case of non spherical molecules, orientation about different axes should require different relaxation times[49].

In solids, the orientational or rotational freedom is normally small and the value of the dielectric constant is around 2 or 3. Losses are also generally small. In some solids, however, polar

molecules can acquire rotational freedom, i.e. they possess sufficient energy to overcome the potential barriers and move from one equilibrium position to another. Examples are known of molecules showing rotational freedom on or before melting and during orientational order-disorder transformation in solids. The onset of rotation of a symmetrical group in a crystal should not effect the dielectric constant values apart from that due to the slight change in density[50].

3.1.2. Interfacial polarization in Heterogeneous materials.

In addition to the contributions to the total polarization from the sources given above, there is another type of polarization; this is interfacial or Maxwell-Wagner polarisation[51] in heterogeneous dielectrics with more than one phase. For such polarization to take place, the phases must have different dielectric constants and D.C. electrical conductivities. It is commonly associated with the presence of conducting impurities, dislocations, vacant sites etc, which form interfaces. If there are free charge carriers (electrons, ions) migrating through the crystal, they may pile up against a defect or be trapped by it. This localised accumulation of charge will induce opposite charges on the electrodes and contribute to the total polarization. This accumulation of charge requires flow of current through the dielectric which may require a very short time if one phase has high conductivity, or may require seconds or minutes. Therefore, this polarization is observable generally in the very low frequency range, but may also occur at even radio frequencies.

The variation of ϵ' of a two phase dielectric with frequency follows precisely the same relaxation equation as before, but the variation of ϵ'' is different. For a simple two phase model[52], it is given by:

$$\epsilon'' = \frac{9v(\epsilon_1')^2}{2\epsilon_1' + \epsilon_2'} \cdot \frac{\omega\tau}{1+\omega^2\tau^2}$$

where v is the volume fraction of conducting impurity present in the mixture, ϵ_1' is the real part of the relative permittivity of the material and ϵ_2' is the real part of the relative permittivity of the impurity phase.

Hamon[53] dispersed some copper phthalocyanine and liquid n-primary alcohols in paraffin wax and obtained the graphs shown in Fig.37a, from measurement of the loss factor ϵ''. It will be seen that as the frequency decreases the d.c. conductance increases.

3.1.3. Ferroelectrics. There is a special class of crystals, whose permittivity increases to very high values because of the distortion of the atoms of particular molecular groups. These are polar crystals within the pyroelectric class of crystals, the direction of the spontaneous polarisation of which can be reversed under the influence of a sufficiently strong applied field. In these crystals the permittivity increases with increasing temperature and at the transition from a ferro to a para electric phase, there is a large increase followed by a fall to a lower value.

Spontaneous polarization in ferroelectrics leads to domain formation. In these domains all the dipoles are parallel to each other. An external field applied to such a crystal tends to align the domains along the field. With increasing temperature, domains grow co-operatively and the ferro-para electric transition is the culmination of this growth process, when the crystal is on the point of moving out of the region of spontaneous polarization due to thermal agitation. The applied field at that temperature is able to produce relatively large shifts with big changes in permittivity.

3.2. The Measurement of Capacity and Conductance

3.2.1. Theoretical. It is usual to use alternating fields for the measurement of dielectric properties. The most convenient frequency range for such measurements lies between 10^{-2} Hz to 10^{7} Hz, because the impedance of the condenser containing the dielectric can be balanced against known combination of discrete capacitances, resistances etc. For higher frequencies, a circuit can no longer be represented by discrete circuit elements and the connecting wires cannot be considered as free of inductance and capacitance, so they are considered as distributed impedances and complicated circuits have to be devised for measurements in that range.

With increasing frequency, sources of error in the measurement also increase. Imperfectly clean electrodes, imperfect contacts, voids in the dielectric etc become increasingly important with increasing frequency. Imperfect contact and unclean electrodes act

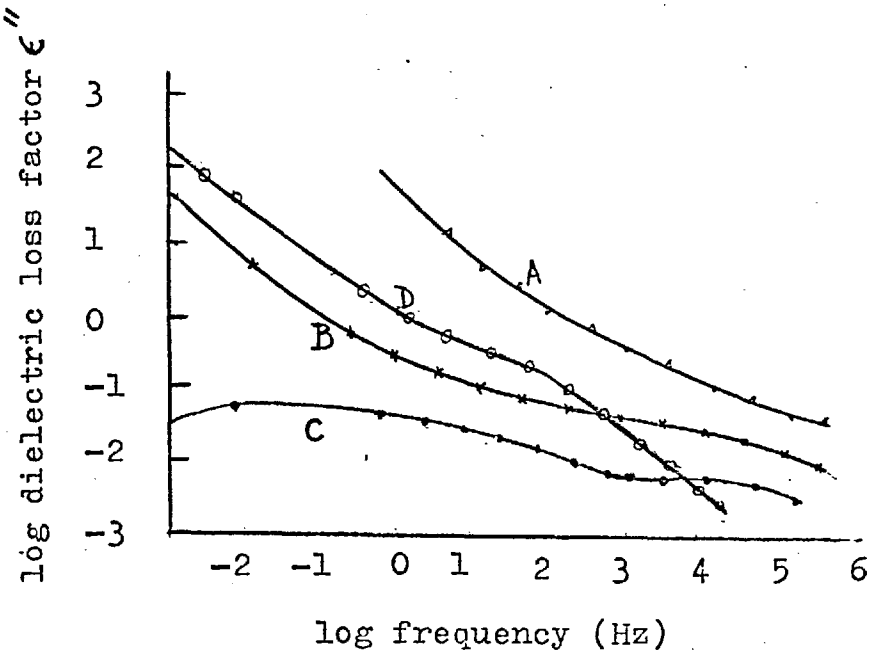

Fig.37(a) Plot of $\log \epsilon''$ vs. log frequency showing D.C. conductivity and interfacial polarisation absorption due to conducting inclusions in a dielectric. Curves A, B, C : 1.9,0.62,0.19 per cent by vol. respectively of copper phthalocyanine and curve D: 1 p.c. n-decyl alcohol dispersed in paraffin wax(after Hamon[53]).

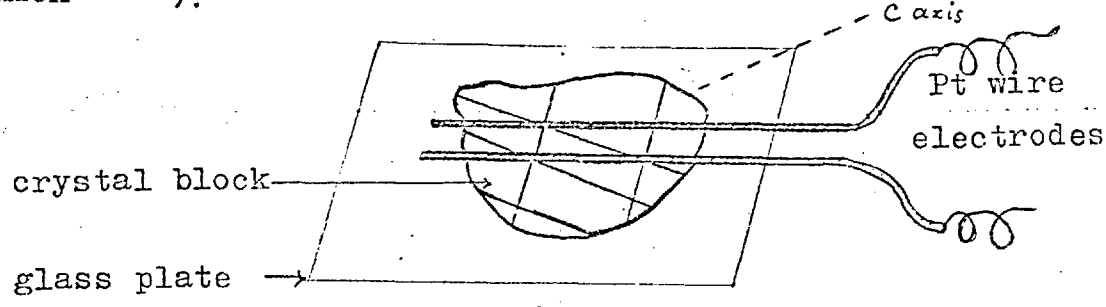

Fig.41. Dielectric cell for measurement of capacitance and conductance along b and c axes of potassium acetate multicrystalline block.

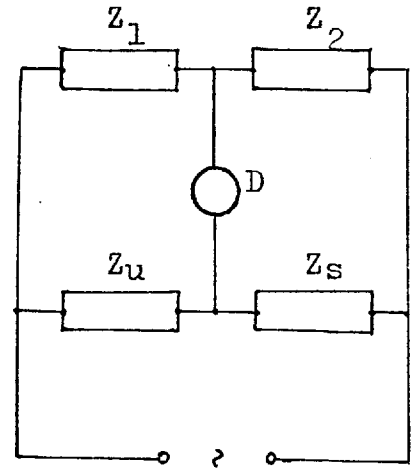

Fig.38. Comparision of impedances in a Wheatstone a.c. bridge.

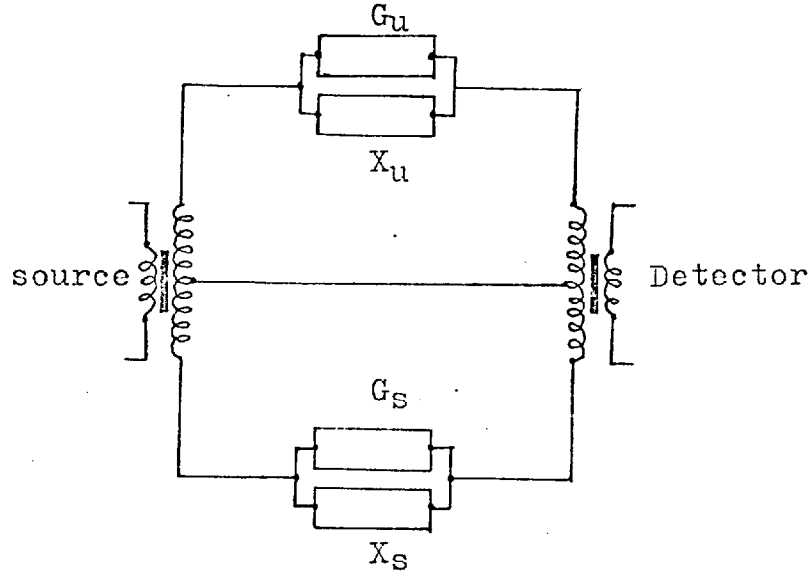

Fig.39. Practical arrangement of the Transformer ratio-Arm Bridge.

as series resistances on the circuit and introduce errors in the measured values of conductance. At very high frequencies, the shapes of the specimen also effect the measurement.

For reasons stated above, the measurements were restricted to a frequency range 500 - 20,000 Hz. The equipment comprised

(1) An A.C. Bridge

(2) A generator

(3) A detector.

(1) The working principle of the ratio-arm bridge can be explained by reference to the simple Wheatstone bridge (Fig.38).

The four arms of the bridge consist of two standard impedances Z_1 and Z_2 whose ratio Z_1/Z_2 can be varied in decade steps, the unknown impedance Z_u which is to be measured and a variable standard impedance Z_s which can be adjusted to balance the bridge.

In the commercial bridge employed (Wayne Kerr Model B221), the source and detector were isolated from the bridge circuit by the use of transformers (Fig.39). In practice, the impedances are divided into their resistive and reactive components as indicated in the figure.

The bridge measures directly capacitance C_p and conductance G_p as a parallel combination.

The range of measurement of the bridge was

C_p, 0.002 pF - 11.1 μF

G_p, 0.00002 μmho - 10 mmho.

The nominal accuracy of the measurements of the bridge was $\pm$ 0.1%.

To minimise the effect of external connections, a low capacity cable was used to link the experimental condenser cell to the bridge. Care was taken to ensure that the disposition of the cables remained unchanged during a series of measurements. Even a small movement of these leads changed the measured capacity to some extent.

(2) The frequency of the internal generator of the bridge was fixed at 1592 Hz so that angular frequency $w = 2\pi f = 10^4$ rad s^{-1}.

For other frequencies, an oscillator generating frequencies in the range 200 Hz - 30 kHz, was used. Below 500 Hz the output wave form was significantly distorted. The upper frequency limit of 20 kHz was imposed by the design of the bridge.

(3) When using the internal generator, the detector system consisted of a two stage amplifier circuit. A double-shadow 'magic eye' is connected to each stage. Balance was indicated by maximum shadow. These were tuned to the generated frequency and for other frequencies were replaced by a cathode ray oscilloscope in which was displayed the off-balance voltage of the bridge. The amplitude of this display was minimised at the balance point. This detector imposed a lower limit of 1% on the accuracy with which low values of the conductance could be measured.

3.2.2. Preliminary experimental work and Dielectric cells.

Initially dried powdered potassium acetate was melted between two small circular brass plates which were connected to the equipment described in the previous section. When the condenser was placed on a small

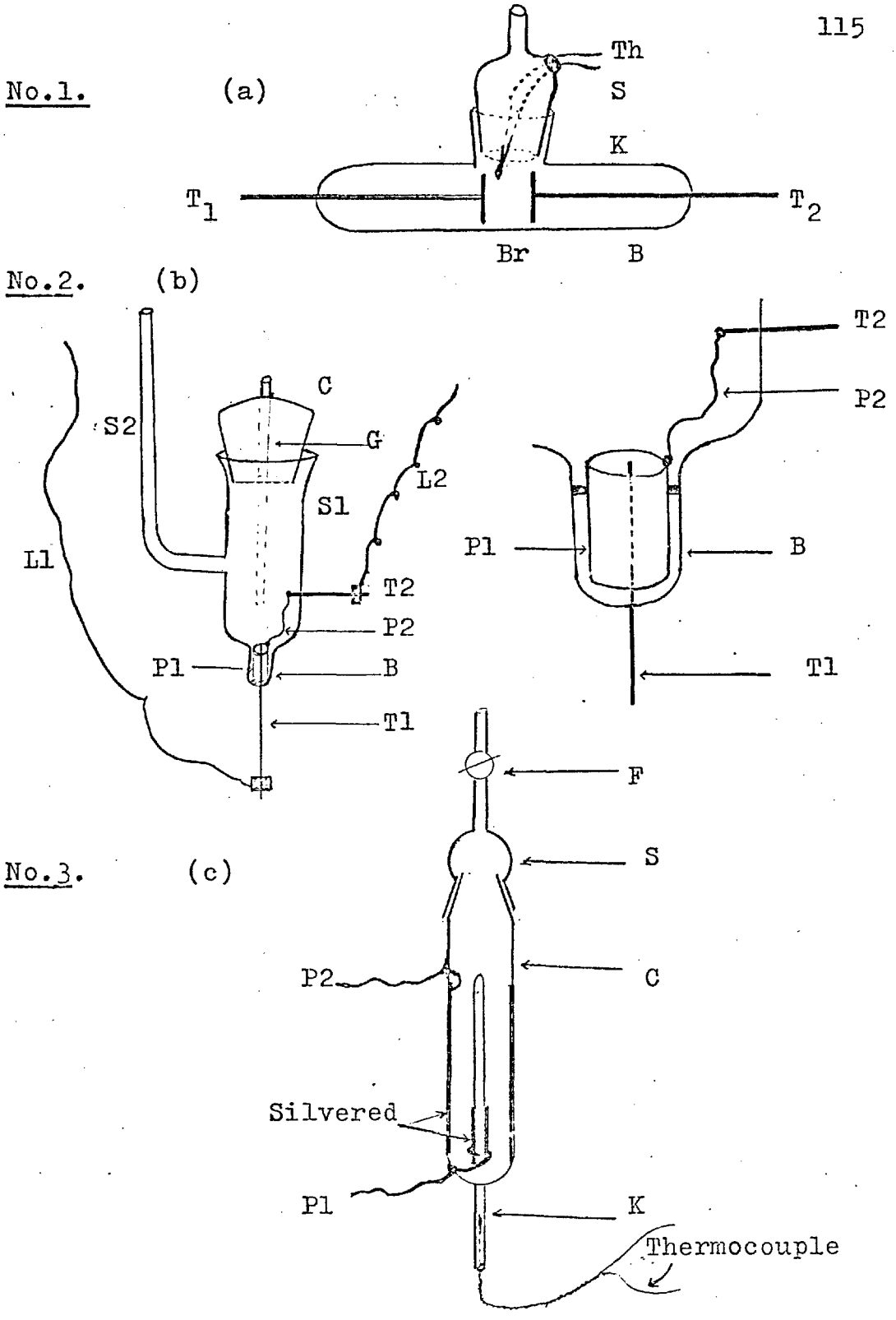

Fig.40. Dielectric cells (a) Cell No. 1 (b) Cell No. 2 (c) Cell No. 3.

heater, both the capacity and conductance of the condenser were found to increase very rapidly when the temperature rose to about 150°C. The temperature fluctuations of this heater were high and moisture attacked the sample as soon as it was cooled. It was, therefore, decided to design dielectric cells which could be evacuated.

Dielectric cell No.1. This was in the form of a glass tube G closed at both ends (Fig. 40a). A socket joint K was inserted into the middle of the tube which could be sealed by a mating cone-joint S and vacuum tap. For measurement of sample temperature, a thermocouple Th was inserted through a small hole on the cone S, so that the thermocouple junction was as close to the condenser plates as possible. The hole was later sealed by a paste of alumina cement with waterglass. Two brass electrodes were welded on to the tungsten rods T1 and T2 which passed through the glass and formed the electrical connections. The cell was thoroughly cleaned before use. Dry powder was packed into the tube, through the socket which was then closed by the cone and the far end of the vacuum tap connected to the vacuum system by pressure tubing. The tungsten rods were connected to the bridge via the low capacity leads. A flexible heater wire was wound round the cell and connected to a Variac. The dielectric behaviour of the sample was observed as before.

This cell has two disadvantages: the temperature of the sample fluctuated by several degrees and the values of the measured capacity and conductance were sensitive to the positions of the heating coil round the cell. To overcome the temperature fluctuations it was

decided to use a thermostatically controlled oil bath. This meant that the design of the cell had to be changed so that it could be submerged under oil without contaminating the sample. Two further cells were therefore designed.

Cell No.2 This was constructed in the form of a cylinder S1 sealed at one end with a side tube S2, bent at right angles which is then connected to the vacuum system (Fig. 40b). The sealed end was drawn to form an elongated bulb B. The open end was closed by a cone-stopper C, through which a small glass tube G closed at one end was inserted and joined so that a thermocouple could be introduced as near to the sample as practicable. T1 was the tungsten rod sealed vertically through the bulb B. Around T1 was a platinum tube P1 which together with T1 formed a co-axial cylindrical condenser. P1 was connected to a horizontal tungsten rod T2 with a short piece of platimum wire P2, by fusing the ends. T1 and T2 were at right angles, so their contribution to the capacity is nil. Thick copper leads were screwed to T1 and T2 for connections to the low capacity cables of the A.C. bridge.

This cell has the advantage that it could be submerged in the oil to keep the temperature steady. There was a slight lag in reaching thermal equilibrium across the cell: this took less than 10 seconds at the highest temperature of measurement and the maximum temperature difference between the inside of the condenser and the oil outside was not more than one degree. With the increase in temperature the drift of the balance point could be followed and the maximum value of capacity and conductance was always recorded when the sample had attained thermal equilibrium with the bath.

Cell No.3 The third cell was specially constructed to allow the sample to be dried to constant weight while still allowing the capacitance and conductance to be measured. This was also in the form of a cylindrical condenser but the central electrode was hollow allowing a thermocouple to be inserted. For ease of construction, the cell was made of glass and subsequently silvered to provide the electrodes. Accurate dielectric measurements were made as before in the oil bath but the cell could be removed and a separate electric heater used for the drying experiments: the relative changes in the capacity and conductance could still be monitored during these drying experiments.

A small bore (2 mm) glass tube K sealed at one end forms the inner cylinder of the condenser. The outer cylinder C was a glass tube of about half an inch diameter. K was fixed concentrically to C by fusing at the bottom end as shown in Fig.40c. The open end of C was a cone on to which was fitted a socket S, joined to a tap F through which the cell was connected to the vacuum system. Two platinum wires P1 and P2 passed through the wall of the tube C, one near the bottom and the other some 5 cm above, served as electrical connections to the electrodes. The inside ends of the wires were bent to proper shape so that P1 connected to the inner cylinder and P2 to the inside wall of the outer cylinder firmly.

Pieces of wax were introduced into C and melted at the bottom so that the level of molten wax was below the end of platinum wire P1. Tube K was covered by a cellophane tube so that except a gap of about a cm on the surface of K, above the level of wax, the whole surface

of K was kept covered. Solutions for silvering were poured down up to a level where P2 contacts the tube. After silvering, the cellophane was removed and the wax was dissolved away by solvents and the cell was properly cleaned.

The capacity of cell No.3 with the sample inside was about 1 pF.

Modified Cell No.3 In view of the low capacity of the cells, at 1592 Hz, the capacity of cell No.3 was increased after the drying experiments by silvering the whole of the inside electrode K, as a precaution against having any low values below the range of the bridge at some frequencies.

This precaution was unnecessary, at least with samples other than potassium acetate where the measurements could be done with cell No.2 at all frequencies without any inconvenience.

Arrangements for Study of Anisotropic Dielectric Behaviour

An attempt was made to examine roughly any anisotropy in the dielectric behaviour of a single crystal of potassium acetate. On a glass plate placed over the microscope hot stage a little dried powder was melted in between two fine platinum wires held close together (Fig.41). The resulting solid was not a single crystal but was multi-crystalline with b and c axes oriented as shown in the figure. The platinum wires were connected to the bridge by the low capacity cables. The temperature was measured by a thermocouple with one junction placed inside the solid mass; temperature variations were about $\pm 5^{\circ}C$.

To examine the a-axis anisotropy, a little powder was melted in between two gold foils, which were used as electrodes. Measurements were taken as before.

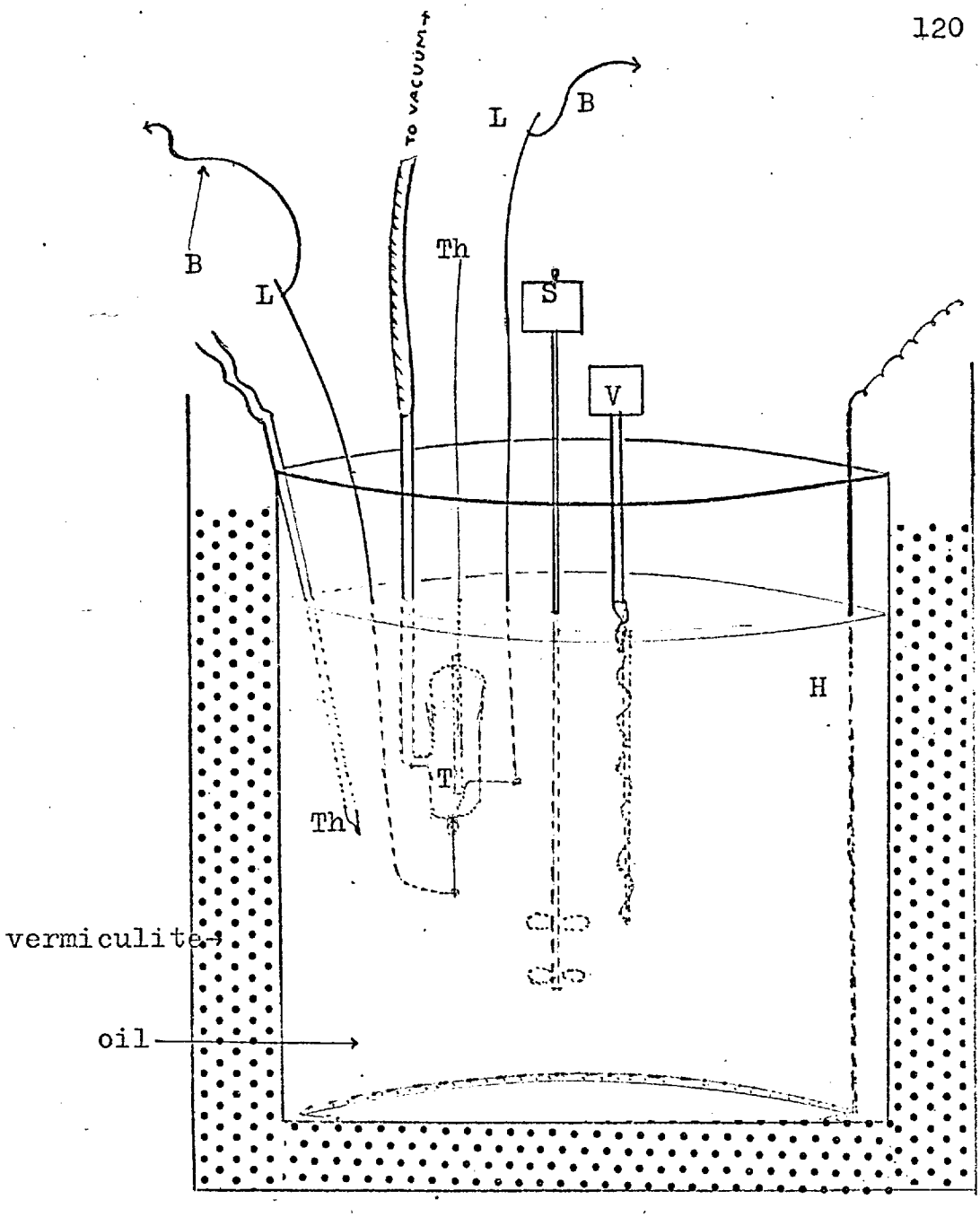

Fig.42. The oil bath for temperature control in dielectric measurements (description in the text)

3.2.3. Method of Achieving Temperature Control. The oil bath mentioned earlier was used to keep the temperature of the dielectric cell steady. At room temperature, the hydrocarbon oil used was very viscous but the viscosity diminished very rapidly with temperature and above about 80°C was quite low. It was capable of withstanding temperatures up to about 200°C without decomposition and up to 250°C with some decomposition. About 3500 ml of the oil was placed in a 5 litre beaker. The beaker was kept inside a bigger metal drum and the space between the outside of the beaker and the inside of the drum was filled with expanded granules of vermiculite. A 2 kW heater H immersed in the oil was connected to a Sunvic bimetallic temperature sensing element V with a sensitivity of ± 0.5°C. A stirrer S whose speed could be controlled, was fixed between the heater and the bimetallic strip V. The arrangement is shown in Fig.42. The thermocouple was placed as near to the sample T as possible. T was clamped in position and the electrical connections were made.

The temperature control was set at a particular temperature and it controlled the temperature of the oil-bath by making and breaking the heater circuit. The bath temperature could then be varied through ± 10° at 1°C inervals. Thus, the total range covered for any particular setting was 20°C after which the control must be re-set.

3.2.4. The Drying Experiments. It has already been seen that the capacity and the conductance of potassium acetate increased very rapidly after the transition II ⟶ I. These experiments were performed to ascertain whether the effect was due to retained moisture or decomposition product, if any.

Experiment with Cell No.3

About 63 g of the dried polycrystalline material were put into the cell and weighed. The heater wire was coiled round and the cell was connected to the high vacuum system. The temperature was measured by inserting a thermocouple into the inner electrode. The initial room temperature capacity C_p and conductance G_p were noted (before the heater wire was coiled) and the cell was then cycled in temperature between about 170°C and room temperature. The heating and cooling cycle was repeated several times in a day. Overnight, the cell remained at room temperature but was pumped continuously. The experiment was continued for 4 days. Every morning, the weight of the cell was taken and the room temperature capacity and conductance recorded. It appeared from the results given in Table 3.2.4.1., that from the third day, the weight of the sample and the dielectric properties became essentially constant.

Table 3.2.4.1.

Data of drying experiment: Cell No. 3.

	Initial values	Day 1	Day 2	Day 3	Day 4
Weight g	63.3656	63.3382	63.3296	63.3286	63.3290
Capacity pF	1.27	0.94	0.92	0.94	0.93
Conductance µmho	0.003	0.002	0.002	0.002	0.002

Ignoring the slight variation in weights on the 3rd and 4th days, which probably arise from trivial causes, it can be concluded

that after the 3rd day the condition of the material remained unchanged.

Having established that the sample reached constant weight in about two days and that the state could be detected by the constancy of the dielectric measurements, the final experiments were made using cell No.2 in the oil bath whose temperature could be controlled to great accuracy. This necessitated a repetition of the drying experiment but now using only the constancy of the dielectric properties to establish that the sample was free from water.

This experiment was performed over five days. Each morning the sample was heated rapidly from room temperature to 180°C under vacuum and then cooled down to about 140°C. The temperature was cycled between 140° and 180° several times during the day and the bath with the sample inside was allowed to cool down to room temperature overnight. Each morning, the capacity and conductance were measured at room temperature and near 180°C. The ratio C_p (room)/C_p(180°C) was recorded (Table 3.2.4.2.).

It was observed that the ratio increased daily and after the third day it remained steady. After the 5th day, the sample was melted and the capacity of the condenser with solidified melt in between the condenser electrodes increased by about 3% (at room temperature); this increase was attributed to the increase in quantity of the material between the two electrodes.

Table 3.2.4.2.

Ratio of Capacity change in the drying Experiment: C_p(pF)

day	the ratio C_p(room temp.)/C_p(180°C)
1	1 : 1.44
2	1 : 1.36
3	1 : 1.24
4	1 : 1.23
5	1 : 1.23
melt 5	1 : 1.41

It was concluded that the values of capacity and conductance should not be effected (by moisture etc) if the sample was dried for at least three days in the manner described above. Abnormal values of the dielectric constant and conductance can arise because of decomposition of a sample[54]. In potassium acetate, besides the initial decrease in capacity due to removal of moisture (absorbed by P_2O_5 in one trap), no condensed decomposition product could be observed in the liquid nitrogen traps indicating either that there was no decomposition with production of gases which could be pumped out or there was no decomposition at all, in the temperature range used. The latter was more likely, because the sample was in high vacuum and the atmospheric oxygen was definitely excluded which was established to be the cause of decomposition of the melt by electron transfer[7].

3.3. Measurement of Capacity C_p and conductance G_p with potassium, ~~rubidium and cesium~~ acetate as dielectric material

3.3.1. Experimental procedure. Measurement of capacity and conductance of the dielectric cells with dried polycrystalline powders of potassium, acetate as dielectric materials were made following similar procedures to those described in the drying experiment.

The sample was tightly packed inside the condenser of the cell and the cell was connected to the vacuum system. It is then fixed in position under the oil in the bath and necessary electrical connections were made as before.

3.3.2. Results.

(a) Potassium acetate: (single frequency). Three runs of measurements on capacitance and conductance at frequency 1592 Hz, from room temperature to about 180°C were recorded, with cell No.2. The first run was made on heating. The sample was then cooled to room temperature. The second run was again made on heating from room temperature to about 170°C, in order to check the reproducibility of the result. The third run consisted of a complete heating and cooling cycle. The results are shown in Fig.43. From the graphs, the reproducibility is evident.

To check whether the dielectric behaviour was effected by the electrodes (electrode effect[55]), cell No.3 was used in another measurement. The graphs of capacitance and conductance plotted against temperature are shown in Fig.44. It will be seen that while

the actual values were slightly altered due to the difference in the room temperature capacity of the two cells, the general features remain essentially the same.

From both sets of results, it is evident that both C_p and G_p values increase rapidly, particularly after the transition from form II to form I at 154°C, although the rise is evident at temperatures as low as 100°C. At the transition, a small peak appears, which is more prominent in the capacitance than the conductance graphs. It appears as though the peak is superimposed on an otherwise continuous but rapidly rising background, suggesting that the mechanisms responsible for the general background and the peak at the transition are different.

(b) Different frequencies: With the modified cell No.3, a run of C_p and G_p measurements for a complete cycle of heating and cooling with temperatures ranging from 20°C to 220°C were made at frequencies 500 Hz, 1 kHz, 1592 Hz, 5 kHz, 10 kHz, 15 kHz, 20 kHz.

The values of C_p and G_p against temperature are plotted and are shown in the Fig.45. The variation of C_p and G_p with frequency for three temperatures are shown in Fig.46. The three temperatures are arbitrarily chosen at 170°C and above, because, below 170°C, the G_p values were too small for recording. This set of values of C_p and G_p will be used for discussion later.

The sample was recrystallised after melting in the cell to check for any change in dielectric property. The result is shown in Fig.47. A comparison of the values of C_p and G_p with those of Fig.46, shows that the values are now somewhat higher. This can be

due to the increase in the quantity of material between the electrodes.

(c) Single crystal measurements: The results of single crystal measurements are shown in Fig.48. Although the transition II $\longrightarrow$ I is not apparent (due to the wide fluctuations of temperature), the general tendency of a rise in the values with increasing temperature is similar to that found in the powder samples.

(d) Relative permittivity and loss factor: The relative permittivity ϵ' and loss factor ϵ'' were calculated over a range of temperatures using the measured values of C_p and G_p obtained during the heating of the samples (results from Fig.45). The equations used for the calculations were:

$$C_o\epsilon' = C_p, \quad C_o\epsilon'' = G_p/\omega$$

where C_o is the capacity of the cell with no dielectric inside, and $\omega = 2\pi f$, f is frequency in Hz.

To display the variation of ϵ' and ϵ'' with frequency, ϵ' and ϵ'' are plotted against log frequency and are shown in Fig.49.

B. DIFFERENTIAL THERMAL ANALYSIS OF POTASSIUM ACETATE

3.1. Introduction

For reasons outlined in Chapter 2, it would be extremely valuable to supplement the structural aspects of this investigation with data on the specific heat of potassium acetate. The information is not available in the literature and it was beyond the scope of the present investigation to consider obtaining the data experimentally. However, it was possible to locate a Du Pont 900 Differential Thermal Analyser and use this instrument to study qualitatively the general thermal behaviour of this salt.

3.2. Principle of working

Differential thermal analysis is a technique for comparing the thermal behaviour of a standard sample with that of other materials which undergo physical and chemical changes during heating or cooling. Heat is applied to both the standard and the unknown sample so that the temperature of the standard sample rises at a constant rate. The temperature difference between the standard and the unknown is recorded.

Hence the basic apparatus consisted of two thermocouples A and B connected in opposition (Fig.50). Thermocouple A was inserted into the sample and thermocouple B into inert fine silica powder (glass beads) which did not undergo any thermal transformation over the range of temperature studied. When the temperature of the sample t_1 and the reference material t_2 were identical, the net output voltage from the

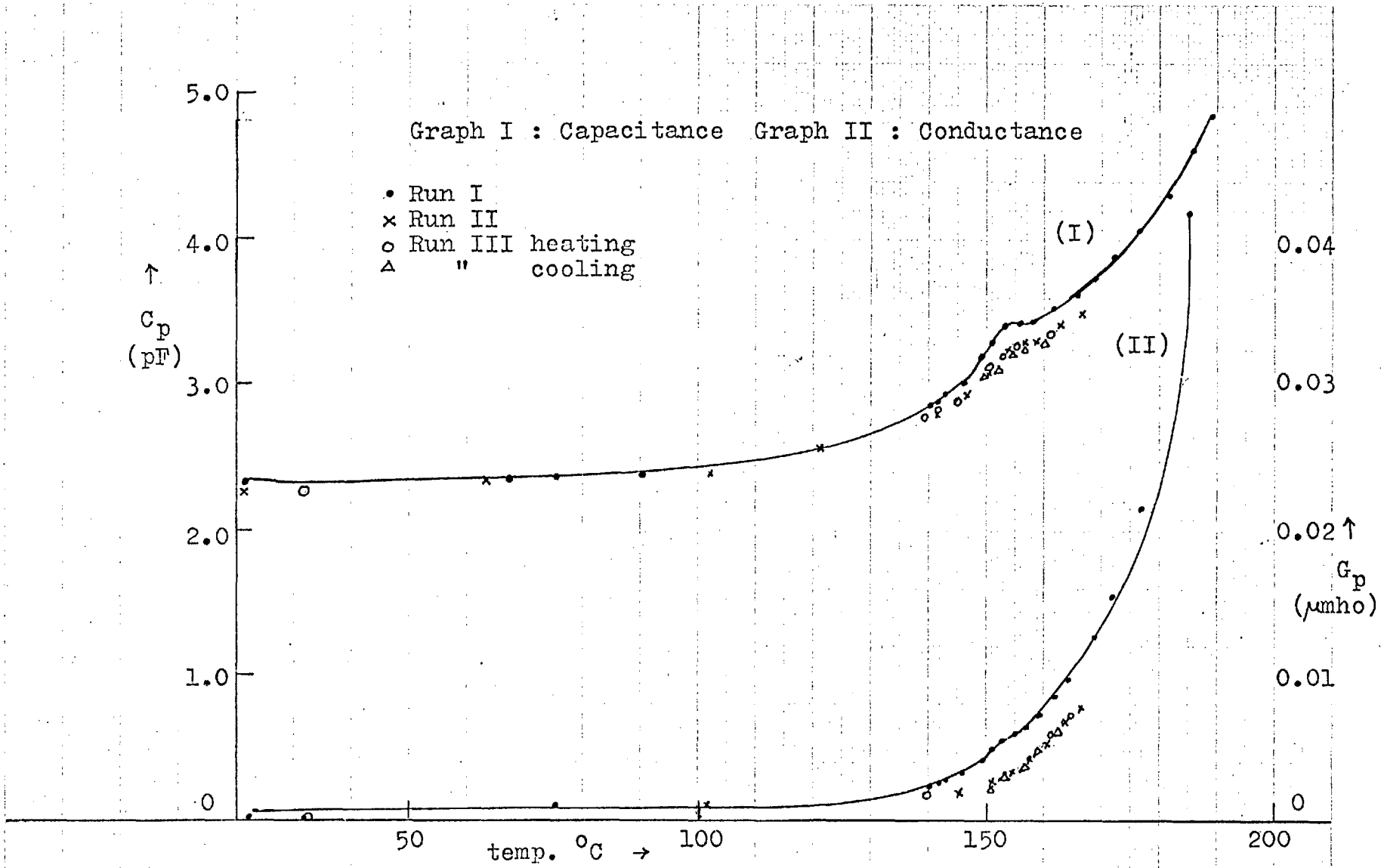

Fig.43. Capacitance and conductance of Cell no. 2 at 1592 Hz, with potassium acetate as the dielectric material

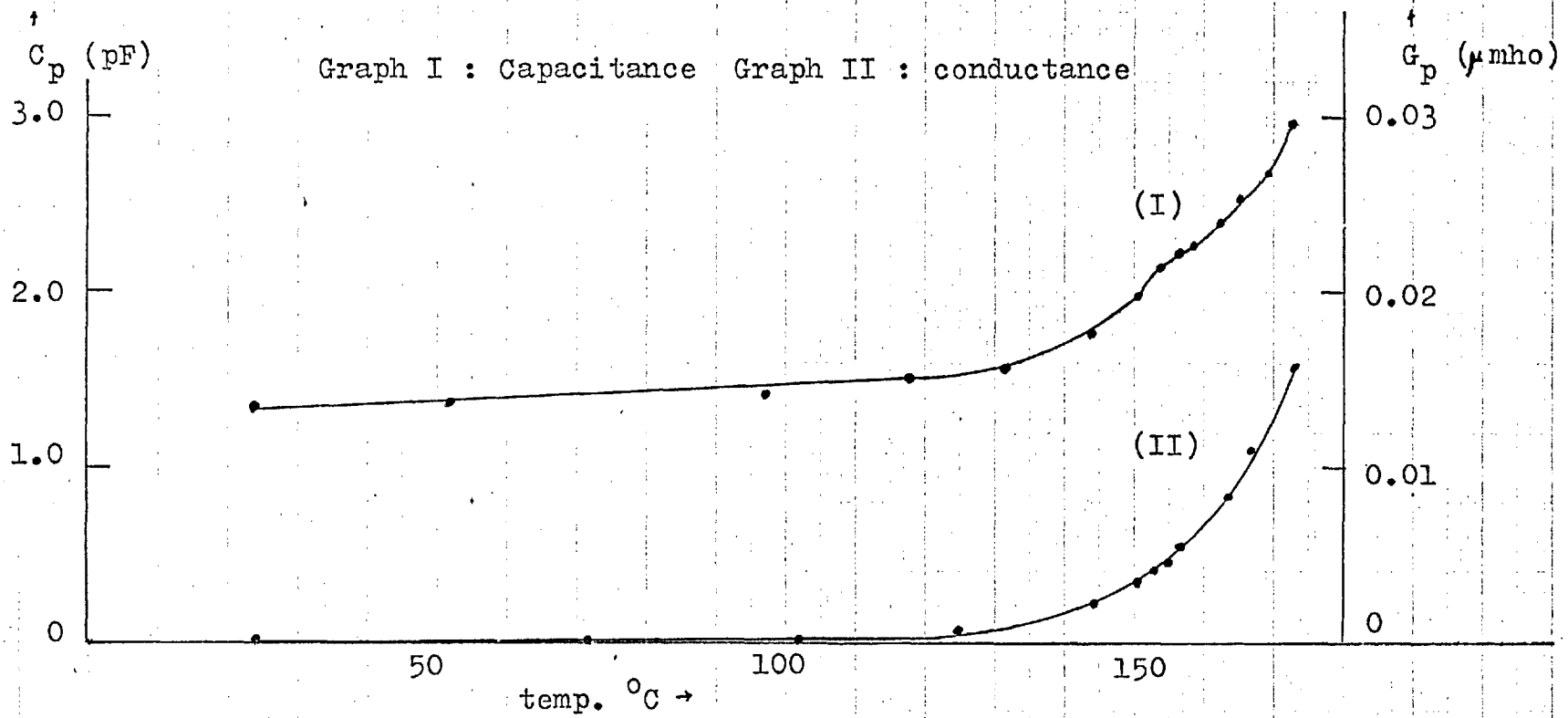

Fig.44. Capacitance and conductance of cell no. 3 at 1592 Hz, with potassium acetate as the dielectric material.

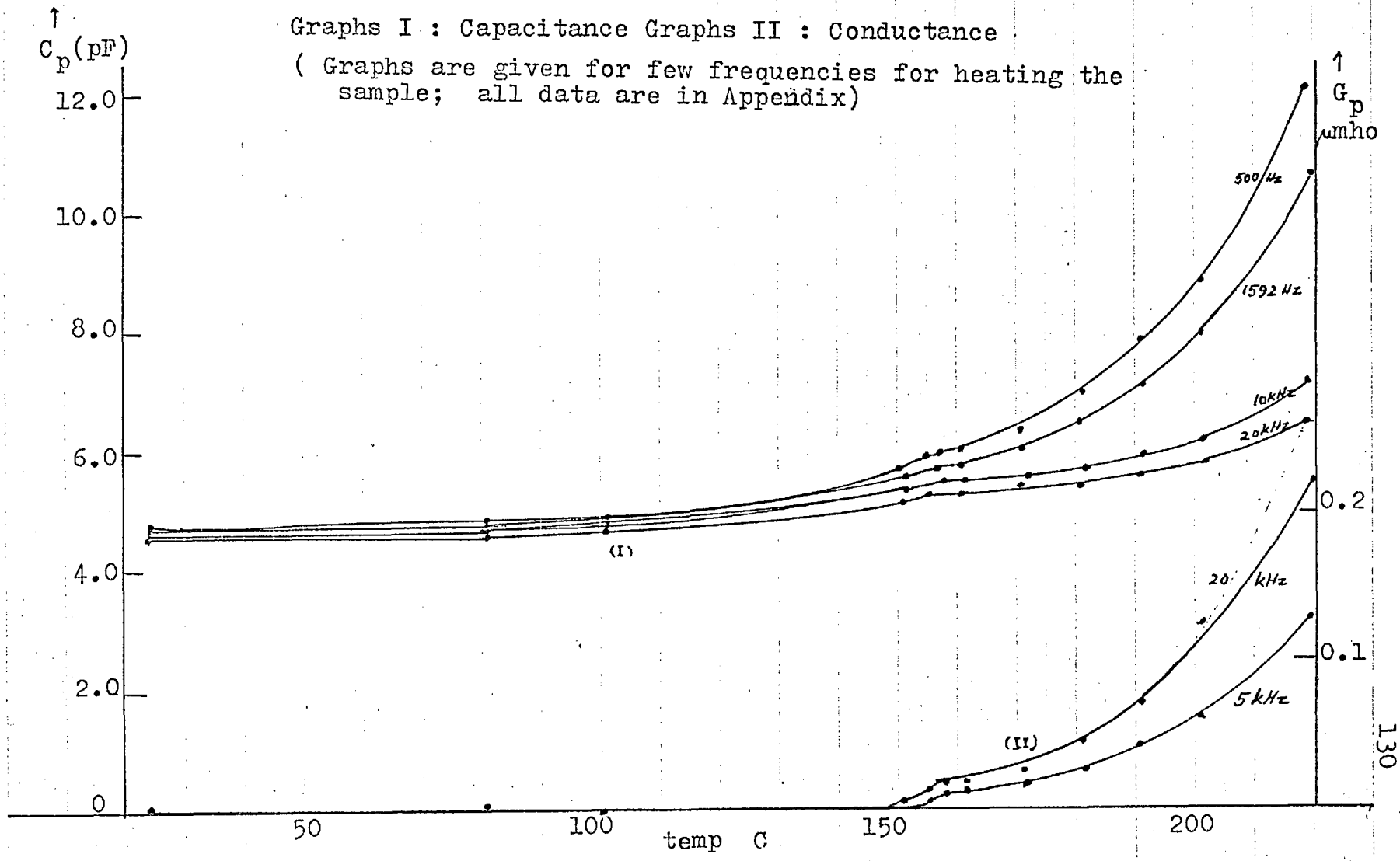

Fig.45. Capacitance and conductance of Cell no. 3 with potassium acetate as dielectric material, at different frequencies. For full description see text.

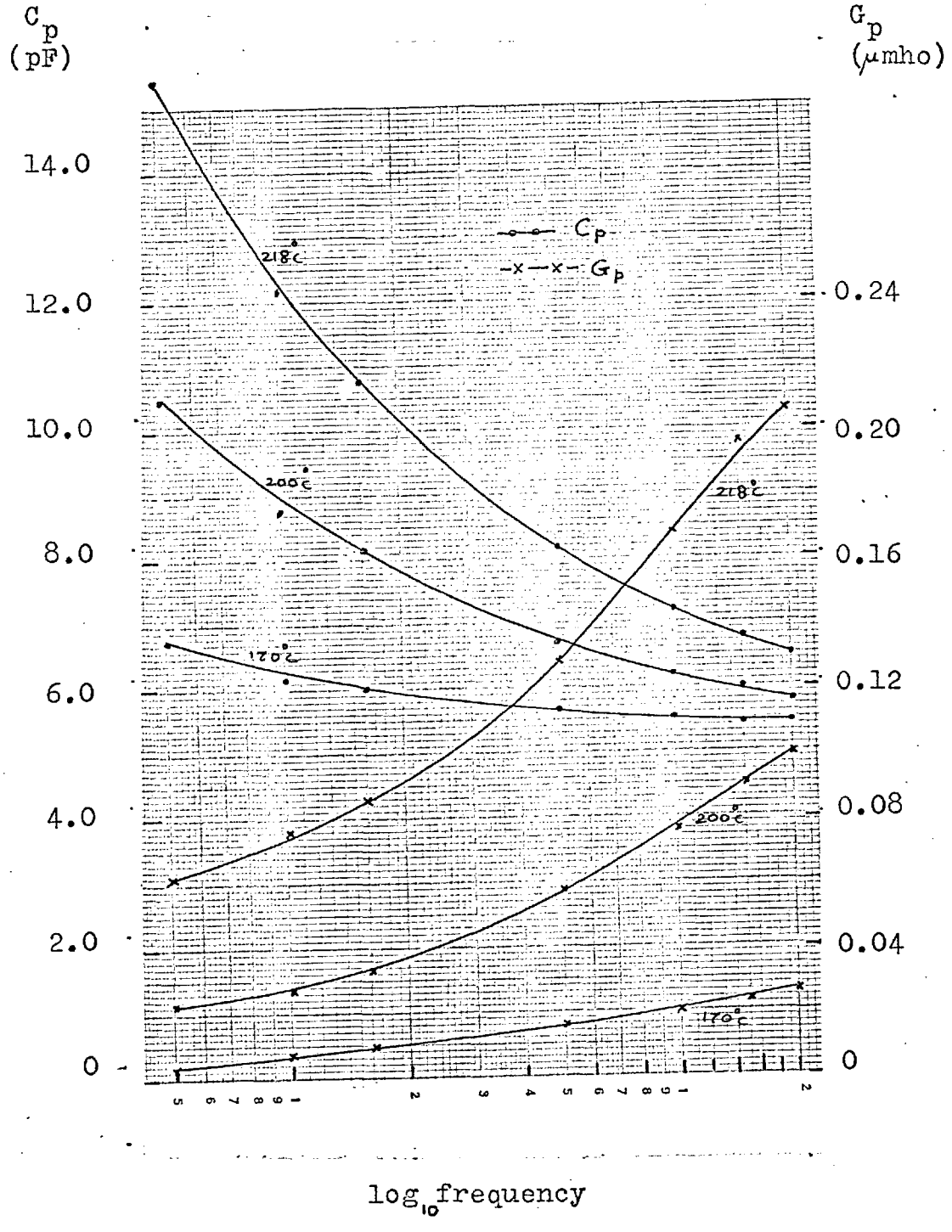

Fig.46. Variation of C and G with frequency, of Cell no.3; dielectric sample: potassium acetate; numerical data are given in Table 4, Appendix.

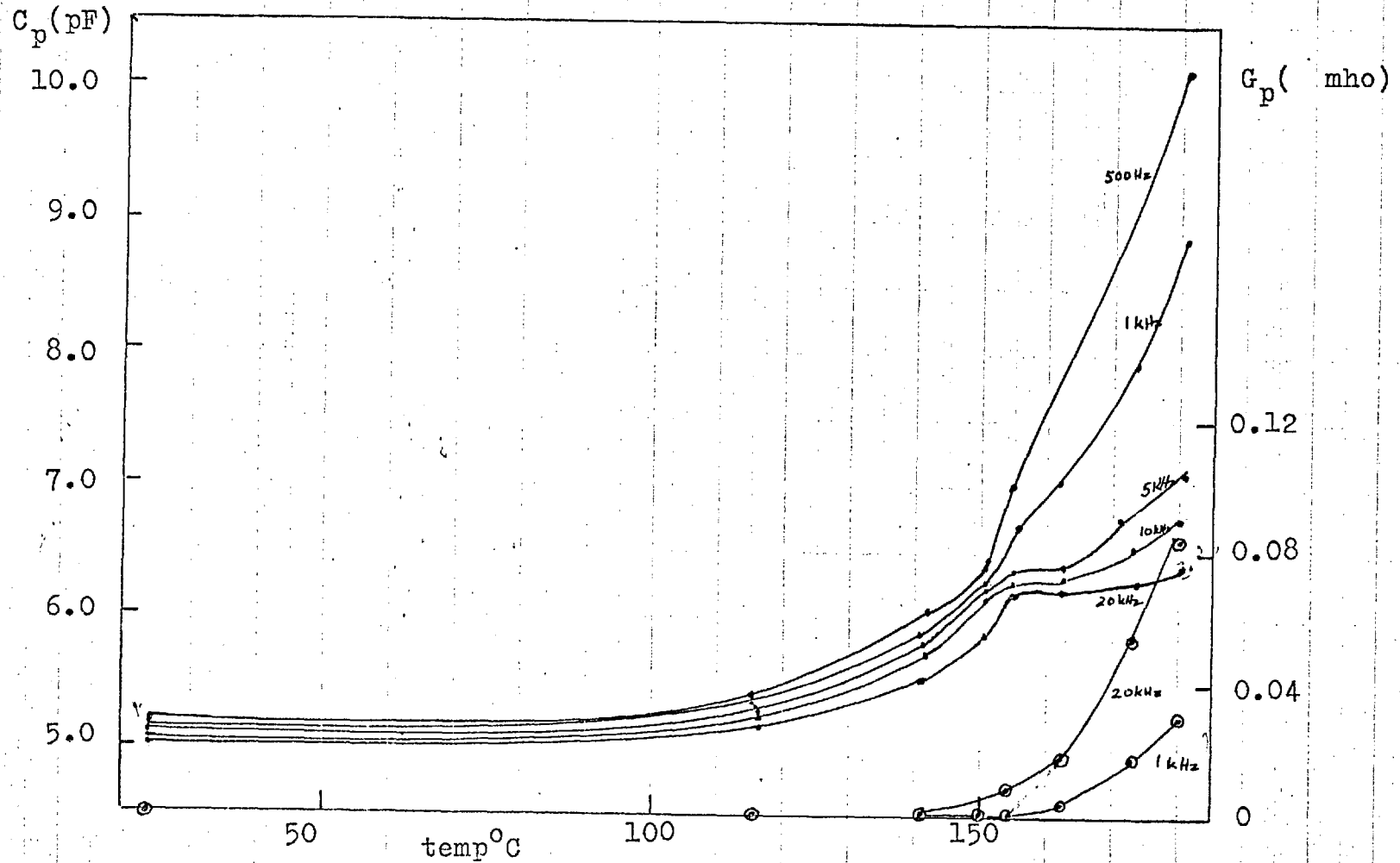

Fig.47. Variation of C and G with temperature of Cell no. 3 with dielectric material same as in Fig.45. Note that the values have now increased due to density effect

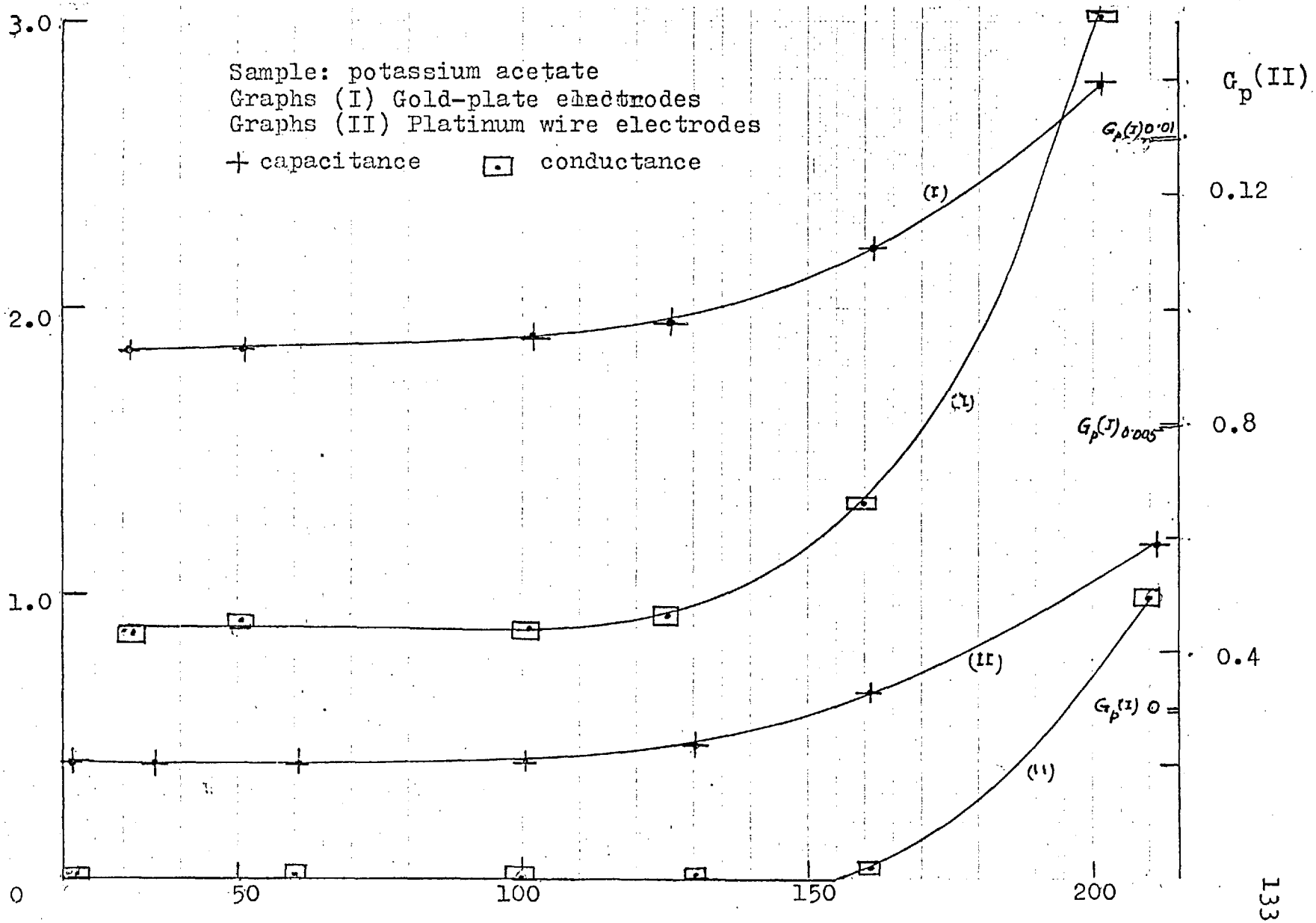

FIG.48.(see text)

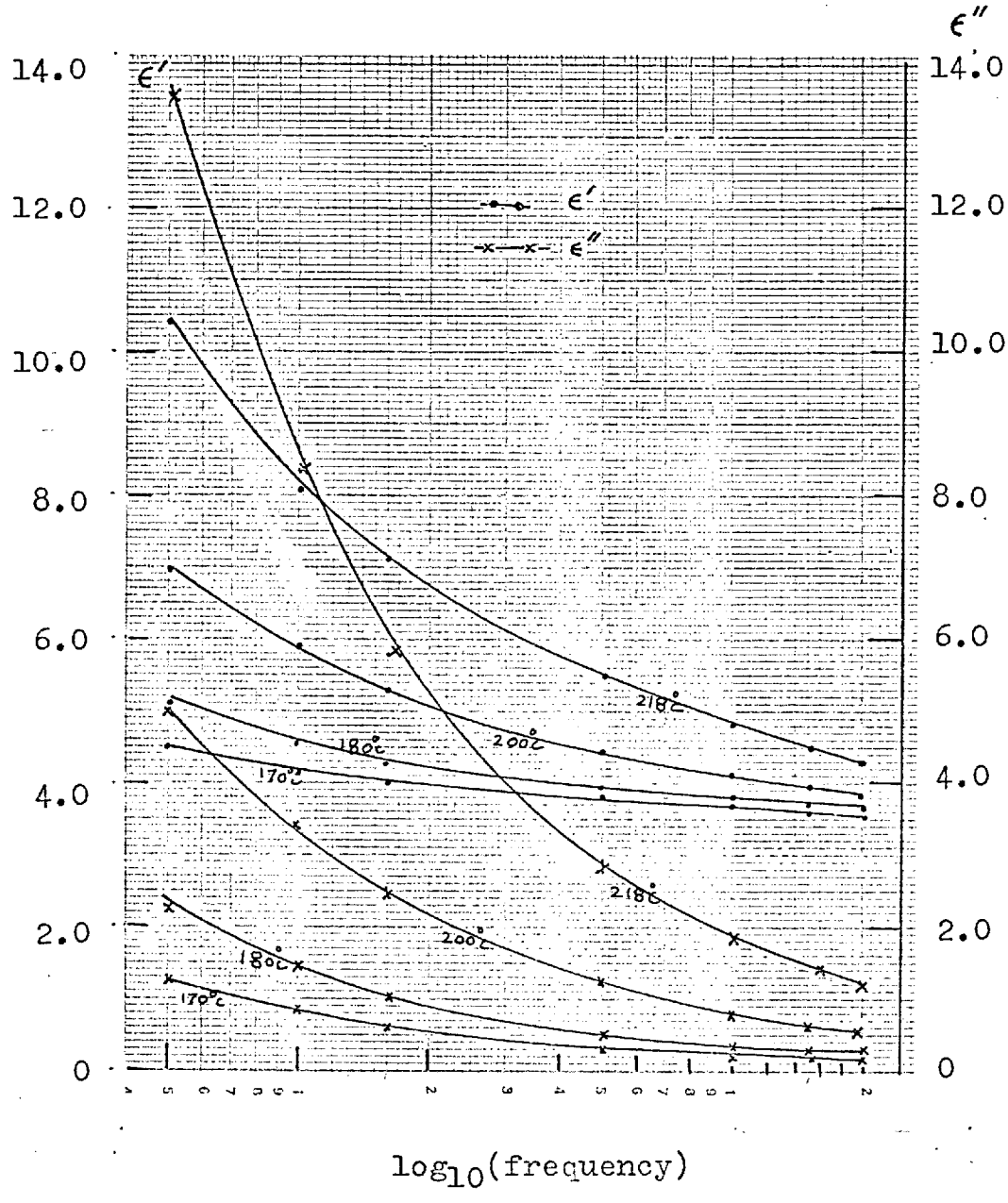

Fig.49. Variation of ϵ' and ϵ'' with frequency
Sample: Potassium acetate(numerical data are given in Table 12, Appendix)

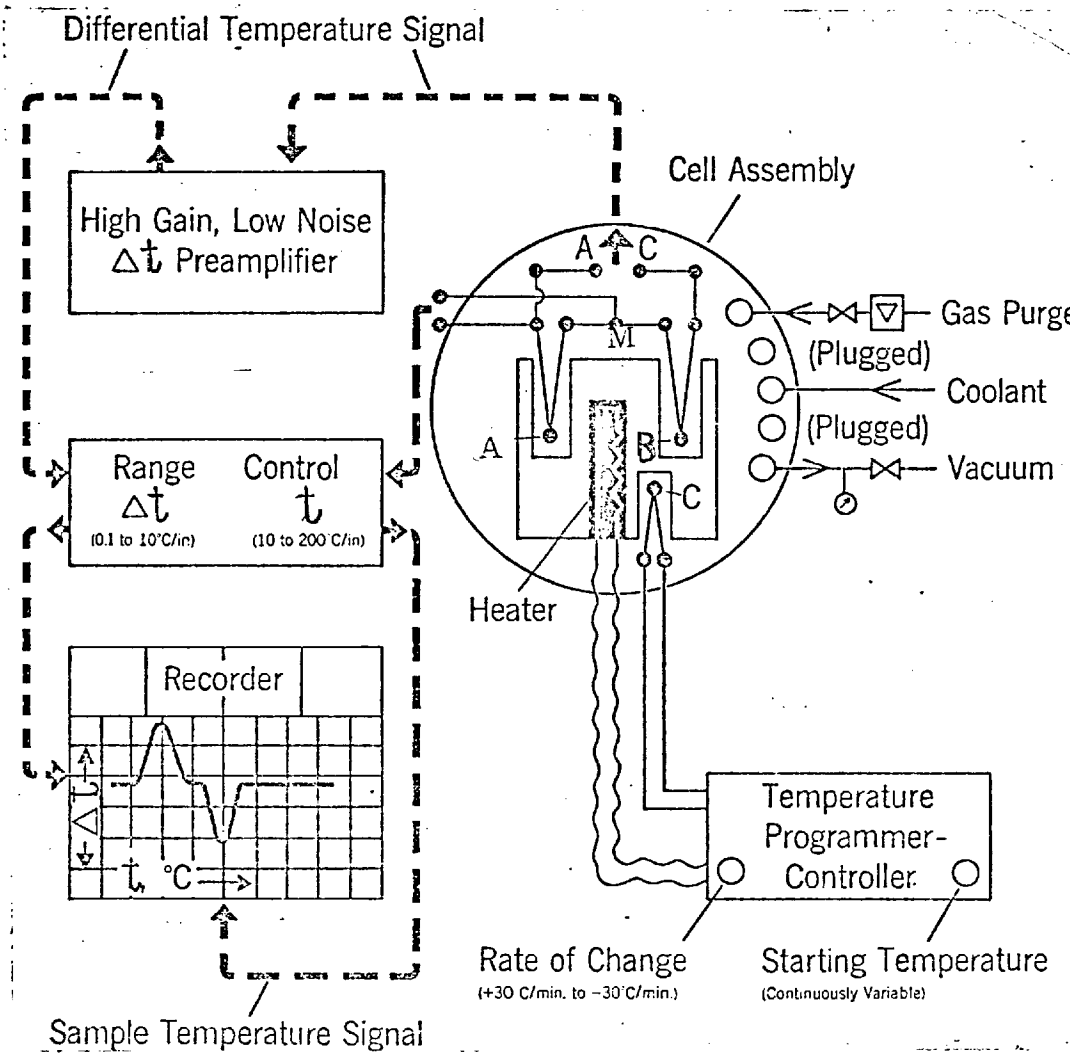

Fig.50. Schematic diagram of Differential Thermal Analyser System.

two thermocouples was zero, i.e. $\Delta t = 0$. Any difference in their temperatures arising from abnormal thermal properties of the unknown material gave a resultant net voltage which was recorded on a potentiometer. The sample and the reference material were placed close together in an environment which was a block of silver M, whose temperature could be changed at a uniform rate by means of a temperature-programmer-controller. A third thermocouple C measured the temperature t_3 of the block. With the change of the temperature of the metal block, the temperatures of the reference material and of the sample also changed, in absence of any thermal anomaly in the sample,

$$\Delta t = t_1 - t_2 = 0$$

When such an anomaly occurs Δt would no longer be equal to zero and its variation with time or temperature is called a thermogram.

The interpretation of such a thermogram can be conveniently described by considering what happens when the sample is melted. Suppose the heat capacity and the thermal conductivity of the sample and the reference material were equal and invariant with temperature. Until the sample reached its melting point, $\Delta t = 0$, but once melting commenced t_1 remained constant until the sample completely melted, but t_2 rose. Given a rise of temperature with time as shown schematically in Fig.51a, the corresponding change in Δt will be as shown in Fig.51b. As the temperature of the reference material rose at the melting point, Δt became negative; Δt reached a minimum when the sample had completely melted and subsequently returned to zero. When Δt is plotted against the reference temperature, the result is

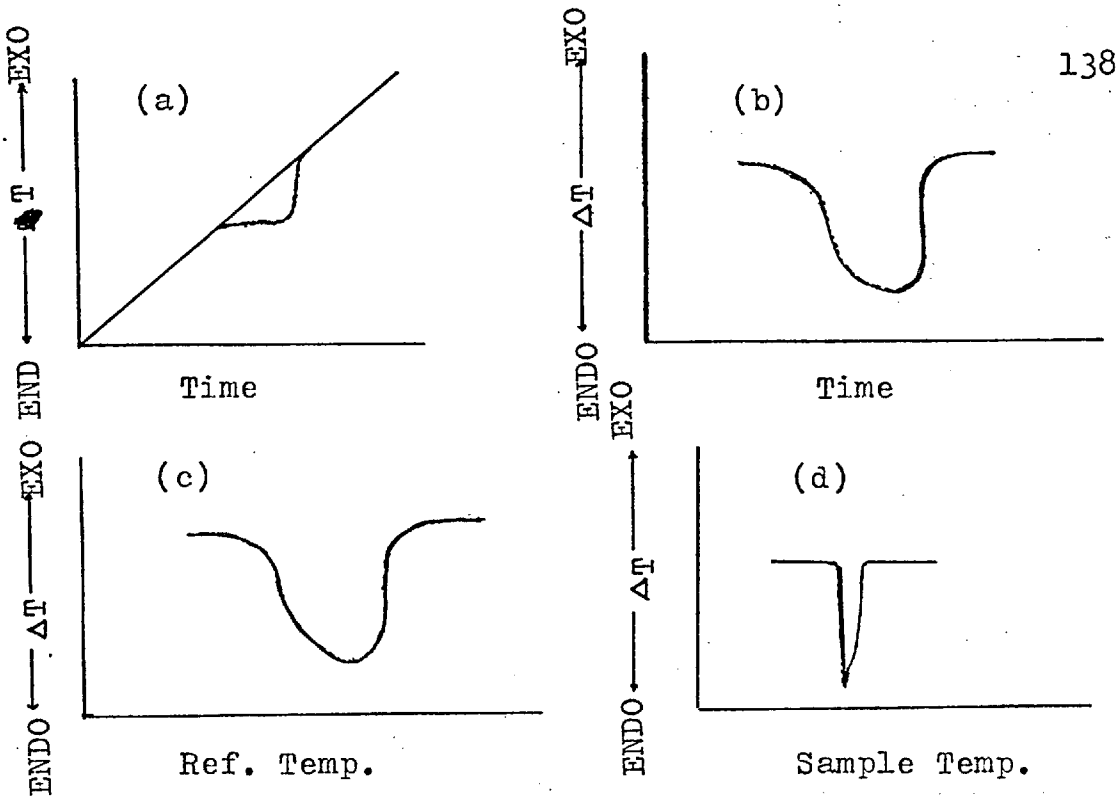

Fig.51. Schematic representation of a thermogram in the DTA (see text)

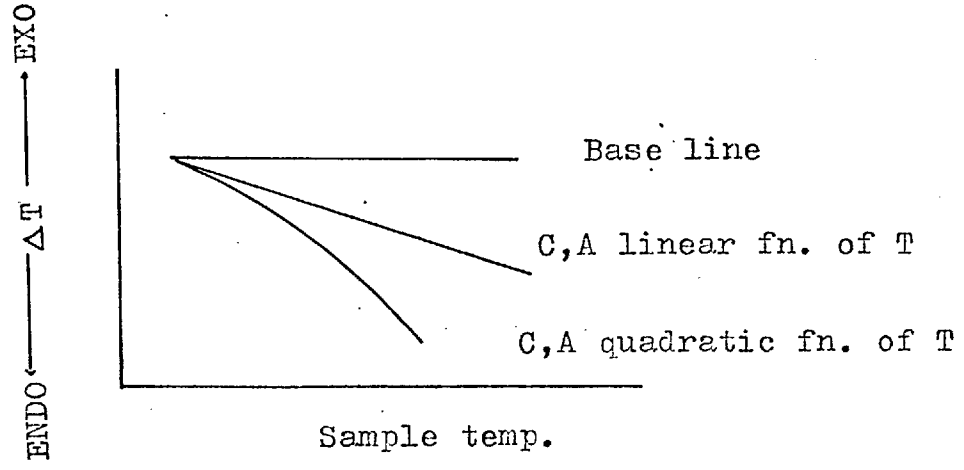

Fig.52. Effect of change of heat capacity and/or thermal conductivity on the slope of the base line.

essentially the same (Fig.51c) but when Δt is plotted as a function of temperature of the sample, the result is a very sharp peak or endotherm (Fig.51d). In the present DTA, the thermogram was a plot of Δt against temperature of the sample.

The magnitude of $t_2 - t_3$ is approximately proportional to the rate of heating H, the weight W of the reference sample, its heat capacity C and thermal conductivity A[56], i.e.

$$t_2 \approx t_3 - H_2 \ (WC/A)_2$$

Similarly for an inert sample

$$t_1 \approx t_3 - H_1 \ (WC/A)_1$$

Thus, $\Delta t = t_1 - t_2 \approx H_2 \ (WC/A)_2 - H_1 (WC/A)_1$.

The present apparatus ensured $H_2 = H_1$. Containers for the reference material and the sample were made of the same material and shape, and were located in identical holes in the heating block.

Then $\Delta t \approx H\left[(WC/A)_2 - (WC/A)_1\right]$

If the variation of WC/A with temperature is the same for both reference and the sample then $\Delta t = 0$ at all temperatures and the thermogram is a horizontal straight line.

However, if any of these quantities, say, heat capacity and/or thermal conductivity vary with temperature, then Δt versus t_1 will, in general, be curved (Fig.52).

Under certain experimental conditions, the area under the peak of a thermogram, produced when a material with a thermal change (phase change) as above is examined, is proportional to the heat of reaction[57].

The change of heat of reaction divided by temperature of transition gives the entropy change at constant pressure.

In the present experiments, sample holders for the reference and the unknown material were of the same shape. They were put in the same environment and the thermal gradient was kept to a minimum by taking the minimum quantity of the sample. Thus almost all of the conditions were fulfilled except that the heat capacity and thermal conductivity of the sample and the reference could not be made alike by mixing a little of the sample with the glass beads. This was not possible because of the deliquescence of potassium acetate.

Thus, although the areas under the peaks of the thermographs obtained could not be considered as heats of reaction, they would indicate the relative change of entropy in the transformations.

Precautions

Certain precautions must be taken to obtain reliable results:

(1) The rate of heating must be kept constant, which was done by the temperature programmer controller in the apparatus used.

(2) The rate of heating should not permit the sample to approach thermal equilibrium with the source. Heating rates in the present measurements were decided by several trial runs.

(3) The samples were tightly packed.

3.3. Present experiments

In the present thermal analysis of potassium acetate, no quantitative study has been attempted. Lack of complete reproducibility in the measurements was attributed to the difficulty of ensuring a completely dry sample. The apparatus did not allow the initial setting up of the sample to be done in a dry atmosphere. The sample surface invariably came into contact with atmospheric moisture if only for a short while.

In spite of these difficulties a few reproducible thermograms were obtained. This required that every part of the DTA apparatus which could come into direct contact with the sample must be thoroughly dried. A specimen tube A was filled to the specified level in the dry box, packed tightly with a glass rod and taken to the DTA cell in a desiccator. The thermocouple junction T was then inserted into the specimen which was then placed in the hole H of the heating block. The glass cover G was then fitted to the cell base B. The whole operation from the insertion of thermocouple to the replacement of the bell-jar took about 15 seconds during which period the acetate powder surface remained exposed to the atmosphere. Subsequently, dry nitrogen gas was passed through the cell and in an attempt to remove the surface moisture, the sample was heated to 200°C very rapidly (at 30°C per minute) and then allowed to cool down to room temperature. Various heating rates and sensitivities were employed and in one case a sample was heated from room temperature to the melting point, cooled to 200°C and again heated through the melting

point in order to examine the effect of recrystallisation on the thermal behaviour.

3.4. Results

(a) The endothermic transition form II → form I was recorded in all the thermograms. (Fig. 53a,b,c,d), with a slope resembling the specific heat anomaly of a Λ-transition i.e. a slow rise culminating in a sharp drop above the transformation temperature recorded by X-ray diffraction. The pre-transition rise was seen in all the thermograms, but onset temperatures of this rise varied. In different samples, values ranging from about 50°C to about 15°C below the transition temperature were obtained. It was concluded that the transition involves a co-operative effect.

(b) All thermograms showed that from about 90°-100°C to the melting temperature 303°C the base line was inclined to the horizontal and followed a slight curve as shown in the above figures. This indicates that the ratio (C/A) of the sample rises from about 90°C right up to the melting point. Thus, either the specific heat C increases or the thermal conductivity A decreases. Reduction of the thermal conductivity A is unlikely. Hence, probably, there is a general rise in the heat capacity of potassium acetate from about 90°C to the melting point which is independent of the Λ-point anomaly.

(c) Transition from form III to form II was not recorded in any of the thermograms, taken with different heating rates, except perhaps in one in which the base line curved very slightly towards the

exothermic direction from about 50° to 80°C (Fig.53a). The reasons for the absence of a prominent peak may be due to the small heat of transformation involved.

(d) The endothermic peak at the melting point went beyond the recording chart. Even so, the area under the endothermic peak at the melting point was much larger than the area of the peak at the transition II ⟶ I, indicating that entropy involved in the melting is much higher than in the transition II ⟶ I.

The results will be discussed more thoroughly in the discussion chapter.

Fig.53 (a) (b) (c) Traces of the Thermograms of potassium acetate.

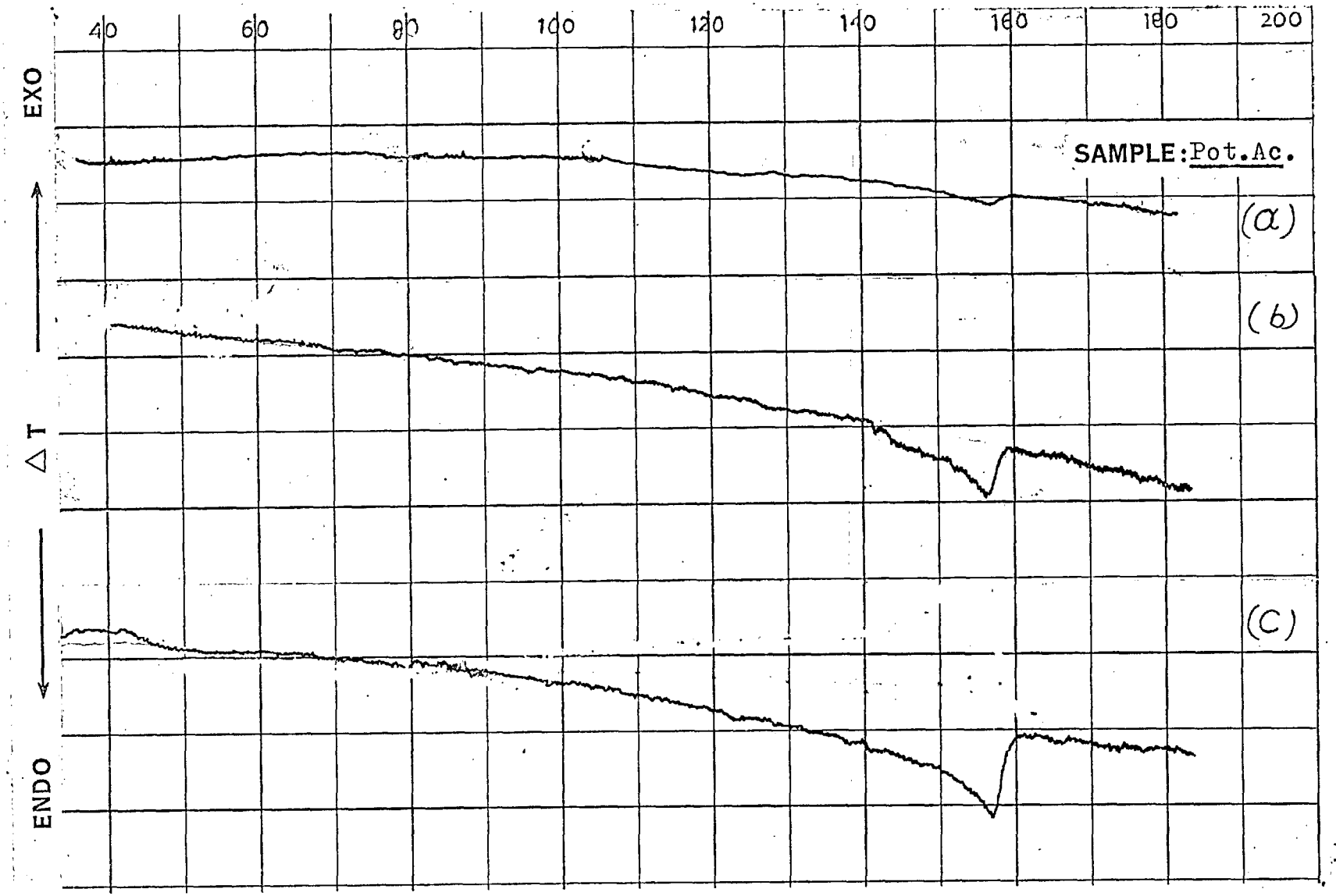

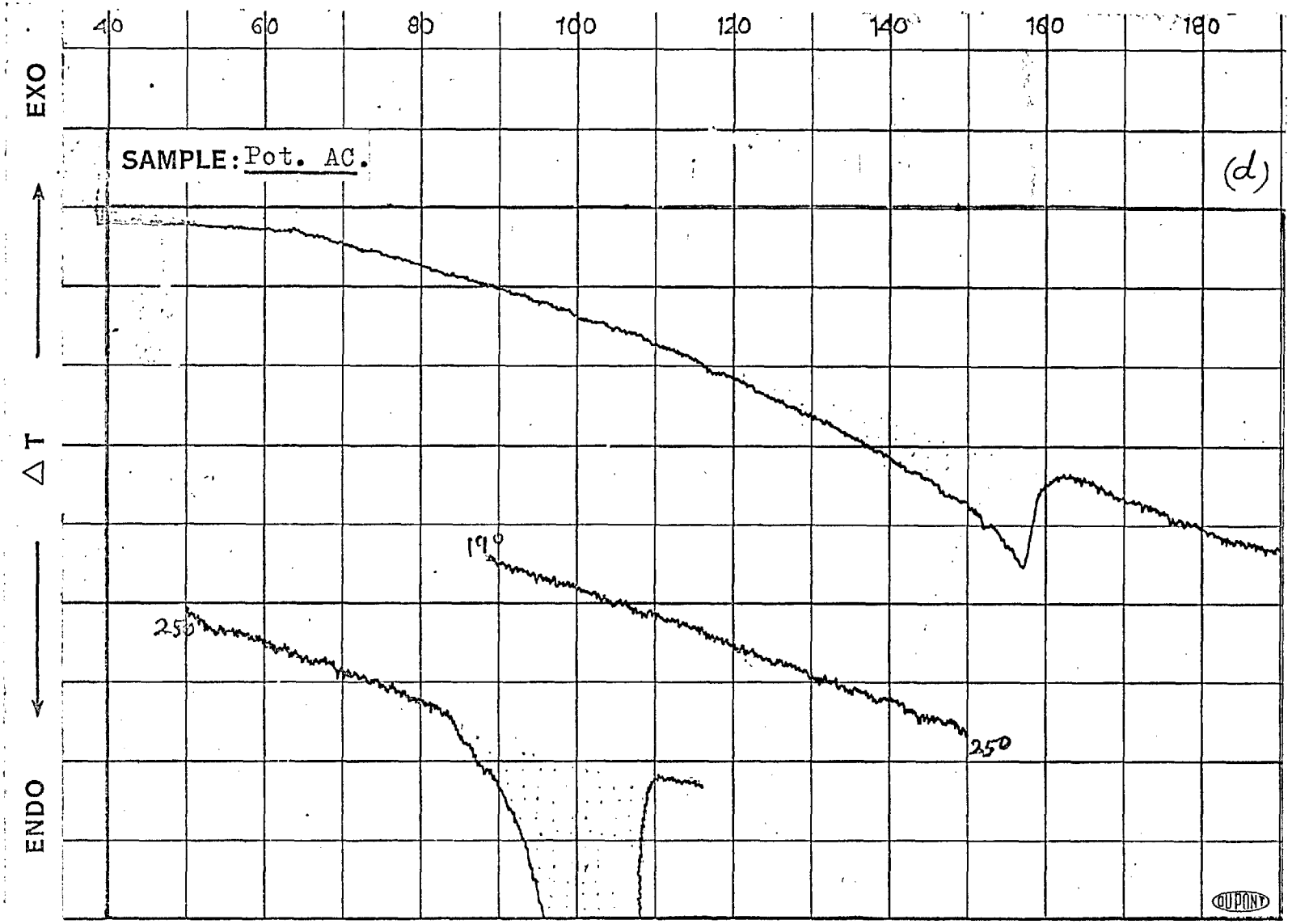

Fig.53 (d) Traces of the thermograms of potassium acetate.

Chapter 4

STRUCTURAL WORK ON POTASSIUM ACETATE

4.1. Introduction

4.1.1. Structure Factor. In ~~the foregoing sections~~ chapter 1, the behaviour of atoms, molecules or ions of a crystal which undergoes solid-solid transformations with change of temperature have been presented theoretically. There are various methods by which these movements of atoms or molecules can be inferred. The only technique by which these movements can be directly detected is the X-ray or neutron diffraction technique of analysing the crystal structure.

To derive or verify a crystal structure from X-ray diffraction data, the intensity of each available reflexion in the diffraction pattern must be measured and compared to that predicted on the basis of some model of the structure.

Intensities of the model structure can be calculated using the formula outlined below.

Theoretically, it has been shown that if a very small block δV of a crystal reflects X-rays, the expression for the integrated intensity of reflexion is

$$\rho \sim \frac{1}{\mathrm{Sin}2\theta} \cdot |F|^2 \cdot \frac{1 + \cos^2 2\theta}{2} \quad .$$

Here 2θ, is angle between primary and diffracted beam. The first term is the Lorentz factor and the last term is the polarisation factor. The two terms are often considered together and referred to as the

Lorentz-Polarisation factor. $|F|^2$ is the square of the structure amplitude. In the case of a single crystal that is rotated about a unique axis, the Lorentz factor is different. The above expression then becomes,

$$\rho \propto \frac{1 + \cos^2 2\theta}{(\sin^2 2\theta - \zeta^2)^{\frac{1}{2}}} \cdot A(hkl)\ \rho'\ |F|^2.$$

Here ζ is a cylindrical co-ordinate of the reflexion, A is a transmission factor, ρ' is the number of superimposed equivalent reflexions.

In the expression for the integrated reflexion given above, the term $|F|$ is to be modified for the following considerations:
The structure factor: The unit cell of a crystal is composed of atoms in various positions. The atoms scatter the incident X-rays and the resultant wave scattered by the atoms in the plane (hkl) of the unit cell is,

$$F(hkl) = \sum f_n \exp 2\pi i(hx_n + ky_n + lz_n)$$

so that, in general,

$$|F(hkl)|^2 = (\sum f_n \cos 2\pi(hx_n + ky_n + lz_n))^2 + (\sum f_n \sin 2\pi(hx_n + ky_n + lz_n))^2$$

Here f_n is the atomic scattering factor of an atom at rest, x_n, y_n, z_n are the fractional co-ordinates of the n-th atom. The structure amplitude $|F|$ is the modulus of the structure factor F(hkl). Only this modulus can be observed experimentally.

For centrosymmetric system,

$$F(hkl) = \sum f_n \cos 2\pi(hx_n + ky_n + lz_n)$$

and $|F(hkl)|^2 = 2(\sum f_n \cos 2\pi(hx_n + ky_n + lz_n))^2$

Values of $|F|^2$ computed from the above equation cannot be directly compared with observed values, because the atoms are not at rest but vibrating randomly about the positive x_n, y_n, z_n. If the amplitude of vibration is independent of direction, atomic scattering factor becomes,

$$f = f_o \exp(-M)$$

where $M = 8\pi^2 u^2 \sin^2\theta/\lambda^2$, u^2 is the mean square displacement of atoms from their equilibrium positions, perpendicular to the reflecting planes[58].

The structure factor is then

$$F(hkl) = \sum f_n \exp 2\pi i(hx_n + ky_n + lz_n) \exp(-M_n).$$

If all atoms are assumed to have the same mean square displacement, this expression becomes

$$F(hkl) = (\sum f_n \exp 2\pi i (hx + ky + lz)) \exp(-B \sin^2\theta/\lambda^2)$$

where the constant $B = 8\pi^2 u^2$ is called the isotropic temperature factor.

B can be evaluated by a method given by Wilson[59] or by variations of it such as the following:[60]

The observed values of the structure amplitudes are on an arbitrary scale. They can be transformed to the absolute scale by multiplying by some factor K. Hence $F(obs.)/F(calc.) = 1/K \exp(-B \sin^2\theta/\lambda^2)$

or $\log_e(F_{obs.}/F_{calc.}) = \log(1/K) - B \sin^2\theta/\lambda^2$. If $\log_e(F_{obs.}/F_{calc.})$ is plotted against $\sin^2\theta/\lambda^2$ for each reflexion the points should be in a straight line, whose gradient gives B and whose intercept gives log (1/K). The $F_{obs.}$ values should then be multiplied by the factor K to get the absolute $F_{obs.}$ values which can then be compared with $F_{calc.}$ values.

In the above estimation of the temperature factor, it is assumed that the atoms are vibrating isotropically and all have the same vibration amplitude i.e. all atoms are of the same mass. In cubic crystals, these conditions can be satisfied, but in crystals of lower symmetry, the amplitudes of atomic vibrations for a given average energy are dependent on direction of vibration. Thus, modern crystal structure refinement techniques allow for the probability that B varies with the type of atom and in different directions.

4.1.2. Discussion on some relevant structures. Crystallographic data on Acetate Structures: Crystallographic data on some acetates and related materials are available although many of the crystals are hydrated.

Lithium acetate crystallises both as an anhydrous form and as a dihydrate. All its crystallographic data are given in Table 4.1.2.(a).

Table 4.1.2.(a)

Crystallographic data on Lithium Acetate

Lithium acetate (anhydrous), triclinic, $P\bar{1}$, z = 8

a = 9.29, b = 12.13, c = 6.76 Å

$\alpha = 101^{\circ}$, $\beta = 100^{\circ}19'$, $\gamma = 105^{\circ}5'$

Lithium acetate (dihydrate), orthorhombic, Cmm2, z = 4

a = 6.86, b = 11.49, c = 6.59 Å

The structure of the anhydrous lithium acetate has not been worked out[61] but that of the dihydrate[62] has been available. Here the lithium ions are surrounded by six oxygen atoms, 4 from acetate ions and 2 from water molecules. The acetate ions are packed along the a axis in sheets and the sheets are linked by hydrogen bonds.

Sodium acetate trihydrate[63] is monoclinic. Its crystallographic data are,

a = 12.32, b = 10.43, c = 10.38 Å

$\beta = 111.7^{\circ}$, z = 8.

space group: C2/c

But nothing is known about the orientation of molecules or co-ordination of atoms.

Among other metal acetates, zinc acetate dihydrate[64] is monoclinic with space group C2/c, with other data:

a = 14.50 b = 5.32 c = 11.02 Å z = 4

$\beta = 100^{\circ}$

In this structure, each Zn^{2+} is surrounded by 4 oxygen and 2 water molecules.

However, hydrated acetate structures are not particularly relevant to the present work. It can be seen that the water of crystallisation plays an essential role in co-ordinating the metal ion. In the anhydrous salts, all oxygen atoms co-ordinating the metal ion must be located in the acetate groups and it can be anticipated that this will impose a severe constraint on the structural geometry.

Another acetate structure of limited relevance is ammonium acetate[65]. The space group $P2_1/c$ is similar to that of one form of potassium acetate. One cell dimension of the structure of ammonium acetate is smaller (~ 4.8 Å) like potassium acetate structure. But above all it gives reliable values of the molecular dimensions. Some of these dimensions are reproduced from that work in Table 4.1.2.(b), along with those of some other similar compounds. The C-C contact length of ammonium acetate is very nearly equal to that obtained by orbital theory.

The average values of bond lengths and bond angles have been used in the present structural work.

As has been discussed in the general introduction, in the ionic crystals co-ordination of the cations by the anions (here oxygens) is an important requirement for the stability of the structure. The minimum co-ordination number of potassium by oxygen is six and since the ratio of the potassium-oxygen in the formula KO_2C_2 is 1 : 2, each orygen must co-ordinate 3 different potassium atoms. In the case of

potassium acetate, it will be seen that severe geometrical constraint is imposed, for such co-ordination to be satisfied. Structures in which similar geometrical constraints exist, are the structures of potassium soaps.

Table 4.1.2.(b)

Some molecular dimensions.

	(C-C)Å	(C-O)Å	(O-$\hat{C}$-O)°
Ammon. trifluoroacetate	1.54	1.26) 1.27)	128.3
Bisglycino copper monohydrate	1.50	1.23) 1.28)	1124.3
Sodium hydrogen diacetate	1.49	1.24) 1.30)	121.7
Ammon. oxalate monohydrate	-	1.25) 1.26)	126
Monopyridine copper acetate	1.47	1.25) 1.25)	127.3
Amino acetic acid	1.52	1.25) 1.25)	125.5
Acetic acid	1.54	1.24) 1.29)	122
Oxalic acid		1.19) 1.29)	
Ammon. acetate	1.504	1.25) 1.25)	123.4

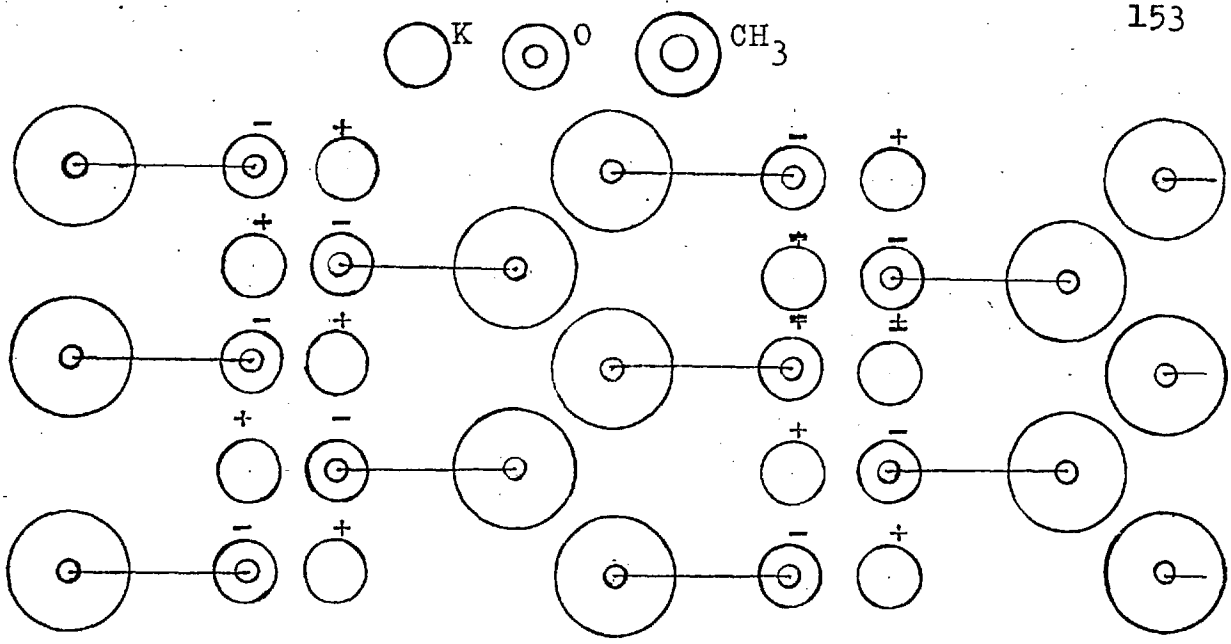

Fig.54(a). Schematic representation of soap structure showing the ionic double layers.

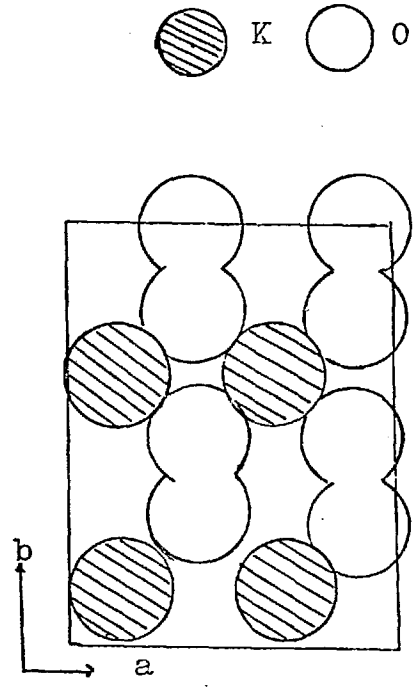

Fig.54. Arrangement of the atoms in one half of the ionic double layer of potassium palmitate, form B structure

Soap Structures

It has already been mentioned that the alkali acetates may be likened to soaps, because both are alkali metal salts of a fatty acid, even though acetic acid has the minimum length of hydrocarbon chain. The soap structures are dominated by the chemistry of the soap molecule, which consists of a long hydrocarbon chain terminated at one end by a hydrophyllic carboxylate ion. A consequence of this molecular geometry is that molecules are limited by ionic forces at one end and by Van der Waals forces (between the terminal methyl groups) at the other. Sheets of ionic double layers (containing potassium and oxygen ions) alternate with sheets of methyl groups. (Fig.54(a)).

Anhydrous soaps (with even number of C atoms) exist in three forms: A, B and C[66]. Form A is monoclinic and occurs when soaps with 4 to 10 carbon atoms are crystallised from alcohol at room temperature. When the number of carbon atoms is greater than 10, form B occurs under the same conditions as form A. It is triclinic. When heated to higher temperature both the forms transform to form C which is monoclinic[67]. Approximate transformation temperatures together with relevant data are shown in the Table 4.1.2(c).

Except for KC_{12} all soaps revert to their room temperature forms when cooled from high temperature. KC_{12} reverts to the B form from the A form (which arises spontaneously on cooling) in a period of months. The characteristic features of these structures are revealed by the typical values of the cell dimensions given in Table 4.1.2.(d).

Table 4.1.2 (c)

Polymorphic transition temperatures of soaps.

Soap	Form	$t^{\circ}C$	transiton temp. $^{\circ}C$	form	obs. d_{001} Å $25^{\circ}C$ - $75^{\circ}C$
KC_4	A (monocl.)	25			
KC_6	A "	25			
KC_8	A "	25	55	C (monocl.)	22.99_6 23.79_8
KC_{10}	A "	25	76	C "	27.525-28.05_7
KC_{12}	B (tricl.)	25	54	C "	
KC_{14}	B "	25	61	C "	
KC_{16}	B "	25	68	C "	
KC_{18}	B "	25	78	C "	

(In the simplified soap formulae, hydrogen and oxygen atoms are deleted),

Table 4.1.2 (d)

Cell dimensions of some even numbered potassium soaps[67]

	$t^{\circ}C$	phase	c(kx)	b(kx)	a(kx)	α°	β°	γ°
KC_8	25	A	7.90	5.67	22.96	90	92.1	90
KC_{10}	25	A	8.06	5.67	27.52	90	93.5	90
KC_{14}	25	B	4.14	5.60	34.00	91.6	91.5	93
KC_{16}	25	B	4.16	5.60	38.19	92.7	91.3	93
KC_8	75	C	8.07	5.72	23.76	90	91.7	90
KC_{16}	75	C	8.03	5.70	40.95	90	90.1	9[illegible]

Thus one of the cell dimensions a is either about 4 Å (form B) or 2 x 4 Å (forms A and C) and the dimension of b is about 5.7 Å in all cases. However, the length of the c-axis increases progressively with the number of carbon atoms in the fatty acid chain from about 14.5 kx (KC_4) to 38.2 kx (KC_{16}).

The structures of potassium caprate, form A[66] and potassium palmitate, form B[68] are known. In all cases the carbon chains are packed in layers around 4 Å thick and almost parallel to (001). In potassium captriate, form A, (KC_{10}) for which C = 2 x 4.06 kx, the doubling of this short cell dimension arises because the axes of the molecular chains in alternate layers inclined to each other when viewed down the c-axis. Accordingly the pattern repeats only after every other layer leading to the doubled C repeat distance characteristic of the form A structure. On the other hand in form B, represented by the structure of potassium palmitate[68], the axes of the molecular chains in each layer are all parallel. The hydrocarbon chains attached to the carboxyl groups make it impossible for the ionic structure of the type AB to be continued in all directions, so that an electrically balanced double ionic layer of K^+ ions and $-C\begin{matrix}=O\\ \diagdown O^-\end{matrix}$ (carboxylate) ions is built. The packing is shown for the top half of the layers (Fig.54). The potassium ions of the bottom half are approximately under the carboxyl groups of the top half and vice versa. Each K atom is surrounded by four oxygen in the same half of the double layer and by two others in the other half. Likewise, each oxygen is surrounded by two K atoms in the same half and one K atom in the other half of the

double layers. This manner of packing satisfies the constraint referred to earlier.

The appropriate unit cell dimensions of potassium acetate show that the b and c repeat distance resemble those of form B soaps. It will subsequently be established that this arises because of a general similarity in structure. In particular, it will be shown that the difference in the potassium-oxygen distances found in potassium palmitate between those within an ionic layer 2.71, 2.73, 2.73, 2.78 Å and those between ionic layers 2.82 Å is accentuated in potassium acetate.

Halfway along the axis of the unit cell, the methyl groups form a second double layer. A methyl group in one layer of the cell is in contact with two others in the same layer and with four methyl groups in the other layer of the cell. The average methyl-methyl separation is 4.21 Å.

4.1.3. Additional reflexions - their origins and thermal behaviours.

In view of the fact that potassium acetate, form III, shows additional reflexions of unknown origin accompanying Bragg reflexions, which disappear on heating and re-appear on cooling, it is proposed to discuss all known types of additional reflexions which may accompany the Bragg reflexions, in order to facilitate discussions later.

One class of structures which show additional reflexions in their diffraction patterns is ordered structures of substitutional solid solutions, which has been already discussed in Section 1.3.1. of Chapter 1. Here, only the diffraction theory, leading to the formation

of the superlattice reflexions will be discussed with the help of an example of an ordered structure.

It has been stated earlier in this chapter that the structure factor of a centrosymmetric structure is

$$F(hkl) = \sum f_n \cos 2\pi (hx_n + ky_n + lz_n)$$

where f_n are the scattering factors f_1, f_2, f_3 ... of the atoms in the unit cell.

Taking the body centred α-iron structure as an example, the iron atoms are at (0, 0, 0) and $(\frac{1}{2}, \frac{1}{2}, \frac{1}{2})$. So

$$F(hkl) = f_{Fe} (1 + \cos \pi(h + k + l))$$

For (h + k + l) odd, F = 0, i.e. when the sum of the indices are odd, the reflexion is absent.

In the case of the ordered FeAl structure, the iron atoms are at (0, 0, 0) and aluminium atoms are at $(\frac{1}{2}, \frac{1}{2}, \frac{1}{2})$.

Therefore, for this solid solution

$$F(hkl) = f_{Fe} + f_{Al} \cos \pi (h + k + l)$$

$$= (f_{Fe} - f_{Al}) \text{ when } h + k + l \text{ is odd.}$$

Thus in this structure, even when the sum of the indices are odd the reflexion is present, the intensity being given by the difference of the scattering factors of iron and aluminium atoms. Intensity is therefore weaker than those given alone by iron or aluminium atoms. These reflexions are the superlattice reflexions; the effect of temperature

on superlattice reflexions is shown in the section referred to above.

Other types of crystal forming superlattices due to ordering are the anti-ferroelectrics. These constitute a subdivision of a general type of crystal called antipolar. Such a structure has a superstructure although it may not have multiple cells, if there is an even number of equivalent molecules in the basic unit cell. A representative of a one dimensional antipolar structure, together with a nonpolar and polar lattice is shown in the figure (Fig.55). It is obvious from the figure that the repeat distance d of the antipolar structure is double that of the nonpolar structure.

A recent study of the phase transitions in $NaNO_2$ [69] has revealed that it has an antiferroelectric phase. At room temperature it is body centered orthorhombic. This polar structure (ferroelectric) transforms to a centrosymmetric (paraelectric) structure when heated to about 164°C. But between the two phases, within about 1°C, there is a third phase which is antiferroelectric with a repeat distance 8 times as long as the original one. Two models have been proposed to explain the origin of the superlattice along a-axis. In both, successive (100) planes of the original cell have a residual dipole moment with a certain order, but the variation in the order parameter of the successive planes differs in the two models. Thus both predict a long period along the a-axis. The difference in the order parameter can be effected in two ways, as shown by the two models (Fig.56a,b). Because the total polarity must vanish for the whole crystal, antiphase domain structure should always satisfy the conditions that the poles of

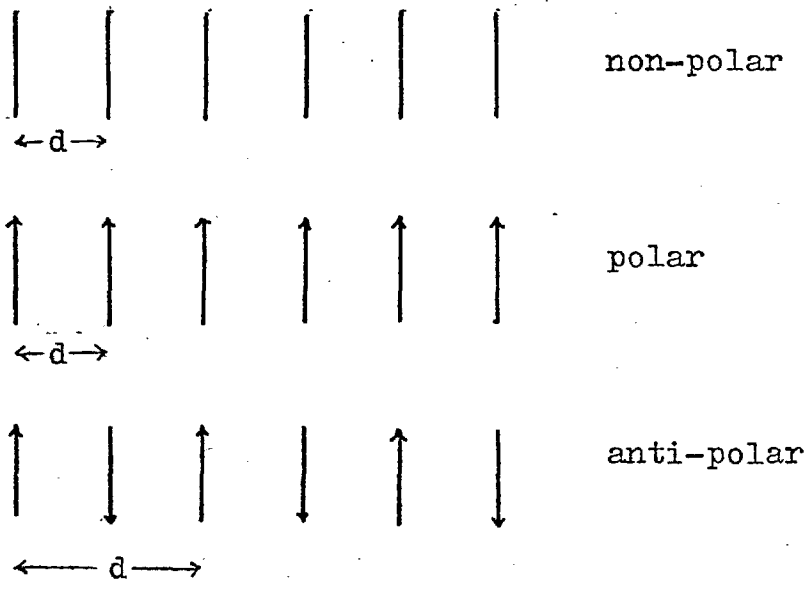

Fig.55. Schematic diagram of the anti-polar arrangement of an arrowhead representating a molecule, compared with polar and antipolar arrangements.

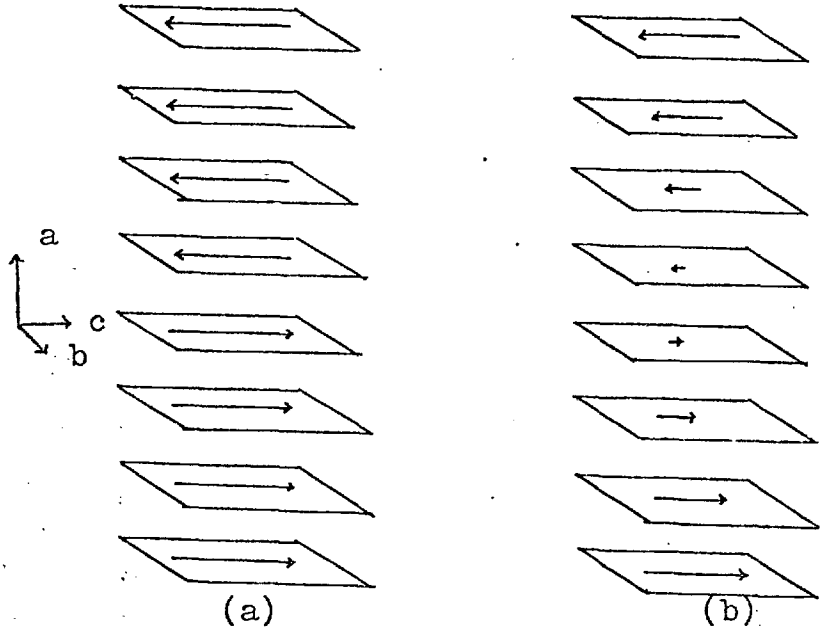

Fig.56. Two models of the structure of $NaNO_2$(after Ref. 69)

four consecutive domains point one way and poles of the next four point the other way as shown in Fig.56(a). However an alternative model in which the residual dipole moment is assumed to be given by a sine function accounted for the observed reflexions in a better way (Fig.56.(b)).

There are a few more examples of inorganic and organic structures in which additional reflexions (superlattice) have been detected under ordinary conditions of temperature. The dependence of these additional reflexions on temperature has often not been investigated. For example DL-norleucine ($CH_3.CH_2.CH_2.CH_2.CHNH_3^+COO^-$, an amino acid) crystallises in two forms, α and β. The β-form shows[70] partially ordered superstructure at room temperature. The structure is of double layer type - layers being stacked along c. The origin of superlattice has been attributed to ordered sequence of two packing arrangements, which will be presently explained. In the β-form the primitive translation $c_\beta = \frac{7}{4}c_\alpha$, where c_α is that of the α-form. From the reflexion conditions it has been deduced that a double layer is retained as a unit during symmetry operations. This unit has been termed L and when it is translated $\frac{1}{2}(a+b)$ with respect to L, it is termed M. (Fig.57).

The proposed model for the explanation of the appearance of the superlattice reflexions is that in the α-form, the stacking arrangement of the double layer is LLLL etc and in the β-form, it is LMLM (Fig.58). But reflexions $\ell = 4n+2$ are almost absent which suggests that four units of L and M are packed together in the sequence LLMM to form a unit cell. If the structure is perfectly ordered in the above sequence,

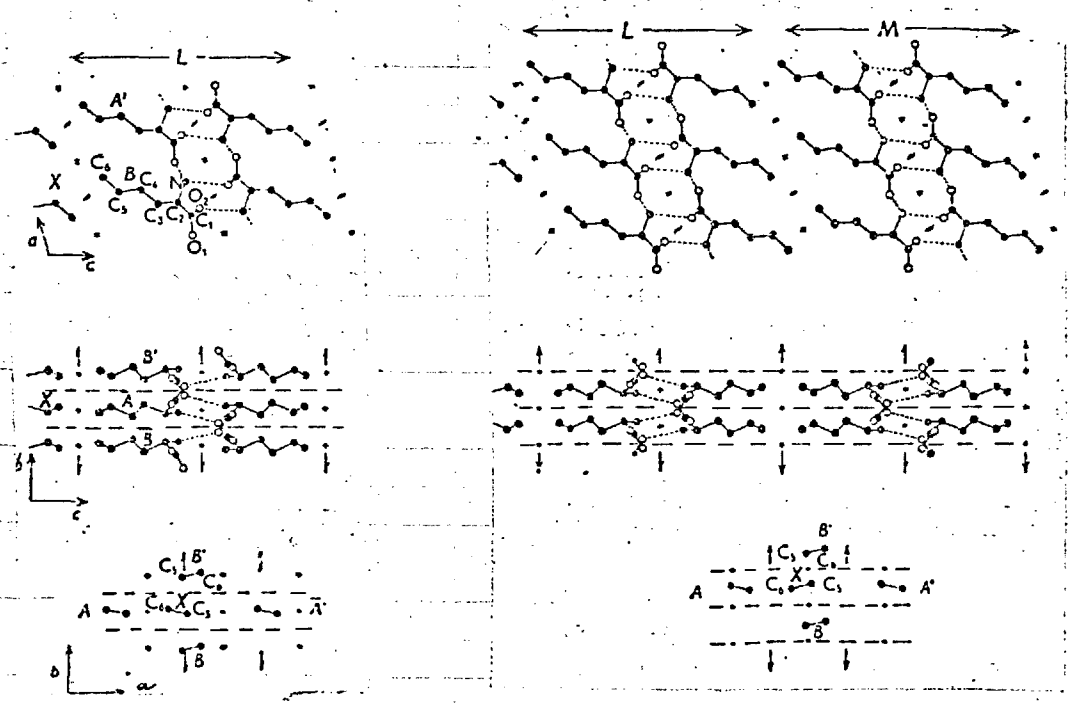

α-Norleucine β-Norleucine

Fig.57. Crystal structures of DL-Norleucine (reproduced from Ref. (70) to show packing fault of a whole unit).

Fig.58. Schematic representation of the crystal structure of β-DL-Norleucice given above. The double layer unit L is retained as a unit and when it is translated by $\frac{1}{2}(a+b)$ with respect to L, it is called M.

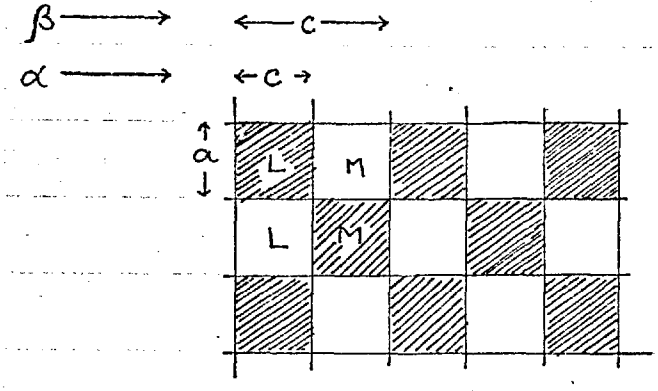

the reflexions present should be $\ell = 4n + 1$, but the presence of very weak $\ell = 4n$ reflexions suggests that the stacking is not perfect. Such structures containing faults of random nature have been dealt with by Wilson's[83] method.

Some other structures showing periodic faults have been studied by Chao and Taylor[71]. They found that some felspars had shown additional layer lines in between the usual layer lines at room temperature. These usual layer lines correspond to a structure with the c-axis of 7 Å, but the appearance of the additional layers corresponding closely to the positions of the second, third, seventh, eighth lines suggested that the actual c-axis was 5 x 7 Å.

They explained the phenomena as due to a structure which consists of two closely related structures. These are in layers approximately parallel to (001). One structure has a repeat of 7 Å and the other is about twice as great. The structures are packed alternately which gives the periodic variations giving rise to the ghost reflexions as in a ruled grating with periodic error in rulings.

Another example where the periodic variation of structure has been shown to be the reason of appearance of additional reflexions is some complexes of 4 : 4' dinitro diphenyl with 4-bromo and 4-iododiphenyl[72]. The c-axis oscillation photographs show two groups of layer lines, one sharp group and the other diffused (diffuseness varied from order to order) and elongated parallel to b. Optically independent fragments in a crystal with the smallest domain extending parallel to b would show the same elongation of spots, but then the diffuseness will

all be equal. The effect (diffused layer line) is therefore attributed to random faults occurring in the b direction. A model has been proposed where the halogen molecules in different (020) planes are displaced relative to each other.

In titanium tetrammine tetrachloride ($TiCl_4.4NH_3$)[73], heating causes diffused superstructure reflexions to appear. This has been accounted for as the disproportionate break up of the β-form (tetragonal) into two structures (cubic) i.e. $2NH_4Cl + TiCl_2(NH_2)_2$, so that one structure is contained within the other as in the felspar structures.

In the discussion of the structure of the alloy Cu_4FeNi_3[74] which shows satellites[75] when heated at 650°C, it has been suggested that additional lines appear due to a periodic variation of lattice spacing rather than superposition of two nearly equal structures as in felspars. This conclusion has been reached because the intensities of the satellites varied with the order of the spectra.

4.2. Models of the Structure : Form I

It should be emphasized that the primary aim in investigating the crystal structure of potassium acetate is to obtain some understanding of the nature of the thermal phase transformation from the structural points of view. Whilst it cannot be gainsaid that it is of utmost importance to determine the crystal structure in full, nevertheless, the aim in the present work is not to establish accurate crystal structures, but to obtain some approximation to the correct structure to understand the structural changes at the transformation.

It has been proposed to envisage some models of form I structure, on the consideration of space group, intensities of reflexions and structures of related compounds and calculate the intensities of the different reflexions for those model structures and qualitatively compare the sequences of these with the observed intensity sequences. If the model predicts the correct sequence of intensity, then it must be essentially correct. Form I structure was investigated first, because it was the easiest of the three structures, with highest symmetry (orthorhombic). Another reason was that the structures of form II and III should be derivable from that of form I by reducing its symmetry, as there was no drastic change in the transition form I $\longrightarrow$ form II, which was indicated by small change in dielectric properties, lattice constants etc.

Now, the number of formula units that must be accommodated in the unit cell was discovered to be 2 from Hazlewood et al.[7]'s density data, D = 1.52 g $cm.^{-3}$ at 155°C, with molecular weight M = 98.14 and measured cell volume = 224 $Å^3$ at 155°C. Thus, the unit cell must accommodate 2 potassium atoms, 4 oxygen atoms, 2 carboxyl carbon atoms and 2 methyl groups.

Now in the determination of space groups, it has been shown that the form I has three alternative space groups. Although the lower symmetry space groups were allowed by systematic absences it is reasonable to take the space group of form I as Pnmm, for continuous phase transitions in single crystals lead to structures of high symmetry as the temperature is raised.

This is a centrosymmetric space group, so that the number of atoms in the asymmetric unit that must be considered are 1 potassium, 2 oxygen, 1 carboxyl carbon and 1 methyl carbon, if the origin is taken at the centre of symmetry.

Now the dimensions of the acetate ion taken from the structure of ammonium acetate discussed in the introduction to this chapter show that its symmetry in potassium acetate above 155°C can be taken as 2mm (Fig.59). The 2-fold axis normal to the two planes of symmetry perpendicular to each other, is along the C-C bond of the ion. It was discovered as given above that there are two acetate ions in the unit cell. The space group Pnmm has two special positions with point symmetry mm i.e.

$$x, \frac{1}{4}, \frac{1}{4} \quad \text{and} \quad \bar{x}, \frac{3}{4}, \frac{3}{4}$$

$$\text{and} \quad x, \frac{3}{4}, \frac{1}{4} \quad \text{and} \quad \bar{x}, \frac{1}{4}, \frac{3}{4}$$

The acetate ions must occupy any one of the two special equivalent positions given above, because otherwise the number of symmetrically equivalent acetate ions in the unit cell must be increased to at least 4 because of the symmetry operations m and $\bar{1}$ of the space group. Now the point symmetry of these equipoints are mm, so the molecular and space group symmetry must coincide, so the C-C bond of the acetate ion lie parallel to an axis of the unit cell.

Now, the dimensions of the unit cell are a = 9.71, b = 5.91 and c = 3.99 Å and the dimensions of the acetate ion is length (i.e. the distance from carboxyl oxygens to the methyl group along the C-C bond)

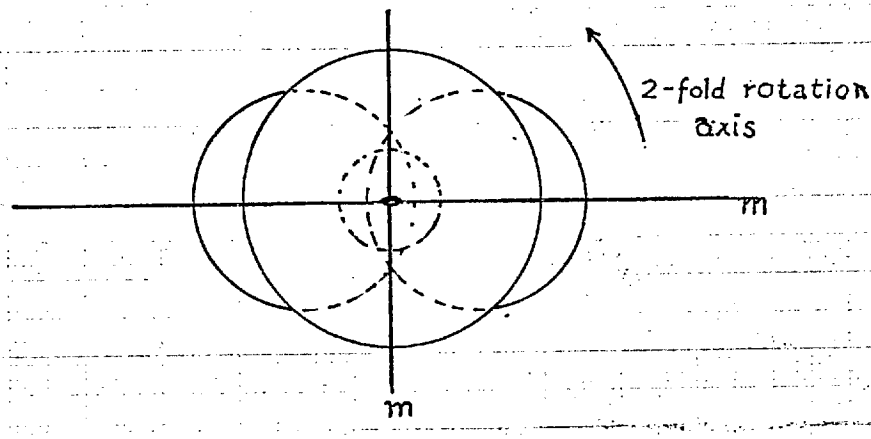

Fig.59. 2mm - symmetry of the acetate ion. With decreasing diameter : methyl group, oxygen atoms, carbon.

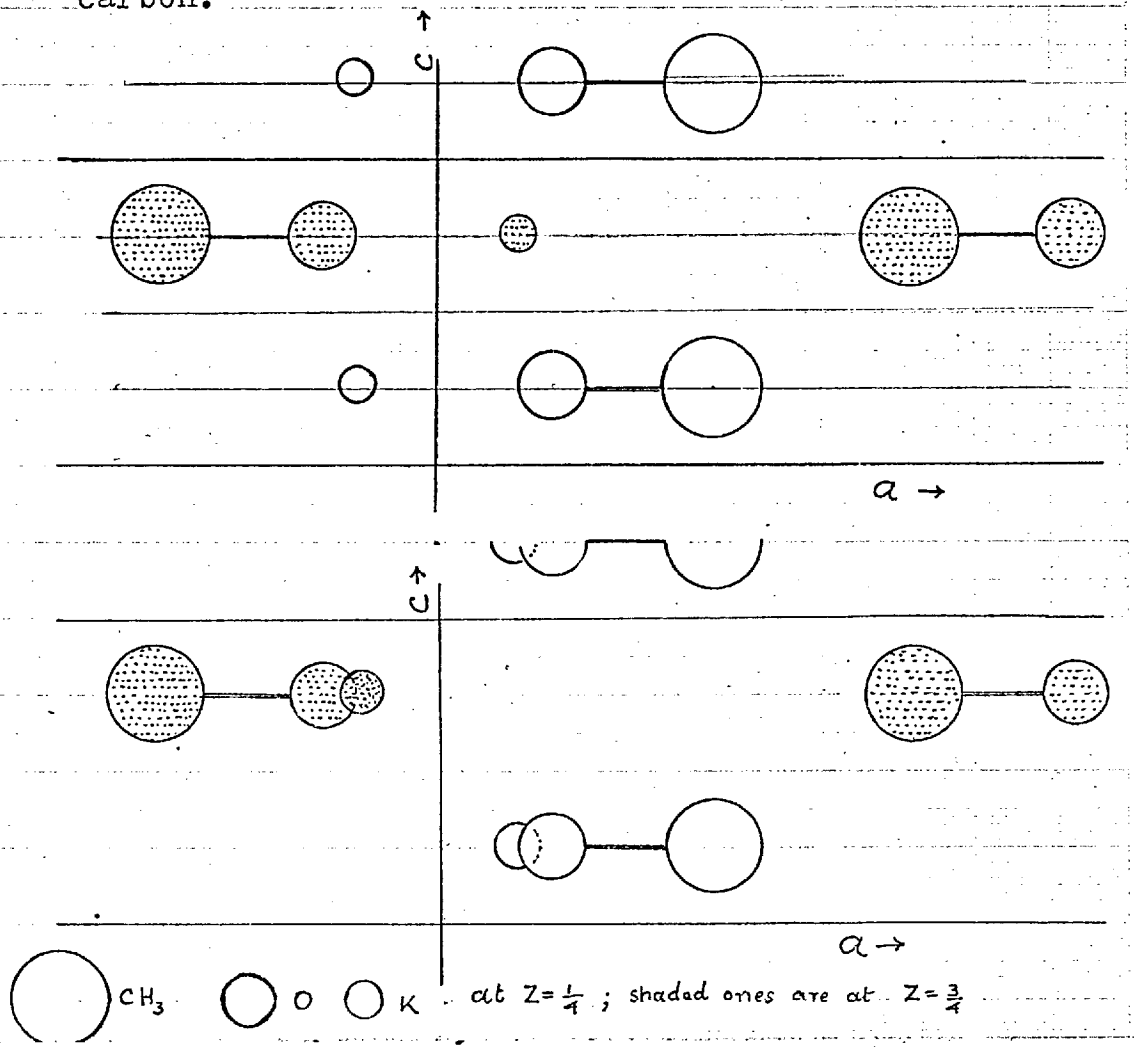

Figs.60 (top) and 61 (bottom). Schematic diagram of the two models of the crystal structures of potassium acetate form I (viewed along the b axis)

= 2.16 Å and its width (i.e. the distance between carboxyl oxygens) = 2.05 Å, ideal diameter of the methyl group = 4 Å. With these dimensions, the acetate ions could be arranged in a close packed structure only when the plane of the ion was parallel to (001) and the a axis of the unit cell. In all other planes and directions, either the packing of the acetate ions resulted in large voids or geometrically impossible. Moreover, consideration of the special equipoints shows that if one acetate ion lies along one of the three 2-fold axes of the space group at $(x, \frac{1}{4}, \frac{1}{4})$, the second ion must lie in antiparallel orientation along the 2-fold axis at $\bar{x}, \frac{3}{4}, \frac{3}{4}$ (Fig.60). There are only 2 potassium ions; so they must also occupy any one of the two special positions, for the same reasons as those given for the acetate groups. They may be located on 2-fold axes which may be either those occupied by the acetate ions or the alternative equipositions at $x, \frac{3}{4}, \frac{1}{4}$ and $\bar{x}, \frac{1}{4}, \frac{3}{4}$ (Fig.61). Thus two models of the structure were envisaged on the basis of these two alternative sets of equipoints for potassium atoms:

Model (1) both acetate and potassium ions at

$$x, \frac{1}{4}, \frac{1}{4} \text{ and } \bar{x}, \frac{3}{4}, \frac{3}{4}$$

(2) acetate ions at

$$x, \frac{1}{4}, \frac{1}{4} \text{ and } \bar{x}, \frac{3}{4}, \frac{3}{4}$$

potassium ions at

$$x, \frac{3}{4}, \frac{1}{4} \text{ and } \bar{x}, \frac{1}{4}, \frac{3}{4}$$

In both models the acetate ions being planer (as in ammonium

acetate), its methyl carbon and carboxyl carbon have the above co-ordinates in the acetate ions and the two oxygen atoms in the carboxyl group being equally inclined to the C-C bond at 61.5°, have different x and y co-ordinates. For two acetate ions in the unit cell four such equivalent positions with $z = \frac{1}{4}$ and $z = \frac{3}{4}$ are needed. Of the two alternative sets of equivalent positions,

(i) $x, \frac{1}{4}, z;\ \bar{x}, \frac{3}{4}, \bar{z};\ x, \frac{1}{4}, \frac{1}{2}-z;\ \bar{x}, \frac{3}{4}, \frac{1}{2}+z$

(ii) $x, y, \frac{1}{4};\ \bar{x}, \bar{y}, \frac{3}{4};\ x, \frac{1}{2}-y, \frac{1}{4};\ \bar{x}, \frac{1}{2}+y, \frac{3}{4}$

The second set is the needed set of points. Moreover, this set of equipoints will reduce easily to the fourfold general positions of form II, monoclinic structure (if the space group of form II is taken as $P2_1/m$) after the thermal transformation form I ⟶ form II.

Thus, the atomic co-ordinates are,

K(1) : either $x_1, \frac{1}{4}, \frac{1}{4}\ (\bar{x}_1, \frac{3}{4}, \frac{3}{4})$ for model 1

or $x_1, \frac{3}{4}, \frac{1}{4}\ (\bar{x}_1, \frac{1}{4}, \frac{3}{4})$ for model 2

and for both models

O (2) (carboxyl oxygens) $x_2, y_2, \frac{1}{4}\ (x_2, \frac{1}{2}-y_2, \frac{1}{4})$

C (3) (carboxyl oxygen) $x_3, \frac{1}{4}, \frac{1}{4}(\bar{x}_3, \frac{3}{4}, \frac{3}{4})$

C (4) (methyl carbon) $x_4, \frac{1}{4}, \frac{1}{4}(\bar{x}_4, \frac{3}{4}, \frac{3}{4})$

Remembering that the C-C bond of the planer acetate ion lies along the a-axis in (001) and taking the dimensions of the acetate ion as:

$$C\text{-}C = 1.50\ \text{Å},\quad \angle\, OCO = 123.4^\circ,\quad O\text{-}C = 1.25\ \text{Å}$$

and an ideal methyl-methyl distance of 4 Å the two models could be

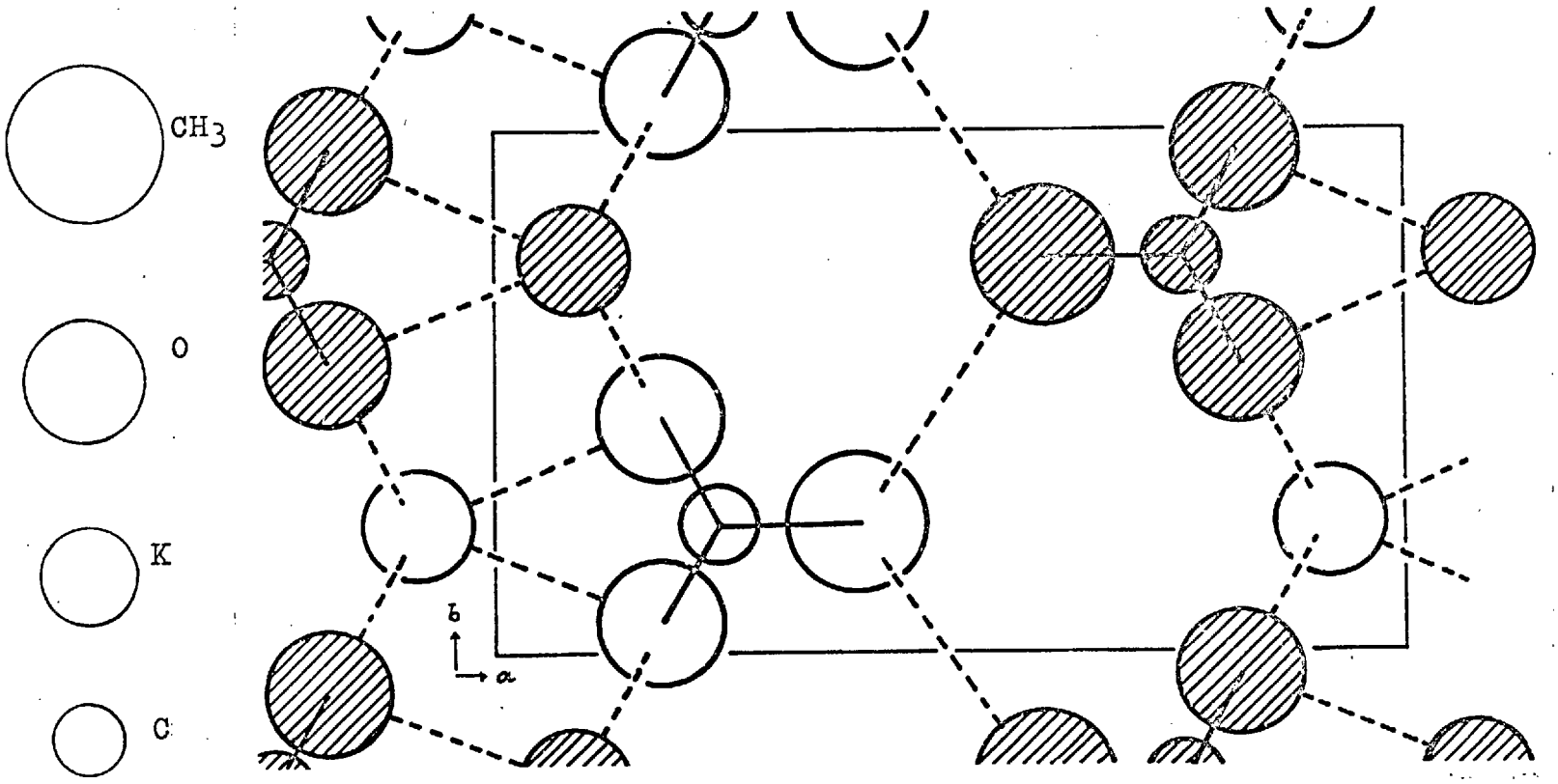

Fig.62. Model (1) of Form I (potassium acetate) structure. The shaded atoms are at $z=\frac{3}{4}$ and the others at $z=\frac{1}{4}$

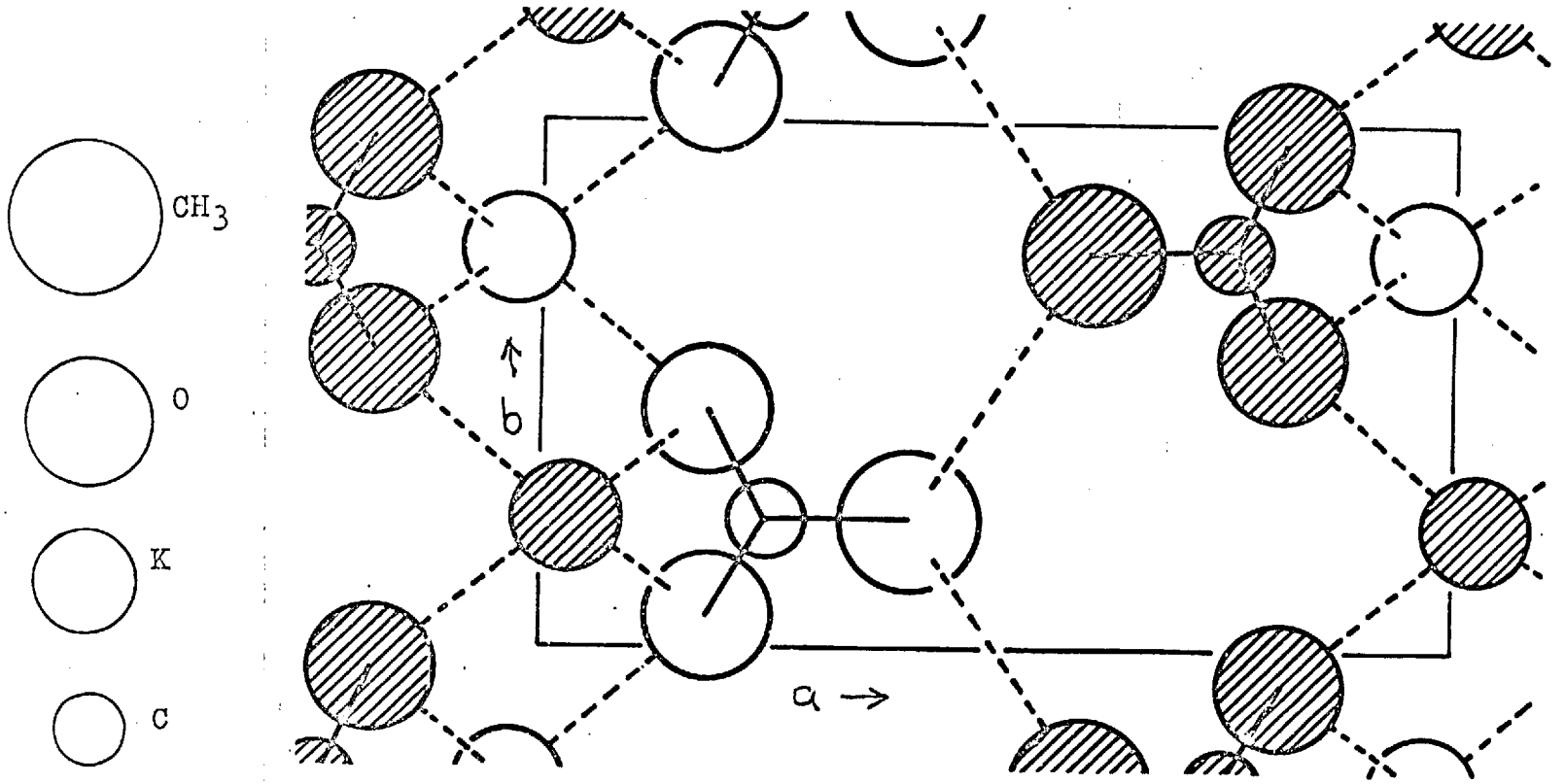

Fig.62. Model (2) of Form I (potassium acetate) structure; the shaded atoms are at z = $\frac{3}{4}$ and the others are at z = $\frac{1}{4}$

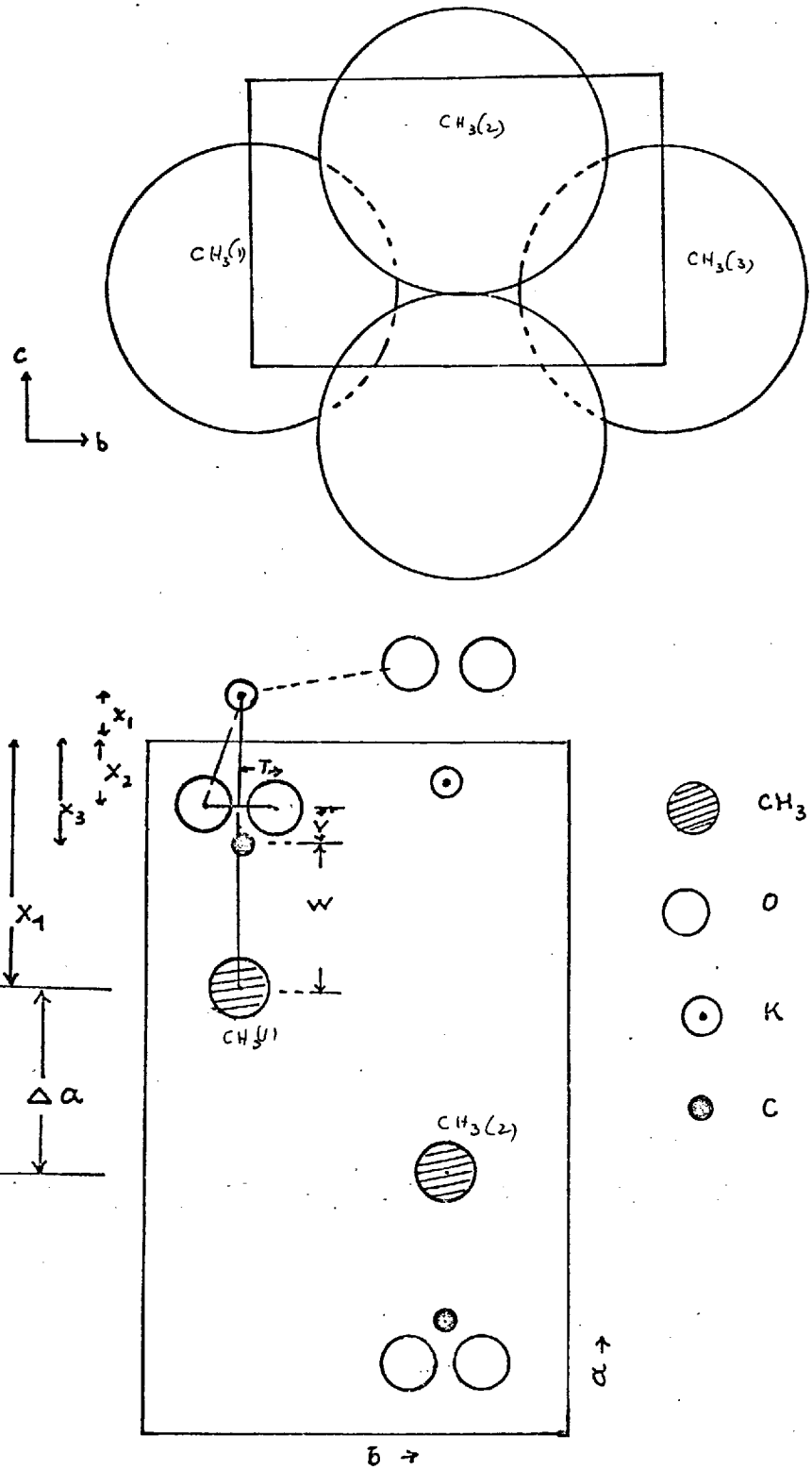

Fig.63 (top). Packing of the methyl groups in potassium acetate form I structure.
Fig.64.(bottom).Diagram for the preliminary calculation of the coordinates of the atoms in the above structure.

drawn with the different atoms in the unit cell (Fig.62).

The standard requirements for the building up of the structure are that the maximum potassium co-ordination must be satisfied and the methyl packing must be within the geometrical limitations of the unit cell.

From the above, it is seen that the nearest neighbours of a potassium atom are six oxygen atoms at $(x_2, y_2, \frac{3}{4})$; $(x_2, y_2, \frac{1}{4})$ $(x_2, \frac{1}{2}-y_2, \frac{1}{4})$; $(x_2, \frac{1}{2}-y_2, \frac{3}{4})$; $(\bar{x}_2, \bar{y}_2, \frac{3}{4})$ and $(\bar{x}_2, \frac{1}{2}-\bar{y}_2, \frac{3}{4})$.

To check the correctness of the proposed models for detailed structure factor calculation, some initial calculations were done, taking the potassium-oxygen distances to be all equal. The packing was done from the methyl ends. It was assumed that the methyl-methyl distances were also equal. Because the width of the unit cell = 5.91 Å and methyl group radius was taken as 2 Å, the methyl group (CH_3) (2) at the end of the antiparallel acetate ion must be packed in between and C/2 above the methyl groups (CH_3) (1) of the acetate ions on the same side as shown in Fig.63.

Let the methyl-methyl distance be nÅ and their separation measured along the a-axis = Δa Å.

Then from geometrical consideration

$$\Delta a = \sqrt{(n^2 - (b/2)^2 - (C - /2)^2)} \qquad (1)$$

Therefore, the co-ordinate of the methyl group $X_4 = (a/2 - \Delta a/2)$ Å and in fractional co-ordinate

$$x_4 = .5 - \frac{\Delta a}{2a} = (.5 - \Delta x) \qquad (2)$$

Let (Fig.64), V = C-O cos (<OCO/2)Å

T = C-O sin (<OCO/2)Å

W = C-C Å

Then the X-co-ordinate of the oxygen atom is

$$X_2 = X_4 - (V + W)\text{Å}$$

and $$x_2 = X_2/a \qquad (3)$$

The potassium X-co-ordinate is

$$X_1 = -[((c/2)^2 + (b/2)^2 - bT)/4X_2]\text{Å}$$

and $$x_1 = -X_1/a \qquad (4)$$

The X-co-ordinate of the carboxyl carbon atom is

$$X_3 = (V + X_2)\text{Å}$$

and $$x_3 = X_3/a \qquad (5)$$

The y-co-ordinate of all atoms except of the oxygen atom, are 0.25 and that of the oxygen is

$$Y_2 = (b/4 - T)\text{Å}$$

and $$y_2 = Y_2/b \qquad (6)$$

The z-co-ordinates of all non equivalent atoms in model (1) is 0.25 and for potassium atoms in model (2), it is $z_1 = 0.75$.

The potassium-oxygen distances can be calculated from the general geometrical relation

$$D^2 = (X_1 - X_2)^2 + (Y_1 - Y_2)^2 + (Z_1 - Z_2)^2 \qquad (7)$$

Using the above relations, the co-ordinates were calculated with the following approximate cell and molecular dimensions. The latter were those commonly found in other structures:

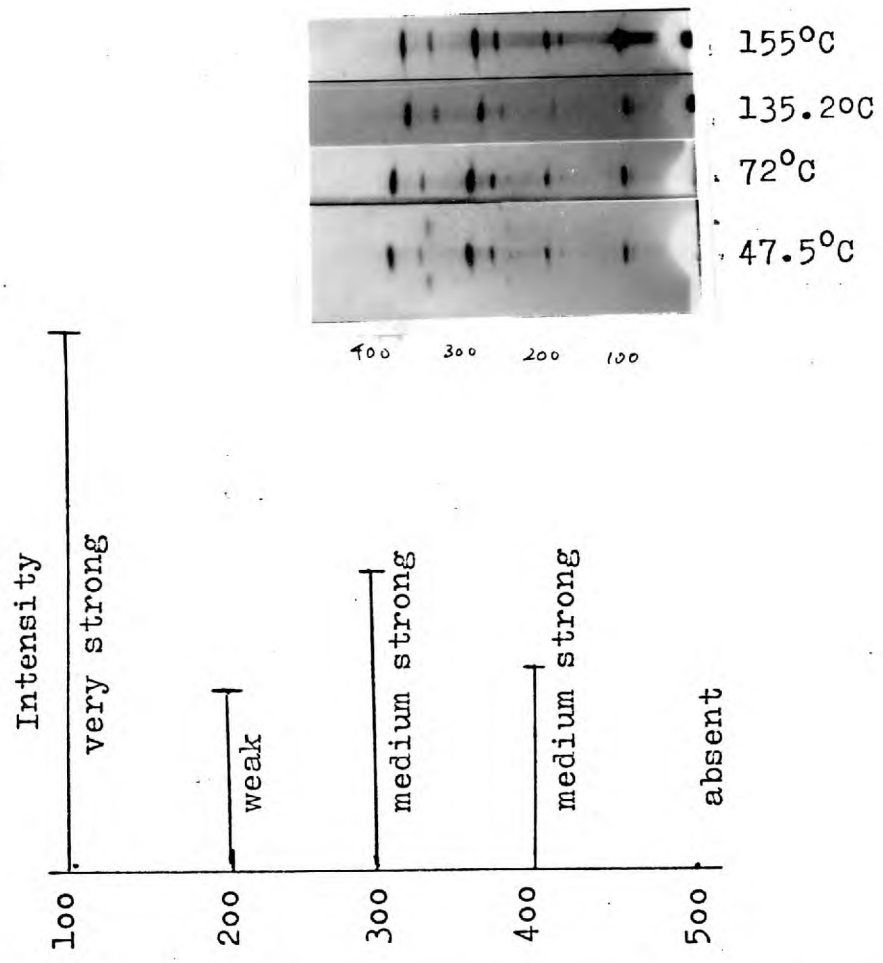

Fig.65. Photographs showing the distribution of intensity in reflexions of the type hoo. Note the large thermal expansion and the additional layer line in form III, potassium acetate.

$a = 9.71$ Å, $b = 5.91$ Å, $c = 3.96$ Å

C-C = 1.54 Å, C-O = 1.23 Å, $\angle OCO = 120^\circ$

With approximate values of co-ordinates, for both models, thus obtained, structure factors for some reflexions of the type hoo were calculated and are tabulated below along with the sequence of observed qualitative intensities. (The oscillation photographs giving these reflexions are reproduced in Fig.65).

hkl	100	200	300	400	500
Intensity (observed)	vs	w	ms	ms	absent
" (calculated $\lvert\sum F\rvert^2$)					
Model 1	49.31	4.45	88.66	121.22	4.0
Model 2	74.77	14.18	5.77	140.6	30.12

Even with these approximate calculations the agreement in the sequence of intensities for model 1 were in fair agreement with the observed intensities. Particularly striking was the result of the intensity of 500; in model 1, it was very small and in model 2, it was stronger than even 300. Also, in model 2, 200 was calculated stronger than 300 whereas the observed intensity was in the other way round which was correctly predicted by calculation of model 1.

Evidently model 1 followed the observed intensity sequence. This suggested structure factor calculation of all reflexions by sophisticated methods. The extent of these calculations makes it imperative to take the help of the computer. Although a considerable

number of structure factor programs exist, none was immediately suitable for calculating intensities, rather than F or F^2. Therefore, a Fortran IV program has been prepared for this purpose which is reproduced in the appendix.

4.3. Identification of equations used in the program

The flow diagram for the program used in the calculation of intensity is shown in Fig.66. The formulae used there are shown below. The paragraph numbers refer to the block number of the flow diagram.

(2) $RA = a^* = \lambda/a \sin \beta^*$

$RB = b^* = \lambda/b$

$RC = c^* = \lambda/c \sin \beta^*$

Used for both monoclinic and with $\beta^* = 90^\circ$, to orthorhombic system.

(6) $RHO = \rho \sin \theta = \sqrt{((ha^*)^2 + (kb^*)^2 + (\ell c^*)^2 + 2h\ell a^* c^* \cos \beta^*)}$

$\beta^* = 90^\circ$ gives 2 sin θ values for the orthorhombic system.

(8) Lp-factor $= (2 - \rho^2 + \rho^4/4)/\sqrt{(\rho^2(4-\rho^2) - 4\xi^2)}$

where $\rho = 2 \sin \theta$; $\xi = k\lambda/b$ (for b axis photographs).

This is a simplified form of

$Lp = (1 + \cos^2 2\theta)/\sqrt{(4(L^{-1})^2)}$

with $L^{-1} = (\sin^2 2\theta - \xi^2)^{\frac{1}{2}}$

(10) The trigonometrical terms

$GI = \cos 2\pi (hx_n + ky_n + lz_n) + \cos 2\pi (hx_n - (\frac{1}{2}+y)k_n + lz_n)$

for all atoms except oxygen where it is taken as 2 GI.

Fig.66. Flow diagram of the program for Intensity calculation.

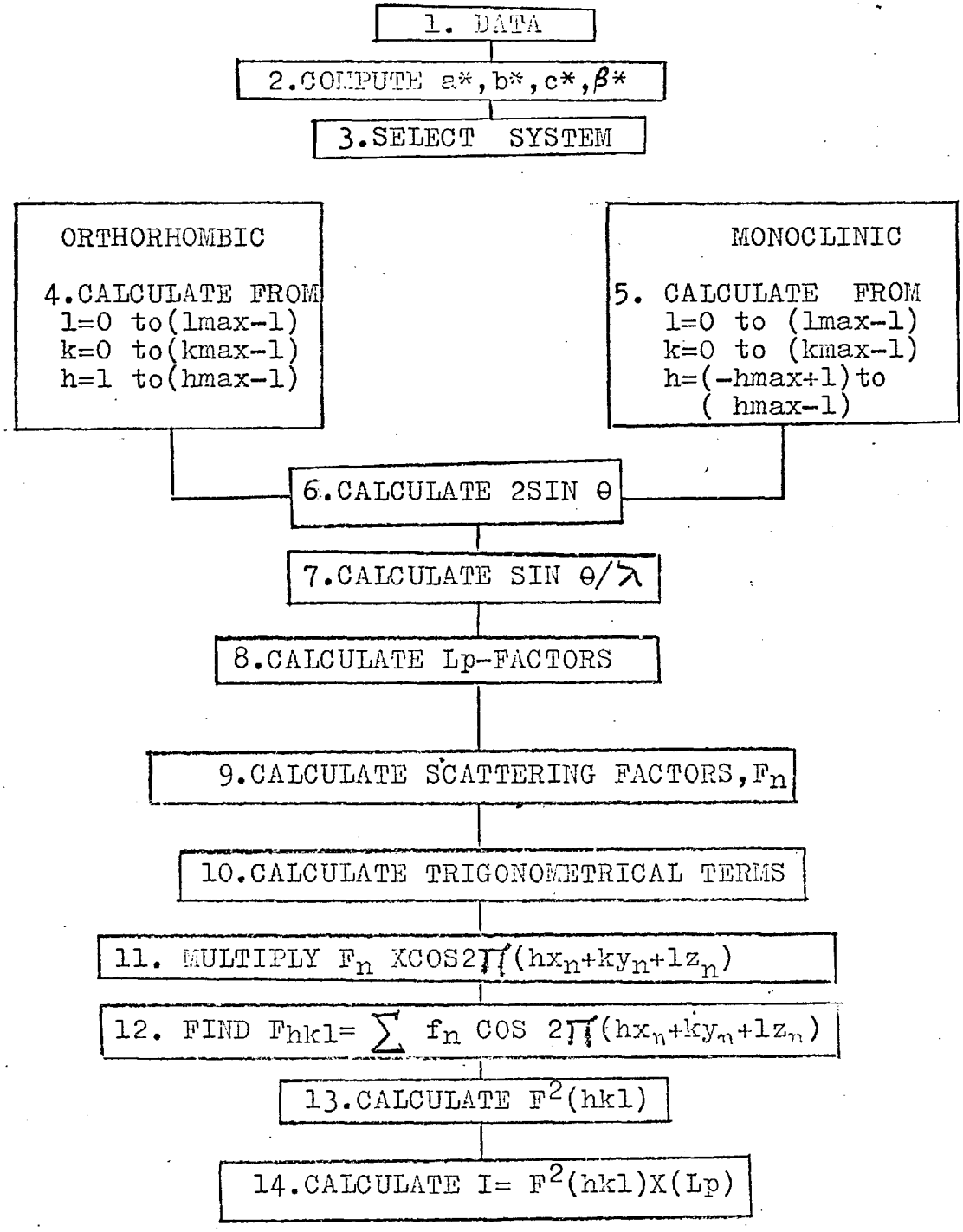

(13) $F(hkl) = \sum f_n \times GI.$

(14) $F^2(hkl)$.

(15) OBINT = Intensity = $F^2(hkl)$ x (Lp factor).

Calculation of Intensities : Trial No. 1(a).

With the above program the first trial given was the same calculation which had already been done with hand machine, for hoo reflexions, h = 0 to 5, with approximate values of lattice parameters and inappropriate values of atomic parameters.

Now, the calculation was done with the correct parameters for all obtainable reflexions. Other atomic parameters were taken from the recent measurement of Ammonium Acetate Structure discussed earlier in this chapter. Ammonium acetate being ionic crystal, it might have similar atomic parameters with potassium acetate. How far this assumption is correct would only be revealed by full structure determination.

At 155°C, the appropriate values of the lattice parameters of potassium acetate, form I, are

a = 9.744 Å, b = 5.750 Å, c = 3.993 Å and

n = 4.0 Å, C-C = 1.504 Å, C-O = 1.251 Å, $\angle$ OCO = 123.4°

Calculated Atomic Co-ordinates

Model 1

	x	y	z
K(1)	0.0841	0.2500	0.2500
O(2)	0.1858	0.0588	0.2500
C(3)	0.2467	0.2500	0.2500
CH_3(4)	0.4010	0.2500	0.2500

Model 2

K(1)	0.0289	0.2500	0.7500
O(2)	0.1858	0.0588	0.2500
C(3)	0.2467	0.2500	0.2500
CH_3(4)	0.4010	0.2500	0.2500

Observed (Fig.67) and calculated intensities are shown in the Table 4.3. In this table the first 12 reflexions of the zero layer are shown in a qualitative way. It is seen that, except for some details, model 1 gives more correct sequence of intensities than model 2. So no more calculations were done on the basis of model 2. Further trials were continued on the basis of model 1. On examining the details in the sequence of intensities for model 1, it was found that reflexions 401, 002, 102 etc were not in proper sequence; this indicated that although the basic idea of model 1 was correct, further refinement was needed in the co-ordinates. For further refinement, therefore, help was sought from known structures of allied nature, i.e. soap structures discussed in the introductory section of this chapter.

Table 4.3

Reflexions	100	200	101	300	201	301	400	401	002	102	500	202
Observed	vs	w	vs	s	w	w	ms	w	s	ms	absent	w
Calculated												
Model 1	36.87	1.67	12.30	4.89	4.27	18.31	1.25	23.11	16.25	5.76	.025	.21
Model 2	45.02	0.26	12.49	0.23	0	3.63	3.82	8.72	16.25	3.52	8.02	.15

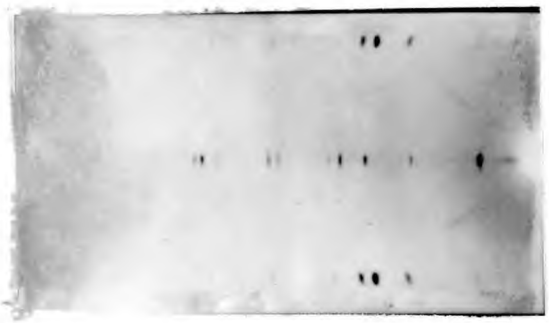

Fig.67. A rotation photograph of potassium acetate form I, about b axis showing the distribution of intensities.

Fig.67a. A rotation photograph of potassium acetate form II,about b axis showing intensity distribution.

4.4. Calculation of Intensities, Form I and the Structure

From the earlier discussion of soap structures, we can ~~safely~~ assume a few things - that our previous assumption of taking an ideal methyl-methyl distance (4 Å) and hence calculation of coordinates of the atoms giving potassium-oxygen distances all equal, is not necessarily correct. So in the light of the soap structures, another assumption is made: that co-ordinates are controlled primarily by the potassium-oxygen distances and that these distances are not all equal. Assumption is made that distances of the two neighbouring oxygen atoms from the potassium atom in the other half of the double ionic layer are equal and = 2.82 Å, as in the potassium palmitate, form B; but unlike it, the K-O distances in the same half of the layer are taken to be all equal and the value is taken to be the average of the distances given in the potassium palmitate, form B structure, and = 2.74 Å. The difference between the palmitate and the acetate structure is that the former is triclinic and the latter is monoclinic. So the co-ordination polyhedron formed by the oxygen atoms in the monoclinic structure cannot be as irregular as that in the triclinic structure. Orthogonality of the ionic sheets to the lengths of the acetate ions, is preserved if this assumption of equality of K-O distances of the same side is made. Another virtue of this notion is that the picture of the structure depicted in the previous section remains almost intact - difference being only that now we must take two K-O distances D_1 and D_2, the values of which can be obtained from the same equation (7), i.e.

$$D_1^2 = (X_2 - X_1)^2 + T^2$$

$$D_2^2 = (X_1 + X_2)^2 + (b/2 - T)^2 + (c/2)^2$$

from which

$$X_2 = 0.5\{\sqrt{(D_1^2 - T^2)} + \sqrt{[D_2^2 - (b/2 - T)^2 - (c/2)^2]} = P \quad .. \quad (8)$$

$$X_1 = -0.5\{\sqrt{(D_1^2 - T^2)} - \sqrt{[D_2^2 - (b/2 - T)^2 - (c/2)^2]} = Q \quad .. \quad (9)$$

Symbols have their meanings as before. The co-ordinates of carboxyl carbon and methyl groups are,

$$X_3 = (X_2 + V) \text{ Å}$$

$$X_4 = (X_3 + W) \text{ Å}$$

y and z co-ordinates remain unchanged.

Now, for the calculation of the co-ordinates of the trial structures, a series of D_1 and D_2 values are needed which can be obtained from a matrix formed by the two extreme values (2.82 and 2.74 Å) of K-O distances given above. At the diagonal extremities $D_1 - D_2 = 0$ Å and $D_1 - D_2 = .08$ Å. Along the rows the differences are 0, .04, .08 Å. The first row is the average $(D_1 + D_2)/2$. For the second row, the two D values are 0.02 Å apart from the average on both sides, hence forming a difference of 0.04 Å and for the third row, these are 0.04 Å apart from the average; so $D_1 - D_2 = 0.08$ Å. The matrix with nine elements is shown below: (all in Å)

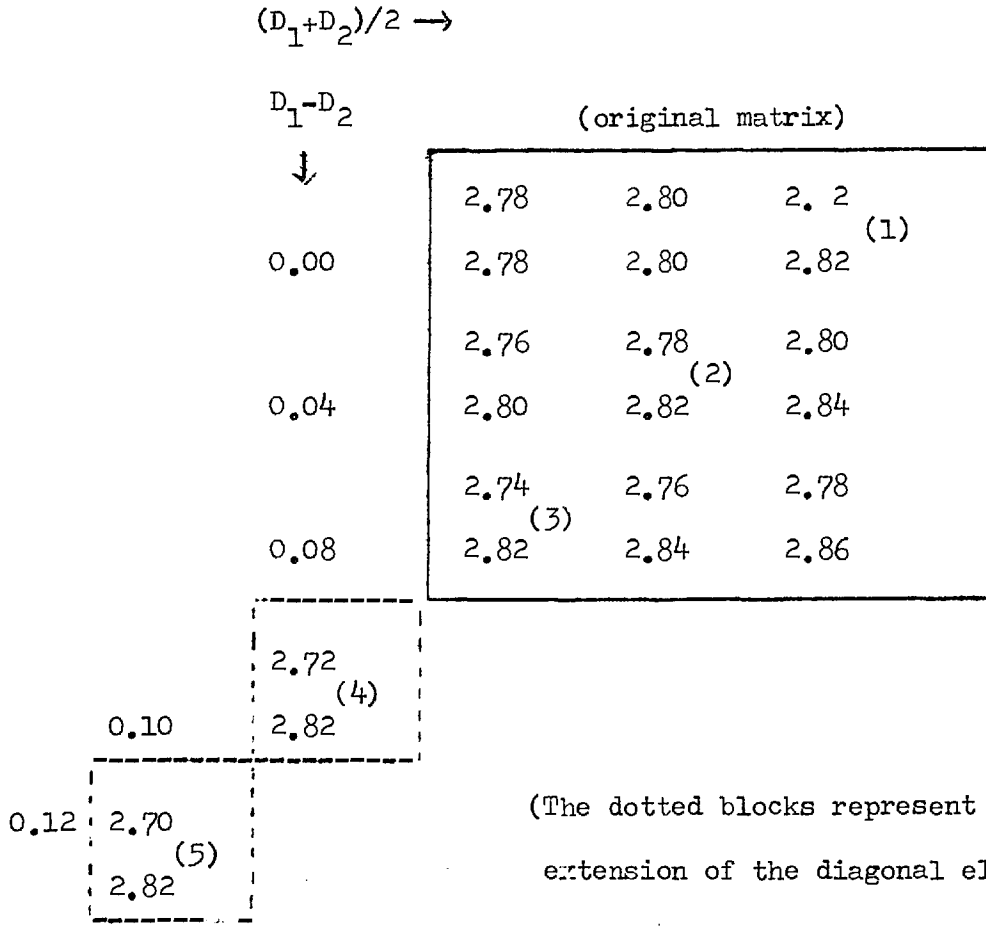

(The dotted blocks represent the extension of the diagonal elements)

Once the co-ordinates for the atoms from these trial K-O distances were computed, the intensities have been calculated feeding the data to the program mentioned before. Comparison of the calculated intensities with the observed ones showed that marked improvements have taken place in the sequence of intensities of some reflexions whereas some remain quite insensitive. This improvement was observed in a systematic way along the diagonal elements of the trial matrix (1), (2) and (3). But even so, the sequence of the critical reflexions were not completely correct, even in trial no.3. We propose to

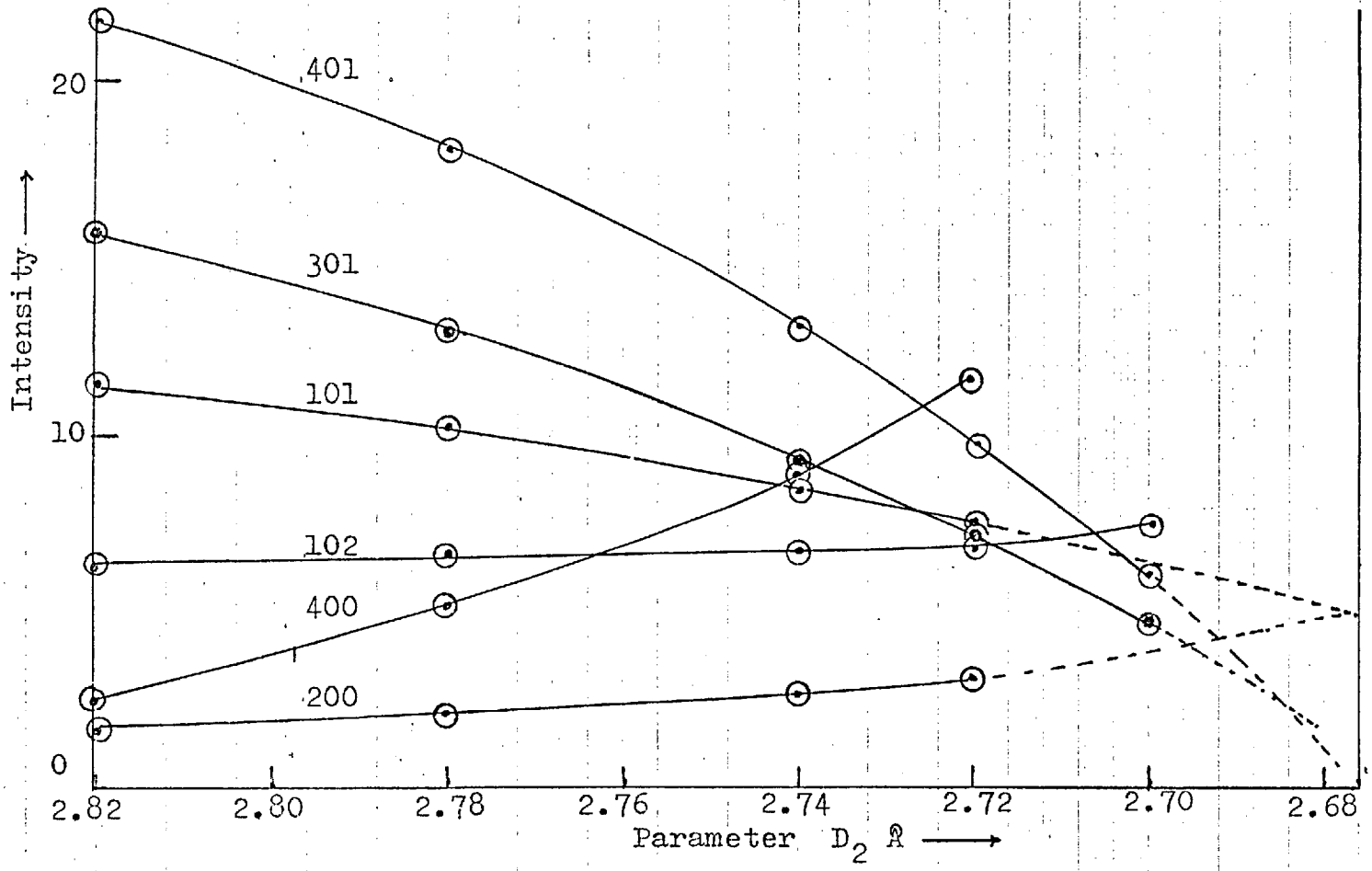

Fig.68. Variation in the intensities of some reflexions with the change in the parameter D_2. Reflexions such as 401,301,101 etc. which converged,helped in finding an optimum value of D_2 (see text)

discuss this point with the calculated values of intensities shown in the Table 4.4(a); here the multiplicity of intensities has been accounted for and the calculated values were scaled down. The critical reflexions that suggested the improvement from (1) to (3) trial calculations were 401, 002, 102. Observed intensities for these three are, $I_{002} > I_{102} > I_{401}$. With trials 1(a), (1), (2) and (3) calculated intensities were $I_{002} > I_{401} > I_{102}$. But from (1) to (3) there was increase in intensity of 102 and decrease in 401. It will be apparent from this that the difference of D_1 and D_2 should be still increased, say, to 0.12 Å i.e. extending the diagonal elements of the matrix. But before passing over to those values, it was safer to examine whether that might upset some other reflexion sequence. Such an examination was graphically possible along the line of Bradley and Lu's determination of the single parameter in Cr_2Al, mentioned by Lipson and Cochran[76]. If calculated intensities for different reflexions are plotted against the parameter D_2 (because $D_1 = 2.82$ Å was kept constant along the diagonal of the matrix), there should be value of D_2 where the intensity sequence of at least some of the critical reflexions would correspond to that of the observed ones. Such plots are shown in Fig.68. The reflexions which do not show any strong trends are not shown. Only those that appear to be sensitive to the change in the parameter are shown. It is observed that the curves 401 and 102 are approaching and the sequence of their intensities is likely to reverse before the value $D_2 = 2.72$ Å in between, is taken and this is the trial no.4. Trial no.5 with $D_2 = 2.70$ Å shows that the

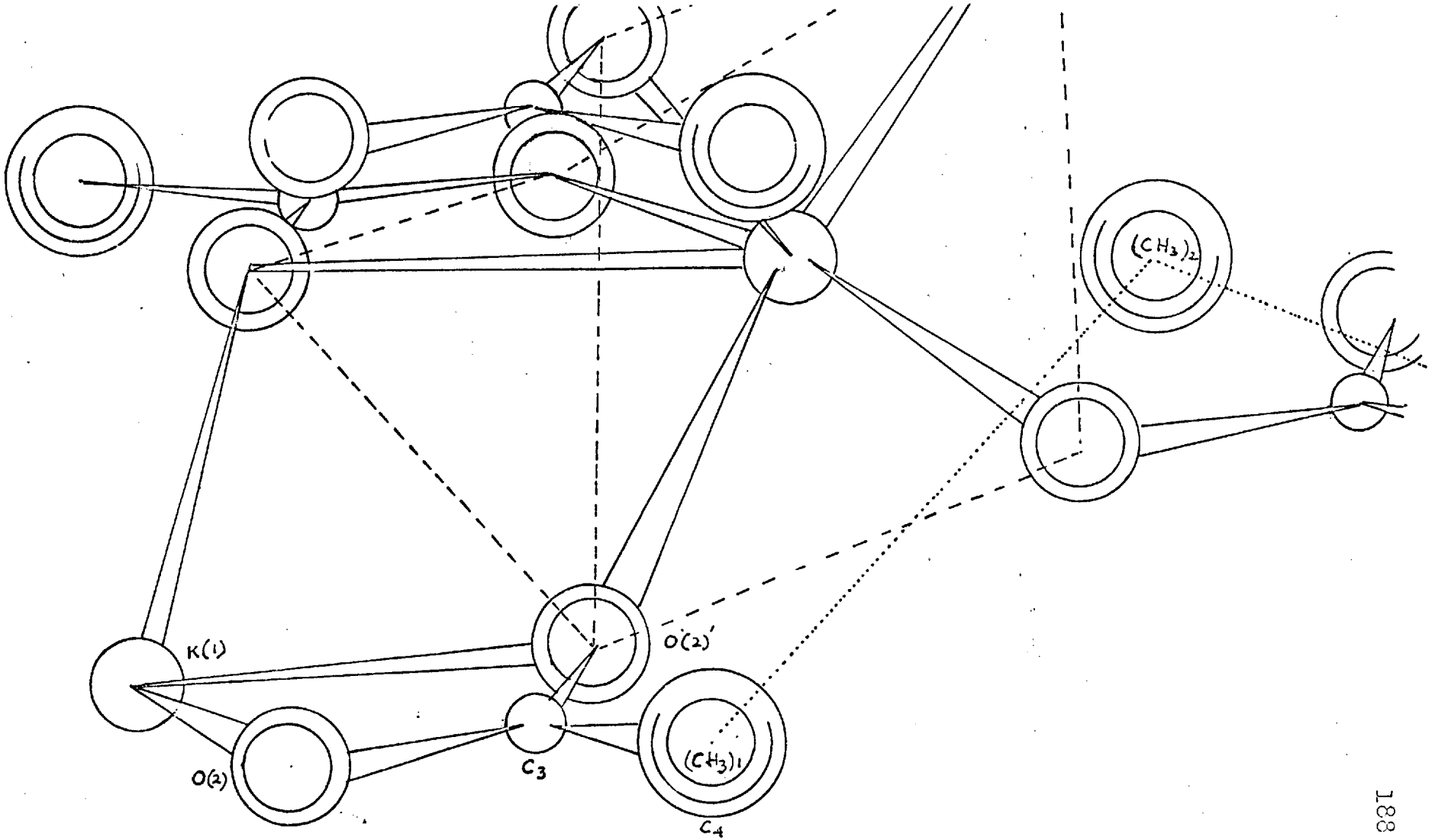

Fig.69. The crystal structure of potassium acetate, form I; coordination polyhedron is shown by dashed lines and methyl groups are joined by dotted line.

Fig.70. Intensity distribution in the zero layer line of the rotation photograph of Form I (potassium acetate). Heights are proportional to intensity. Below each line is given the calculated intensity for comparision.

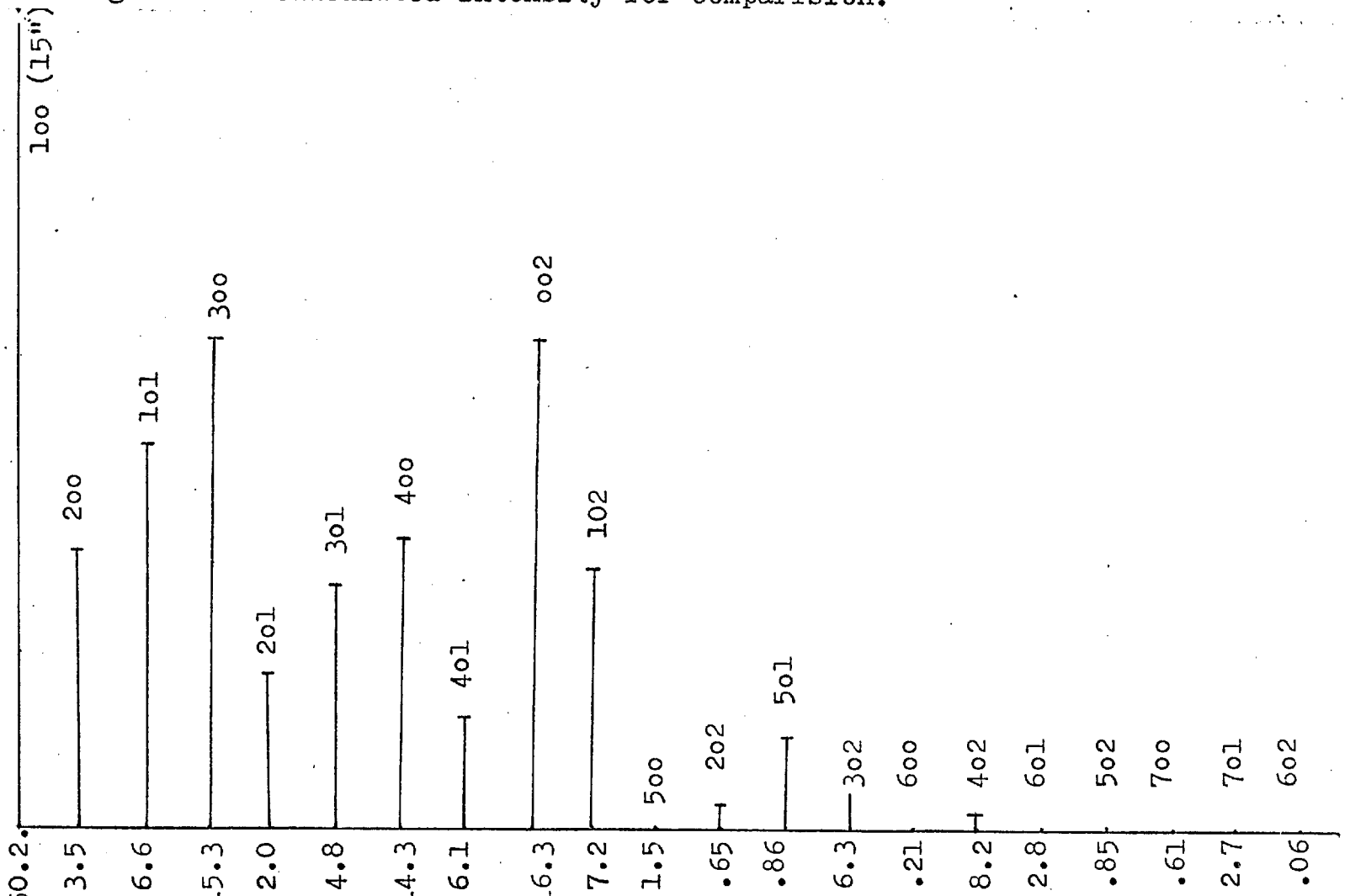

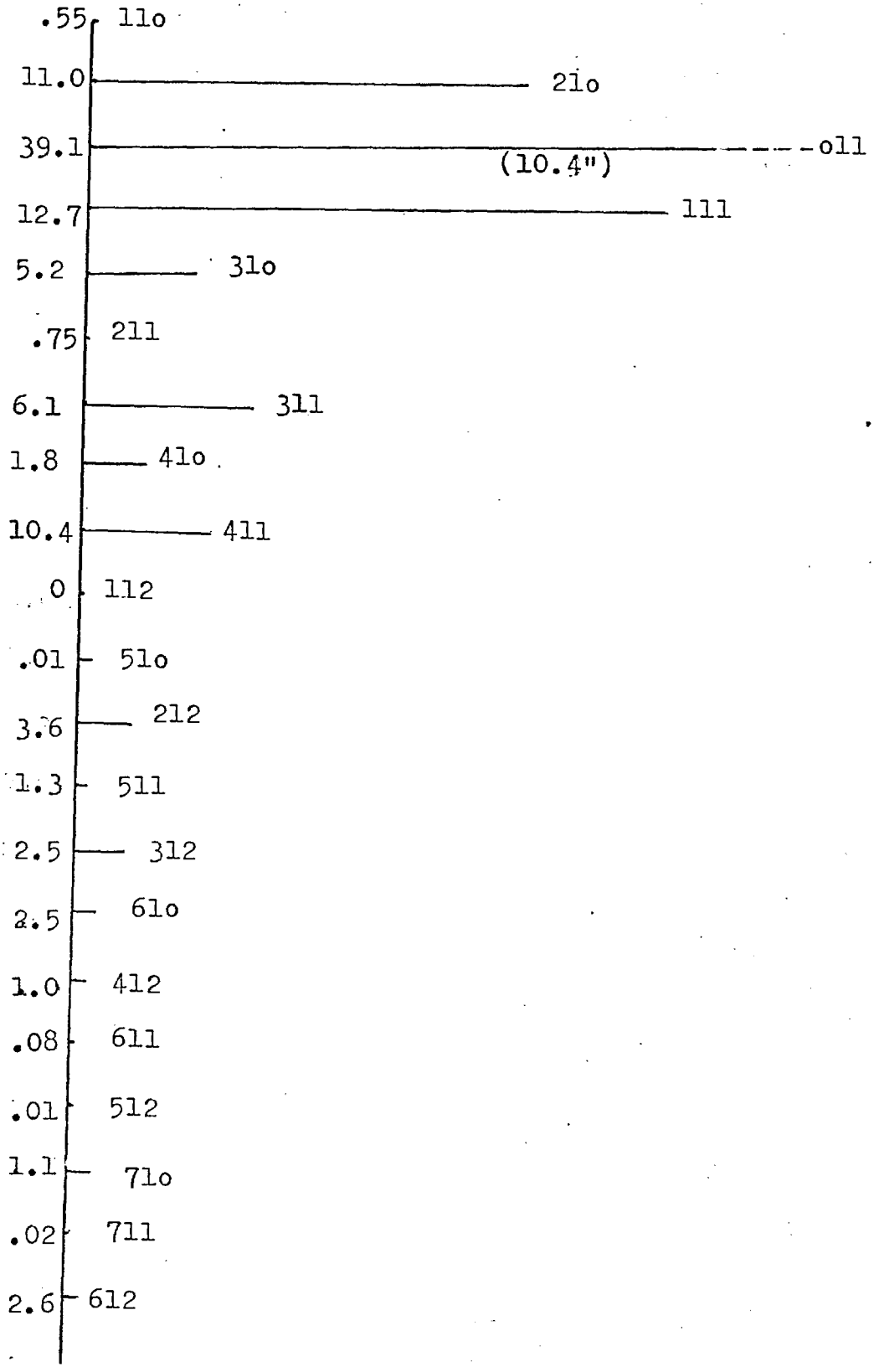

Fig.71. Intensity distribution of the same photograph as Fig.70, in the first layer line.

sequence of the above two reflexions have actually reversed as it should be.

This established that the poor agreement could be systematically corrected. The significance of the precise value of D_2 = 2.70 Å is uncertain and would require a complete structure analysis for its confirmation. What has been established was that the structural aspect of form I is as shown in Fig.69, and that the K-O distances are not all equal.

To compare the intensities calculated from the 5th trial with the observed intensities, a schematic diagram is drawn (Fig.70). Here the intensities of the observed reflexions are made proportional to the heights of the straight lines perpendicular to x-acis. At the bottom of each line, the calculated intensities (5th trial) are also given.

From Fig.70 (Table 4.4(a)), it can be seen that most of the reflexions are in correct sequences. A notable exception is 301 and 401 reflexions. Throughout all the trial calculations 401 has been calculated stronger than 301 while their observed intensities are the other way round. In the Fig.68, the curves 401 and 301 are approaching only slowly and there is no likelihood of crossing each other before D_2 = 2.68 Å is reached. But then some other reflexions would be radically altered. For example, 400 could increase to unreasonably high values. It is already calculating a high value.

Such considerations lead to the conclusion that unless full scale structure determination work is done, no more information about the

form I structure could be obtained in this way.

For the present work, therefore, the co-ordinates from trial no.5 were taken as the final co-ordinates for form I structure.

In addition to the zero layer, calculated intensities for the first layer has also been compared with the observed intensities, which is shown in Fig.71 (Table 4.4(b)). It will be seen that the sequence of observed and calculated intensities agree quite well. This thus confirms the correctness of the structure proposed for form I.

It is to be noted that the temperature factor for the reflexions was not taken into account in the estimation of the intensities. Proper calculation of B was not possible because of lack of enough data. Although statistically unpermissible an approximate calculation, by the method outlined in the introduction to this chapter, with 14 reflexions of the zero layer gave a value of about 10 for isotropic temperature factor B, from which residual R ~ .24. It is to be noted that value of B differs from atom to atom and with directions.

Thus, the final parameters for the potassium acetate structure are as follows: (Form I)

temp. = 155°C
a = 9.744 Å
b = 5.760 Å
c = 3.993 Å

D_1 = 2.82 Å
D_2 = 2.70 Å
methyl methyl distance = 4.35 Å

	x = X/a	y = Y/b	z = Z/c
K(1)	-0.1138	0.25	0.25
O(2)	0.1526	0.0588	0.25
C(3)	0.2135	0.25	0.25
C(4)	0.3678	0.25	0.25

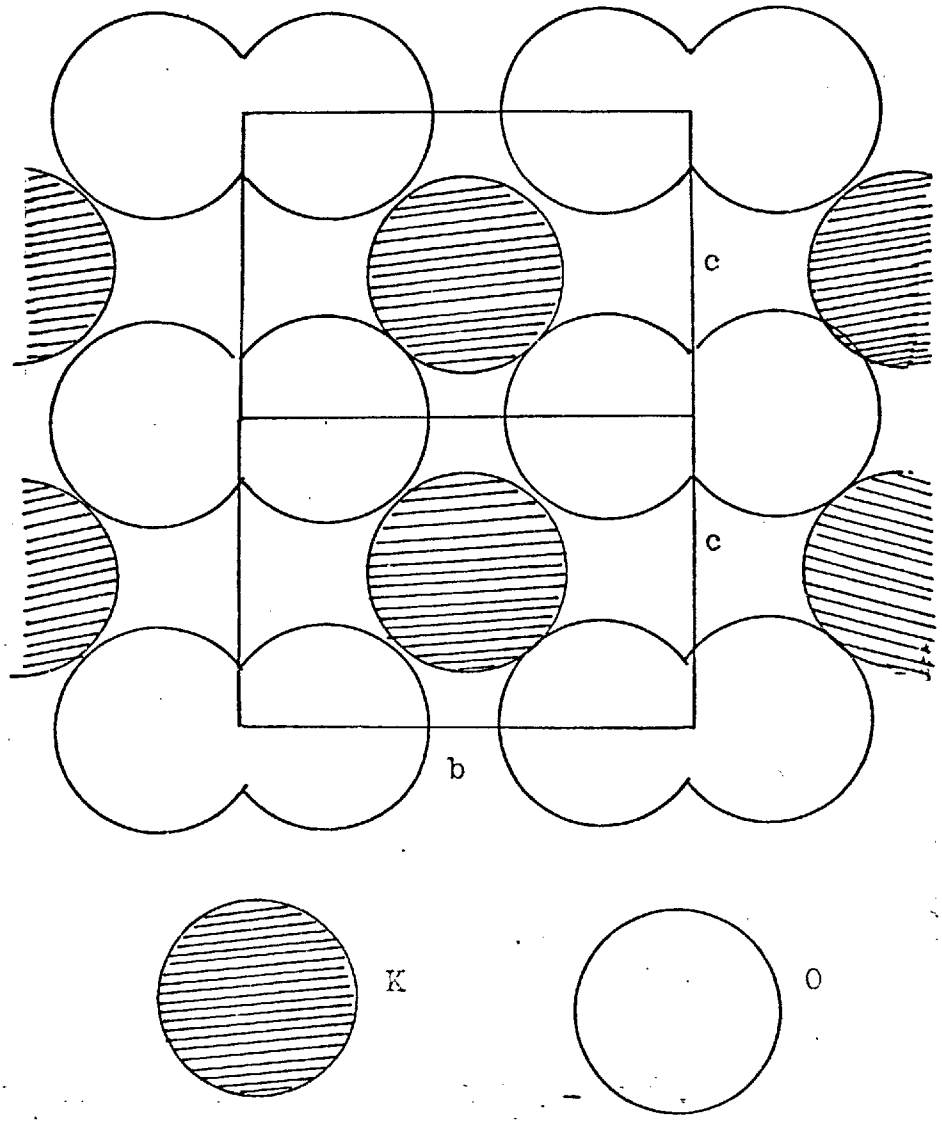

Fig.72. The top half of the ionic double layer of potassium acetate , form I structure

The structure of potassium acetate, form I based on the above parameters are shown in Fig.69. This is essentially the same figure as the one of Model no.1 (Fig.62).with the difference that potassium oxygen distances are no longer equal. Each potassium atom is co-ordin by six oxygen atoms, four of which are equivalent and belong to four different acetate groups and the other two from a different acetate group in the antiparallel position to the other acetate groups. The potassium atom is not at the centre of the polyhedron formed by the co-ordinating oxygen atoms but displaced towards the four equivalent oxygens on the same side, thus forming ionic double layers of K(1)' - O(1)' - O(2) etc on one half and K(1) and its nearest oxygens on the other half, layers being parallel to (100). Such a double layer is shown in Fig.72; only the top half of it is shown. The ionic sheets are almost identical with those of soap structures, except some differences in cell dimensions. The methyl groups attached to the carboxyl groups also form double layers parallel to (100), approximately at a/2. In the figure[63] $(CH_3)_2$ belonging to one sheet sits in between $(CH_3)_1$ and $(CH_3)_3$ belonging to the other sheet, each separated from its nearest neighbour by a distance of 4.35 Å.

Table 4.4(a)

Comparison of Calculated and Observed Intensity, Potassium Acetate, form I.

Zero layer line

hkl	Calculated						observed
	Trial 1(a)	Trial 1	Trial 2	Trial 3	Trial 4	Trial 5	
100	36.87	40.34	43.02	46.13	47.97	50.15	15.02
200	1.67	1.70	2.15	2.72	3.08	3.50	1.69
101	12.30	11.59	10.21	8.62	7.69	6.60	2.35
300	4.89	6.17	8.59	11.58	13.35	15.32	3.01
201	4.27	3.56	3.17	2.67	2.36	1.98	0.94
301	18.31	15.78	12.90	9.33	7.31	4.83	1.51
400	1.25	2.67	5.32	9.13	11.54	14.32	1.79
401	23.11	21.77	18.19	13.07	9.83	6.12	0.71
002	16.25	16.25	16.25	16.25	16.25	16.25	3.01
102	5.76	6.19	6.48	6.81	6.99	7.21	1.59
500	0.03	0	0.05	0.27	0.47	1.47	
202	0.21	0.22	0.31	0.45	0.54	0.65	0.16
501	1.44	2.02	1.90	1.55	1.25	0.86	0.56
302	1.83	2.34	3.35	4.62	5.39	6.26	0.22
600	1.33	0.87	0.42	0.06	0	0.21	
402	0.80	1.61	3.12	5.27	6.62	8.15	0.13
601	1.27	1.52	2.26	2.85	2.98	2.82	
502	0	0.02	0.16	0.33	0.49	0.85	
700	1.23	0.89	0.36	0.01	0.04	0.61	
701	1.17	1.68	2.57	3.17	3.14	2.69	
602	1.45	1.00	0.53	0.11	0.01	0.06	

Note (1) Sensitivity of the microdensitometer limited the measurement of intensity to a minimum of 1.00. Therefore, a blank indicates intensity lower than this minimum.

Table 4.4(b)

Comparison of Calculated and Observed Intensity, Potassium Acetate, form I.

First layer line

hkl	Calculated						observed
	Trial 1(a)	Trial 1	Trial 2	Trial 3	Trial 4	Trial 5	
110	2.53	2.30	1.74	1.16	0.86	0.55	-
210	12.34	11.91	11.92	11.69	11.43	10.98	26.6
011	39.12	39.12	39.12	39.12	39.12	39.12	104.3
111	11.37	11.98	12.24	12.49	12.61	12.73	35.4
310	9.93	9.39	8.57	7.27	6.36	5.16	6.6
211	0.15	0.06	0	0.16	0.37	0.75	-
311	0.52	0.89	1.90	3.49	4.61	6.08	10.3
410	8.04	7.54	6.12	4.20	3.04	1.76	3.7
411	1.49	2.48	4.43	7.06	8.65	10.39	8.0
112	0.09	0.07	0.03	0.01	0.01	0	-
510	0.35	0.39	0.22	0.06	0.01	0.01	0.5
212	3.77	3.68	3.73	3.73	3.68	3.58	3.2
511	0.61	0.71	0.97	1.21	1.29	1.29	0.6
312	4.73	4.50	4.12	3.52	3.09	2.53	2.6
610	0.22	0.46	1.05	1.85	2.25	2.54	1.1
412	4.85	4.52	3.65	2.48	1.18	1.01	0.6
611	4.90	3.47	2.50	1.22	0.57	0.08	-
512	0.30	0.32	0.17	0.04	0	0.01	-
710	0.14	0.26	0.57	0.93	1.06	1.07	1.6
711	1.53	1.44	0.89	0.28	0.06	0.02	-
612	0.20	0.44	1.05	1.87	2.30	2.62	0.7

Note (2) No.1(a) is obtained from calculation with methyl-methyl distance = 4Å and K-O distance - 2.85Å.

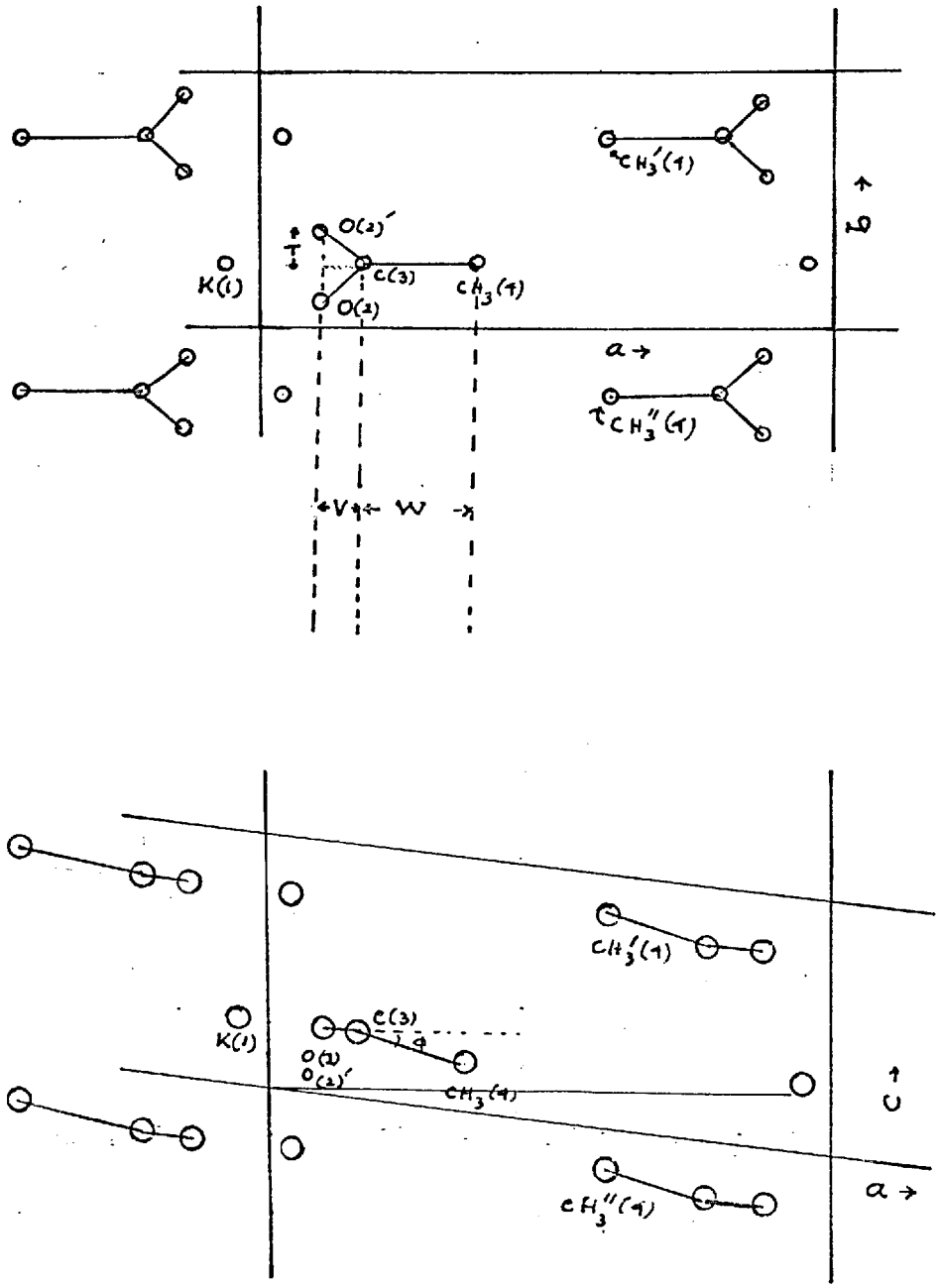

Fig.73. A schematic diagram of the model of potassium acetate, form II (monoclinic structure).

4.5. Potassium acetate: Form II Structure

A Model. As has already been discussed in the previous section, that in the potassium acetate, form I structure, the potassium ion is co-ordinated by six oxygen atoms consisting the ionic double layer parallel to (100) at $x \sim 0$ and the sheets of methyl groups are formed at $x \sim \frac{1}{2}$. While cooling through the transformation I $\longrightarrow$ II, the b and c axes of form I structure remained practically unaffected in magnitude and directions (see Fig. 27 and 28 and also subsection on the persistence of axes in section on cell dimensions at different temperatures, Chapter 2). The direction of the a-axis changed while cooling through the transformation II $\longrightarrow$ I as evidenced by the increase in the angle β between [100] and [001] from 90° in form I.

Physically and hence structurally, it would mean that the co-ordination polyhedron of oxygen atoms around the potassium ion bound by strong electrostatic forces remains thermally stable i.e. co-ordination geometry would remain unchanged through the transformation, while the transition itself originates from the thermal instability in the packing of the methyl groups, bound together by weak Van der Waals forces, resulting in the shear parallel to (100). These considerations enabled a detailed model to be proposed for form II structure. A diagram of the key features of such a model is shown in Fig.73.

Relative to the co-ordinate system used in form I, the positions of the potassium and oxygen atoms in the ionic double layer with $x \sim 0$ remain fixed, but because the a-axis has moved from its former orientation through an angle $(\beta-90^{\circ})$ which is a function of temperature, the

x and z co-ordinates of the potassium and oxygen atoms are now different. Considering such a changing situation, it is convenient to calculate the monoclinic co-ordinates relative to an orthogonal axial system, defined as follows:

Let the monoclinic axes be a_M, b_M and c_M and the orthogonal axes be A, B and C. Let $c_M \| C$, $b_M \| B$. The spacial co-ordinates x,y,z of a point in the monoclinic system of co-ordinates become X,Y,Z in the orthogonal system; the transformation equations are,

$$X = x_M \sin \beta, \quad Y = y_M, \quad Z = z_M - x_M \cos \beta.$$

When transformed, the fourfold general positions of the space group become,

$$X = x \sin \beta, \quad Y = y, \quad Z = z - x \cos \beta$$

$$X = -x \sin \beta, \quad Y = -y, \quad Z = -z + x \cos \beta$$

$$X = -x \sin \beta, \quad Y = \tfrac{1}{2} - y_M, \quad Z = z - x \cos \beta$$

$$X = -x \sin \beta, \quad Y = \tfrac{1}{2} + y, \quad Z = -z + x \cos \beta$$

(The x,y,z of the right hand side of each relation have subscripts M, i.e. x_M, y_M, z_M) while the twofold positions become

$$X = x_M \sin \beta, \quad Y = \tfrac{1}{4}, \quad Z = z_M - x \cos \beta$$

$$X = -x_M \sin \beta, \quad Y = \tfrac{3}{4}, \quad Z = -z_M + x \cos \beta$$

Thus, the co-ordinates X,Y,Z of the atoms (orthogonal co-ordinates), expressed in terms of the monoclinic co-ordinates x,y,z are (in Å)

K(1)	$X_1, Y_1, Z_1,$	$x_1 \sin \beta, b/4, c/4$
O(2)	$X_2, Y_2, Z_2,$	$x_2 \sin \beta, y_2, c/4$
O(2)'	X_2', Y_2', Z_2'	$-x \sin \beta, -y_2, -c/4$
C(3)	X_3, Y_3, Z_3	$x_3 \sin \beta, b/4, z_3 - x_3 \cos \beta$

$CH_3(4)$	X_4, Y_4, Z_4	$x_4 \sin\beta,\ b/4,\ z_4 - x_4 \cos\beta$
$CH_3'(4)$	X_4', Y_4', Z_4'	$(a-x_4)\sin\beta,\ 3b/4,\ (c-z_4)-(a-x_4)\cos\beta$
$CH_3''(4)$	X_4'', Y_4'', Z_4''	$(a-x_4)\sin\beta,\ 3b/4,\ -z_4-(a-x_4)\cos\beta$

To preserve the equality of the methyl separation, the acetate ion must tilt at an angle ϕ to the axis a and it is convenient to define the length of the C-CH_3 bond as w and the projected length of C-O bond as ν (Fig.73). It can be shown that

$$\phi = \sin^{-1}\left(\frac{a_M}{2(\nu + w)}\cos\beta\right)$$

Thus remembering that the orthogonal axial system links the orthorhombic and monoclinic unit cells (with the transformation relations given before), the co-ordinates for the different atoms are:

For oxygen atom O(2):

$$X_2 = x_2 \text{ (form I)}$$
$$= x_2 \sin\beta \text{ (form II)}$$
$$= p \text{ (say)}$$
$$Z_2 = c/4 \text{ (form I)}$$
$$= z_2 - x_2 \cos\beta \text{ (form II)}$$
$$= z_2 - p\cot\beta$$
$$Y_2 = y_2 \text{ (form I)}$$
$$= y_2 \text{ (form II)}$$

For potassium atom K(1)

$$X_1 = x_1 \text{ (form I)}$$
$$= x_1 \sin\beta \text{ (form II)}$$
$$= q$$

$$Z_1 = c/4 \text{ (form I)}$$

$$= z_1 - x_1 \cos \beta \text{ (form II)}$$

$$= z_1 - q \cot \beta$$

$$Y_1 = y_1 \text{ (form I)}$$

$$= y_1 \text{ (form II)}$$

The co-ordinates of the methyl groups can be found in terms of the co-ordinates of the oxygen atom and the dimensions and the tilt of the acetate ion:

$$X_4 = X_2 + (\nu + w) \cos \phi \text{ (form II)}$$

$$= x_4 \sin \beta \text{ (form II)}$$

$$Z_4 = Z_2 - (\nu + w) \sin \phi \text{ (form II}$$

$$= z_4 - x_4 \cos \beta \text{ (form II)}$$

$$Y_4 = y_4 \text{ (form I)}$$

$$= y_4 \text{ (form II)}$$

The co-ordinates of the carboxyl carbon atom can be obtained by writing ν instead of $(\nu + w)$ in the expression for the methyl group co-ordinates:

$$X_3 = X_2 + \nu \cos \phi \text{ (form II)}$$

$$= x_3 \sin \beta \text{ (form II)}$$

$$Z_3 = Z_2 - \nu \sin \phi \text{ (form II)}$$

$$= z_3 - x_3 \cos \beta \text{ (form II)}$$

$$Y_3 = y_4 \text{ (form I)}$$

$$= y_4 \text{ (form II)}$$

Hence the final expressions for the monoclinic co-ordinates in terms of the parameters p, q, ν, w, ϕ, a, b, c and β are:

K(1) $x_1 = q/\sin\beta$

$y_1 = b/4$

$z_1 = c/4 - q\cot\beta$

O(2) $x_2 = p/\sin\beta$

$y_2 = b/4 - t$

$z_2 = c/4 + p\cot\beta$

C(3) $x_3 = (\nu\cos\phi + p)/\sin\beta$

$y_3 = b/4$

$z_3 = x_3\cos\beta + c/4 - \nu\sin\phi$

C(4) (methyl group)

$x_4 = ((\nu+w)\cos\phi + p)/\sin\beta$

$y_4 = b/4$

$z_4 = x_4\cos\beta + c/4 - (\nu+w)\sin\phi$

The numerical data used for the calculation of co-ordinates with the above equations were

$\nu = 0.593$ Å

$w = 1.504$ Å

$T = 1.102$ Å

$D_1 = 2.820$ Å

$D_2 = 2.710$ Å

p and q were calculated by using equations (8) and (9) of section 4.4.

Calculations of co-ordinates

Using the above relations, a subsidiary Fortran IV program was written to calculate the atomic co-ordinates predicted for form II, at four different temperatures, 150°C, 130°C, 100°C and 80°C. The

co-ordinates were then inserted into the program already described for intensity calculation.

Lattice parameters used for these calculations are given in Table 4.5(a).

Table 4.5(a)

Lattice parameters of monoclinic form II structure

$t^{\circ}C$	a Å	b Å	c Å	β°
150.2	9.697	5.763	3.991	93.1
130.0	9.543	5.776	4.002	96.3
100.0	9.414	5.804	4.015	98.3
80.0	9.338	5.820	4.025	99.1

For structure factor calculations the co-ordinates x,y,z must be converted to fractional co-ordinates by dividing by the appropriate lattice parameters. These are given in Table 4.5(b).

Table 4.5(b)

Calculated Atomic Co-ordinates (fractional)

$t^{o}C$		x	y	z
150.2	K(1)	-0.1112	0.2500	0.2354
	O(2)	0.1569	0.0588	0.2706
	C(3)	0.2176	0.2500	0.2600
	C(4)	0.3717	0.2500	0.2332
130	K(1)	-0.1164	0.2500	0.2195
	O(2)	0.1573	0.0592	0.2912
	C(3)	0.2178	0.2500	0.2700
	C(4)	0.3713	0.2500	0.2163
100	K(1)	-0.1247	0.2500	0.2078
	O(2)	0.1539	0.0601	0.3021
	C(3)	0.2142	0.2500	0.2746
	C(4)	0.3669	0.2500	0.2050
80	K(1)	-0.1322	0.2500	0.2015
	O(2)	0.1494	0.0607	0.3048
	C(3)	0.2095	0.2500	0.2750
	C(4)	0.3622	0.2500	0.1994

Using the procedure given above, the equal methyl-methyl separation are calculated as

$t^{\circ}C$	$(CH_3) - (CH_3)$ Å
150.2	4.296
130.0	4.278
100.0	4.313
80.0	4.356

Comparison with observed intensities

With these co-ordinates, the intensities of reflexions for the four different temperatures were calculated and for qualitative comparisons, some observed reflexions of the b-axis rotation photograph at 122°C and a relevant oscillation photograph, and their calculated values are shown in Table 4.5(c). The photograph at 122°C is reproduced for visual comparison (Fig 67 a). It is seen that in spite of overlap of several reflexions, the sequence of the observed and calculated intensities of the given reflexions agree quite well. This indicates the basic correctness of the model of form II structure envisaged. Complete structure analysis would only confirm its final correctness.

Table 4.5(c)

Qualitative Comparison of Calculated Intensity with Observed Intensity.

Form II Structure
zero layer line

Reflexions	I(calc.) at 130°C	I(calc.) at 100°C	I(obs.) at 122°C	
100	44.71	43.20	v.s.	
200	4.52	5.83	m	
300	15.69	17.67	m	
400	12.38	13.14	m	
001)	0	.03)	m	may overlap
$\bar{1}01$)	2.94	2.35)		
101	3.09	2.52	m	
$\bar{2}01$	0.55	0.47	-	
201	1.98	1.67	w	
$\bar{3}01$	1.73	0.92	w	
301	3.42	2.19)		may overlap on 400
$\bar{4}01$	4.10	2.52)		
401	1.83	.60	f	
002	13.31	11.47	m	
$\bar{1}02$	7.25	8.19	m	
102	.44	.06	f	

(observable intensity up to about $\xi = 0.8$)

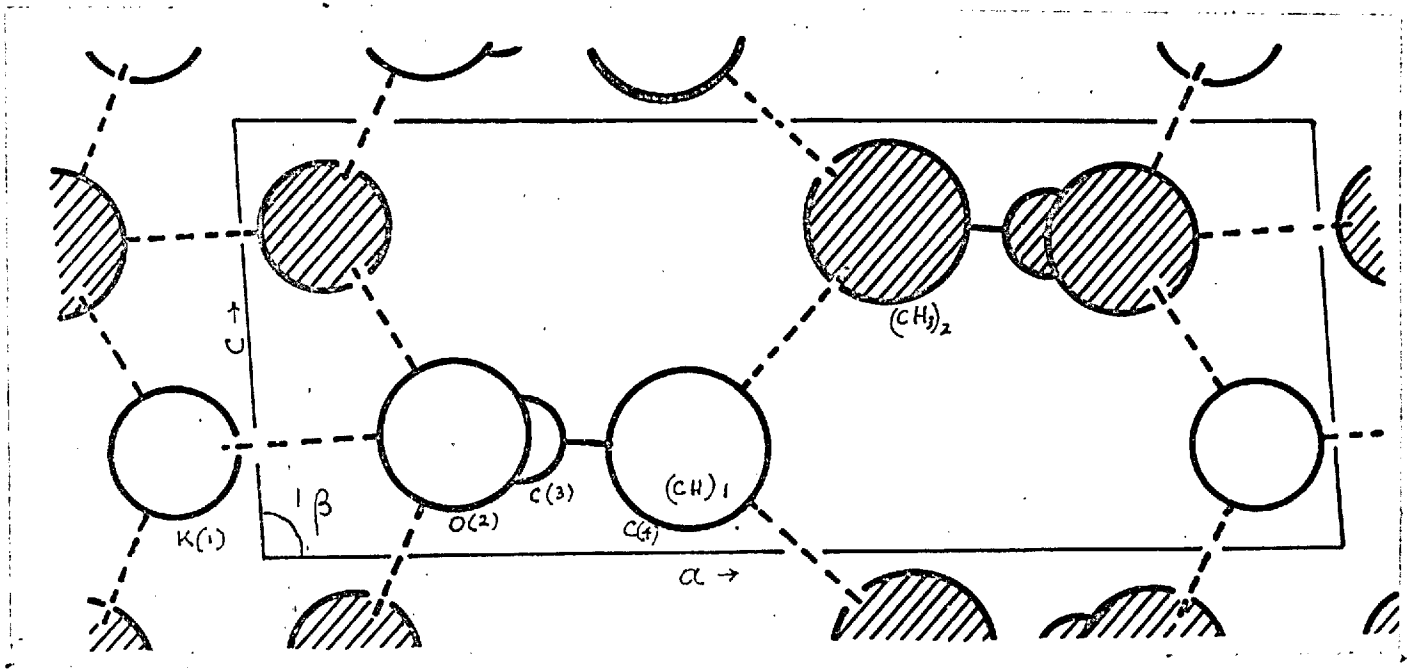

Fig.74. A model of potassium acetate form II structure. The shaded atoms are at z = $\frac{3}{4}$ and the others are at z = $\frac{1}{4}$

Table 4.5 (c)

(continued for other reflexions)

Reflexions	I(calc.) at 100°C	I(obs.)	Remarks
110	0.22	w	First layer at 122°C
210	10.4	s	" " " "
$\bar{3}11$	3.29	w	Oscillation photograph
311	4.43	s	at 114°C
$\bar{4}11$	6.38	s	" "
411	3.35	w	" "

vs, very strong; s, strong; m, medium; w, weak; f, faint.

Conclusion:

It is therefore concluded that the structure of form II is as shown in Fig.74. As in form I, every potassium ion in the ionic double wall structure is surrounded by six oxygen atoms, 4 from the same side of the double wall, all belonging to different acetate ions and 2 from the other layer belonging to the same acetate ion. In the methyl end, the equality of separation was preserved although now its value was increasing with temperature.

4.6. On potassium acetate, form III structure

The room temperature structure of potassium acetate retains the monoclinic of form II but there is an eightfold increase in cell volume which is v = (211 x 8)$\AA^3$. The number of formula units in the unit cell deduced from the dilatometric density at room temperature, $D_{obs.}$ = 1.58 g cm^{-3} and the cell volume gives 16.4 (~ 16) formula units $KO_2C_2H_3$. The calculated density for 16 formula units in the cell is $D_{calc.}$ = 1.55 g cm^{-3}.

Although no detailed structural studies on form III structure have yet been attempted, it is proposed to discuss the various possibilities on the basis of the information available so far.

It has already been discussed in section 2.10, Chapter 2, that the direction of b and c axes were practically constant through the transformation form II → form III, and very little anomalous change in the magnitude of a axis when cooled through the transition except the continuous decrease obtained all along the temperature range in form II through to room temperature (form III). Similarly, no anomalous change in c was found through this transition except the very slow increase in cooling throughout the temperature range from 155°C (form I) to room temperature (form III). The values of β also did not show any anomaly at the transition. The b axis continuously increased in length on cooling throughout the temperature range studied (from 198°C to room temperature), but at the transition form II → form III, there was an anomalous contraction of b axis (form III) (excluding the fourfold increase of its overall length indicated by the appearance

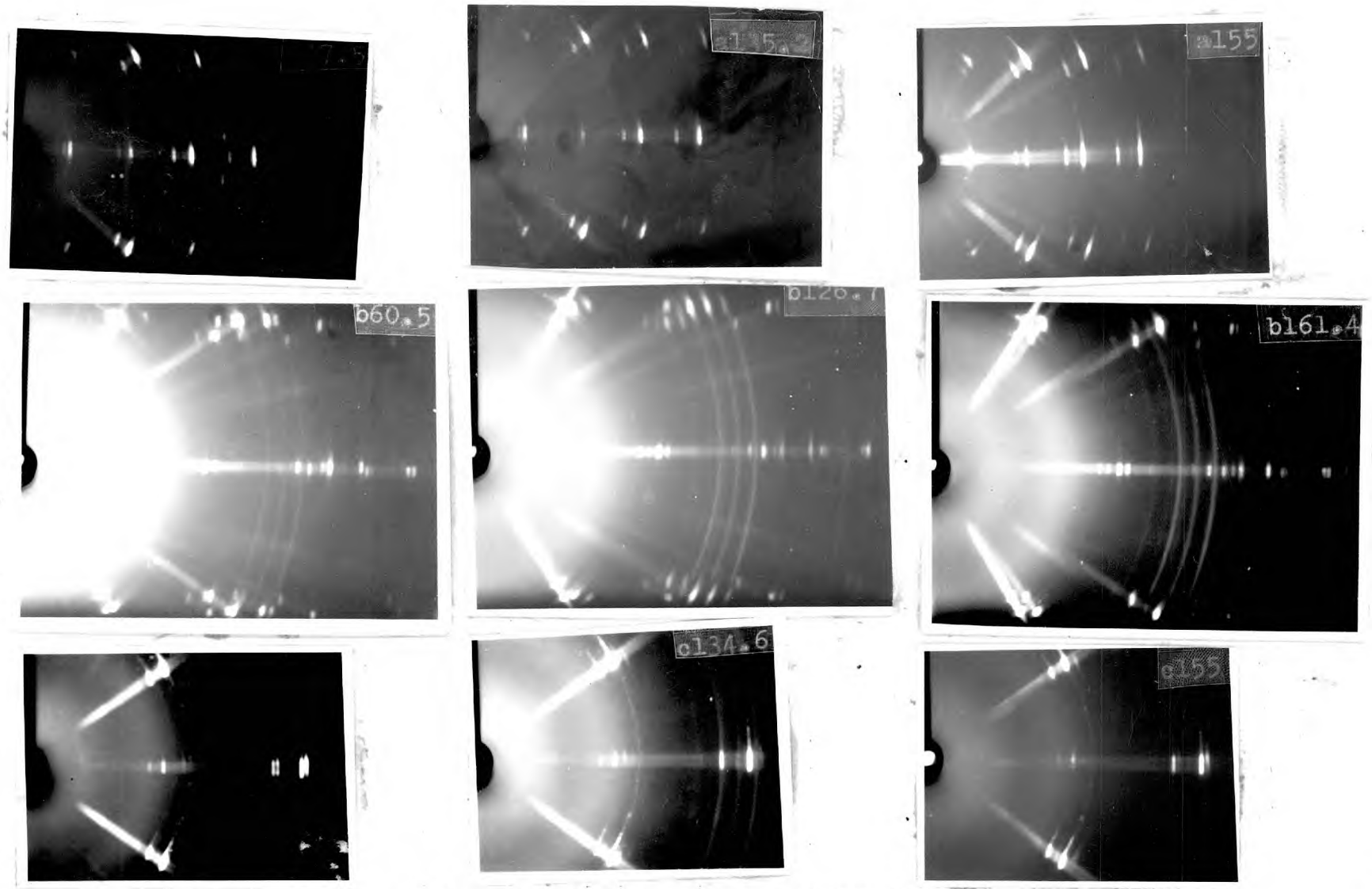

Fig.75. Comparision of the photographs of the three forms of potassium acetate, showing the similarity in their structures.

In Fig.75, shown in the previous page, 'a' denotes the photographs having reflexions 100, 200 etc. in the zero layer; the number gives the temperature at which the photograph is taken. Similarly, 'b' denotes the photographs with reflexions 040 at the extreme end of the zero layer and 'c' denotesn the photographs with reflexion 002 in the zero layer line (last but one reflexion)

of new layer lines). Most of the reflexions of the type hoo, oko and ool of form II were affected very little through the transition. In fact, as referred to above, the transition II ⟶ III could be detected only by the appearance, on cooling through the transition, of new layer lines with weak reflexions in between those on the b-axis oscillation photographs of form II. Some oscillation photographs before and after the transitions are shown in (Fig.75). The transition form II ⟶ form III could not even be detected by the dielectric measurements described in Chapter 3. The DTA thermograms described in the above chapter also did not reveal the transition.

All the above facts suggest that there was no major structural change in the transformation form II ⟶ form III.

Increase in the b cell dimensions are of the following nature:

The b-axis oscillation photographs of form III showed subsidiary layer lines between the prominent layer lines corresponding to the spacings of ~ 5.8 Å. These additional layer lines corresponded closely to the positions of the 1st, 3rd, 5th and 7th lines for a spacing of 4 x 5.8 Å. This showed that in form III structure the b axis had increased fourfold. The unaltered existence of the main layers (i.e. 4th, 8th etc in form III) suggested that form II b-cell length was still a main side of the subcell.

In the case of the a-axis, no direct experimental evidence could be produced in the above way showing additional layers. But there are other strong evidences that a -axis has doubled through the transition II ⟶ III. It was described in Chapter 2 that the indexing

of the Weissenberg photograph of form III about c-axis could be indexed only on the basis that $d_{100} \sim 9.2$ Å has doubled to $d_{100} \sim 18.4$ Å through the transformation. All other oscillation photographs taken about b and c axes could be completely indexed only on the basis of this double interplaner spacing.

Thus the unit cell of form III structure consists of 8 subcells each of which approximate to the unit cell of form II with axial lengths a/2, b/4 and c of form III.

The indices of the Weissenberg photograph referred to above showed that all hkl reflexions were absent for $k = 4n + 2$.

Now in a lattice, if all hkl reflexions were absent with $h + k$ odd, then this would require that the equivalent positions in the space groups be x,y,z and $x + \frac{1}{2}$, $y + \frac{1}{2}$, z, because the general structure amplitude is then

$$F = \sum f_n \left(e^{i\phi} + e^{i\phi \cdot 2\pi(h+k./2)}\right.$$

where $\phi = 2\pi (hx + ky + lz)$. F vanishes when $h + k = 2n + 1$.

Similarly, in the present case, the absence of reflexions with $k = 4n + 2$ requires that the equivalent positions in the lattice must be

$x, y, z;$ $x, y + \frac{1}{4}, z$ and by centering $(x + \frac{1}{2}), (y + \frac{1}{2}), z$ and $(x + \frac{1}{2}), (y + \frac{3}{4}), z,$

because,

$$F = \sum f_n \left[e^{i\phi} \left\{1 + e^{i2\pi k/4} + e^{i2\pi h+k/2} + e^{i2\pi(h/2 + 3k/4)}\right\}\right]$$

This expression becomes zero for $k = 4n + 2$, irrespective of whether h is even or odd.

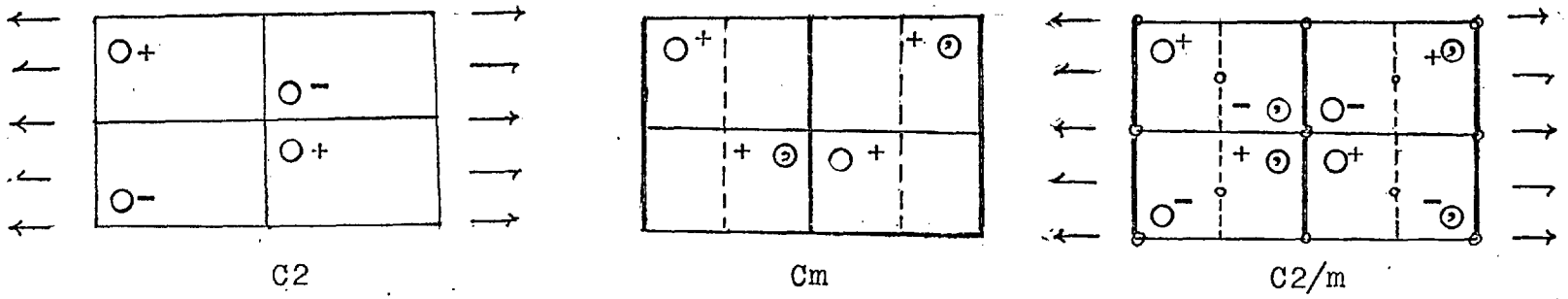

Fig.76. The possible space groups of potassium aceate form III structure. The equivalent general positions and the group of spatially distributed symmetry operators are shown. The rotation diad parallel to b, present in C2 and C2/m rules out these two space groups (see text)

Fig.77. (Identical to Fig.11)

Space group of form III

The possible space group of form III structure are C2, Cm and C2/m shown in Fig.76, where the equivalent general positions and the group of spatially distributed symmetry operations are given. Of these three possible space groups only the space group Cm is acceptable, for, otherwise the twofold rotation axis parallel to b present in the other two space groups would bring the acetate ions to positions where the K^+ ions become nearest neighbours. The situation is shown in the above figure.

Hence, the space group of form III is Cm.

Chapter 5

WORK ON SOME OTHER ACETATES

5.1. Introduction

Some studies of rubidium, caesium and lithium acetates were made in order to see the effect of change in the cation, on the structural and other properties. In the case of lithium acetate, measurements were limited to dielectric properties as some X-ray data were available[61,62]. In these three compounds, the cation radius has changed - it has decreased to 0.6 Å in lithium salt, increased to 1.48 Å and 1.69 Å in the rubidium and caesium salt respectively. Because the co-ordination number of ionic crystals depends on the radius ratio of the metal and oxygen ions, oxygen co-ordination should now increase in rubidium and caesium acetates. On the other hand the salts are anhydrous and even in the case of smaller potassium ion, there were geometrical limitations in co-ordinating the potassium ion with the available oxygen atoms. Therefore, it is of interest to see whether structural and other properties are similar to those of potassium acetate.

5.2. Rubidium and Caesium acetates.

5.2.1. Crystallographic work.

5.2.1.1. Introduction. Anhydrous acetates of rubidium and caesium (Laboratory reagent grade of 98% purity) were supplied by Alfa Inorganics Limited, U.S.A. The white crystalline materials were

very deliquescent. The experimental procedures used followed those already described for potassium acetate.

5.2.1.2. Preliminary work.

(i) Optical: As in potassium acetate, the surface of a crystal plate of rubidium acetate grown from the melt became marked by cleavage cracks as the crystal cooled. The traces of the cleavage directions were found to have a definite orientation relative to the extinction directions (Fig.77). From geometrical considerations, it was found that the cleavage plane was (110) as in potassium acetate.

By contrast the irregular cracks observed on the surface of the caesium acetate crystal plate were found to have no relation to the crystal axes.

In both cases, crystals were cut parallel to the extinction directions prior to mounting in capillaries.

(ii) Diffraction work: Oscillation photographs taken about direction (2) showed a lattice repeat distance of about 4 Å in both rubidium and caesium acetate crystals; those taken about direction (1) at right angles to it gave a repeat distance of about 6 Å for rubidium and 7 Å for caesium acetates. These values are more or less similar to c and b axes for potassium acetates. Hence, directions (1) and (2) were designated as b and c axes respectively. Diffraction photographs of these crystals at elevated temperatures ($\sim 160^{\circ}C$) did not show any significant change nor the anomalous a-axis thermal expansion found in potassium acetate and no further work at high temperature was undertaken.

As in potassium acetate, crystals could not be mounted to record photographs in which the a-axis was the rotation axis again because the lamellar shape and the high absorption of CuK_α radiation.

Linear absorption coefficients are

(i) $\mu = 169$ for rubidium acetate,

(ii) $\mu = 729$ for caesium acetate.

Even if it has been possible to use crystals about 0.05 mm thickness, rubidium acetate would have absorbed 57% of the incident radiation and caesium acetate 96%.

5.2.1.3. Weissenberg photography. Zero layer diffraction photographs of both the salts were taken at room temperature about the b and c axes using a standard Weissenberg goniometer.

5.2.1.4. Lattice parameters and space groups. Interplaner spacings were determined from the Weissenberg photographs by measuring the perpendicular distance x of the relevant reflexion from the central line of the photograph.

The c-axis Weissenberg photograph of rubidium acetate showed that the a^*b^* reciprocal lattice was orthogonal. In the b-axis photograph reflexion of the type hol were split; the effect was interpreted as due to twinning of a monoclinic structure in (100) and the pairs of reflexions were assigned indices hol and $h\bar{o}l$. The interaxial angles were obtained from the θ-values of these reflexions. Details of specific measurements are given in Table 5.2.1.4.

Table 5.2.1.4(a)

Reciprocal cell dimensions of rubidium acetate

Reflexions	θ°	Reciprocal cell dimensions
20, 0, 0	65.90	$a^{*} = 0.09128$
0, 6, 0	48.95	$b^{*} = 0.2495$
0, 0, 4	46.56	$c^{*} = 0.3623$

Table 5.2.1.4(b)

Reflexions	x mm $= \theta^{\circ}$	$\xi = 2 \sin \theta$	$\beta^{*} = \cos^{-1}\left(\frac{\xi_1^2 - \xi_2^2}{4h\ell a^{*} c^{*}}\right)^{\circ}$
602	$\theta_1 = 27.04$	0.90922)	89.4
$60\bar{2}$	$\theta_2 = 27.38$	0.91978)	
802	$\theta_1 = 30.84$	1.02528)	89.3
$80\bar{2}$	$\theta_2 = 31.26$	1.03784)	

Thus, when indexed on the basis of this cell it was found that for all hkl reflexions h+k odd were absent. The axes were accordingly transformed by the equations

$$\underline{a}_2 = 1/2\,(\underline{a}_1 - \underline{c}_1)$$

$$\underline{b}_2 = \underline{b}_1$$

$$\underline{c}_2 = \underline{c}_1$$

$$h_2 = \tfrac{1}{2}(h_1 - \ell_1)$$

$$k_2 = k_1$$

$$\ell_2 = \ell_1$$

where the ubscript 2 refers to the new cell.

Thus, at room temperature, rubidium acetate is monoclinic with cell dimensions $a = 8.689$, $b = 6.18$, $c = 4.26$ Å, $\beta = 104.4^\circ$.

In the case of caesium acetate, the zero layer b-axis Weissenberg photograph showed that a^*b^* net was apparently hexagonal with $a^* = b^* = 0.118$. The crystals were of poor quality which gave multiple reflexions and it was concluded that the crystal was multiple and not a twin as there was no preferred orientation. The question of whether the crystal really belong to hexagonal system will be discussed later.

The cell dimensions are given below:

$$a = b = 13.08 \text{ Å}$$

$$c = 3.98 \text{ Å}$$

$$\gamma = 120^\circ$$

Space groups

For rubidium acetate, the systematic reflexion conditions are:

oko present only for $k = 2n$

There are no other restrictions.

Thus, the transformed cell has the space groups $P2_1$ or $P2_1/m$.

For caesium acetate, there are no restrictions on the presence of reflexions. Inspection of reflexion intensities indicated that the Laue symmetry of the required lattice was 6/m.

Therefore, the allowed space groups are P6, $P\bar{6}$ and P6/m. Of these three space groups $P\bar{6}$ occurs rarely. Only one substance (Ag_2HPO_4) has been tentatively assigned to this space group. Thus, either P6 or P6/m is more probable as the space group of caesium-acetate.

5.2.1.5. Measurement of density. The density of the two salts was measured by the flotation method[77], using a 10 cc specific gravity bottle. Carbon tetrachloride (density ~ 1.5867 g cm^{-3} at 20°C) was added to methylene dibromide (density ~ 3 g cm^{-3}) until the small crystals introduced to it remained suspended in the liquid. All operations were performed inside the glove box. The specific gravity bottle was then filled with the mixture and taken out of the glove box for weighing on a Mettler balance (sensitivity: 0.00001 g). The whole operation from mixing the liquids to obtain the mixture with required density to the weighing of the mixture, was repeated three times and the average of the three readings were taken. The results are given in Table 5.2.1.5, along with other data for the two salts.

Table 5.2.1.5.

Salt	D(obs.) g cm^{-3}	Cell vol. V $Å^3$	No. of formula units N	D(calc.) g cm^{-3}
Rb acetate	2.19	221.56	2	2.17
Cs acetate	2.50	786.86	6	2.42

In the table, the observed values of density were used to calculate the number of formula units in the unit cell.

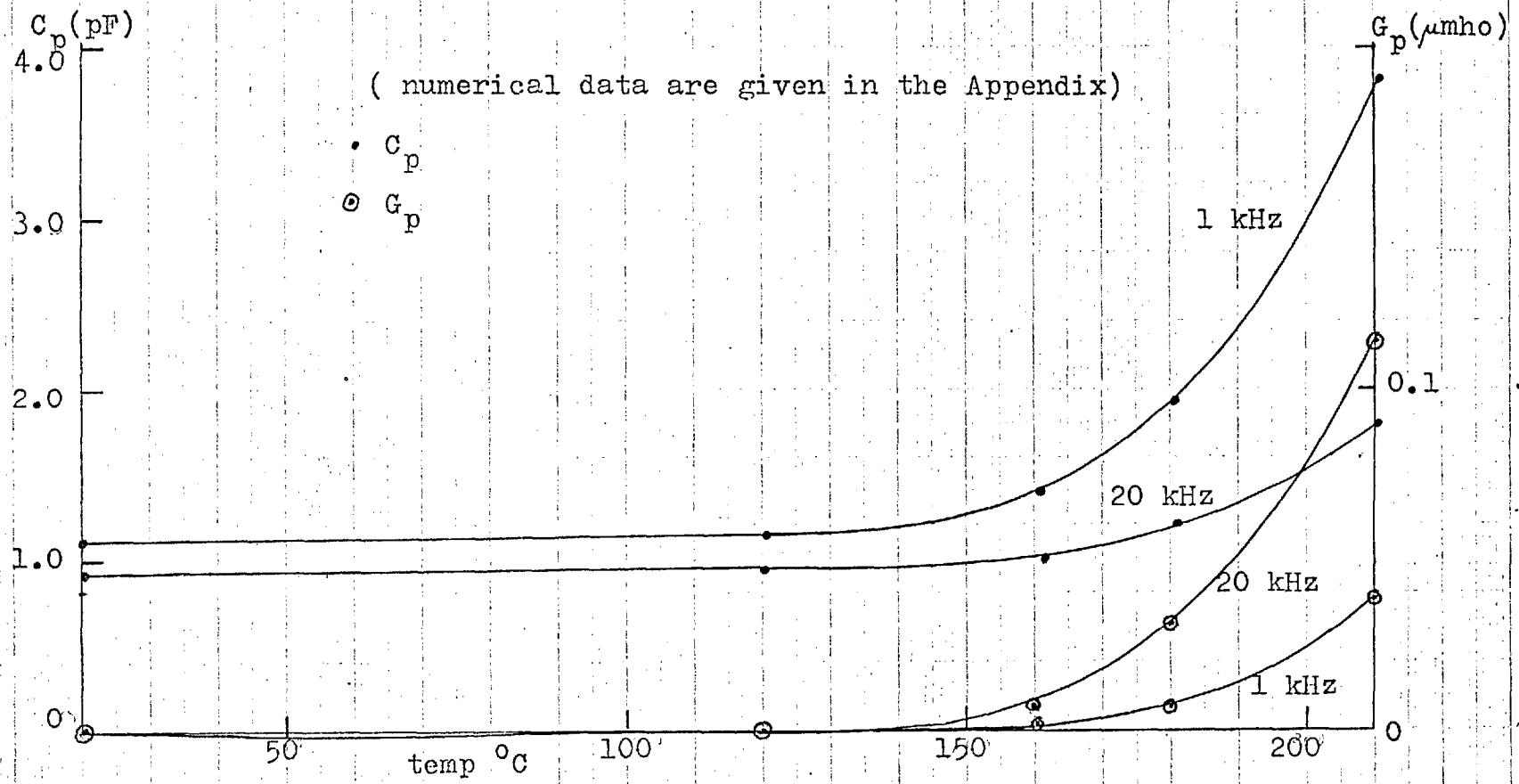

Fig 78. Variation of C and G of Cell no.2 with temperature; dielectric material : Anhydrous Rubidium acetate.

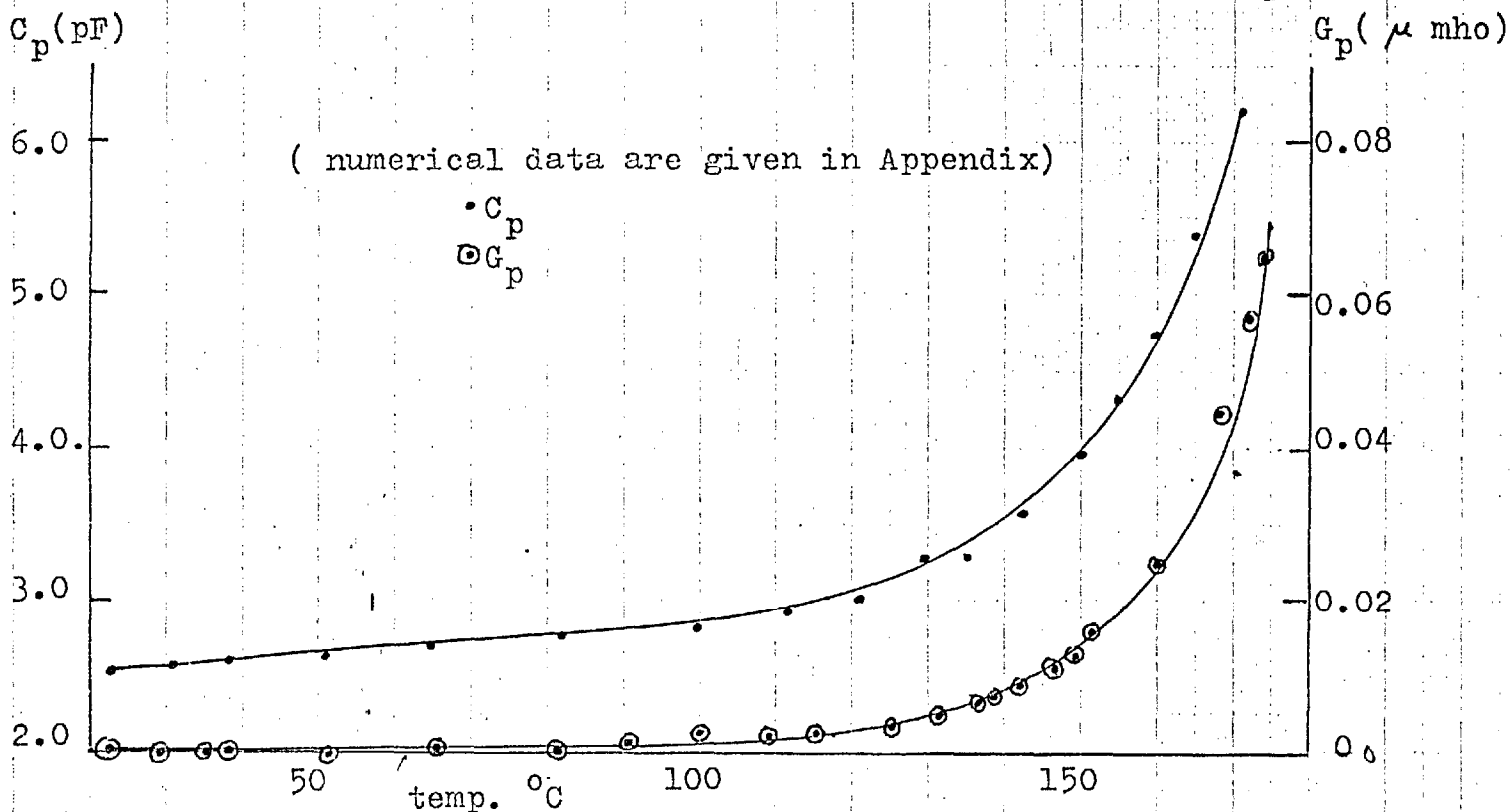

Fig.79. Variation of C and G of Cell no. 2 with temperature: dielectric sample Caesium acetate anhydrous.

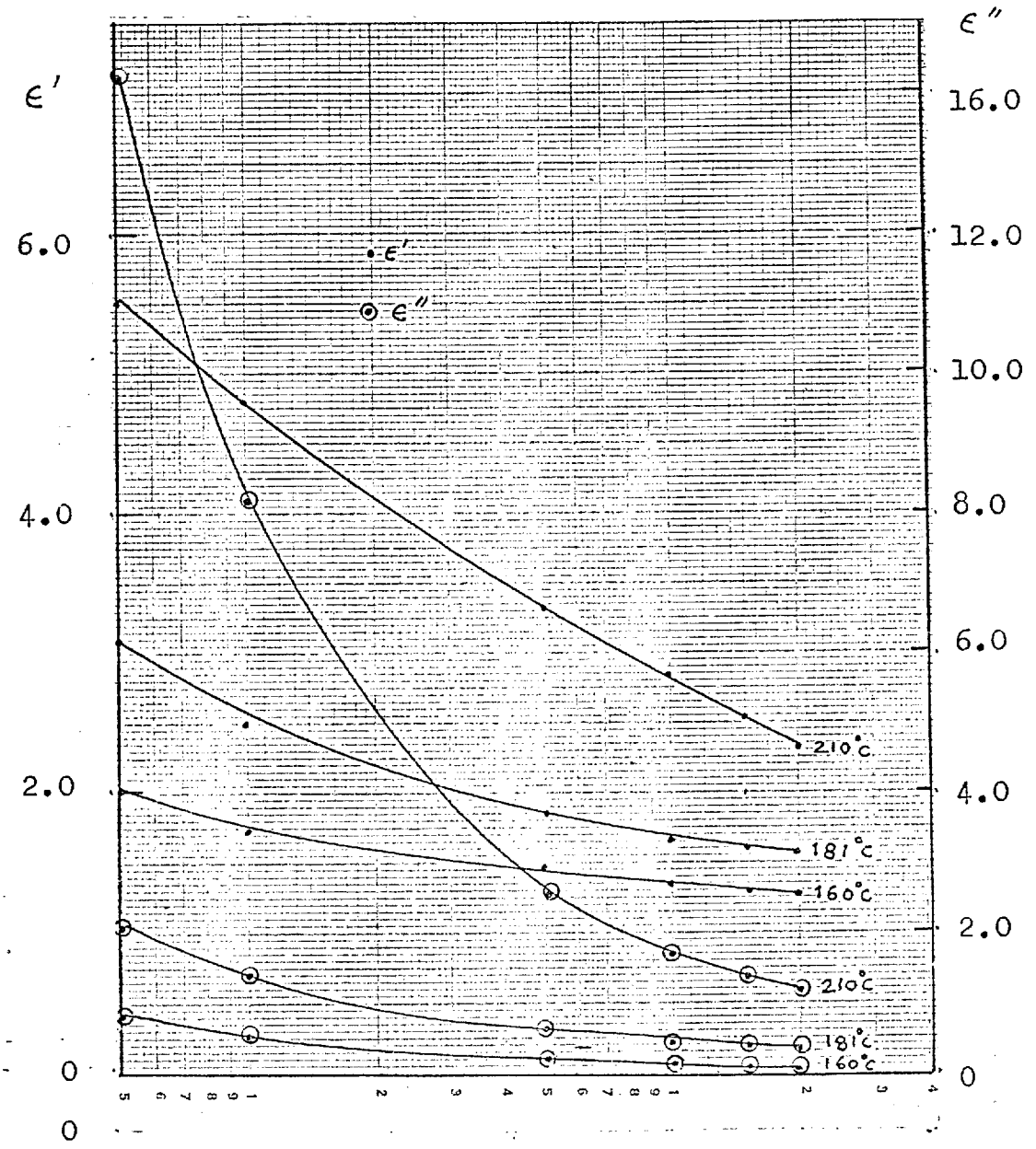

Fig.80. Variation of ϵ' and ϵ'' with frequency of anhydrous rubidium acetate.

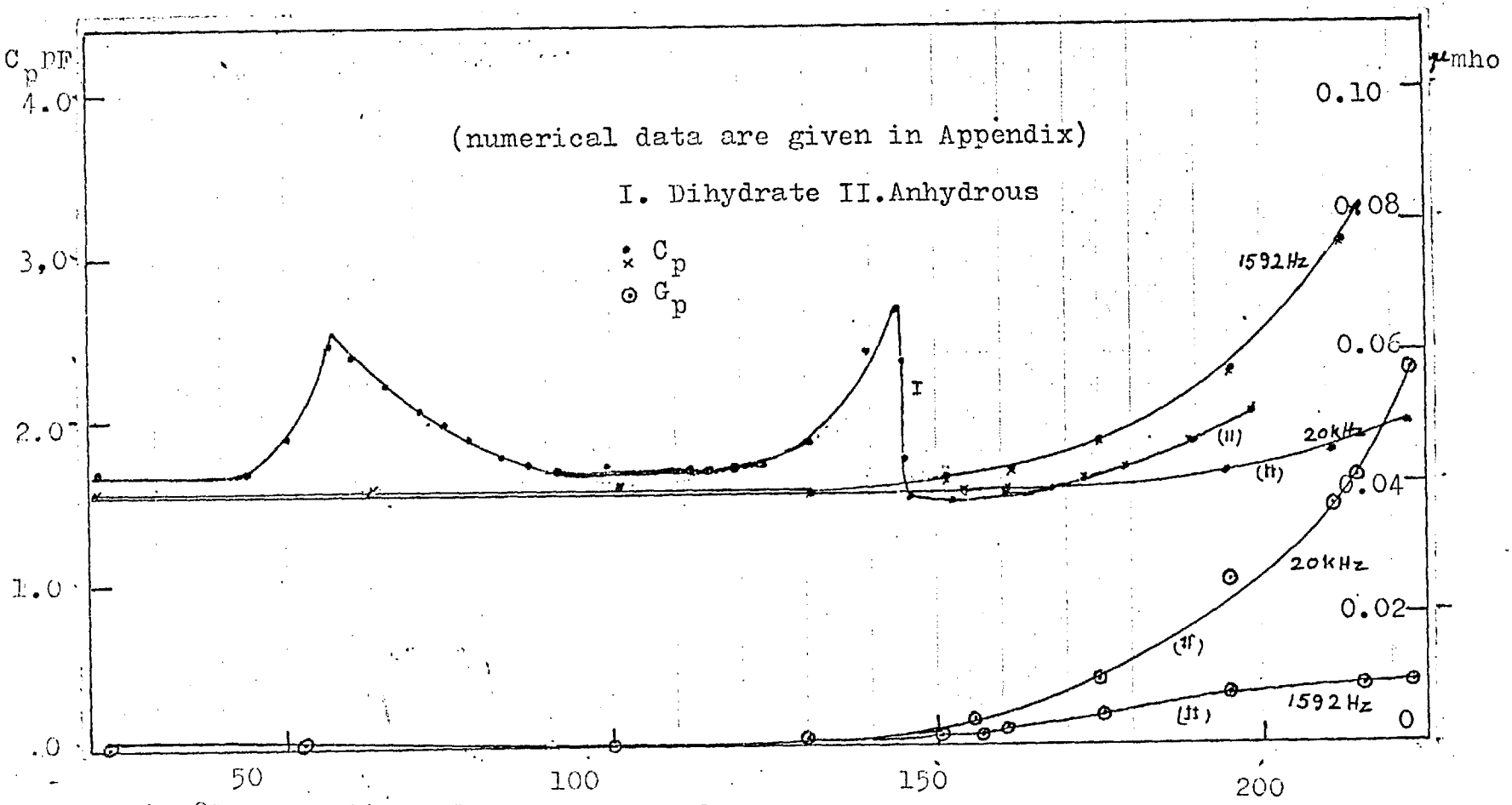

Fig.81. Variation of C and G of Cell no. 2 with temperature; dielectric material: (1) Lithium acetate dihydrate (2) Anhydrous sample made by heating sample (1)

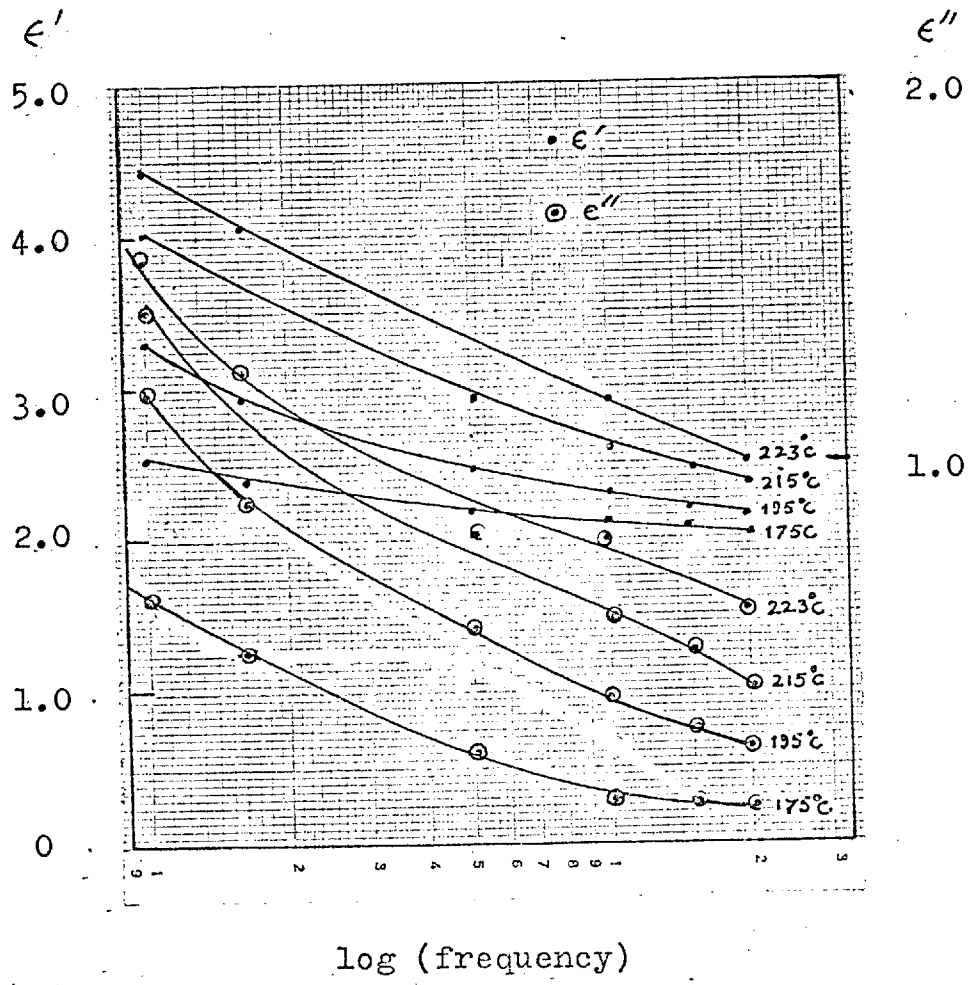

Fig. 82. Variation of ϵ' & ϵ'' with $\log_{10}$ (frequency) of anhydrous lithium acetate

5.2.2. Measurement of dielectric properties of rubidium and caesium acetates.

The procedure followed for the measurement of the conductance and capacitance of the condenser containing other ionic salts as the dielectric material were exactly similar to that of the potassium acetate. The values obtained for C_p and G_p with rubidium acetate powder as the dielectric are plotted against temperature for different frequencies in Fig.78. The tendency of the values to rise with temperature is similar to that of potassium acetate. The result for caesium acetate shown in Fig.79 also reveals the same tendency.

Values of the relative permittivity ϵ' and the loss-factor ϵ'' were plotted against log frequency for rubidium acetate and are shown in Fig.80.

5.3. Dielectric properties of lithium acetate dihydrate

Graphs of variation of C_p and G_p with temperature and at different frequencies are given in Fig.81. The two peaks in the C_p-t curve at about 58°C and in between 140°C and 145°C were due probably to the removal of the two molecules of water of crystallisation in the two temperatures respectively[78]. From the graphs, it is evident that the overall behaviour of the resulting anhydrous material is similar to the other acetates investigated. The graphs of ϵ'' vs log frequency are given in Fig.82.

5.4. A check on the reliability of the dielectric results

To check whether the results obtained so far were reliable, a sample of sodium nitrite powder, which has a well known ferroelectric transition at 163°C, was used as a dielectric in cell No.2 and the C_p and G_p values were measured at 1592 Hz. These values are plotted against temperature and displayed in Fig.83. These graphs correctly show the ferro ⟶ para electric transition at 164°C. Thus, the results obtained with the acetate samples cannot be due to any defect in the experimental system.

5.5. Conclusions

The room temperature cell dimensions of rubidium acetate are similar to those of the potassium acetate, form II structure (say at 80°C). The alternative space groups are the same in both salts, but in the case of rubidium acetate, a has decreased by about 0.647 Å; b and c have increased by 0.36 and 0.23 Å and β has increased by about 3.6°. The increase in the c-axis cannot be wholly accounted for by the difference in the ionic radii of Rb^+ (1.48 Å) and K^+ (1.33 Å), which is only 0.15 Å. It appears that there are minor adjustments in the packing although the basic structure of the ionic double layers may be the same with the rubidium ion being co-ordinated by only 6 oxygen atoms.

In caesium acetate, the ionic radii of Cs (1.69 Å) has increased to a still larger value. Surprisingly the c-axis repeat distance now

falls to 3.98 Å suggesting that a structural change has taken place.

The dielectric properties of the acetates studied so far show the same tendency of rapid rise at higher temperatures. Further discussion of these results is postponed to the Discussion Chapter.

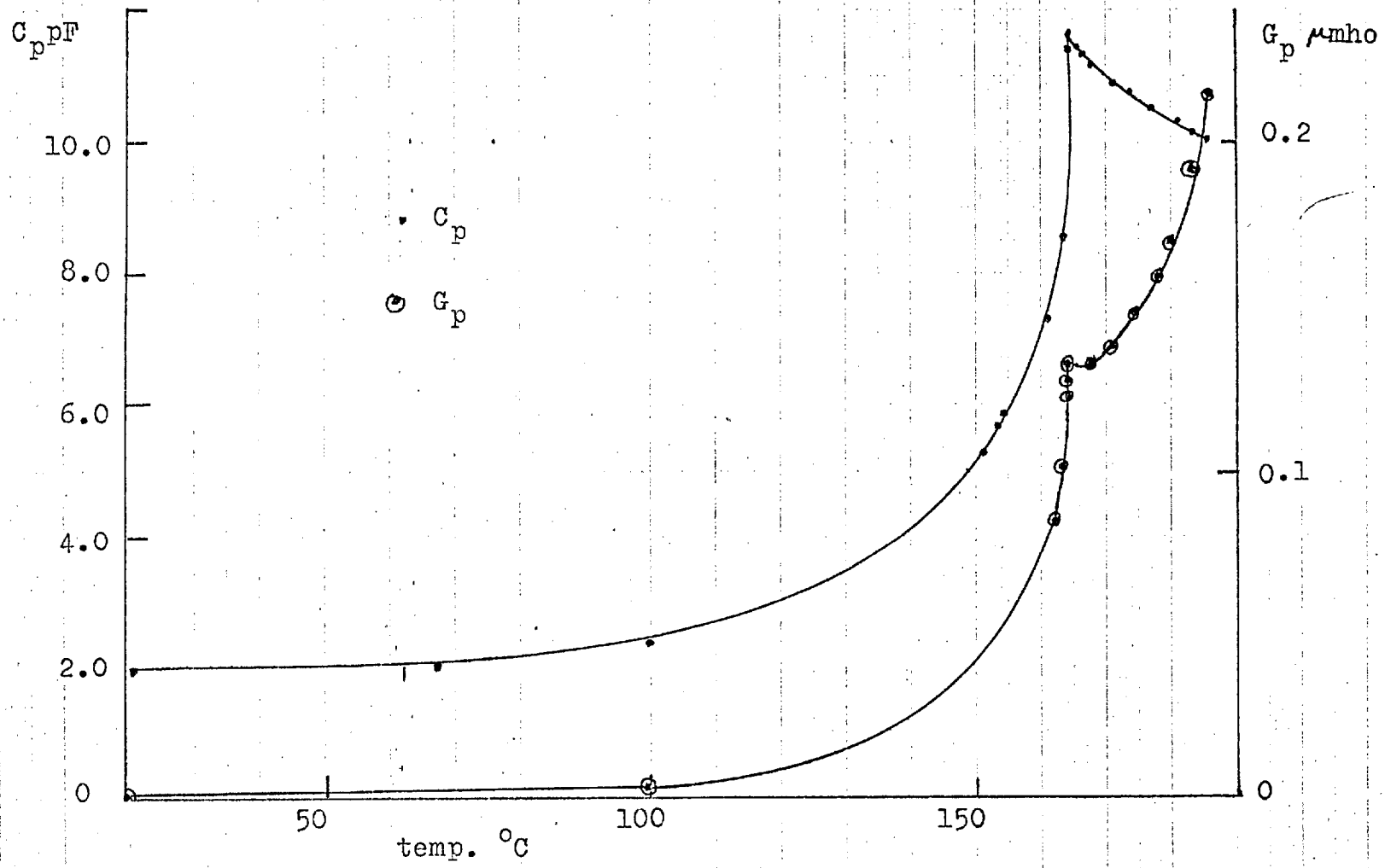

Fig.83. Variation of C and G of Cell no. 2 with temperature; sample: $NaNO_2$ (polycrystalline)

Chapter 6

DISCUSSION

6.1. Introduction

An assessment of the results given by different techniques of measurement has been presented in the last three chapters. Now in the final discussion, the phase transitions of potassium acetate will be discussed in relation to its molecular structure.

6.2. The solid-solid phase transitions

It can now be concluded that potassium acetate has three polymorphs involving two solid-solid phase transformations - one at 155°C and the other at about 75°C. The structure of form I, (above 155°C) is orthorhombic. The structure of form II, (between 155°C and ~ 75°C), is monoclinic and that of form III, stable between ~ 75°C and room temperature is also monoclinic with eightfold increase in volume of unit cell. No evidence for the transition at 230°C, suggested by Hazlewood et al.[7] from dilatometric measurements, could be detected by the X-ray diffraction method. The rotation photographs about b-axis at 160°C and 247°C are indistinguishable apart from changes due to the small thermal expansion (Fig.84). This does not, of course, rule out the possibility of the formation of structural defects at elevated temperature which may not influence the statistical structure detectable by X-ray diffraction. Thus, the production of Schottky defects would lower the density of the material, i.e. increase the volume of a constant mass.

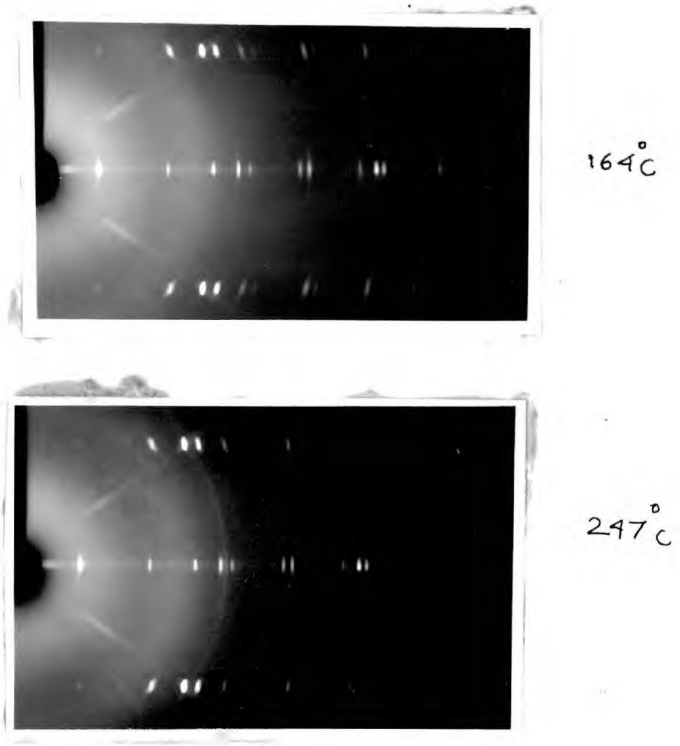

Fig.84. Rotation photographs about b axis of potassium acetate at 164°C and 247°C showing that the structure remains the same.

In this connection it must be noted that the present measurements are based on measurements of a single crystal whereas Hazlewood's graph is an average line based on several measurements of two polycrystalline samples. It may be possible that different crystals behave differently. Moreover, the state of the sample must be significant as the quantitative change in molar volumes determined by macroscopic and microscopic techniques have been shown to differ significantly. Two probable reasons may be considered for this discrepancy:

(i) The first may be errors in either or both of these sets of measurements. As each set appears to be self consistent, it is highly improbable that in either method an error of 2 $cm^3 mole^{-1}$ could occur in a volume change measurement involving only 4 $cm^3 mole^{-1}$. Thus, this reason for the discrepancy is not tenable.

(ii) The most probable reason however is the difference in the state of the sample used for measurement. Hazlewood et al.'s sample was dried at room temperature by evacuation to $\sim 10^{-3}$ mm of Hg, whereas the present measurements show that even after heating through thermal cycles from room temperature to ~180°C several times a day repeatedly passing through the solid-solid phase transition at 154°C and evacuating to $\sim 10^{-5}$ mm of Hg, it needed three days to make the sample effectively free from moisture.

6.2.1. The Form I ⟶ Form II transition. The transition II ⟶ I has been detected by all the three methods of investigation.

X-ray diffraction showed change of structural symmetry from monoclinic to orthorhombic and the rapid increase in the a-axis cell dimension terminates at the transition. The dielectric properties ϵ' and ϵ'' (represented by capacitance and conductance of the dielectric cell) have shown a slight anomalous increase at the transition. The DTA thermograms show a peak resembling a λ-point anomaly. In the three methods, one feature is found common - that there is no evidence for any structural discontinuity at 155°C. There is, however, a pre-transition range (premonitory range of Ubbelohde; see introduction) in which the measured property begins to change before the actual transition. In the X-ray diffraction method, reflexions from the two orientations of the monoclinic structure, i.e. reflexions of the type hol and $h\bar{o}l$ were slightly broadened below the transition temperature and the broadening persisted even when the diffraction geometry indicated that the transformation to the orthorhombic structure is complete (Fig.85). Detectable line broadening is limited to a temperature range of about 10°C around the transition temperature. The anomalous pretransition rise in the dielectric properties and the DTA thermograms also spread over about the same range of temperature. To interpret these observations in terms of structural changes, it is necessary to consider the idealised structures of forms I and II.

In the average structure form I, the C-C bond of the planar acetate ion at x, y = $\frac{1}{4}$, z = $\frac{1}{4}$ in the unit cell lies along the twofold axis of the space group parallel to the a-axis. The second acetate ion at $\bar{x}$, y = $\frac{3}{4}$, z = $\frac{3}{4}$ lies antiparallel to the first. The two

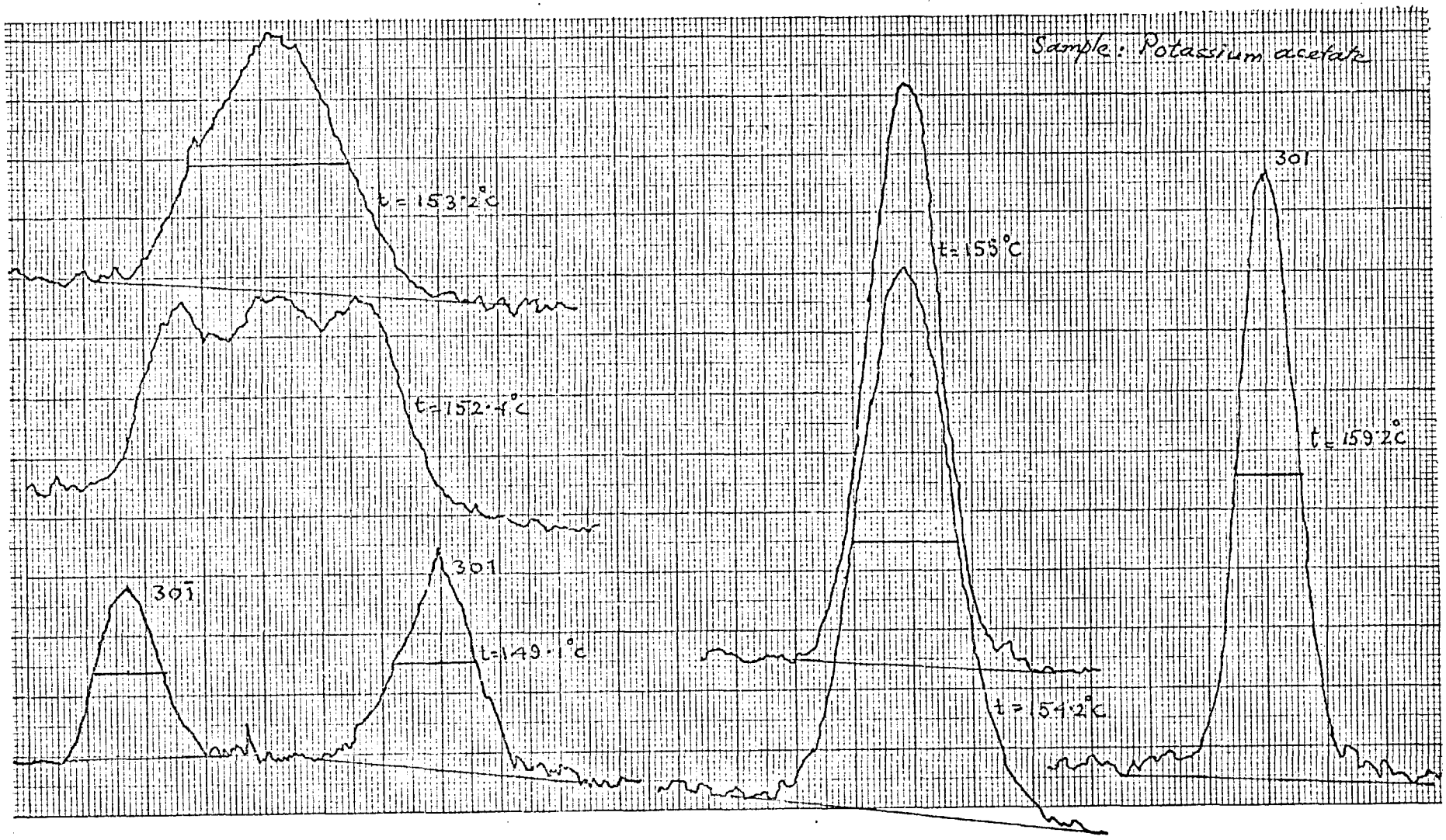

Fig.85. Traces of the line profiles of the 301 and 30$\bar{1}$ reflexions obtained with microdensitometer, around the transition Form II- Form I, which show broadening.

potassium ions have similar co-ordinates to the acetate ions. Thus, each potassium ion is co-ordinated by six oxygen atoms - four from the four acetate ions lying above and below the potassium atom (displaced by $\pm \frac{c}{2}$) and two from the acetate ion having the same z-co-ordinate as the potassium. The structure can, therefore, be considered as containing ionic double layers of potassium and oxygen atoms parallel to (100) firmly bound by ionic forces; between two such parallel double layers are the acetate ions with their methyl groups in contact and attracted by much weaker Van der Waals forces. Consideration of the cell and atomic parameters of potassium acetate, form I structure shows that there is a rather large void in the unit cell of about 1.82 Å x 1.76 Å extending through the whole crystal along [001] (Fig.86). The unusual behaviour of potassium acetate appears to stem from these two peculiarities, viz. the ionic double layer parallel to (100) and the large void (marked in the figure by X) in the structure.

It was established experimentally that the b and c axis directions in the orthorhombic form I and monoclinic form II lattices remained unchanged throughout the phase transitions. This can now be seen to imply that the orientation of the ionic double layers remains constant. In the monoclinic form II structure, the twofold axis identified with the acetate ion orientation in form I, has disappeared, so that the ion is no longer constrained to remain parallel to the a-axis in form II and moves in the plane (010) with respect to the double layers parallel to (100), whose structure does not

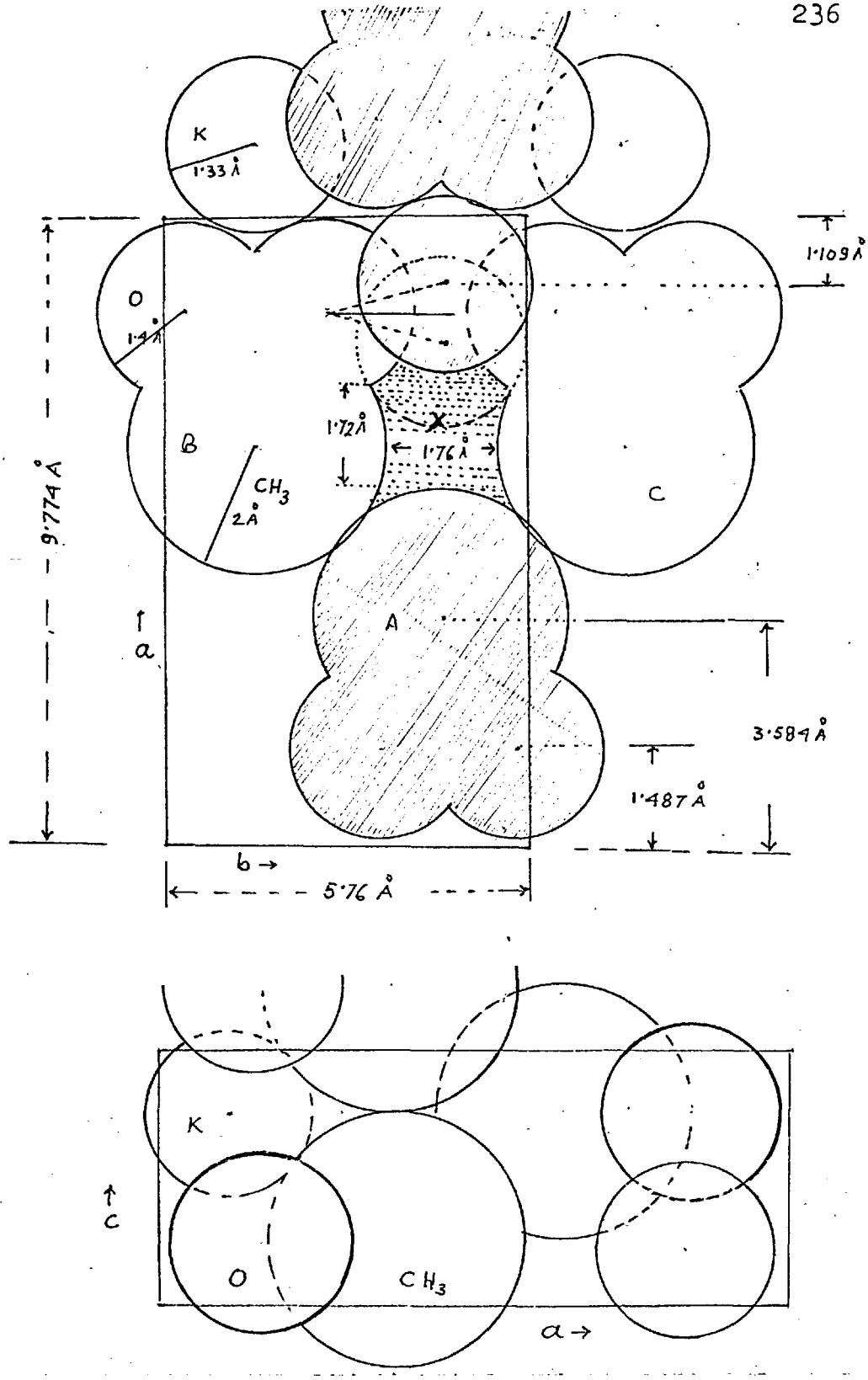

Fig.86. Potassium acetate, form I , unit cell, which has the void marked X. The shaded atoms are at $z=\frac{3}{4}$ while others are at $z=\frac{1}{4}$.

change significantly. The progressive decrease of a-axis below the transition temperature from 9.744 Å at 155°C to 9.330 Å at 80°C and the increase in β from 90° at 155°C to 99.1° at 80°C can be visualised as a shear deformation of the form I structure along [001] parallel to (100).

As has been reported in Chapter 2, direct measurement of β could not be followed right up to T_c (II → I), but indirect evidences had been given to show that even if there is any discontinuity in β, it would be limited to within a degree or so above 90°.

From the above description, the structural behaviour of the transition II → I can be interpreted as follows: On increasing the temperature of form II, acetate ions begin to switch between two alternative sites (represented by the two twin orientations) as the transition is approached. The number of ions switching increases with increasing temperature which accounts for the pretransition phenomenon in different properties. The two sites mentioned above correspond to the 'observed' and 'reversed' position of a displacive transformation discussed in Chapter 1, so that the form I structure is the statistical average of the two positions and forms a higher symmetry structure. At temperature above and below the transition region the sharpness of X-ray reflexions is regained and dielectric and thermal anomaly disappears, suggesting that orientational disorder involving the acetate ions is energetically unfavourable. From the X-ray results this appears to be when the β angle exceeds the value of about 93°. Immediately above the transition temperature,

a continually changing mosaic of small regions "observed" and "reversed" forms in equal amount have been formed. This is the statistical open form. The lack of any detectable discontinuous change in volume at the transition temperature suggests that this is a second order transformation, but it is difficult to confirm this, because the transition is spread over a few degrees. Practical difficulty arises because different parts of the crystal appear to be transforming at slightly different temperatures; probable reasons for this are crystal defects and impurities, anisotropic surface strains or simply a temperature gradient along the crystal in the furnace. The temperature range of the anomalous increase in the dielectric properties at the transition is also broad showing that no abrupt change has taken place at a fixed temperature. The peak in the DTA thermograms which was thought to be representing changes in heat capacity, resembled a co-operative peak rather than that of a first order transition. Thus all evidences suggest that this transition is structurally and hence thermodynamically continuous. But further study by purely thermodynamical methods and dielectric measurement on good single crystals is needed for a final settlement of this conclusion.

Form II structure has already been described earlier in discussing the transition II $\longrightarrow$ I. This structure is temperature sensitive. Here a-axis rapidly contracts and b (also c slightly) expands on cooling. The contraction of a may be considered by referring to Fig.86. To minimise the cell volume as the crystal is cooled, the methyl group of the acetate ion A in contact with

methyl groups on the acetate ions B and C appears to slide over them for close packing so that it pushes towards the void in the unit cell in between B and C. The methyl-methyl separation, given by the model described in Chapter 4, at different temperatures supports the above idea:

$t^{\circ}C$	Methyl contact distance (Å)
155	4.35
150	4.30
130	4.28
100	4.31
80	4.36

Thus, in between 130°C and 100°C, the methyl group of A, when sliding over those of B and C, crosses the nearest point on the saddle formed by them and at 80°C, it enters the void in the structure. The penetration of a large methyl group in between the acetates B and C would, of course, separate them to some extent so that this picture would account both for the contraction of a and for the expansion of b on cooling through form II. If this is the correct explana ion then what has been described as thermal expansion and contraction may in reality be a thermomechanical strain effect[79]. Otherwise, the large anharmonic vibrations along a-axis which must be set up to account for the large thermal expansion of a would not simply account for the other lattice parameter changes observed experimentally.

6.2.2. The Forms II → III transformation. The dielectric and DTA measurements did not reveal any unusual behaviour at this transformation.

It was detected only by the appearance of additional layer lines with k = $\frac{1}{4}$, $\frac{3}{4}$, $\frac{5}{4}$, $\frac{7}{4}$ etc in between the main layer lines of the b-axis (form II) oscillation photographs. This fourfold increase in the b-axis at the transition II $\longrightarrow$ III was accompanied by a twofold increase in the a-axis as evidenced by indexing of reflexions in the Weissenberg photographs. The transition was accompanied by a small contraction of the b-axis which reversed the negative thermal expansion coefficient in the direction of b, but the expansion coefficients along a and c axes were only slightly effected by the transition.

It has already been shown that form II and form III structures are closely related so that the unit cell of form II becomes a sub cell of form III. The big unit cell of form III (Fig.87 a,b) comprises 8 such sub cells as shown in Chapter 4. There, a mathematical model was designed to ensure that reflexions with k = $4n\pm2$ are absent; a schematic diagram of such a model is shown in Fig.87(a). At the same time arguments have been presented in that chapter showing that only the space group C_m is consistent with such a structure. In that case, sub cells marked 1 and 2, 5 and 6, as also 3 and 4, 7 and 8 must be related by mirror symmetry (Fig.87(b)). As each sub cell contains two molecules, this is possible only if one molecule lies in the mirror plane. Thus the mathematical model represented in the Fig.87(a) is inconsistent with the space group; as there is no reason to suspect that the arguments leading to the space group invalid, the mathematical model may be rejected.

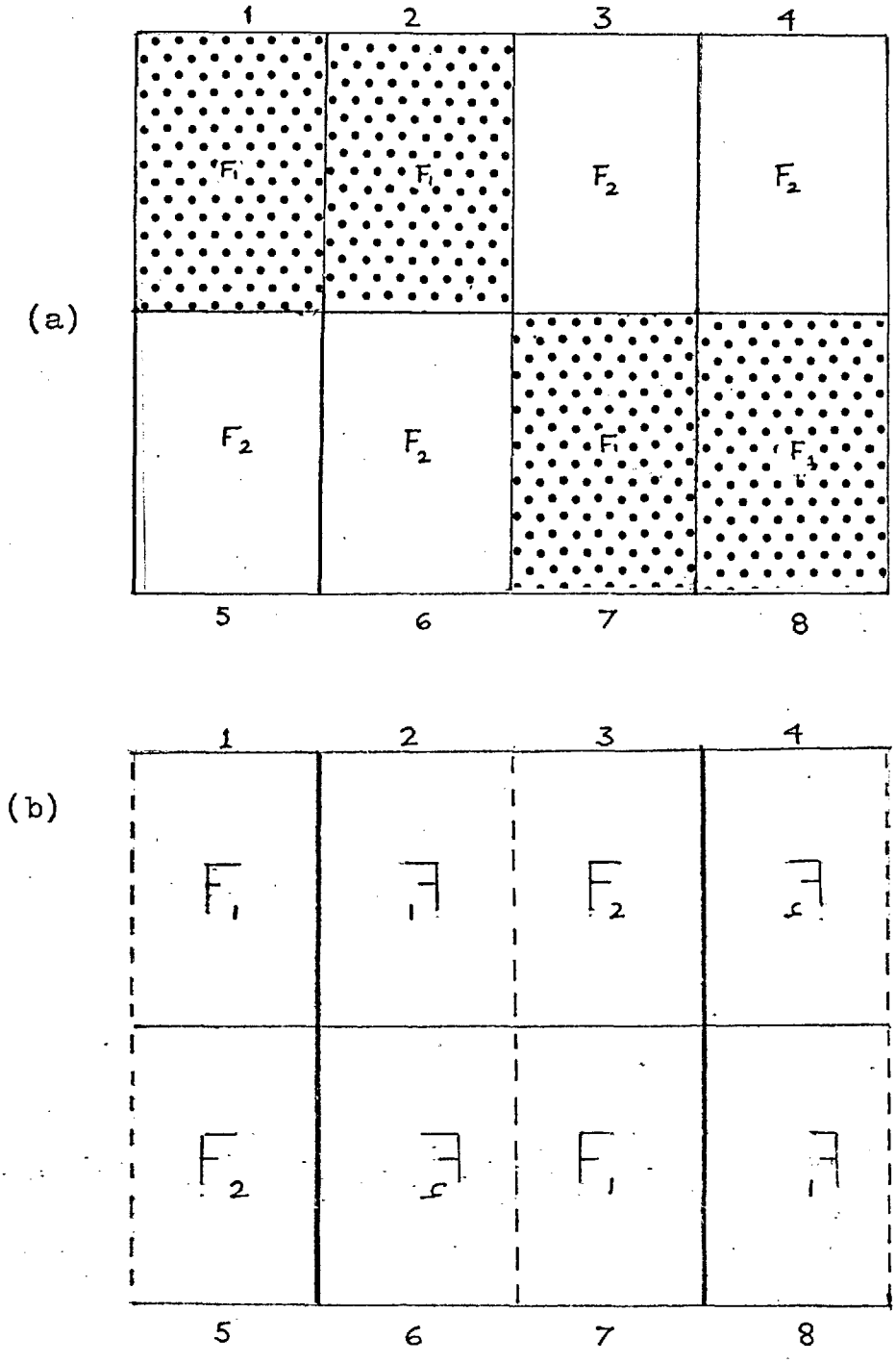

Fig.87a. A schematic representation of the mathematical model which accounts for the absence of the reflexions of the type k= 4n + 2.(potassium acetate, form III)

b. The schematic representation of the space group.

In the absence of experimental evidence any further statements regarding the form III structure are bound to be speculative. The problem is essentially to define the difference in structure between the subcells F(1) and F(2).

In discussing the origins of additional reflexions in the Chapter 4, several mechanisms were described which accounted for the appearance of additional reflexions. Periodic error in the packing of layers as in 4:4' dinitrodiphenyl etc[72] would lead to diffuse superlattice reflexions. In potassium acetate form III, the reflexions in the additional layer lines, although weak, are sharp, not diffused. Regular alternation of two structures as in Felspars[71] would imply that F(1) and F(2) are unrelated. This is permissible provided that the structures are chemically identical. The known impurities of potassium acetate are of very small quantity. If F(1) and F(2) are structurally unrelated it is not possible to proceed further without full structural study. On the other hand, this is unlikely to be the correct interpretation, for it would require all reflexions with $k = 2k+2$ to be absent accidentally. Hence it is more likely that form III is a modulated form II structure in which the periodicity of the modulating function is commensurate with the lattice of the basic structure. The origin of the modulating wave is suggested by the earlier assumption that the acetate ion A passes over and through B and C (Fig.86) so that its methyl group approaches the void X in the unit cell. Further reduction in cell volume may not be possible by this simple mechanism.

Further penetration of the methyl group into the void may force the molecules B and C apart. Conversely, the void volume may be reduced by moving B and C closer together. These alternatives suggest models for the two subcells and these can be arranged to form a reasonable structure. This is thus a continuation of the form II structure. The difference now is that many of the acetate ions have no constraint to remain parallel to (010) and so the packing is much more compact. This model is consistent with the space group symmetry as shown in Fig.88 and possesses the essential requirements that the structural changes can be progressive and reversible. This model has not yet been further investigated through lack of time.

On heating and cooling the intensities of the reflexions in the additional layer lines do not follow the typical curve for the variation of order with temperature (Fig.6). The path followed by the intensity vs. temperature curve on cooling from form II to room temperature through transition II $\rightarrow$ III was different from that obtained on heating over the same range of temperature, so that a hysteresis loop extending over about 15°C was observed in the transformation II $\rightleftharpoons$ III for the crystal used. As discussed in Chapter 1, such hysteresis indicates interfacial (or domain boundary) and volume strain energy in the growth of the new phase in the matrix of the old. The intensity curves referred to above with inflexion points as shown in Fig.35 may perhaps be related to strain in the structure on the basis of the modulated model. A thermodynamic treatment of ferroelectric behaviour given by Devonshire[80] implies

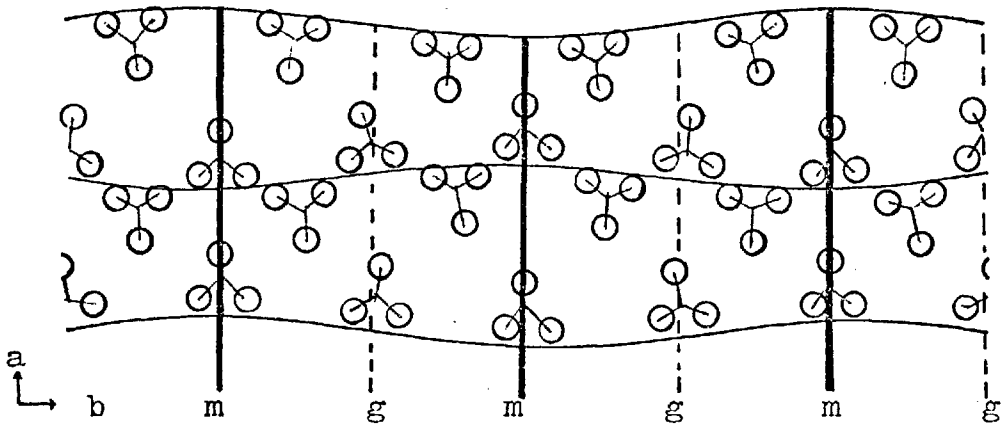

Fig.88. A model of the modulated structure of Potassium acetate, form III. The acetate ions are represented by the group three circles, the potassium ions are not shown. Symmetry elements of the Space group Cm are also indicated.

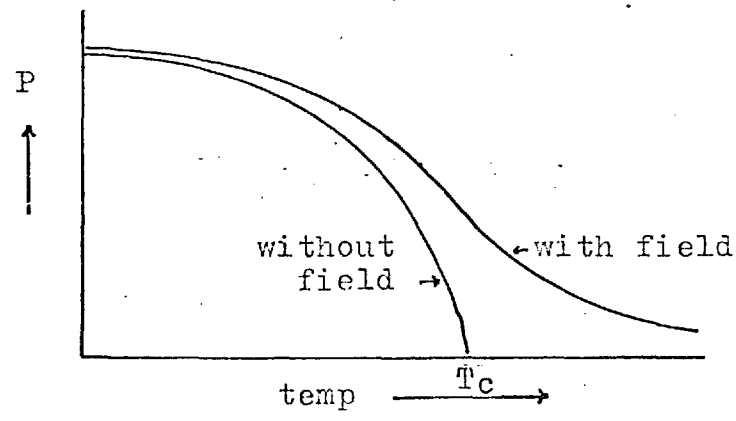

Fig.89. Variation of polarization with temperature with or without field(after Devonshire[80]).

that such curves would be obtained when a stressed crystal undergoes a second order transformation. Taking the free energy relation to be

$$dG_1 = -SdT + x_i dX_i + EdP$$

where G_1 is Gibb's elastic free energy function, S is entropy, x_i and X_i are strain and stress components, E and P are field and polarization. Devonshire showed that when stress is assumed to be zero in a ferroelectric undergoing second order transformation, the polarization varies with temperature at different polarizing fields as shown in Fig.89. Without field and stress, the second order transition would be distinct whereas the effect of an electric field is to blurr the transition so that the plot of polarization against temperature no longer falls sharply to zero but has a point of inflexion at T_c.

This behaviour has some resemblance to the variation of intensity of the reflexions in the additional layer lines with temperature in potassium acetate form III. In this case of course, if the same free energy equation is assumed to be applicable, EdP=0 and $dG_1 = -SdT + x_i dX_i$. If it is further assumed that the internal stress is decreasing with increasing temperature (assuming the decrease in the second term to be faster than the increase in the first term -SdT) and that the resulting strain in the crystal effects the intensity of the additional reflexions (this in effect is an assumption that the additional reflexions originate from internal strain - which supports the modulated model of the structure),

then the X vs. T or Intensity vs. T curve should follow that observed experimentally.

In this connection it may be pointed out that the reason why the transition forms III — II could not be detected even by the DTA method might just be that the interfacial and volume strain involved in the transformation discussed above, has probably smeared the peak beyond recognition under the experimental condition. In fact, in one thermogram (Fig.53a) there is a suggestion of such an effect, where the base line shifted very slightly towards exothermic direction from ~ 40° to ~ 80°C forming a very wide and flat peak.

It must be emphasized that these results of thermal analysis are tentative and more accurate thermal measurements are called for in order to understand the thermodynamic behaviour of the transformations.

6.3. Comparison of rubidium acetate with potassium acetate

The only other acetate studied that resembled potassium acetate in structure is rubidium acetate. Its space group is the same as that of potassium acetate, form II and the β-angle and a-axis are comparable:

	a Å		β°
potassium acetate	9.33 ...	80°C	99.4
	9.10 (x2)	23°C	100.8
rubidium acetate	8.69 ...	22°C	104.4

The b and c axes are slightly larger although of the same order of magnitude as in potassium acetate. Such a comparison calls

for an explanation why rubidium acetate should not show any polymorphic transitions above room temperature. To account for this, one considers the difference in the ionic radii of K^+ and Rb^+ which is 0.15 Å and the difference in the a-axes of the unit cells of potassium and rubidium acetates which is 0.64 Å. This shows that even if a thermal expansion of a-axis and a decrease in β as large as in potassium acetate is assumed to occur (in fact, there was no readily observable displacement of reflexions in rubidium acetate high temperature photographs for which reason its high temperature study was discontinued), at no temperature below melting point will the a-axis of rubidium acetate be long enough to allow the acetate ion to switch over the "neutral" or "toggle" point to another equilibrium position, as occurs during the II ⟶ I transformation in potassium acetate.

6.4. Structure and other properties

6.4.1. Dielectric properties: In the above discussion, the transformations have been correlated with the structures of potassium acetate. The structural basis of the slight anomalous increase in the dielectric properties is now clear. The switching of the acetate ions to the second equilibrium position must contribute to the orientational polarization which gives the anomalous region.

In addition to this anomalous effect there is another effect to be accounted for, which may again be attributed to the presence of the ionic double layers and the void in the structure. In the dielectric measurements, it has been observed that above ~100°C there was a general tendency at any frequency for the capacitance and the conductance of

a cell containing acetate as dielectric, to increase with increasing temperature. At a particular temperature as the frequency decreased, the capacitance increased and the conductance decreased. When converted to relative permittivity ϵ' and loss factor ϵ'', both sets of measurements showed an increase as the frequency is decreased (Figs. 49 and 80). The graphs of log ϵ'' against log frequency for potassium acetate are shown in Fig.90. From these graphs, it is evident that the polarization increases with decreasing frequency suggesting some mechanism with large relaxation time. However, although ϵ' is behaving as if it is approaching a Debye relaxation region, on the other hand ϵ' does not show the increase needed for the formation of a relaxation absorption peak. Such behaviour of ϵ' and ϵ'' cannot therefore be due to a Debye relaxation effect which thus rules out the possibility of rotation of any part or the whole of the acetate ion in the frequency range studied. The effect can be discussed in relation to different mechanisms of polarization:

(i) Ionic polarization: Rising temperature should decrease the dielectric constant of an ionic solid by decreasing the density, but at the same time increase in the distances between the ions weakens the forces between them, thus making ionic polarization easier. The latter effect is much greater than the density effect[49]. In potassium acetate, the main objection against this interpretation is that in the present case the frequency of measurement is below that normally required to excite ionic polarization, (frequency for ionic polarization $\sim 10^{10}$ Hz). Even if this objection is discounted on the

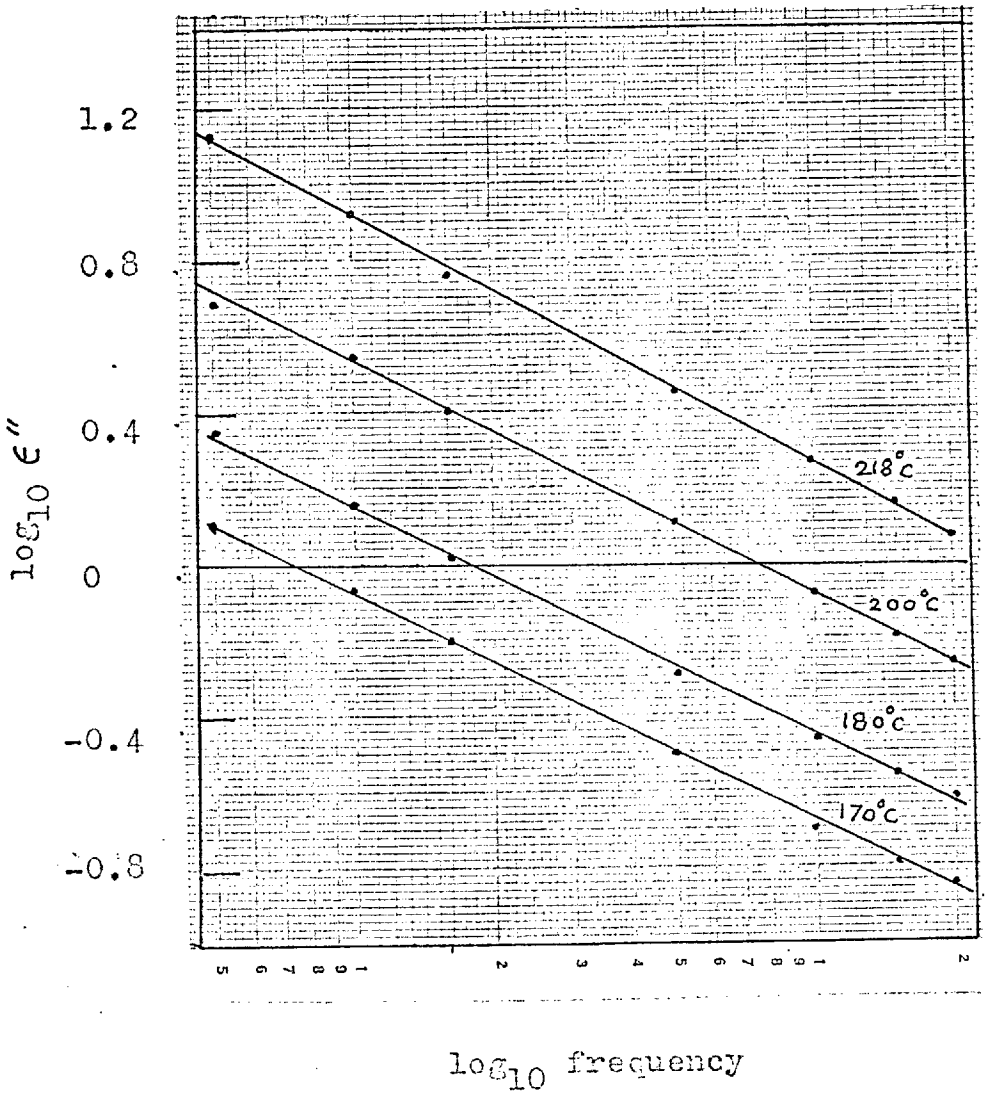

Fig.90. Plot of $\log_{10} \epsilon''$ vs. $\log_{10}$ (frequency) for potassium acetate

grounds that many properties of potassium acetate are unusual, then there are other objections which cannot be dismissed similarly. For example, in potassium acetate K-O distances were assumed to remain constant at least in form II and up to the transition II $\longrightarrow$ I. Such an assumption resulted in reasonable agreement between observed and calculated diffraction intensity. Thus, polarization should have decreased in this region (contrary to observation), for, actually decrease in density was noted. This indicates that the rapid increase in the dielectric properties has some other explanation.

(ii) Interfacial polarization of heterogeneous dielectrics: The origin of this type of polarization has been discussed in the Introduction to Chapter 3. Now the interfacial polarization arising out of any source cannot be distinguished from orientational polarization by measuring ϵ', because its variation with frequency is precisely the same as that for the case of Debye relaxation. But the expression for ϵ' in this case contains additional terms (compared to the Debye expression) inversely proportional to frequency. This means that as frequency $\omega \longrightarrow 0$, the loss represented by $\epsilon'' \longrightarrow \infty$. The interfacial polarization can thus be distinguished from Debye relaxation by observing ϵ'' below the relaxation frequency. In the Debye case $\epsilon'' \longrightarrow 0$ as $\omega \longrightarrow 0$.

For potassium acetate, the log ϵ'' vs. log (frequency) curve has already been shown in Fig.90. It is similar in behaviour to those obtained by Hamon[81] using conducting inclusions such as copper phthalocyanine and liquid n-primary alcohols dispersed in paraffin wax

(Fig.37a). Thus interfacial polarization can be taken as one of the reasons which causes the peculiar behaviour of the dielectric properties in these acetates. Such polarization may arise for one or more of the following reasons:

(a) Impurities. Conducting charge carriers can accumulate at the impurity centres to cause polarization. The difficulties of purifying ionic crystals are well known.

(b) Dislocations. The conducting charge carriers may be trapped at the dislocations and other defects formed during heating. For reproducibility of the results the number of charge carriers and the defects formed must be large so that the measured average behaviour may remain the same for each measurement.

In both cases, there must be thermally activated charge carriers in the absence of conducting inclusions and in potassium acetate these are likely to be potassium ions. In a crystal, the mobility of such ions under the influence of an electric field is closely connected to their diffusional mobility. This is shown by the fact that at higher temperatures, the temperature dependence of both the electrical conductivity (d.c.) and diffusion coefficient can be expressed by a formula of the form:

$$K = A \exp.(-E/kT)$$

where K is electrical conductivity, A is a constant, E is an activation energy, k is Boltzmann constant and T, the absolute temperature.

Now at a particular frequency, the d.c. conductivity in a condenser is proportional to ϵ''. So, in order to test the validity of the arguments given above, in the present case, the values of log ϵ'' were plotted against the reciprocal of absolute temperature T (only for higher values of T) and are shown in Figs. 91(a), (b), (c). The graphs are practically straight lines. At different frequencies the straight lines are all parallel suggesting that some activation process with constant activation energy is involved:

thus

$$\epsilon'' = A \exp.(-E_o/RT)$$

Here A is a constant; E_o, the activation energy in cal.; R = 1.987 cal. per deg. per mol. is the gas constant.

The slope of these curves of $2.303 \log_{10} \epsilon''$ vs. I/T gives E_o/R, whence E_o has been calculated and is given in Table 6.4.1.

Table 6.4.1.

Calculation of activation energy

Compound	Frequency kHz	E_o kcal.mol.$^{-1}$
Lithium acetate	5	17.7 } ≃ 17.4 (av.)
	20	17.1 }
Potassium acetate	5	20.7 } ≃ 20 (av.)
	20	19.6 }
Rubidium acetate	5	26.0 } ≃ 25.4 (av.)
	20	24.8 }

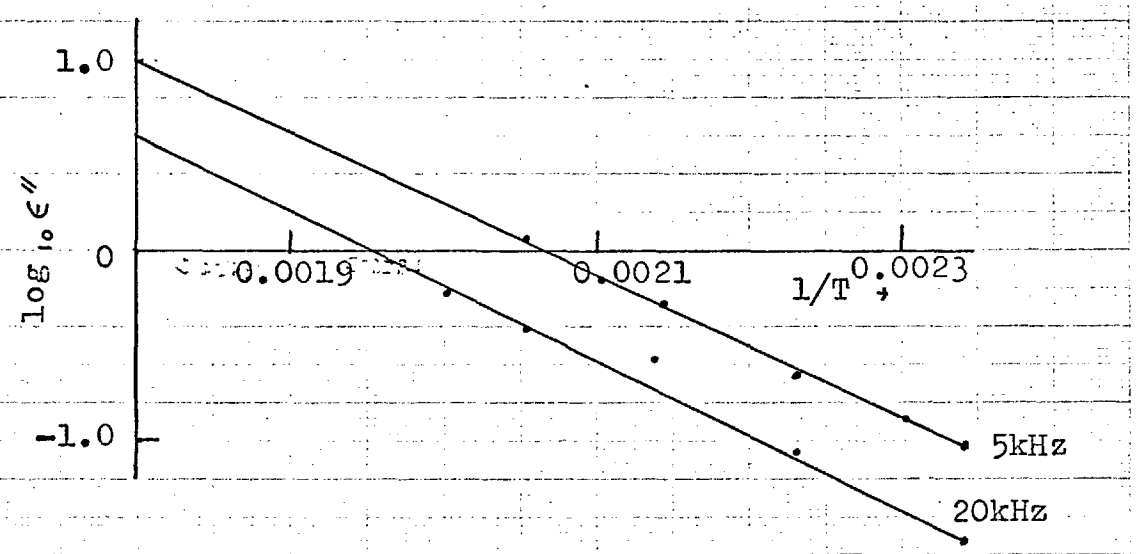

Fig.91(a) The values of $\log_{10}\epsilon''$ are plotted against 1/T; sample : Lithium acetate anhydrous.

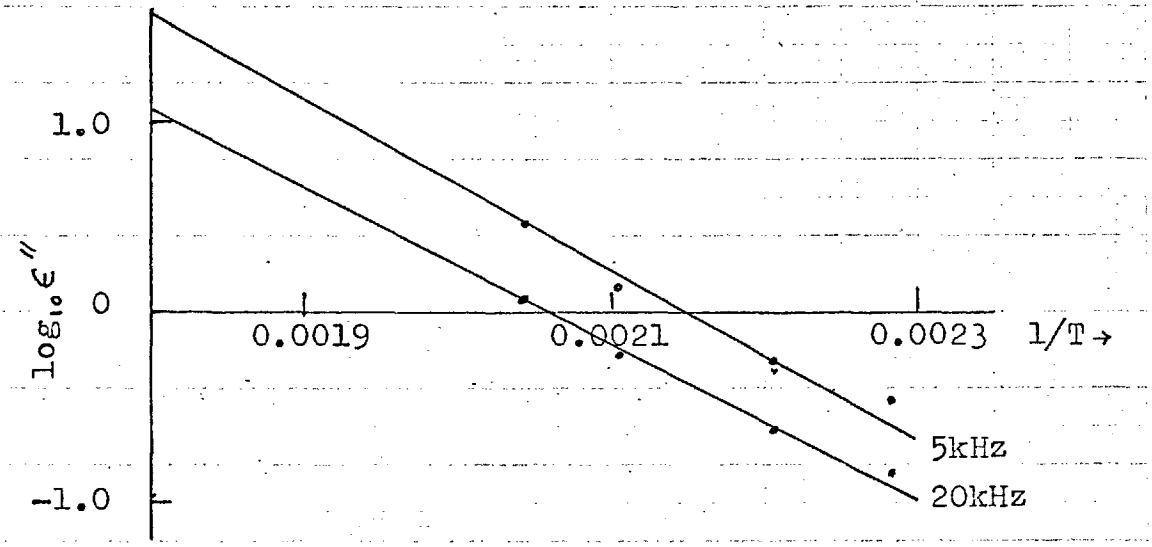

Fig.91(b) The values of $\log_{10}\epsilon''$ are plotted against 1/T; sample : Potassium acetate

(Numerical data are givem in the Appendix)

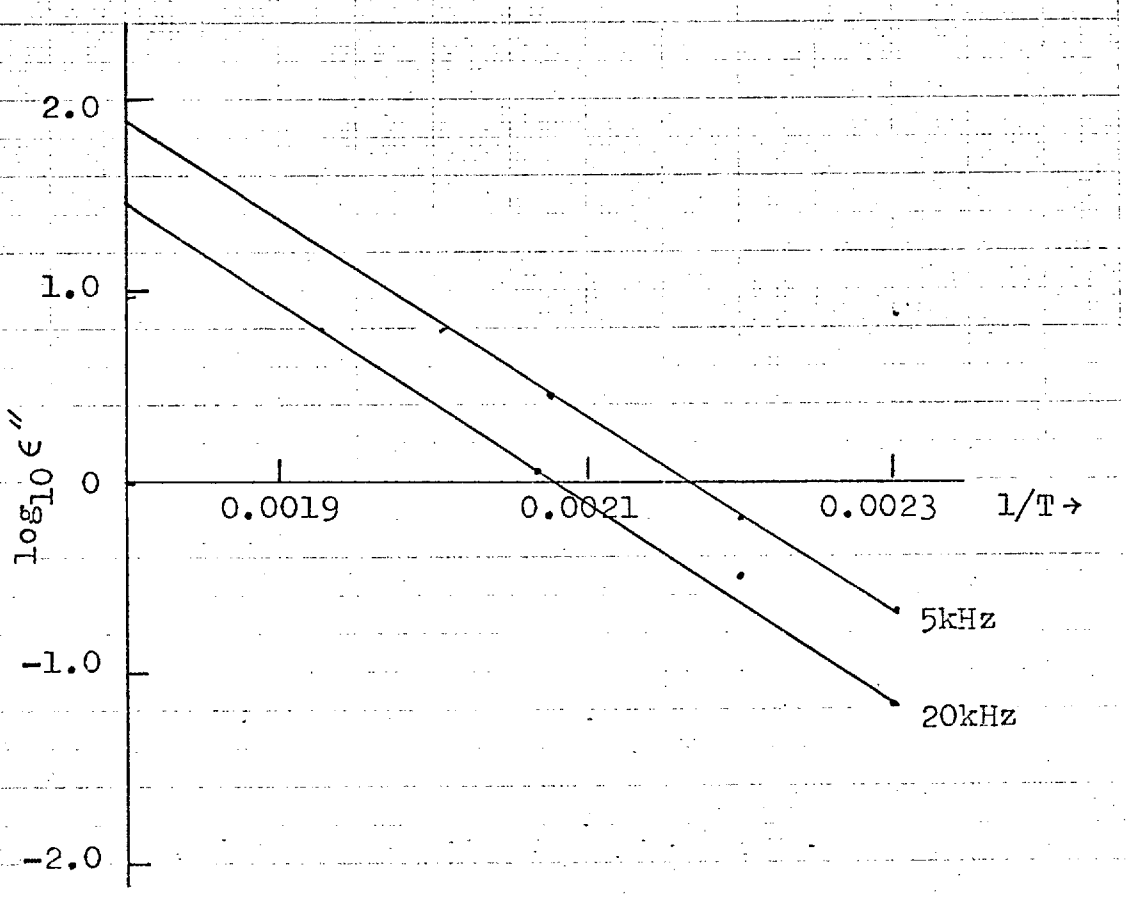

Fig.91(c) The values of $\log_{10} \epsilon''$ are plotted against 1/T; sample : Rubidium acetate

(Numerical data are in Appendix)

It should be noted that the magnitude of the activation energies obtained above are not very accurate when considered as absolute values, because of the use of approximate values of C_o (the capacity of the condenser without any dielectric in between electrodes) in their derivation. Nevertheless, the relative accuracy of the different measurements on the different samples should be accurate enough for their comparison to be significant. It is evident, therefore, that the activation energy increases as the cation size increases. This is taken as confirmation that it is the thermal activation of the cations Li^+, K^+ and Rb^+ that is responsible for the rapid rise in the relative permittivity ϵ' and the loss factor ϵ''. Thus the similar behaviour of the dielectric properties in the acetates studied may be co-related to common features in their crystal structures. These common features may well be that the cations are co-ordinated by oxygen atoms to form an ionic double layer (the rubidium acetate structure probably contains ionic double layers as in potassium acetate; the lithium acetate (anhydrous) structure is unknown).

In this connection, it may be pointed out that the idea of the ionic double layers, with off-centre potassium ion in the co-ordination polyhedron formed by oxygen atoms, was taken from the soap structures. Thus it is quite possible that the soaps would also show similar dielectric behaviour.

In potassium acetate, the movement of the potassium ion from site to site may be accounted for by assuming that the alternative site for potassium (model 2, Chapter 4), permitted by the space group

symmetry, at x, $\frac{1}{4}$, $\frac{3}{4}$ and $\bar{x}$, $\frac{3}{4}$, $\frac{1}{4}$ usually remains vacant, because of packing difficulties. But as the temperature is increased it may be possible that the potassium ions jump to the alternative vacant position limiting the movement of the cations to the ionic double layers. Such a jump would be facilitated if there are some vacant sites already present in the ionic double layers due to formation of Schottky defects. Such defects should always be available in a real crystal. Thus, if this process is responsible for the low frequency dielectric loss (and d.c. conductivity) the maximum effect should be obtained along [010] and [001]. But from experiments with the gold-plate and platinum wire condenser described in Chapter 3, it appears that the effect is slightly greater in the [100] direction (Fig.48). Although the experiment was not very satisfactory (because the measurements were done not on good single crystals, but on a multiple crystal block with preferred orientation), it is more probable that at higher temperatures the potassium ion is not constrained to lie in the double layer but jumps to the void within the unit cell in between the four acetate ions (Fig.86). A jump of about 0.8 Å parallel to the a-axis would bring the potassium ion into contact with four methyl groups while keeping the distance (D_2) to the nearest four co-ordinating oxygen atoms, the same as before. The distance (D_1) from the other two distant oxygen atoms now increases from 2.82 Å to 3.57 Å. Thus, there is always a possibility that on application of an a.c. field to the crystal, at higher temperature, some K^+ ions jump into the alternative site, which would be equivalent

to diffusion of charge carriers and would effect the dielectric properties in the way already described. Such a thermal diffusion causing an ohmic current under the influence of an applied field will not effect the diffraction pattern. This picture can be compared to the jump of Ba^{2+} in $Ba_x(Ti_{8-x}Mg_x)O_{16}$ [82] along a tunnel in the structure, but there is a difference that the activation energy is small in Ba^{2+} jumping ($\sim$ 4 kcal.). Whether there is really any appreciable anisotropy in the dielectric behaviour to confirm the potassium ion jump to the void in the structure can only be decided by accurate measurement on good single crystals. Besides, to investigate any possible Debye relaxation of these molecules in the crystals, the dielectric investigation needs to be extended to higher frequency range.

6.4.2. Other properties: On the same peculiarities in the structure of potassium acetate do depend other physical properties. For example, Hazlewood et al.[7] found that potassium acetate contracts on melting. Because long range order disappears on melting, there will be no necessity for the void in the liquid structure.

The influence of ionic forces in the double layer, is evidenced by the off-centre position of the K^+ in the oxygen co-ordination polyhedron. This effect may be due to the nearest neighbour $K^+ - K^+$ repulsion in the double layer and probably some influence due to co-ordination of the K^+ to the next nearest neighbour oxygens lying in the next ionic double layer.

The ionic double layer again is responsible for the shape of the potassium acetate crystals formed from melt inside a glass tube. As has been shown in Chapter 2 that on recrystallisation, the crystals formed a cross-section as shown in Fig.12, where the face (100) tends to remain parallel to the glass surface. It is now known that the face (100) of a potassium acetate crystal is the ionic double layer formed by potassium ions co-ordinated by only 6 oxygen atoms. The basic structure of a simple glass (fused quartz) on the other hand is a three dimensional network of silicon and oxygen atoms - oxygen atoms forming a distorted cage round the silicon atoms. The glass surface is thus a sheet of atoms where oxygen atoms are abundant. The ionic double layer of potassium acetate with insufficiently co-ordinated K^+ ions thus finds a ready source of oxygen sheet in the glass surface and extends co-ordination to the surface, suggesting why the crystal surface (100) tends to remain parallel to the glass surface.

Prior to this study practically nothing was known about the structure and properties of potassium acetate; this investigation has revealed the structural basis on which, apparently, many of its unusual properties depend. Moreover, potassium acetate appears to be the only known example of an organic salt exhibiting behaviour resembling that of super lattice formation in an alloy. Only complete crystal structure analysis can establish the validity of the model proposed but the basis has been laid for such a study and for a more accurate analysis of the other structures exhibited by this unusual compound.

Appendix I

Table 1

Observed Lattice Parameters of Potassium Acetate. $\lambda = 1.5418$ Å

$t^{\circ}C$	d_{100}(A)	d_{001}(A)	$\theta_{301}{}^{\circ}$	$\theta_{30\bar{1}}{}^{\circ}$	$t^{\circ}C$	$d_{010} = b_o$(A)
23	8.942	3.976	20.807	17.311	25	23.301
36.1	8.986	3.972	20.694	17.297	50	23.233
47.5	9.026	3.983	20.594	17.309	60.5	23.243
55.2	9.091	3.986	20.405	17.186	67.4	23.241
67.8	9.167	3.986	20.255	17.200	68.3	23.278
72.0	9.168	3.984	20.205	17.686	70.6	23.287
73.6	9.184	3.972	20.189	17.191	86	5.816
75.7	9.197	3.972	20.183	17.228	126.7	5.780
86.0	9.255	3.975	20.010	17.185	152.7	5.762
95.3	9.283	3.973	19.951	17.258	161.4	5.758
105.0	9.342	3.971	19.776	17.246	198.5	5.748
113.3	9.397	[illegible]	[illegible]	17.146		
124.0	9.443	3.978	19.406	17.253		
135.0	9.518	3.974	19.118	17.250		
146.0	9.602	3.984	18.786	17.405		
147.6	9.621	3.983	18.729	17.467		
149.7	9.679	3.979	-	-		
150.2	9.683	3.985	18.480	17.518		
151.7	9.665	-	-	-		
152.7	9.693	3.990	-	-		

Table 1 (continued)

$t^{\circ}C$	d_{100}(A)	d_{001}(A)	$\theta_{301}{}^{\circ}$	$\theta_{30\bar{1}}{}^{\circ}$
153.1	9.711	3.990	-	-
153.3	9.694	3.991	-	-
154.3	9.757	3.990	-	-
155.0	9.744	3.993	-	-
160	9.744	-	-	-
247	9.853	4.021	-	-

Table 2

Calculated Lattice Parameters of Potassium Acetate

t°C	β°	a Å	c Å
23	100.8	9.103	4.048
36.1	100.5	9.139	4.040
47.5	100.2	9.171	4.047
55.2	100.1	9.234	4.049
72	99.6	9.298	4.041
73.6	99.3	9.306	4.025
75.7	99.2	9.317	4.024
86.0	98.8	9.365	4.022
95.3	98.5	9.384	4.017
105.0	97.9	9.432	4.009
113.3	97.5	9.478	4.005
124.0	96.8	9.510	4.006
135.0	95.7	9.565	3.994
146.0	94.4	9.630	3.996
147.6	94.0	9.645	3.993
150.2	93.1	9.698	3.991

Table 3

Interpolated Values of Lattice Parameters and Molar Volumes

$t^{o}C$	d_{100}(A)	b (A)	c (A)	V(A^2)	$V_{molar} = \frac{NXV}{2}$
23	8.942 x 2	5.824 x 4	4.048	210.9	63.51
30	8.970 x 2	5.818 x 4	4.047	211.2	63.60
40	9.020 x 2	5.812 x 4	4.042	211.9	63.81
50	9.057 x 2	5.811 x 4	4.037	212.4	63.96
60	9.115 x 2	5.810 x 4	4.034	213.6	64.32
67	9.150 x 2	5.812 x 4	4.030	214.3	64.50
68	9.160 x 2	5.820 x 4	4.030	214.8	64.68
70	9.167 x 2	5.822 x 4	4.030	215.1	64.78
75	9.195	5.822	4.026	215.5	64.90
80	9.220	5.820	4.025	216.0	65.05
90	9.270	5.814	4.020	216.7	65.25
100	9.315	5.804	4.015	217.1	65.38
110	9.370	5.794	4.015	217.7	65.56
120	9.420	5.785	4.007	218.4	65.77
130	9.485	5.776	4.002	219.3	66.04
140	9.551	5.769	3.997	220.2	66.31
150	9.660	5.764	3.992	222.3	66.94
155	9.744	5.762	3.991	224.1	67.49
160	9.744	5.760	3.991	224.1	67.49
247	9.853	-	4.021	-	

Table 3A

Approximate calculation of intensities.

$a = 9.7$ Å, $b = 5.9$ Å, $c = 3.96$ Å, $CH_3\text{-}CH_3 = 4$ Å, C-C = 1.54 Å, C-O = 1.23 Å, $\angle OCO = 120^\circ$

l = even

k = 0

	h =	1	2	3	4	5
Model 1	$\frac{\sin\theta}{\lambda}$ x	.0515	.1030	.1545	.2060	.2575
$K(\frac{1}{2}f_k)$	-.0999	7.34	2.90	-2.63	7.17	-.90
$O(f_o)$	.1996	2.45	-6.24	-6.38	2.22	.78
$C(\frac{1}{2}f_c)$	.2634	-.24	2.83	-.70	2.72	1.14
$C(\frac{1}{2}f_c)$	.4220	-2.53	-1.60	.29	-1.09	-2.21
Model 2						
$K(\frac{1}{2}f_k)$	.0185	8.962	8.772	8.781	8.014	7.464
Model 1	$\sum F$	7.02	-2.11	-9.42	11.01	-2.0
Model 2	$\sum F$	8.65	3.77	2.40	11.86	5.49
Model 1	$\lvert\sum F\rvert^2$	49.31	4.45	88.66	121.22	4
Model 2	$\lvert\sum F\rvert^2$	74.77	14.18	5.77	140.6	30.12

Table 4

Polycrystalline potassium acetate; Cell no.3 (Heating). Values of capacitance and conductance at different temperatures and frequencies. C_p, (pF); G_p, (μmho).

t°C	20 kHz		15 kHz		10 kHz		5 kHz		1592 Hz		1 kHz		500 Hz	
	C	G	C	G	C	G	C	G	C	G	C	G	C	G
23	4.66	-	4.70	-	4.73	-	4.75	-	4.75	-	4.78	-	4.79	-
70	4.69	-	4.73	-	4.78	-	4.80	-	4.82	-	4.83	-	4.84	-
100	4.72	-	4.82	-	4.84	-	4.86	-	4.87	-	4.88	-	4.92	-
150	5.18	-	5.24	-	5.31	-	5.40	-	5.64	-	5.64	-	5.77	-
154	5.30	.0011	5.38	-	5.44	.0100	5.54	.0080	5.74	.0044	5.85	.0036	5.95	.0030
156	5.32	.0148	5.39	.0133	5.46	.0110	5.56	.0087	5.76	.0053	5.88	.0044	6.08	.0032
160	5.31	.0160	5.40	.0160	5.48	.0155	5.60	.0098	5.86	.0062	5.97	.0050	6.24	.0040
170	5.36	.0260	5.46	.0228	5.56	.0190	5.70	.0150	6.04	.0092	6.25	.0077	6.76	.0058
180	5.45	.0454	5.56	.0390	5.69	.0320	5.91	.0240	6.47	.0151	6.89	.0130	7.60	.0010
190	5.60	.0670	5.75	.0630	5.91	.0530	6.26	.0390	7.13	.0240	7.70	.0200	8.92	.0150
200	5.77	.102	5.97	.0890	6.20	.0770	6.68	.0580	7.97	.0367	8.80	.0310	10.45	.0230
218	6.48	.2180	6.76	.2010	7.22	.1700	8.20	.1300	10.70	.0870	12.06	.0750	15.55	.0620

(A blank (-) indicates a very small value)

Table 5

Polycrystalline potassium acetate; Cell no.3 (Cooling). Values of Cp (pF), Gp (μmho) at different temperatures and frequencies

t°C	20 kHz		15 kHz		10 kHz		5 kHz		1592 Hz		1 kHz		500 Hz	
	C	G	C	G	C	G	C	G	C	G	C	G	C	G
20	4.66	-	4.70	-	4.73	-	4.75	-	4.79	-	4.79	-	4.80	-
70	4.66	-	4.71	-	4.74	-	4.76	-	4.78	-	4.79	-	4.82	-
100	4.70	-	4.80	-	4.85	-	4.85	-	4.86	-	4.88	-	4.92	-
140	5.05	.0068	5.09	.0068	5.13	.0060	5.20	.0048	5.28	.0027	5.36	.0022	5.45	.0015
151	5.26	.0090	5.34	-	5.40	-	5.49	.0064	5.66	.0040	5.80	.0035	5.88	.0030
155	5.30	.0135	5.37	.0138	5.47	.0110	5.55	.0076	5.77	.0052	5.88	.0042	6.08	.0032
161	5.35	.0174	5.42	.0160	5.48	.0160	5.61	.0100	5.84	.0067	5.96	.0050	6.25	.0045
182	5.45	.0490	5.59	.0430	5.72	.0372	5.97	.0275	6.58	.0170	6.94	.0144	7.88	.0110
190	5.59	.0680	5.74	.0670	5.92	.0520	6.29	.0405	7.18	.0250	7.79	.0210	8.70	.0160
199	5.84	.1154	6.03	.1005	6.27	.056	6.85	.0650	8.25	.0410	9.09	.0340	10.77	.0260
220	6.96	.3230	7.38	.2940	7.35	.2500	9.18	-	12.20	.1360	13.50	.1100	16.50	.0984

(A blank (-) indicates a very small value)

Table 6

Capacitance and Conductance of recrystallised solid potassium acetate

C (pF), G (μmho)

temp. °C	20 kHz		15 kHz		10 kHz		5 kHz		1 kHz	
	C	G	C	G	C	G	C	G	C	G
23	5	-	5.06	-	5.08	-	5.09	-	5.09	-
115	5.17	-	5.23	-	5.24	-	5.25	-	5.33	-
141	5.53	-	5.65	-	5.76	-	5.80	-	5.85	-
150	5.86	-	5.93	-	6.14	-	6.06	.006	6.26	.0036
154	6.16	.0130	6.26	.0130	6.29	.0100	6.34	.0078	6.67	.0050
162	6.15	.0180	6.26	.0170	6.33	.0150	6.48	.0120	7.05	.0095
173	6.26	.0510	6.37	.0460	6.48	.0415	6.76	.0335	7.89	.0190
180	6.36	.0850	6.51	.0750	6.72	.0660	7.09	.0520	8.87	.0310

(A blank (-) indicates a very small value)

Table 7

Potassium Acetate; cell: two pt. wires, powder melted in between and the crystals grown. (temp. $\pm$ 5°C to $\pm$ 10°C).

Frequency 1592 c/s.

t°C	CpF	G µmho
20	.4	0
35	.4	0
60	.4	0
100	.405	0
130	.47	.001
137	.50	.0013
160	.67	.01
210	1.2	.517
245	1.5	.7

Table 8

Pot. Acetate; powder allowed to melt in between two gold plates (thin); upper plate (~ 4 mm sq); temp. ± 5°C to ± 10°C.

freq. 1592 c/s.

t°C	CpF	G µmho
30	1.85	.0014
50	1.86	.0012
100	1.9	.0012
124	1.94	.0015
160	2.22	.0036
200	2.8	.0125
258	8.00	-

Table 9

Capacity and conductance of the dielectric cell no.2 with rubidium acetate as dielectric material, at different temperatures and frequencies

Cp (pF), Gp (μmho).

t°C	500 Hz		1 kHz		5 kHz		10 kHz		15 kHz		20 kHz	
	C	G	C	G	C	G	C	G	C	G	C	G
20	1.10	-	1.08	-	1.00	-	0.95	-	0.93	-	0.92	-
120	1.12	-	1.10	-	1.04	-	0.97	-	0.95	-	0.93	-
160	1.55	0.0020	1.35	0.0025	1.15	0.0050	1.05	0.0055	1.02	0.0070	0.98	0.0070
180	2.40	0.0050	1.95	0.0066	1.45	0.0155	1.30	0.0225	1.25	0.0280	1.20	0.0300
210	4.30	0.0345	3.75	0.0383	2.60	0.0610	2.20	0.0830	2.00	0.1000	1.80	0.1140

Table 10

Capacity and conductance of the dielectric cell no.2 with caesium acetate as dielectric material, at different temperatures; frequency 1592 Hz. C (pF), G (μmho).

$t^{\circ}C$	C	G	$t^{\circ}C$	C	G	$t^{\circ}C$	C	G
23.5	2.56	0.00001	76.0	2.74	0.0009	142.5	3.55	0.0077
30.5	2.57	0.00001	82.0	2.75	0.00095	147.0	3.77	0.0104
35.5	2.59	0.00001	90.5	2.77	0.0010	149.5	3.91	0.0122
38.5	2.60	0.0002	95.5	2.79	0.0011	152.5	4.11	0.0149
40.5	2.60	0.0002	100.5	2.81	0.0013	155	4.30	0.0175
42.0	2.61	0.0002	104.5	2.84	0.00145	157	4.38	0.0187
43.5	2.615	0.0003	109.5	2.88	0.0018	160	4.74	0.0243
45.5	2.62	0.00039	115	2.92	0.0020	162.5	5.02	0.0292
48.5	2.63	0.00039	121	3.00	0.0026	165.0	5.36	0.0350
50.0	2.635	0.0004	124	3.06	0.0030	168.0	5.82	0.0441
54.5	2.66	0.0005	128.5	3.13	0.0037	172	6.48	0.0576
60.5	2.68	0.0006	132.0	3.22	0.0043	174	6.78	0.0647
64.0	2.69	0.0007	136.5	3.35	0.0054	175	6.94	0.0684
72.0	2.71	0.0008	138.0	3.40	0.0060			

Table 11

C_p and G_p values of Lithium acetate dihydrate : cell no.2.

C_p, pF; G_p μmho. (This sample was made anhydrous for next measurements).

t°C	C_p	G_p	t°C	C_p	G_p
22	1.69	-	103	1.72	0.0008
37	1.71	-	106	1.71	0.0009
44	1.70	-	112	1.70	0.0012
51	1.68	-	118	1.70	0.0016
57	2.47	0.0017	123	1.72	0.0020
62	2.42	0.0006	131	1.87	0.0035
65	2.26	0.0006	140	2.45	0.0055
70	2.10	0.0006	146	1.65	0.0014
75	2.00	0.0006	152	1.54	0.0009
78	1.90	0.0006	158	1.55	0.0010
83	1.80	0.0006	164	1.57	0.0013
87	1.76	0.0006	172	1.62	0.0021
92	1.73	0.0006	179	1.70	0.0030
99	1.72	0.0007	190	1.85	0.0047
			199	2.04	0.0065

Table 11 (continued)

C_p and G_p values of Lithium acetate anhydrous. Cell no.2. C_p, pF.; G_p μmho

temp. °C	20 kHz		15 kHz		10 kHz		5 kHz		1 kHz		1592 Hz	
	C	G	C	G	C	G	C	G	C	G	C	G
22	1.53	-	1.55	-	1.55	-	1.56	-	1.56	-	1.55	-
52	1.53	-	1.55	-	1.55	-	1.56	-	1.56	-	1.56	-
100	1.53	-	1.55	-	1.55	-	1.56	-	1.58	-	1.56	-
130	1.54	-	1.55	-	1.56	.-	1.58	-	1.60	.-	1.58	0.0003
151	1.54	-	1.56	-	1.58	0.0020	1.60	0.0016	1.66	0.0010	1.62	0.0012
156	1.55	0.0027	1.58	0.0020	1.58	-	1.60	0.0020	1.70	0.0013	1.64	0.0015
161	1.56	-	1.58	-	1.60	-	1.63	0.0032	1.76	0.0016	1.68	0.0020
175	1.58	0.0090	1.62	0.0078	1.64	0.0062	1.70	0.0057	1.97	0.0030	1.85	0.0040
195	1.67	0.0250	1.71	0.0220	1.80	0.0187	1.93	0.0135	2.57	0.0055	2.26	0.0071
210	-	-	1.87	0.0320	1.99	0.0260	2.20	0.0185	-	-	-	-
212	1.81	0.0380	1.88	0.0330	1.99	0.0265	2.20	0.0185	3.04	0.0062	3.04	0.0065
215	1.84	0.0405	1.92	0.0375	2.02	0.030	2.27	0.0260	3.14	0.0065	3.82	0.0090
223	1.96	0.0580	2.09	-	2.26	0.040	2.57	0.0250	3.45	0.0072	3.17	0.0097

Table 12

Values of ϵ' and ϵ'' calculated on the basis of Tables 4, 9, 11 for calculation of activation energy.

Potassium acetate: cell no.3 : Co $\simeq$ 1.5 pF.

Freq.	T°K	I/T	ϵ'	ϵ''
20 kHz	491	0.00204	4.32	1.15
	473	0.00210	3.85	0.54
	453	0.00220	3.63	0.24
	443	0.00228	3.57	0.14
15 kHz	491	-	4.51	1.42
	473	-	3.98	0.63
	453	-	3.71	0.28
	443	-	3.64	0.16
10 kHz	491	-	4.81	1.80
	473	-	4.13	0.81
	453	-	3.79	0.34
	443	-	3.71	0.20
5 kHz	491	-	5.47	2.80
	473	-	4.45	1.25
	453	-	3.94	0.51
	443	-	3.80	0.32
1592 Hz	491	-	7.13	5.80
	473	-	5.31	2.45
	453	-	4.31	1.01
	443	-	4.03	0.61

Table 12 (continued)

Freq.	T°K	I/T	ϵ'	ϵ''
1 kHz	491	-	8.04	8.33
	473	-	7.87	3.44
	453	-	4.56	1.44
	443	-	4.17	0.86
500 Hz	491	-	10.37	13.55
	473	-	6.97	4.94
	453	-	5.07	2.25
	443	-	4.51	1.25

Rubidium acetate : Cell no.2 : Co $\simeq$ 0.78 pF.

Freq.	T°K	I/T	ϵ'	ϵ''
20 kHz	483	0.00207	2.31	1.16
	454	0.00220	1.54	0.34
	433	0.00230	1.26	0.07
15 kHz	483	-	2.56	1.36
	454	-	1.60	0.38
	433	-	1.31	0.10
10 kHz	483	-	2.83	1.68
	454	-	1.67	0.46
	433	-	1.35	0.11

Table 12 (continued 2)

Freq.	$T^{o}K$	I/T	ϵ'	ϵ''
5 kHz	483	-	3.33	2.52
	454	-	1.86	0.64
	433	-	1.47	0.21
1 kHz	483	-	4.81	8.18
	454	-	2.50	1.41
	433	-	1.73	0.53
500 Hz	483	-	5.51	14.27
	454	-	3.07	2.07
	433	-	2.00	0.82

Lithium acetate : Cell no.2 : Co $\simeq$ 0.78 pF.
(Anhydrous)

20 kHz	496	0.00200	2.51	0.59
	488	0.00205	2.36	0.41
	468	0.00214	2.14	0.25
	448	0.00223	2.01	0.09
	429	0.00234	2.00	0.03
15 kHz	488	0.00205	2.46	0.51
	485	0.00206	2.41	0.45
	468	0.00214	2.19	0.30
	448	0.00223	2.07	0.11
	429	0.00234	2.03	0.03

Table 12 (continued 3)

Freq.	T°K	I/T	ϵ'	ϵ''
10 kHz	496	0.00200	2.90	0.81
	488	0.00205	2.59	0.61
	485	0.00206	2.28	0.54
	468	0.00214	2.31	0.38
	448	0.00223	2.10	0.13
5 kHz	488	0.00205	2.91	1.08
	485	0.00206	2.82	0.77
	468	0.00214	2.47	0.56
	448	0.00223	2.18	0.23
	434	0.00231	2.09	0.13
	429	0.00234	2.05	0.09
1592 Hz	496	0.00200	4.06	1.24
	483	0.00207	3.50	1.15
	468	0.00214	2.90	0.91
	448	0.00223	2.37	0.51
	434	0.00230	2.15	0.26
	429	0.00234	2.10	0.19
1 kHz	497	0.00200	4.42	1.54
	488	0.00205	4.03	1.39
	468	0.00214	3.30	1.18
	448	0.00223	2.53	0.64
	434	0.00230	2.26	0.34
	429	0.00234	2.18	0.28

Appendix 2

Program for Intensity Calculation

The aim of the program is to calculate the diffraction intensities theoretically, given the calculated values of the co-ordinates of the atoms, for all reflexions obtainable. The maximum limits to the values of h, k and l are set by the dimensions of the camera. The same reason sets maximum limits to 2 sin θ values.

It is now known that potassium acetate has three structures, form I - orthorhombic, form II and III monoclinic. So it would be convenient if the same program can be used for both systems. The values of the monoclinic angle β decide whether the calculation of a^*, b^*, c^* is for monoclinic or orthorhombic system. These parameters are then used to calculate 2 sin θ and sin θ/λ, needed for Lorentz-Polarization factor calculation. Again in the orthorhombic system, the calculation is limited to reflexions of the type hkl, whereas in the monoclinic system calculation is to be done both for hkl and $\bar{h}kl$.

The equation used for 2 sin θ calculation is

$$\rho = 2 \sin \theta = \sqrt{((ha^*)^2 + (kb^*)^2 + (lc^*)^2 + 2hl\, a^* c^* \cos \beta^*)}$$

For Lp-factor calculation, the expression used is (from International Tables for X-ray crystallography):

$$\text{Lp-factor} = \frac{1 + \cos^2 2\theta}{\sqrt{(4\,(L^{-1})^2)}}$$

where $L^{-1} = (\sin^2 2\theta - \xi^2)^{\frac{1}{2}}$

Here $\xi = k\lambda/b$. Putting $\rho = 2 \sin \theta$

$$\text{Lp-factor} = (2 - \rho^2 + \rho^4/4) \sqrt{(\rho^2(4 - \rho^2) - 4\xi^2)}.$$

The values of atomic scattering factors are obtained from interpolation of those given in the International Tables for X-ray crystallography.

The trigometrical terms were calculated with the formula:

Trigonometrical terms = $\cos 2\pi(hx + ky + lz) + \cos 2\pi(hx-k(y + \frac{1}{2}) + z)$

(taking into account the two formula units per unit cell. For oxygen atoms the above sum is doubled). The rest of the calculation is proceeded as usual, and the calculated intensity is obtained. The flow-diagram is given in Fig.66 and the program is reproduced below:

```
      DIMENSION FX(32,3),ATOM(4),SF(4),X(4),Y(4),Z(4),TERM(4)
      WRITE(6,16)
   16 FORMAT(1H1,25HPOTASSIUM ACETATE,FORM II)
      WRITE(6,17)
   17 FORMAT(1HO,36HCALCULATION OF OBSERVED INTENSITIES.)
      WRITE(6,18)
   18 FORMAT(1HO,21HOSCILLATION AXIS IS B)
      WRITE(6,30)
   30 FORMAT(1HO,26HRADIATION IS COPPER KALPHA)
C READ DATA
      READ(5,20) JM,KM,LM,ICS,A,B,C,BETA
   20 FORMAT(4I5,4F8.3)
      WRITE(6,70) A,B,C,BETA
   70 FORMAT(1HO,9X,3HA =,F8.3//10X,3HB =,F8.3//10X,3HC =,F8.3//10X,6HBE
     1TA =,F8.3)
      READ(5,21) NF,NA,RHOMAX,WL
   21 FORMAT(2I3,2F10.5)
      WRITE(6,71) RHOMAX,WL,NF,NA
   71 FORMAT(1HO,9X,8HRHOMAX =,F10.5//10X,4HWL =,F10.5//10X,4HNF =,I3//1
     10X,4HNA =,I3)
      READ(5,22)((FX(I,N),I=1,32),N=1,NF)
   22 FORMAT(8F9.3)
      DO 23 I=1,NA
   23 READ(5,24) ATOM(I),SF(I),X(I),Y(I),Z(I)
   24 FORMAT(A6,3X,4F9.6)
C     ATOMIC PARAMETERS X,Y,Z
      DO 40 I=1,NA
   40 WRITE(6,41) ATOM(I),X(I),Y(I),Z(I)
   41 FORMAT(1HO,A6,3X,3F9.6)
C     CALCULATE RECIPROCAL CELL DIMENSIONS
      RBETA =180.0-BETA
      BR =RBETA/57.29578
      COSB = COS(BR)
      RA = WL/(A*SIN(BR))
      RB = WL/B
      RC = WL/(C*SIN(BR))
      WRITE(6,90) RA,RB,RC
   90 FORMAT(1HO,9X,4HRA =,F10.5//10X,4HRB =,F10.5//10X,4HRC =,F10.5)
      WRITE(6,19)
   19 FORMAT(1HO,3X,1HJ,4X,1HK,4X,1HL,5X,3HRHO,7X,9HLP FACTOR,4X,9HINTEN
     1SITY)
      IF (ICS) 50,50,51
   50 AJM=0.0
      GO TO 52
   51 JM=2*JM
      AJM=FLOAT(JM)
   52 CONTINUE
C     START LOOPS THROUGH JKL
      DO 6 L=1,LM
      AL=FLOAT(L-1)
      DO 7 K=1,KM
      AK=FLOAT(K-1)
      DO 8 J=1,JM
      AJJ=FLOAT(J)
      AJ=-0.5*AJM+AJJ-1.0
```

(CONTINUED)

```
C CALCULATE RHO AND SINWL
      RHO=SQRT((AJ*RA)**2+(AK*RB)**2+(AL*RC)**2+(2.*AJ*AL*RA*RC*COSB))
      IF (RHO-RHOMAX) 100,100,28
  100 SINWL=RHO/(2.*WL)
C     CALCULATE LORENTZ-POLARISATION FACTOR
      ZETA=AK*WL/B
      DENOM=((RHO**2)*(4.0-(RHO**2))-4.0*(ZETA**2))
      IF(DENOM.LE.0.00001) GO TO 28
      FACLP=(2.0-(RHO**2)+.25*(RHO**4))/SQRT(DENOM)
C     CALCULATE STRUCTURE FACTOR
C     CALCULATE ATOMIC SCATTERING FACTOR
      SFAC=0.0
      DO 101 I=1,NA
      PT=SINWL/.05+1.0
      IPT=PT
      FRACPT=PT-FLOAT(IPT)
      M=SF(I)
      FI=FX(IPT,M)+(FX(IPT+1,M)-FX(IPT,M))*FRACPT
C     CALCULATE TRIGONOMETRICAL TERMS
      THETA1=6.2831853*(AJ*X(I)+AK*Y(I)+AL*Z(I))
      THETA2=6.2831853*(AJ*X(I)-AK*Y(I)+AL*Z(I)-.5*AK)
      IF(Y(I)-.25) 103,102,103
  102 GI=COS(THETA1)+COS(THETA2)
      GO TO 104
  103 GI=2.0*(COS(THETA1)+COS(THETA2))
  104 TERM(I)=FI*GI
  101 SFAC = SFAC+TERM(I)
      SFACSQ = SFAC**2
      OBINT = SFACSQ*FACLP
      WRITE(6,105)(AJ,AK,AL,RHO,FACLP,OBINT)
  105 FORMAT(1HO,3F5.0,F10.6,3X,F10.6,3X,F10.3)
   28 CONTINUE
    8 CONTINUE
    7 CONTINUE
    6 CONTINUE
      STOP
      END
```

Glossary of symbols used in the program for calculation of Intensity

JM, KM, LM: Maximum values of h, k, l respectively.

ICS: A digit to denote crystal system : 0 for orthorhombic, 1 for monoclinic.

A, B, C: Dimension of a, b, c axes respectively.

Beta: Cell angle in degrees (= 90° if orthorhombic).

NF: Number of different atom types.

NA: Number of atoms in asymmetric unit.

RHOMAX: Maximum value of 2 sin θ.

WL: Wavelength of X-rays in $\mathring{A}$

FX (IPT, N): The value of atomic scattering factor of N atom type at sin θ/λ given by IPT.

ATOM (I): A particular atom type I (up to 6 characters to denote).

SF (I): The atomic scattering factor table to be used for Ith atom.

X(I), Y(I), Z(I): x, y, z parameters for the ith atom.

J, K, L: hkl in integral form.

AJ, AK, AL: hkl in floating point form.

AJJ: h in floating point form for monoclinic structure.

AJM: 2JM in floating point form for monoclinic structure.

AJ: $-\frac{1}{2}$ AJM + AJJ + 1.0

RBETA: β^{*} (180 - β).

BR: β^{*} in radians.

RA: $a^{*} = \lambda/a \sin \beta$

RB: $b^{*} = \lambda/\bar{b}$

RC: $c^{*} = \lambda/c \sin \beta$

RHO: $2 \sin \theta$

COS B: Cos (β^{*} in radians).

SINWL: $\sin \theta/\lambda$

ZETA: $k\lambda/\bar{b}$ (oscillation along $\bar{b}$)

FACLP: Lorentz polarization factor.

PT: $(\sin \theta/\lambda)/0.05 + 1.0$

IPT: Integral part of Pt

FRACPT: Fractional part of PT

FI: FX(IPT, M) + (FX(IPT + 1, M) - FX(IPT, M)) FRAC PT.

THETA 1: θ_1 = Trigonometrical term for atom at x y z.

THETA 2: θ_2 = Trigonometrical term for atom at x, $\frac{1}{2}$-y, z.

GI: Cos θ_1 + cos θ_2 or 2(cos θ_1 + cos θ_2) according to y co-ordinate.

TERM: Product of atomic scattering factor FI and cos terms GI.

SFAC: $F = \sum f \cos(\ ) = \sum$ TERM over each atom in asymmetric unit.

SFACSQ: F^2

OBINT: F^2 x Lorentz polarization factor.

REFERENCES

1. Pauling, L., "The Nature of the Chemical Bond", (Ithaca, New York, Cornel University Press), 3rd Edition, 1960, pp.382.
2. Zhdanov, G.S., "Crystal Physics". (Edinburgh and London, Oliver and Boyd), 1st Edition, 1965, pp.154.
3. Kitaigorodsky, A.I. (Ref.2).
4. (i) Ketelaar, J.A.A. and Strijk, B., Rec. trav. chim, 64, 174, 1945.
   (ii) Tahvonen, P.E., Ann. Acad. Scient, Fennicae, Sr. A.I. Math. Phys., 43, 3, 1947.
   (iii) Siegel, L.A., J. Chem. Phys., 17, 1146, 1949.
5. Evans, R.C., An Introduction to Crystal Chemistry (Cambridge University Press), 2nd Edition, 1966, pp.370.
6. Ref. 1, pp. 171.
7. Hazlewood, F.J., Rhodes, E. and Ubbelohde, A.R., Trans. Faraday Soc., 62, No.527, part II, 3101, 1966.
8. Ehrenfest, P., Leiden Commen. Supp. 75, 1933.
9. Justi, E. and Laue, von, Phys. Z., 35, 945, 1934.
10. For example, Jaffray, J., Ann. Phys., 3, 5, 1948.
11. Nix, F.C. and Shockley, W., Revs. Modern Phys., 10, 1, 1938.
12. Messer, C.E. and Zeigler, W.T., J. Amer. Chem. Soc., 63, 2703, 1941.
13. Shirane, G. and Takeda, A., J. Phys. Soc. Japan, 7, 1, 1952.
14. Temperley, H.N.V., "Changes of State", (London, Cleaver-Hume Press), 1st Edition, 1956, pp. 247.
15. Ubbelohde, A.R., Quart. Rev. Chem. Soc., 11, 247, 1957.

16. Ubbelohde, A.R. and Woodward, I., Proc. Roy. Soc., A, 188, 358, 1946.

17. Kennedy, S.W., Ubbelohde, A.R. and Woodward, I., Proc. Roy. Soc., A, 219, 303, 1953.

18. Cleever, B., Rhodes, E. and Ubbelohde, A.R., Proc. Roy. Soc., A 276 437, 458, 1963.

19. Kennedy, S.W. and Patterson, J.H., Proc. Roy. Soc., A 283, 498, 1965.

20. Ubbelohde, A.R. and Woodward, I., Nature, 155, 170; 156, 20, 1945.

21. Buerger, M.J., "Phase Transformations in Solids" (New York, John Wiley and Sons) 1951, pp.183.

22.(i)Parry, G.S., Schuyff, A. and Ubbelohde, A.R., Proc. Roy. Soc., A 285 360, 1965.

(ii) Hazlewood, F.J. Rhodes, E. and Ubbelohde, A.R., Proc. Roy. Soc., A 285, 360, 1965.

23. Cimino, A., Parry, G.S. and Ubbelohde, A.R., Proc. Roy. Soc., A 252, 445, 1959.

24. Ubbelohde, A.R. "Koninkl. Nederl. Akademie Van Wetenschappen-Amsterdam", Proc. Sr. B, 65, No.5, 1962.

25. Ubbelohde, A.R., "Consiglio Nazionale Dele Ricerche Fondazione" F. Giordani "Corsi E Seminari Di Chimica", Vol.5, 85, 1966.

26. (Ref. 25).

27. Ubbelohde, A.R. and Woodward, I., Proc. Roy. Soc., A 185, 448, 1946.

28. Gallagher, K.J., Ubbelohde, A.R. and Woodward, I., Proc. Roy. Soc., A 222, 195, 1953.

29. (Ref. 21).

30. Buerger, M.J., American Mineralogist, 30, 469, 1945.

31. Buerger, M.J., J. Chem. Phys., 15, 1, 1947.

32. Bilby, B.A. and Christian, J.W., "Mechanism of phase transformations in metals", Inst. of Met. Monograph and Rept. Sr., No.18, 121, 1955.

33. Frank, F.C., Acta Met., 1, 15, 1953.

34. Kaufman, L. and Cohen, M., Prog. Met. Phys., 7, 165, 1958.

35. Ubbelohde, A.R., "Reactivity of Solids", Proc. of the 4th International Symp. on the Reactivity of Solids, Amsterdam, 1960, pp. 255.

36. Bragg, W.L. and Williams, E.J., Proc. Roy. Soc., A 145, 699, 1934.

37. Pauling, L., Phys. Rev., 36, 430, 1930.

38. Fowler, R.H., Proc. Roy. Soc., A 149, 1, 1935.

39. Einstein, A., Ann Physik, 22, 180, 800, 1906; 34, 170, 1911.

40. Debye,,P., Ann Physik, 39, 789, 1912.

41. Blackman, M., Repts. Progr. Phys. 8, 11, 1941.

42. For example, Kellermann, E.W., Phil. Trans., A 238, 513, 1940; Proc. Roy. Soc., A 178, 17, 1941.

43. Seidell, A. "Solubilities of Organic and Metal organic Compounds" (D. Van Nostrand Co.), 3rd Edition, pp. 700.

44. (Ref. 22(i)).

45. Lefkowitz, I. and Megaw, H.D., Acta Cryst., 16, 753, 1963.

46. Young, R.A., J. Sci. Instrum., 43, 449, 1966.

47. Buerger, M.J., "Crystal Structure Analysis" (John Wiley), 1960, pp. 78.

48. Kittel, C., "Introduction to Solid State Physics" (John Wiley), 2nd Edition, 1956, pp. 480.

49. Smyth, C.P., "Dielectric Behaviour and Structure" (McGraw-Hill), pp. 66.

50. Ref. 49, pp. 133.

51(a) Daniel, V.V., "Dielectric Relaxation", (London, Academic Press), 1967, pp. 203.

(b) Ref. 49.

(c) Meakins, R.J., "Progress in Dielectrics" Vol.3 (London, Heywood and Co.), 1961, pp. 153.

52. Ref. 51(c).

53. Hamon, B.V., Aust. J. Phys., 6, 304, 1953.

54. Glasser, L., Hall, P.G. and Leibenberg, D.D., J. Chem. Soc., A 295, 1967.

55. Ref. 51(a) pp. 211.

56. Borchardt, H.J., J. Chem. Ed., 33, 103, 1956.

57(a) Ref. 56.

(b) Spiel, S. (Referred to by Ref.56).

(c) Wittel, M., Am. Mineralogist, 36, 615, 1951.

58. Int. Tables for X-ray Crystallography (The Kynoch Press, Birmingham, England), 2nd Edition, 1967, pp.241.

59. Wilson, A.J.C., Nature, 150, 152, 1952.

60. Buerger, M.J., (Ref. 47) pp. 233.

61. Saunderson, C. and Ferguson, R.B., Acta Cryst. 14, 321, 1961.

62. Amrithalingam, V. and Padmanabhan, V.M., Acta Cryst., 11, 896, 1958.

63. Kalman, A., Acta Cryst., 19, 853, 1965.

64. Van Neikerk, J.N., Schoening, F.R.L. and Talbot, J.H., Acta Cryst. 6, 720, 1953.

65. Nahringbauer, I., Acta Cryst., 23, 956, 1967.

66. Vand, V., Lomer, T.R. and Lang, A., Acta Cryst., 2, 214, 1949.

67. Lomer, T.R., Acta Cryst., 5, 11, 1952.

68. Dumbleton, J.H. and Lomer, T.R., Acta Cryst., 19, 301, 1965.

69.(a) Yamada, Y., Shibuya, I. and Hoshino, S., J. Phys. Soc. Japan, Vol. 18, No.11, 1594, 1963.

(b)Hoshino, S., J. Phys. Soc. Japan, 19, 140, 1964.

70. Mathieson, McL.A., Acta Cryst., 6, 399, 1953.

71. Chao, S.H. and Taylor, W.H., Proc. Roy. Soc., A 176, 76, 1940.

72. Saunder, D.H., Proc. Roy. Soc., A 188, 31, 1946: A 190, 508, 1947, A 190, 518, 1947.

73. Brager, A., Acta Phys. Chim., URSS, 10, 88790, 1939 (Struct. Rept. 8, pp. 140).

74. Daniel, V. and Lipson, H., Proc. Roy. Soc., A 181, 368, 1943.

75. James, R.W. "Crystalline State", Vol. II, (G. Bell and Sons) pp.563.

76. Lipson, H. and Cochran, W., "The Determination of Crystal Structure" (London, G. Bell and Sons), 3rd Edition, 1966.

77. "International Tables for X-ray Crystallography" (The Keynoch Press, Birmingham, England), Vol. III.

78.(i) Ref. 43, pp. 901.

(ii) Sidgwick, N.V. and Gentle, J.H.H.R., J. Chem. Soc., 121, 1837, 1922.

79. Lefkowitz, I., Lukaszewicz, K. and Megaw, H.D., Acta Cryst., 20, 670, 1966.

80. Devonshire, A.F., Advan. Phys., 3, 85, 1954.

81. Ref. 53.

82. Dryden, J.S., Trans. Faraday Soc., 54, 1574, 1958.

83. Wilson, A.J.C., Proc. Roy. Soc. A.180, 277, 1942.